DESIGN AND OPTIMISATION OF EXTRACELLULAR MICROELECTRODES

Robert Lind B.Eng

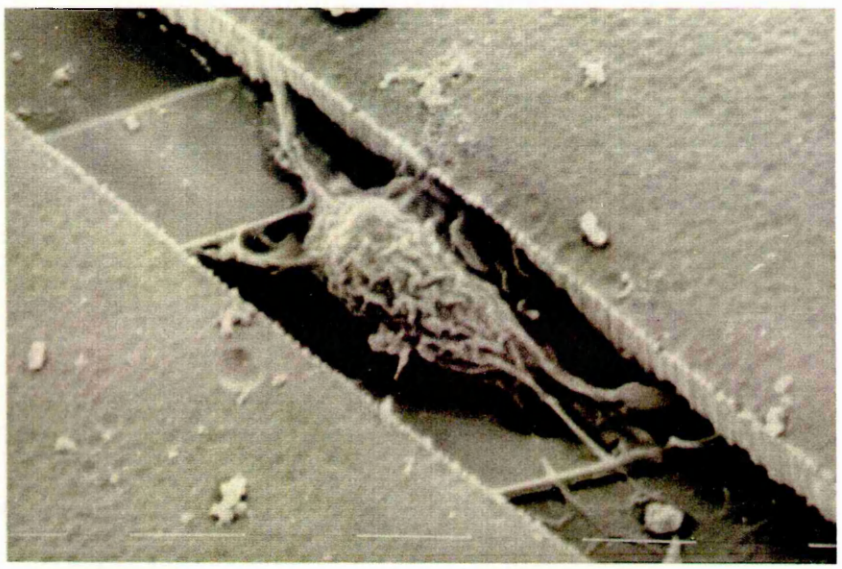

A thesis submitted to the Faculty of Engineering of the

University of Glasgow

for the degree of

Doctor of Philosophy

April 1991

ProQuest LLC.
789 East Eisenhower Parkway
P.O. Box 1346
Ann Arbor, MI 48106 – 1346

ACKNOWLEDGEMENTS

The completion of this thesis has only been possible with the help and encouragement of many people, both inside and outside the department of Electronics and Electrical Engineering. I wish to thank Professor J Lamb for providing the facilities for this work, and Dr P Connolly for her supervision and support. The active interest and helpful discussions provided by Professor C D W Wilkinson is also appreciated.

The excellent technical facilities made available to me are appreciated, made possible by the efforts of Bill Monaghan and Mary Robertson within the Bioelectronics group, Dave Clifton, Dave Lawson, and Ray Darkin in Dry Etching, and Lois Hobbs and Joan Carson in the Clean room. Thanks are also given to the staff of the USSL including Douglas McIntyre, Dave Gourlay, Helen Wallace, and Susan Capie. The willingness of George Boyle to lend anything and everything is appreciated, as are the cheerful efforts of Lawrence Bradley in the stores. Many of the photographs and diagrams in this thesis were prepared with the help of Kenny Melvin.

Throughout this work help and advice has been freely given by many people, including Drs P Clark, J Dow, G Moores, and L Breckenridge of the Department of Cell Biology. Professor A S G Curtis is thanked for allowing me access to the facilities of his Department, and I am especially grateful for the interest shown by Richard Wilson. Dr R Thomson is due thanks for the help given in carrying out much of the theoretical work involved.

My time time spent in the Department of Electrical Engineering was made easier by the friendship show by the above people, and by fellow students and researchers. In particular Ken Thomas, Andy Jennings and Rory MacCleod (with whom I shared an office) are thanked, as are John Bebbington, Brian Grahame, Iain Thayne, Thomas Krauss, Philipe Nadel, Dave Statton, Callum Cossar, Giovanni Barbarossa and laterly Jie Shen.

Finally I thank my parents and my sisters, Mary and Elizabeth, for supporting me during my (too) many years of study.

TABLE OF CONTENTS

SUMMARY

The work described in this thesis concerns the development and application of design methods for the optimisation of thin film metal microelectrodes, to be used for recording the electrical signals generated by neurons in culture.

The importance of carrying out studies into neural networks using these devices are discussed, emphasising the important role that small networks play in the functioning of the nervous system and the difficulties of studying them *in situ*. A survey of the various techniques available suggests that thin film metal microelectrodes are the only way to monitor networks for long periods of time (with the exception of MOSFET devices, which are inherently noisy) and which do not inflict serious damage on the cell. Several models and analytical calculations are used to estimate the extracellular potentials present around the cell during the firing of an action potential, which it is hoped to detect with the microelectrodes.

Consideration of previously reported recordings obtained with devices such as this, suggests that signal to noise ratios are often inadequate and that electrode surface roughness may play an important role in its determination. This is thought to be due to the effect of roughness on cell adhesion, which in turn determines the amplitude of the resulting potential. In order to study and quantify the dynamic process of cell adhesion, electrode impedances were continuously monitored during the attachment and development of variety of cultured cell types. The application of small, low frequency fields across electrode and cell was shown not to produce obvious deviations in normal cell development.

The theoretical properties of the electrode-electrolyte interface are compared to those obtained experimentally, and the behaviour of the impedance with respect to frequency, current density, and time is shown to be linear within certain estimated limits. Initially for relatively large electrodes (0.2×0.7mm), with the attachment and spreading of a permanent fibroblast cell line, impedance changes are only observed when the electrode surface possesses a suitable degree of roughness. This roughness is produced by the electrodeposition of either platinum black or gold. Less significant changes are shown to occur after smooth electrodes have been exposed to a plasma etch. Impedance rises are correlated with microscopically observed cell activity.

By reducing the size of the electrode used to below $100\mu m^2$, it is shown to be possible to detect the attachment and spreading of a single fibroblast cell, with the measured impedance increasing by up to 20%. Results of preliminary experiments concerning the attachment of neurons from the snail *Lymnaea stagnalis* are presented, but relate only to initial cell attachment as consistent spreading and process outgrowth has been difficult to achieve.

In order to consider the effects of electrode geometry on the extracellular potentials generated by neurons, a range of models are constructed and analysed using the field solution method known as the 'finite element method' (FEM). It is shown that in particular, the presence of insulating boundaries close to the cell membrane will significantly increase the extracellular potential at and near to it. It is suggested that locating the planar metal microelectrode at the bottom of either a groove or pit, into which the cell can fall, will lead to major improvements in the signal to noise ratios with which action potentials

generated by vertebrate neurons can be recorded.

Given the unavailability of a suitable electrically active vertebrate neuronal cell type during these studies, two methods are used to show that such devices will indeed significantly improve recordings. The first involves the use of micropipettes to inject a constant current into groove structures, directly above the electrodes. This shows the trend of increasing electrode potential with increasing groove depth. A more realistic method of verifying the computer simulations however, is the use of cardiac myocytes obtained from the heart of chick embryos. These generate action potentials similar to those produced by vertebrate neurons and, from the limited data obtained, again the recorded signal amplitude appears to increase with groove depth.

CHAPTER ONE

INTRODUCTION

CONTENTS

1.1 GENERAL INTRODUCTION TO THE NERVOUS SYSTEM

A complete understanding of the structure and functioning of the nervous systems of higher animal species has long been sought, with a great deal of research currently being directed towards achieving this goal. In addition to answering fundamental neurophysiological questions, such work will have major implications in the fields of both medicine and computing. Currently available technology offers enormous opportunities for the real time observation of the behaviour of the nervous system, employing a huge range of quasi biological and electronic (bioelectronic) sensing devices.

The enormous complexity presented by approximately 10^{12} neurons however, each of which is morphologically distinct and which may make many hundreds of interneuronal connections, has meant that research to date has only succeeded in answering a fraction of the related questions. The advances which have been achieved however, are not in themselves insignificant with perhaps the most important being the identification of the basic unit of the nervous system, the neuron. Although other cell types also play a significant role in the functioning of the nervous system, it is the neuron with its distinct morphology and electrical properties that allows humans to perform specialised tasks substantially faster than even the most powerful modern computers.

1.1.1 The neuron and neuronal organisation

Neurons exhibit a huge variety of three-dimensional shapes, although they are often modelled in a much simplified stylised form. Figure 1.1a illustrates such a neuron, with the important features being the relatively large cell body (soma) and the numerous processes emanating from it. The soma diameter of a typical vertebrate neuron is generally less than 10μm whilst that of an invertebrate neuron may vary from 20μm to 200μm; the diameters of the processes being only a fraction of these values. Generally there are considered to be two main categories of processes, termed dendrites and axons, although it is not always possible to distinguish between these at the resolution provided by a light microscope. Dendrites act as receptors for the electrical signals generated by other neurons, relaying these into the soma itself. The net result of all the signals arriving at the soma is a shift in the potential existing across its membrane, which if of sufficient magnitude may trigger the transmission of a short electrical pulse, termed an action

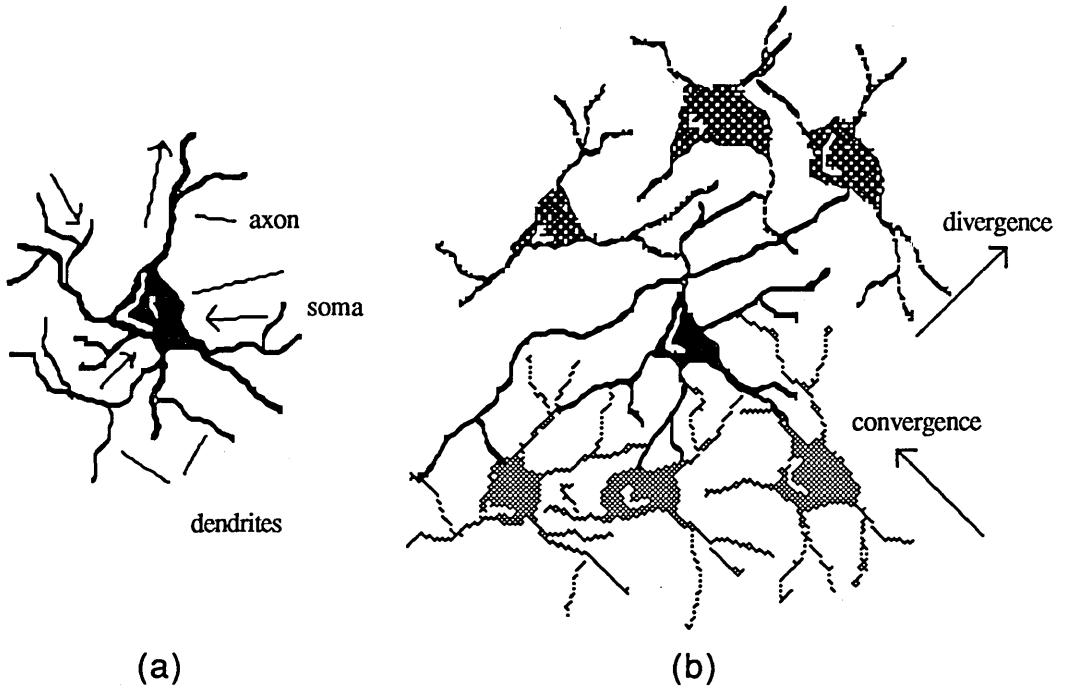

Figure 1.1 (a) A typical neuron possessing a relatively large cell body (soma) and a mass of fine processes. These consist of dendrites which transmit electrical signals to the soma, and a single axon which transmits signals initiated near the soma away from it. (b) A basic parallel architecture that allows signals to converge to and diverge from a single central neuron (shown in black).

potential, along the second category of process, known as an axon. Action potentials may be triggered either singly or in short bursts (a train).

There is only a single axon proceeding directly from the soma although this may branch many times along its length, and it is capable of the lossless transmission of action potentials (action potential transmission is often likened to a line of toppling dominoes or to a line of gunpowder ignited from one end). The axon terminates on the soma or on the processes of other neurons, in a junction termed a synapse. Although the existence of 'electrical' synapses has been observed, which allow ionic current to flow between cells through mediated gap junctions, the commonest form of termination junction is the 'chemical' synapse (Purves and Lichtman 1985). Here an intermediate substance, known as a neurotransmitter (e.g acetylcholine, γ-aminobutyric acid), serves to bridge the gap. The arrival of an action potential at a chemical synapse, via the axon, stimulates the release of this neurotransmitter which in turn elicits an electrical response in the post-synaptic cell. This response may either depolarise the cell towards the threshold for action potential generation, excitatory post-synaptic potential, EPSP, or may inhibit firing, inhibitory post-synaptic potential, IPSP. In addition to the generation of EPSP's and IPSP's, signal transmission via synapses may also affect action potential transmission along axons and may also induce the release of transmitters which modify the cells behaviour (both electrical and other) over a period of seconds, minutes, or even hours.

The conventional view that it is the soma which carries out all processing operations, with the dendrites and axons acting merely as conduits of signal transmission has been recently reassessed. The motivation for this is based on both experimental observations and on the conclusion that such a simple

system is incapable of performing the complex functions which are observed of the nervous system. Experimental results demonstrate for example that various regions of the dendritic tree may be capable of generating action potentials, which may or may not be propagated to neighbouring regions (Miller and Dacheux 1976). This suggests that within a single neuron there may exist a number (possibly very great) of subunits each capable of independent activity. The function of so called dendritic spines (small protrusions which occur on the surface of many dendrites at the site of a synapse) has also been questioned, with suggestions that they may be electrically active (Miller, Rall, and Rinzel 1985) and that they may be capable of rapidly changing their shape in response to the arrival at the synapse of an action potential (Crick 1982). This could result in a modulation of the amount of electrical signal transmitted from the pre- to the post-synaptic cell. All of these observations and hypotheses concerning the distribution of signal processing around the cell imply that the processing power of the central nervous system (CNS) is infinitely more powerful than was suggested by earlier models.

The study of individual neurons has revealed many of the complex properties detailed above, but it has proved exceptionally difficult to theoretically construct a model using these, which will predict accurately even relatively simple animal behaviour. An alternative approach which it was hoped would achieve this aim is that of behavioural psychology, which treats the entire body as a black box, and is concerned with external stimuli and the resulting responses. This may be looked on as the uppermost approach to the study of the nervous system, with the study of individual neurons being the lowermost. Two intermediate levels may also be identified, the first in which the black boxes consist of relatively large zones, each identified with specific functions, e.g. the visual cortex, the olfactory bulb, and the hippocampus. A second intermediate level is that of small groups of interconnected neurons, known as neural networks.

Intuition would suggest that neurons will interact to a greater extent with neighbouring cells than with those which are geographically distant. Such an arrangement would lead primarily to a reduction in the length of interconnecting processes resulting in reduced signal propagation delays (especially significant for axonal transmission which is relatively slow, $\approx 10 m.sec^{-1}$) and also lessening the risk of damage to fragile processes (Shaw, Harth, and Scheibel 1982).

An important question however, is whether small groups of cells can act as a single unit, receiving inputs and delivering outputs, or whether they are merely neighbouring links in a continuous chain. There is evidence that networks reconstructed in culture can perform as simple circuits exhibiting bistability (Kleinfeld, Raccuia, and Chiel 1988) and oscillatory behaviour (Droge et al. 1986), which could conceivably be incorporated into more complex networks. It may be simplistic however, to suggest that there is a 'library' of such small units which are slotted into place during development, as this ignores the dynamic and evolutionary nature of this process.

This last point indicates that it is not only the equilibrium behaviour of neural networks that is of interest, where the relationship between structure and function is observed, but in addition concern must be given to the dynamic processes whereby the network achieves this state, involving as it almost certainly will, their ability to adapt by 'learning'. Various explanations for this latter, fundamental property, have been suggested including changing morphologies, adaptation of membrane excitability, and 'synaptic

plasticity'. Of these synaptic plasticity has been the most widely discussed and investigated (Zucker 1989), and refers to the ability of the synapse to modulate the amount of neurotransmitter released upon the arrival of an action potential via the axon (the fraction of the axonal signal which passes through to the post-synaptic cell is known as the 'synapse weight'). For example the neurons controlling the gill withdrawal reflex in the marine mollusc *Aplysia californica*, produce habituation and sensitization which are two simple forms of short term learning, by reducing and increasing respectively the amount of neurotransmitter released from presynaptic terminals with repeated stimulation (Rayport and Schacher 1986)

1.1.2 Artificial neural networks

Out of attempts to reproduce the processing techniques used by the brain, for the purposes of robotics and computing, the field of artificial intelligence (AI) has arisen. In particular the development of artificial neural networks is of great current interest, where circuits are loosely based on digital and analogue equivalents of neurons and their interconnections. Figure 1.2(a) illustrates one such simulated neuron having two inputs and one output (Widrow and Lehr 1990), which is known as an Adaline (adaptive linear element). The two inputs, X_{1k} and X_{2k}, represent dendritic inputs; W_{1k} and W_{2k} represent the corresponding synapse weighting; W_{0k} is the bias weight; S_k is the summation of the three inputs times their weights, and represents the integration occurring at the soma; Y_k is the output which can take on a value of either 1 or -1, depending on whether S_k is positive or negative, and represents the output along the axon. Figure 1.2(b) shows the four possible input configurations in pattern space, which is divided in two by a line whose slope and intercept is determined by the values of the three weights. Points lying below this line will produce a positive output whilst those lying above it will produce a negative output.

Whilst this represents only a trivial example of a pattern recognition circuit, it is possible to combine Adalines (and to incorporate non-linear inputs, e.g. X_{1k}^2) to produce systems which can recognise complex regions of pattern space and which can perform conventional Boolean logic operations. In addition artificial networks have been designed which can perform optimisations (Hopfield and Tank 1985), exhibit bistability (Tank and Hopfield), and act as simple content addressable memories (CAM) (Hopfield 1983). Such simulated networks were never seriously intended to mimic completely the operations of real nervous systems, but they may offer an indication of some of the complicated functions which relatively small parallel networks can perform. Although these models take as their basic unit the neuron, it is clear from the above discussion of the complex nature of the neuron that these might well be zones distributed around both the cell body and its arborisations.

1.1.3 Introduction to neuronal recording

The combined evidence, both experimental and theoretical, supports the view that small networks are one of the foundations upon which the nervous system is built, operating as either processing, pattern generation, or memory circuits, or as a combination of each. These will vary in complexity but initial studies must necessarily concentrate on the more simple networks, due to the technical limitations of recording the activity from every neuronal member. In addition there is the difficulty involved in analysing data recorded over time periods sufficient to observe adaptive behaviour, where the volume of data will increase disproportionately with network size. It is also important to note that even in these small

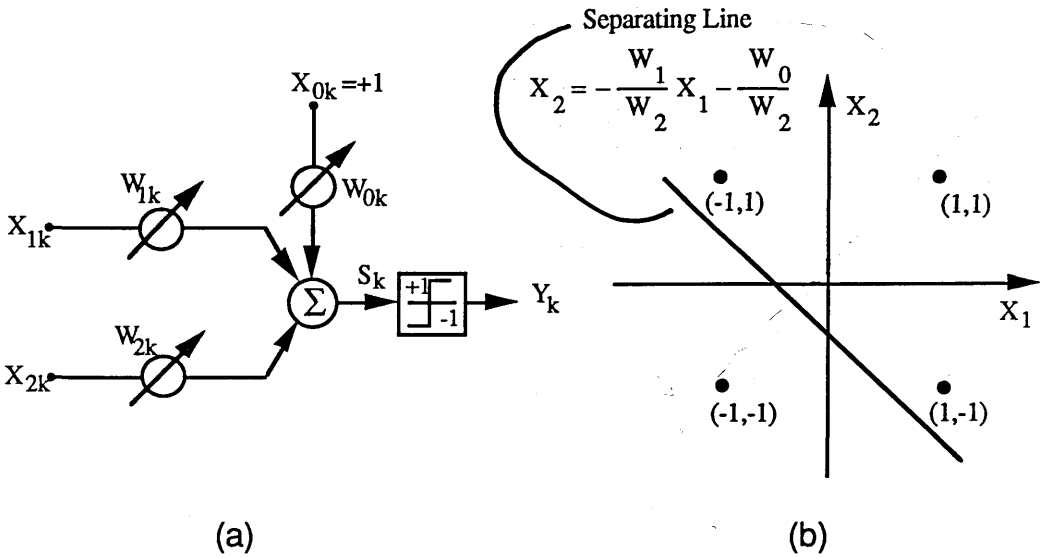

Figure 1.2 (a) The two input Adaline where X_{1k} and X_{2k} are the dendritic inputs with W_{1k} and W_{2k} being the synapse weights. The products of the inputs times the weights are summed at the 'soma' with a bias signal $X_{0k}.W_{0k}$ to produce an output S_k. If S_k is positive then Y_k=1, otherwise Y_k=-1. (b) The output can be represented in pattern space, with two distinct regions.

networks, individual neurons may be under the influence of many other cells outside the network in addition to a myriad of chemical effects, which must either be monitored or eliminated.

Studies concerning the behaviour of such small neural networks have progressed slowly over the last few decades, limited chiefly by the inability to monitor simultaneously the activity of all of the cells in a network and by the unpredictable effects of external factors. The importance of simultaneous multi-site recording is apparent from the above discussion on the dynamic nature of the neuronal network, given that the state of the output of a neuron is dependent on the integrated effect of the inputs, both in temporal and in spatial terms. Simply observing the behaviour of each neuron in turn will not indicate how the overall system operates, as the properties of the network may change over the time between successive recordings (it is also important to note that neurons do not behave in a consistent manner, with a degree of noise always present in their response to a repeated stimulus). The possession of this multi-site recording capability is probably the single most important criterion for any technique, but has been satisfied by the recent introduction of a range of devices fabricated using methods previously the sole preserve of the semiconductor industries. The past decade, over which these methods have been more fully utilised, has therefore seen an intensification of research with some noticeable successes.

In addition to possessing the ability to record in parallel, any successful technique must satisfy several other important criteria, namely:
(a) that the materials used must be biocompatible for long term use, and that the recording technique must be as non-invasive and non-disruptive as possible,
(b) that it allows the study of networks that exhibit real and relevant behaviour,
(c) and finally that the signals recorded should be repeatable, with good signal to noise ratios.

Several methods exist which satisfy all of these conditions to a greater or lesser extent, but which rely on different effects caused by neuronal electrical activity. In order to compare their relative merits, it is

necessary first to understand the underlying processes of cellular electrical activity and to be aware of the additional effects caused in the surrounding environment.

1.2 THE MEMBRANE ACTION POTENTIAL AND ITS ASSOCIATED EXTRACELLULAR FIELDS

1.2.1 Underlying processes of membrane excitability

The manner in which transmembrane action potentials are generated is well understood and is detailed in most elementary cell biology textbooks (Alberts et al. 1983). Briefly, the potential difference existing across the lipid bilayer cell membrane is determined by both the relative ionic concentrations in the intra and extra-cellular regions, and by the rate at which these ions can leak from one side to the other. The Nernst equation,

$$E_m = \frac{RT}{hF} \ln \frac{a_e}{a_i} \qquad (1.1)$$

allows the potential difference across the membrane, E_m, to be calculated, provided that the membrane is permeable to only one ionic species. R is the gas constant, F is Faraday's constant, T is the absolute temperature, and h is the valence of the ion. a_i and a_e are the intracellular and extracellular ionic activities respectively.

Obviously in the case of a neuron the situation is more complex with ionic imbalances existing for a number of ions, most notably sodium and potassium (where the extracellular concentration greatly exceeds the intracellular concentration for Na^+ and vice versa for K^+). The membrane potential existing under these conditions is that potential which causes the net current flow across the membrane to be zero. Individual ionic currents may still flow however. The electrical properties of a small patch of membrane can be represented in terms of the equivalent circuit shown in figure 1.3 (Hodgkin and Huxley 1952).

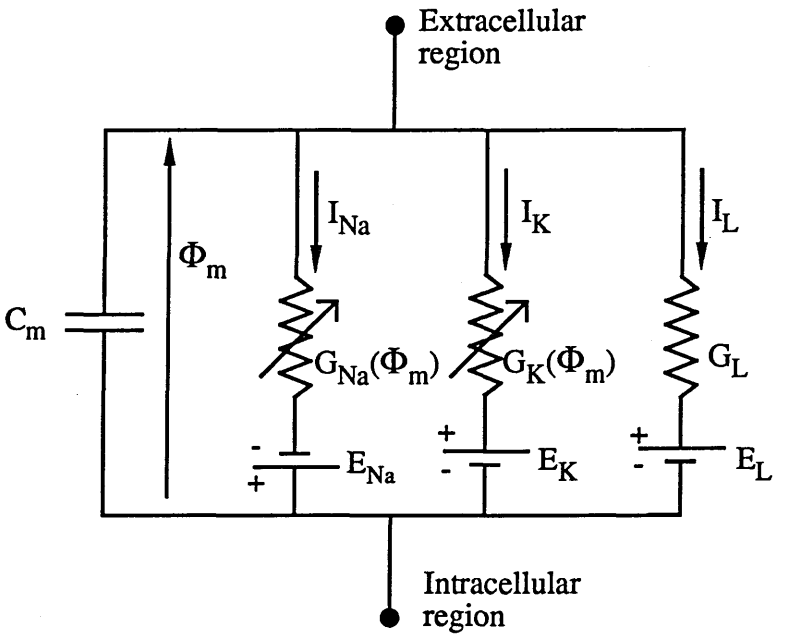

Figure 1.3 Model of the electrical properties of a patch of neuronal cell membrane. C_m represents the membrane capacitance, G the ionic conductances, and E the nernst potential for each ion. I represents the ionic current flow through the conductances.

Current can be carried across the membrane by either sodium (Na), potassium (K), or other non-specified ions (L).
These flow through ion specific channels whose permeability or conductivity G, is dependent on the transmembrane potential Φ_m. The potential difference driving each ion through these channels is the difference between the transmembrane potential and the Nernst potential for that particular ion E. In addition to the current carried through the membrane, there is an additional contribution from the charging and discharging of the membrane capacitance.

When the membrane is at rest, its conductance to potassium is much greater than that for sodium. Examining figure 1.3, the potential drop across G_K will be negligible and C_m will be charged to approximately E_K. From (1.1) E_K can be shown to lie between -70 and -100mV. It is observed experimentally that a depolarisation (a positive increase) of the membrane by about 10mV or more, leads to a further transient increase of between 70 and 90mV (figure 1.4). This can be explained by the triggering of a rapid rise in the sodium conductance to a value far greater than that for potassium. The potential thus moves towards the Nernst potential for sodium (50 to 65mV). This rise in conductance lasts for 1-2mS before returning to its original value, with the membrane potential also recovering to its resting value aided by a temporary rise in the potassium conductance. The latter effect causes a slight overshoot in the potential to occur. Although potassium and sodium concentration imbalances dominate the electrical behaviour of the majority of neurons, other ions, notably calcium, play a major role in a significant minority of neuronal cell types, while the basic mechanisms of action potential generation remains the same.

It is clear from figure 1.3 that when the transmembrane potential is at its resting value, individual ionic currents are still flowing across the membrane. If no mechanism existed to reverse this leakage, the ionic concentrations inside and outside the cell would eventually equalise. There is in fact a mechanism involving proteins which are integrated into the lipid membrane, and which pump the leaking ions back across the membrane thus maintaining the dynamic steady state situation described above. These pumps are powered by adenosine triphosphate (ATP).

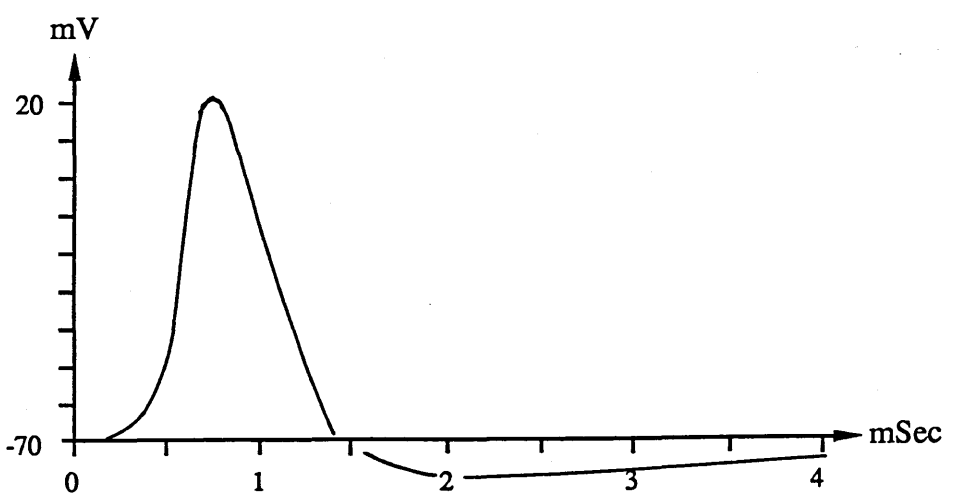

Figure 1.4 A typical vertebrate neuronal action potential

The voltage gated channels which facilitate increased ionic leakage during an action potential are distributed unevenly throughout the neuronal membrane, and the total current is the sum of currents through individual channels. Channel densities are observed to be highest at the junction between axon and soma, which is known as the axon hillock or initial segment. This latter term arises from the fact that due to the large channel densities present the threshold for depolarisation at this point is relatively low, and action potential generation is often initiated at this point (Eccles 1964). This then leads to a depolarisation of the adjacent axonal membrane and the firing of an action potential, a process that continues along the length of the axon. By describing each portion of membrane by the equivalent circuit of figure 1.3, and linking adjacent regions by the conductivities of both the intra and extra-cellular fluid (Hermann 1879), it is clear how the sodium influx at one point will cause a depolarisation of its neighbouring areas. Figure 1.5 illustrates this 'core conductor' model. The occurrence of a refractory period after depolarisation, that is a period in which no further action potentials can be triggered, causes the transmission to be unidirectional.

This model has to be modified if the axons are insulated with glial cells, which wrap tightly around the process with a periodic length of approximately 1mm. In the gaps, known as nodes of Ranvier, between these insulating cells, the exposed axonal membrane possesses a large accumulation of voltage dependent channels (these are chiefly sodium channels with potassium channels being less localised). The process of action potential transmission in this case consists of passive electrotonic flow between two adjacent nodes, with regeneration occurring on arrival at the node. This 'hopping' increases the speed of conduction down the axon, as electrotonic spread is substantially faster than continuous local circuit depolarisation (which is limited by the relatively slow response of the voltage dependent channels). Since myelination, as this process is known, only occurs in longer fibres and is not generally observed in culture the following discussion is confined to the extracellular fields generated only by unmyelinated fibres.

It is clear that in the case of an axonal action potential, currents will flow in the extracellular region adjacent to the membrane currently active. The core conductor model does not indicate how the resulting extracellular field is distributed as it represents the extracellular region only as a lumped conductance. In order to achieve this a continuous field solution in either 2 or 3 dimensions is required.

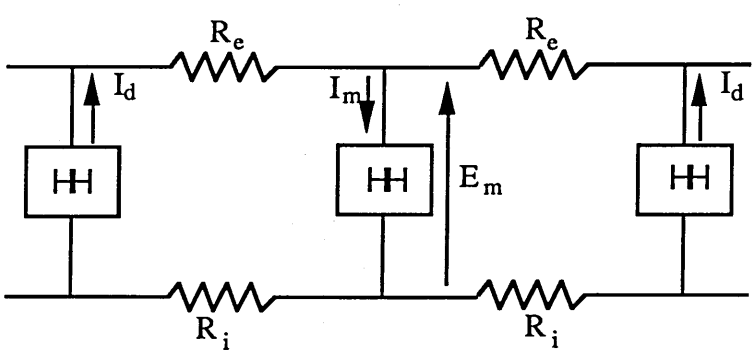

Figure 1.5 The core conductor model illustrates how action potentials are transmitted unattenuated along an axon. The properties of the membrane are represented by distributed components (HH) consisting of Hodgkin-Huxley elements (see figure 1.3), linked by the resistance of both the intracellular, R_i, and extracellular, R_e, fluids. The current I_m flowing across an excited patch of membrane causes depolarisation of the neighbouring regions, via I_d.

1.2.2 Estimation of extracellular potential fields

An analytical solution can be obtained for an AP travelling along an axon in an homogeneous volume conductor (Clark and Plonsey 1966)(Geselowitz 1966), by solving Laplace's equation in cylindrical coordinates (considering the axon to be a cylinder of radius a, and of infinite length with its longitudinal axis in the z direction). Laplace's equation,

$$\nabla^2\Phi = 0 \qquad (1.2)$$

gives the potential Φ everywhere in a bounded region inside which no net charge is present, provided that either the potential or its derivative with respect to the boundary normal are known over the entire boundary. In terms of cylindrical coordinates (1.2) can be written as

$$\nabla^2\Phi = \frac{1}{\rho}\frac{\partial}{\partial\rho}\left(\rho\frac{\partial\Phi}{\partial\rho}\right) + \frac{1}{\rho^2}\frac{\partial^2\Phi}{\partial\varphi^2} + \frac{\partial^2\Phi}{\partial z^2} = 0 \qquad (1.3)$$

Where ρ is the radial distance from z axis, and φ is the angle of rotational symmetry.

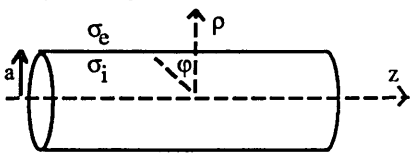

Given the boundary conditions that $\Phi=0$ as the radial distance ρ approaches infinity, and that the transmembrane potential Φ_m occurs over an infinitely thin membrane at a radius $\rho=a$, the solution for the extracellular region is shown to be

$$\Phi_e = \frac{1}{2\pi}\int_{-\infty}^{\infty}\frac{\Phi_m(k)K_0(|k|\rho)e^{-jkz}}{\alpha(|k|a)K_0(|k|a)}dk \qquad (1.4a)$$

where

$$\alpha(|k|a) = -\left[\frac{\sigma_e K_1(|k|a)I_0(|k|a)}{\sigma_i K_0(|k|a)I_1(|k|a)} + 1\right] \qquad (1.4b)$$

given rotational symmetry around the axon.

I, K = modified bessel function of the first and second kind respectively

σ_i, σ_e =conductivity of the intracellular and extracellular fluid respectively

$\Phi_m(k)$ = Fourier transform of the transmembrane potential

k = inverse space dimension

For simplicity, Clark and Plonsey approximated the transmembrane potential Φ_m by a simulated action potential consisting of the summation of three appropriate Gaussians (figure 1.6a), making it straightforward to evaluate the fourier transform. Figure 1.6b illustrates the variation in potential with time that would be present at a radial distance of 260μm from a 60μm diameter axon#. This characteristic triphasic shape may also be thought of in terms of the variation in potential along the axon at a single point in time. Figure 1.6c shows the radial variation in the peak potential for axons varying in diameter from 1 to 60μm. The maximum extracellular potential for a 10μm diameter axon is 45.5μV at the surface of the membrane.

It is important to note the dependence of the extracellular potential on the ratio of the intracellular and the extracellular conductivities. By decreasing the latter it would be possible to increase the signal

Calculations assume an axoplasmic conductivity of 0.01S.cm^{-1}, and an extracellular conductivity of 0.0033S.cm^{-1} (McNeal 1976)

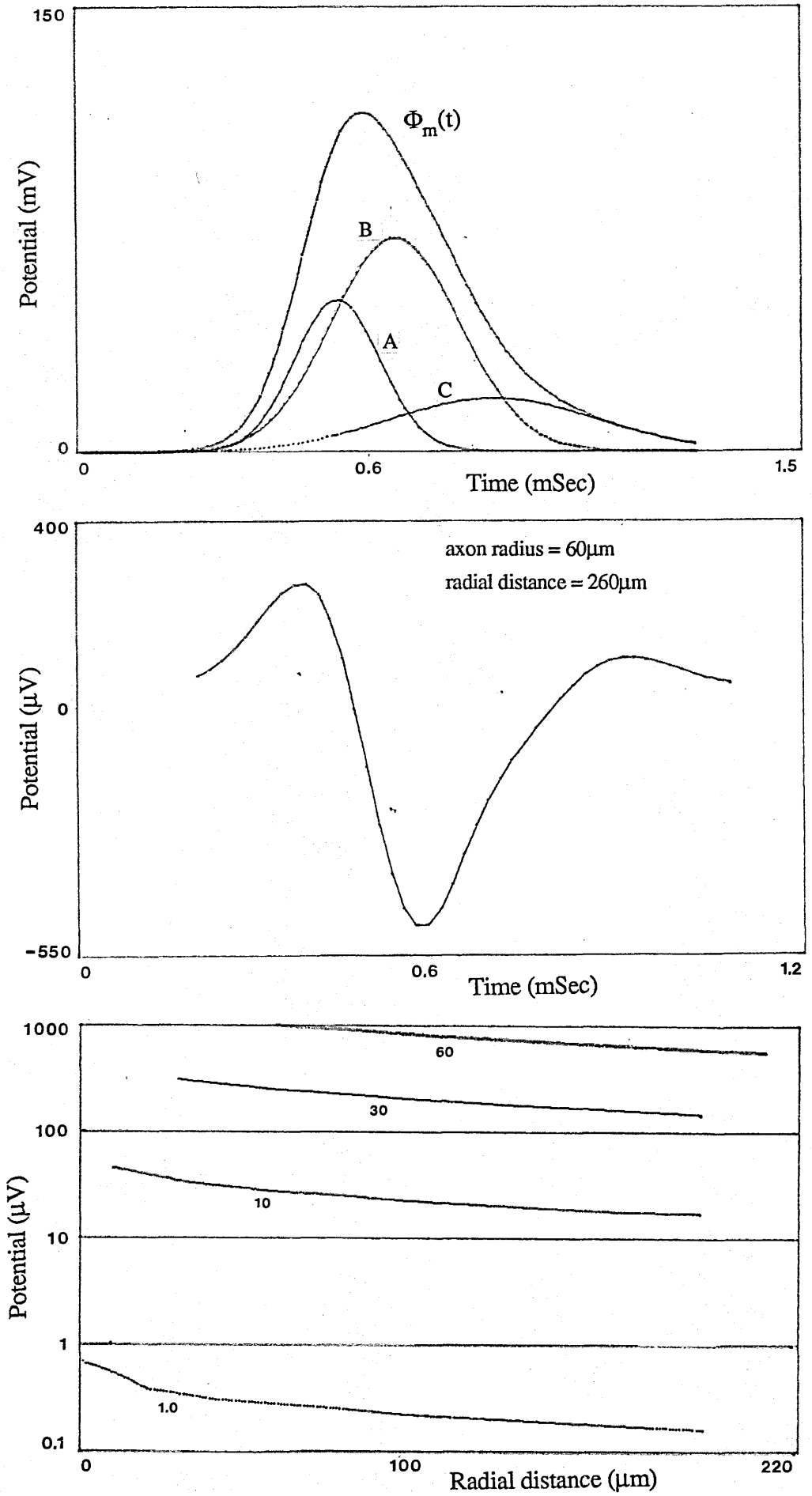

Figure 1.6 (a) Simulated transmembrane action potential, obtained by the summation of three gaussians, A B and C. (b) The axial variation in potential along a 60μm diameter axon, at a radial distance of 260μm, obtained from (1.3) and (c) the decay in peak potential with radial distance, for a variety of axonal radii.

amplitude. Such a situation exists in nervous tissue where the processes are tightly surrounded by both connective tissue and other neurons, and consequently much larger extracellular potentials will occur.

These figures suggest that it would be possible to record extracellularly from large isolated axons (>10μm in diameter) with a reasonable signal to noise ratio. Such axons would probably be those belonging to large invertebrate neurons, and indeed several successful attempts have been reported (Wilson 1990). Whilst the signal amplitudes obtained were similar to those calculated here, the precise shape of the waveform does show some variations. It is probable that this is due to the failure to take into account the finite length of a real axon, and the presence of the large cell body (electrode properties and inappropriate signal filtering can also seriously alter the waveform). Given that action potential transmission occurs at a velocity of around $10m.Sec^{-1}$ in unmyelinated axons, with a duration of 1-2mSec, theoretically a region of over 1cm in length would be simultaneously depolarised. Axonal lengths in culture are generally only a few hundred microns, and hence the cell body will affect the flow of local circuit currents along the entire length of the axon.

Although action potential generation on axons has been the concern of the majority of theoretical calculations, an important question is whether they can also be generated on the cell body itself. An indication of membrane excitability can be obtained from the distribution of voltage dependent sodium channels, which in turn can be found by the specific attachment of various neurotoxins (Catterall 1984). The β-scorpion toxin can be labelled with the ^{125}I isotope and attaches only to voltage dependent sodium channels. Channel densities thus obtained for rat spinal chord neurons are in the range $50\text{-}110\mu m^{-2}$ on the soma and unmyelinated axons, and $350\text{-}500\mu m^{-2}$ at the axon hillock. The high channel density on the soma, which is comparable to that present on the axon, would indeed suggest that the soma membrane can be stimulated to fire an action potential. This is supported by the use of voltage sensitive dyes (section 1.3.2) to map the transmembrane potential distribution over the entire membrane of cultured neurons from the snail *Aplysia* (Parsons et al. 1989). In this method the absorption of light is proportional to the transmembrane potential, and illustrates that the amplitude of action potentials generated on the soma is only fractionally less than that on the initial segment and on the axon.

As discussed above, the magnitude of the extracellular potentials in the vicinity of an excited axon are small due to the small membrane surface area that is activated. It would be expected that larger potentials would be present near a soma that was similarly active, due to its much greater surface area (in proximity to a recording electrode). Predicting the form and magnitude of these extracellular fields is far from trivial, due to the non-uniform morphology of the soma (including extensive folds in the membrane surface) and the often massive number of processes emanating from it. In addition, compared to the simple 1-dimensional propagation (in the z direction) of the action potential in the axon, the propagation over the soma may involve some complicated 3-dimensional spreading pattern.

A much simplified situation is achieved by assuming the cell to have a spherical soma and by modelling all the dendrites as a single cylinder emanating from it (Rall). This latter assumption is justified if the cylinder has the same passive electrical properties as the dendrites when looking out from the cell body. In addition the soma membrane is taken to depolarise uniformly, with the incoming current flowing out through the single cylindrical dendrite (the effect of the axon is assumed to be negligible due

to its relatively small surface area). Rall calculated the potential around such an idealised neuron given the peak current density into the soma, using cascaded RC networks to simulate the cylindrical dendrite. For a 25-50μm diameter cell suspended in an homogeneous, infinite volume conductor, the maximum extracellular potential is in the region of 800μV at the soma surface.

A further simplification is achieved by considering the cell body in isolation, removing the effects of the processes. In this case the entire membrane is again considered to depolarise simultaneously with the current being drawn from a grounded reference electrode at infinity (instead of through the cylindrical dendrite). If the transmembrane current density is J_m, and the soma is spherical with a radius b, the current density at any radial distance ρ ($b < \rho > \infty$) is

$$J_\rho = \frac{J_m b^2}{\rho^2} \qquad (1.5)$$

The electric field at this point is given by $J_\rho = \sigma_e E$, where σ_e is the conductivity of the extracellular media and hence the electric potential at a distance ρ from the centre of the cell is

$$\phi_e = -\int_{\infty}^{a} E dr = \frac{J_m b^2}{\sigma_e \rho} \qquad (1.6)$$

The maximum attainable potential occurs at the surface of the cell where ρ=b, and is proportional to the cell radius. In the region very near to the cell, this solution approaches that obtained when including the lumped dendrites in the model.

This much simplified model for calculating extracellular potentials would also suggest a 1/ρ decay of potential with distance from the cell membrane. A similar decay has been observed experimentally using a metal filled glass micropipette (Tank and Kleinfeld 1986) with dissociated mouse spinal chord neurons in culture, and is also suggested by recordings made with planar metal electrodes from slightly displaced cells (Pine 1980)(Gross and Lucas 1982).

A further refinement in predicting the extracellular potential field around the cell body is to take into account the perturbation caused by extracellular boundaries. It was noted above that extracellular tissue surrounding a cell *in vivo* will cause a decrease in the conductivity around the cell, hence increasing the potential in certain regions. Introducing electrodes which are often mounted on substantial insulating surfaces will cause a similar, though non-symmetrical disturbance of the field. Models, such as that described by Rall, despite their simplicity offer the opportunity to quantify these effects. For example, considering the perturbation caused by a wide flat electrode support, a distance of four soma radii from a neuron (Drake et al. 1988) and utilising the finite difference solution method, demonstrates a substantial increase in extracellular potential of up to 60%.

The influence of boundaries, either insulating or conducting, on the extracellular potential field has often been neglected, due mainly to the difficulties in incorporating them into the initial mathematical problem. This is especially true when an analytical solution, which often provides a clearer picture, is sought. The increasing power of digital computers combined with the versatility of the graphics available means that this need no longer be the case, and the modelling of neurons situated in complicated 3-dimensional surfaces is possible by a variety of methods.

1.3 RECORDING NEURONAL ELECTRICAL ACTIVITY

Section 1.1 noted the major features that are required of a recording device if it is to monitor successfully the behaviour of electrically active neurons, and it is also clear from the foregoing discussion that there are several locations around the cell from which recordings may be made. A variety of devices and techniques have been proposed and utilised which fulfil certain of these requirements, although no single method has yet proved to be ideal. The most successful of these are discussed below, but it is necessary first to consider the advantages and disadvantages of studying neural networks either *in vivo* or *in vitro*.

1.3.1 *In vivo* versus *in vitro* systems

The study of nervous tissue *in vivo* offers the most natural environment in which to observe neuronal behaviour, and in addition the presence of surrounding insulating tissue will cause increased signal amplitudes. Problems arise both in determining the pattern of intercellular connections, and in identifying which cells are being recorded from. In addition there will be electrical interactions with many cells outwith those under observation, and a host of uncontrollable chemical factors. Other problems include the deposition on electrodes of organic material (Elbicki and Weber 1989) leading to variations in electrode properties, and the trauma and mechanical stress produced by penetrating into the tissue.

An alternative method of observing networks is under defined culture conditions *in vitro*. This can be divided into either tissue culture or dissociated cell culture. The former involves maintaining tissue slices or fragments in culture medium (Levi-Montal Chini and Seshan 1982), but retains many of the problems inherent to *in vivo* observation. Dissociated cell culture on the other hand, overcomes all of these while introducing limited problems of its own. Dissected nervous tissue can be enzymatically treated to loosen the connective tissue holding the cells together, allowing the dissociated cells to be plated onto a suitable planar substrate. A long list of neuronal cell types exists for which suitable culture conditions have been obtained, and which have been maintained in culture over a period of many weeks (Nelson, Neale, and Macdonald 1981). Two primary factors are a suitable surface onto which the cells can attach, and culture media containing the correct balance of salts, proteins, nutrients, and other organic compounds.

In general most of the processes are removed from cells upon dissociation due to the mechanical trauma involved, and it is only the cell body which initially attaches to the artificial substrate. Subsequently however, a distinctly neuronal morphology develops with extensive arborisation which often displays a similar shape to that observed *in vivo* (eg unipolar, bipolar and pyramidal). The electrical properties of the cell membrane depend on the age of the cell, as would be expected. Mature neurons from invertebrates are observed to be electrically active immediately after dissociation, while embryonic neurons may take several days to reach this state (Nerbonne and Gurney 1989),(Ahmed 1988). The ability of cultured neurons to form inter-neuronal synapses, both chemical (Fuchs, Henderson, and Nicholls 1982) and electrical (Hadley, Kater, and Cohan 1983) has also been demonstrated. The possibility exists therefore, that dissociated neuronal cell cultures will reform networks which will allow access to individual cells and which will allow the pattern of interconnections to be observed under optical microscope examination. In

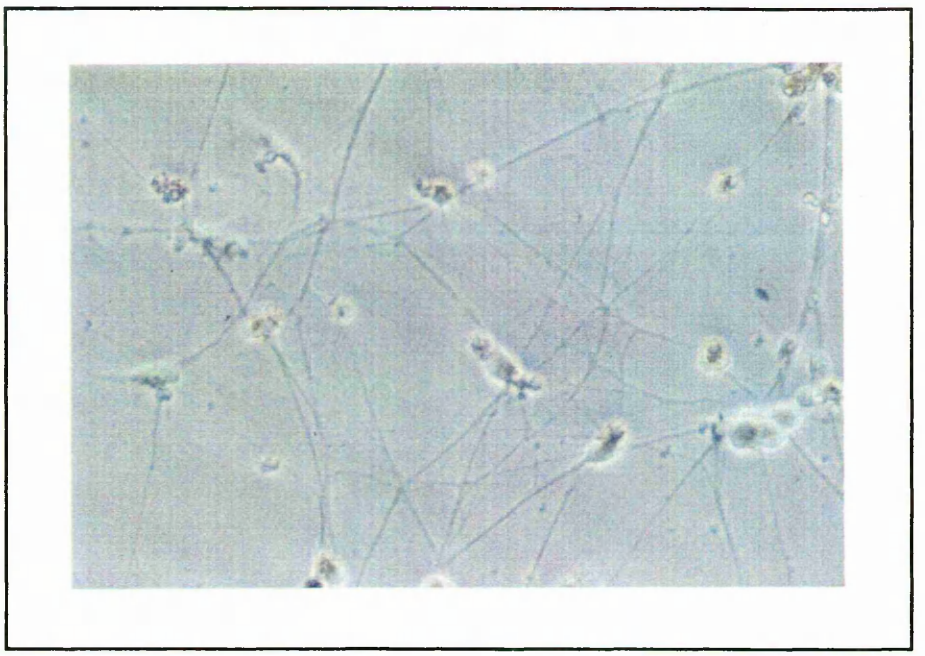

Figure 1.7 Neurons from embryonic chick dorsal root ganglia, after 2 days in culture.

addition the outside influences upon it can be strictly controlled by maintaining constant culture conditions, and the problem of interconnections with outside cells can be eliminated.

Whilst culturing can simplify networks enormously, there still exists a great deal of complexity if even a small number of cells are allowed to form a mass of interconnections. As an example figure 1.7 shows an interconnected network of chick dorsal root ganglia neurons, after 2 days in culture. This problem has been addressed by several authors. Higgins (Higgins, Smith, and Gross 1980) first considered the elimination of unwanted cells and neurites (the processes of cultured neurons are commonly termed neurites) by laser surgery. This has the advantage that the effect of the removal of one or several inputs to a cell can be observed, but it will not allow repeated experiments to be carried out as the neurites are initially allowed to grow randomly. A second approach has been the use of substrate surface topography to guide neurite outgrowth. Cultures of both vertebrate (Clark et al. 1987)(Clark et al. 1990)(Hirono et al. 1988) and invertebrate neurons (Wilson, Dow, and Blackshaw 1991) show neurite alignment along grooved substrata, the degree of alignment being dependent on groove depth, width, and periodicity for gratings. Alignment obtained is probabilistic, but providing that cells can be accurately positioned this method should allow outgrowth to be directed towards specific target cells. Finally, a technique which allows the patterning of molecules that promote (eg amines) and inhibit (eg alkane chains) cell adhesion and neurite outgrowth (Kleinfeld, Kahler, and Hockberger 1988)(Britland et al. 1989) has recently been developed. Neurite outgrowth has been shown to be confined along 10μm wide lines defined photolithographically. Either this method, or that of topographic guidance should be able to produce defined and repeated networks consisting of a small number of cells (2-5), that are simple enough to be monitored and analysed.

Initial studies have demonstrated the ability of cultured networks to operate as bistables and rhythm generators (see section 1.1.1), functions which would be expected *in vivo*, and indicate the important part they can play in neurophysiological research. There are however, two directions in which investigations

can proceed. The first is to culture identified neurons, which by necessity must be large enough to manipulate individually and are generally taken from invertebrates. These have the advantage that their behaviour *in vivo* is known (through intact brain studies using glass micropipette electrodes) and networks can also be partially reconstructed in culture. Such a reconstructed circuit, consisting of three identified neurons from the snail *Lymnaea stagnalis*, has recently been demonstrated and its electrical behaviour was shown to resemble that observed *in vivo* (Syed, Bulloch, and Lukowiak 1990). The main results from such studies will probably concern synaptic transmission and plasticity, but are unlikely to reveal any complex network behaviour. The second direction involves culturing smaller vertebrate neurons into 'novel' networks. There is no guarantee that these will exhibit any of the properties of *in vivo* networks, but it is probable that they will tend towards some kind of steady state behaviour (Hopfield 1982). This will offer opportunities to observe the emerging collective properties, an analogy to early development, and also how the steady state behaviour can be modified by appropriate stimuli. This latter point may provide some insight into learning processes, in addition to suggesting how it is possible for regions of the brain to alter their function, for example after serious brain damage has occurred.

In summary, dissociated neuronal cultures offer greater access and the prospect of 'designer' circuits, neither of which are available *in vivo* or in tissue culture. There exist a variety of techniques for recording electrical activity generated by these cultured cells, some of which are also applied to *in vivo* recording.

1.3.2 Recording from dissociated cell cultures

Intracellular glass microelectrode

Saline filled glass microelectrodes remain the most commonly used device for recording from dissociated neurons in culture, and have proved the most successful to date (Standen, Gray, and Whitaker 1987). The small tip diameter which can be obtained (<1μm) allows the penetration of the cell membrane (figure 1.8a) and the direct measurement of the transmembrane potential. Intracellular recordings can therefore record the full deviation in potential during an action potential, as well as subthreshold deviations such as excitatory and inhibitory post synaptic potentials. Stimulation is also possible by intracellular current injection. After penetration the cell membrane often forms a relatively tight seal around the electrode, allowing recording to continue for several hours before leakage of the cytoplasm becomes critical. On removal, the cell membrane can reseal itself and it is often possible to carry out several recording sessions on the same cell.

Despite the large signal to noise ratios obtainable with this method, intracellular penetration does not allow observation of the neuronal electrical activity over a period greater than about 48 hours, and in addition the trauma caused by penetration often results in so called 'damage' action potentials. Such uncontrollable stimuli would not allow a systematic study of a neural network to take place.

A second method of recording using glass microelectrodes of larger tip diameters is available, which does not involve rupturing the membrane. In this, the electrode is pressed against the outside of the membrane to obtain a 'loose patch clamp' (also figure 1.8a). Sometimes a slight backwards pressure is applied to increase the tightness of the seal, forming a 'tight patch clamp'. Action potentials of up to 5mV have been recorded using patch clamping, and sub-threshold changes in transmembrane potential (eg, EPSP's and IPSP's) have also been observed. Stimulation is also possible by current injection via patch

clamp electrodes. This method is ideal for the long term monitoring of cultured networks, provided sterility can be maintained in what is necessarily a semi-exposed environment. It does however suffer, in common with intracellular methods, from the difficulty of independently manipulating in excess of 3 or 4 electrodes in the same culture due to the bulky micromanipulators required.

Voltage sensitive dyes

A class of potentiometric dyes exists which when bound to the cell surface, display an optical absorption linearly dependent on the transmembrane potential (Cohen and Salzberg 1978). By mapping the cells of interest onto a planar array of photodiodes (or photomultipliers) using a specially adapted optical microscope (figure 1.8b), it is possible to observe the changes in absorption due to the firing of action potentials. The spatial resolution of this technique depends on both the size of the photodetector elements and on the magnification available with the microscope, but is unlikely to be better than 10μm. Arrays are commercially available with the use of up to 124 channel devices being successfully demonstrated for recording from intact ganglia (Grinvald et al. 1981). Similar techniques have been applied to cell culture with signal to noise ratios of up to 50 being achieved for Aplysia neurons (Parsons et al. 1989), where recordings were made from both soma and neurites. Results obtained with vertebrate neurons have proved less successful (signal to noise ratios of <2), due to the smaller surface area to which the dyes are able to bind.

Early problems were encountered with the toxicity of these dyes which tend to break down under illumination (Arvanitaki and Chalazonitis 1961)(Pooler and Oxford 1973), severely limiting the length of recording periods. Gradual improvements have now allowed continuous recording for up to 30 minutes without serious damage occurring (Parsons et al. 1989), although this time period could only be achieved by a reduction in illumination intensity and hence a reduction in the signal to noise ratio.

A second optical method has recently been suggested and demonstrated, which overcomes the problems of dye toxicity (Stepnoski et al. 1991). This relies on the phenomenon that the light (from a laser beam) scattered by a cell during excitation is increased, and can be observed by an angled detector. As with the voltage sensitive dyes this method does not possess the resolution to record from individual neurites, but may allow sites of activity around the cell to be mapped.

Modulation of MOSFET gate voltage

It is possible to construct an active extracellular recording array, where the cell lies on top of the gate of a metal oxide semiconductor field effect transistor (MOSFET). Using standard photolithographic techniques, devices and electrodes can be fabricated to single cell dimensions. Recordings rely on the extracellular potentials generated by cells overlying the gates, modulating the conductivity of a narrow strip of doped semiconductor beneath the gate insulator. One suitable configuration, shown in figure 1.7c, would be a depletion mode FET with the culture medium biassed to allow the detection of both positive and negative potentials. Evoked potentials from rat brain slices have been recorded using an array of 9 similar devices on a single substrate (Jobbling, Smith, and Wheal 1981), with signal amplitudes in excess of 1mV while noise levels remain about 50μV. The use of similar devices for recording from dissociated cell culture, based on the ion sensitive field effect transistor (ISFET), have recently been given theoretical consideration (Cambiaso et al. 1990), with predicted peak drain-source currents of several micro-amps.

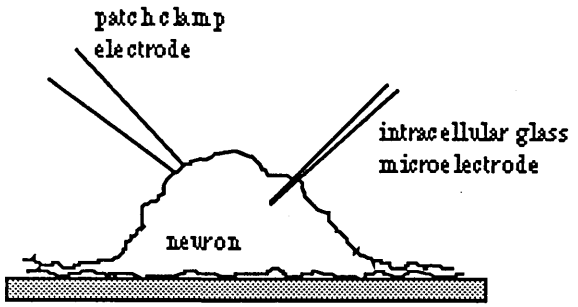

(a) Intracellular and patch clamp recording techniques

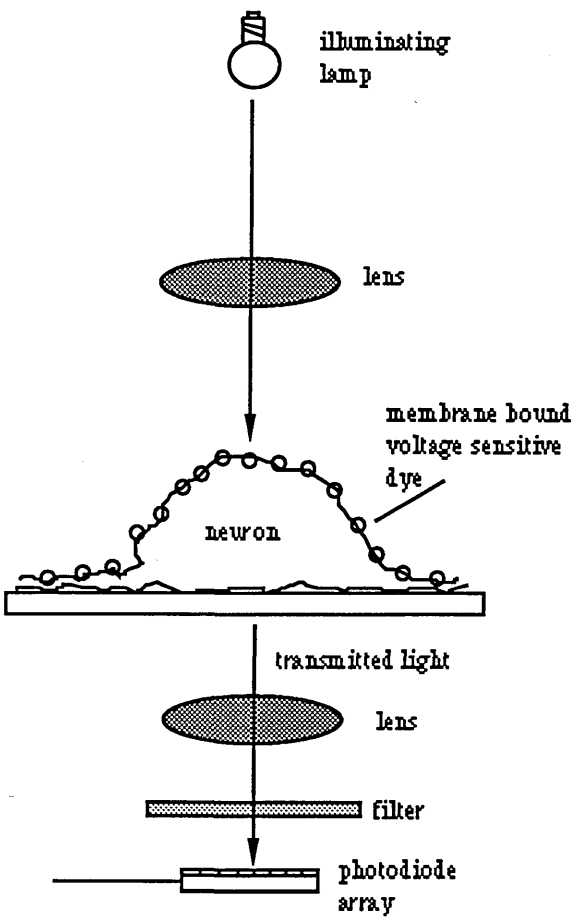

(b) Action potentials can be detected by measuring the amount of light absorbed (or refected) by a neuron, to which is bound a voltage sensitive dye.

Figure 1.8(a) and (b) Methods of recording neuronal action potentials

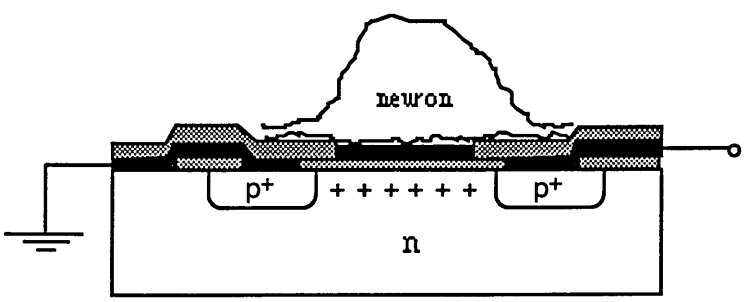

(c) Extracellular action potential modulates the conductance of the source drain channel of a depletion mode MOSFET

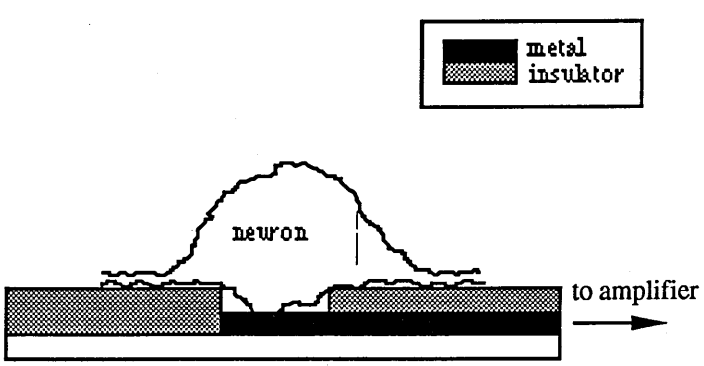

(d) Extracellular signals are picked-up by thin film metal microelectrodes

Figure 1.8(c) and (d) Methods of recording neuronal action potentials

It is believed that the use of MOSFET's will reduce noise levels below that produced by other techniques as the amplifier is so close to the recording electrode. MOSFET noise is dominated by flicker noise (McNeil, Clark, and Edell 1987) arising from the semiconductor-metal gap, having a root mean square value of

$$V_{noise} = \sqrt{\frac{K_f \Delta f}{WL\frac{\varepsilon_o \varepsilon_r}{d} f}} \qquad (1.7)$$

Given the typical values of the parameters shown in table 1.1, this would produce a rms gate-drain noise of 25μV. This noise value is somewhat higher than could be achieved with planar microelectrodes coupled to low noise amplifiers (see below), typically in the region of 5μV. It does however have the advantage that the signal is amplified at the cell itself, removing the necessity for bulky and intricate screening. Thus, whilst MOSFET devices may be capable of recording large amplitude signals from invertebrate neurons, their suitability for cultured vertebrate recordings must be questioned. Due to the isolated nature of the electrodes in these devices, extracellular stimulation of cells is not possible and would have to be carried out with additional glass microelectrodes. Fabrication is also difficult and expensive, although this could be offset by the simplification in the overall recording set-up.

Extracellular metal microelectrode arrays

The requirement for multi-site detection has also been met by utilising extracellular microelectrode arrays (figure 1.7d), fabricated using techniques required in the manufacture of semiconductor devices. That is photolithograthy, thin film deposition, and dry and wet etching. In addition to offering multiple electrodes, such devices are robust for long term use in culture (or *in vivo*), are non-invasive allowing normal cell development, and allow visual observation of both cell and network morphology.

Successful electrode arrays have differed slightly in the materials used and in their dimensions, but it

symbol	parameter	value
ε_r	dielectric constant of the gate insulator	4 for silicon dioxide
ε_o	permittivity of free space	$8.85\times10^{-12}C/Nm^2$
W	gate width	8μm
L	gate length	20μm
d	insulator depth	0.12μm
Δf	recording bandwidth	10KHz (10-10KHz)
f	centre frequency of action potential	1KHz
K_f	a process dependent parameter	$3\times10^{-24}V^2F$

Table 1.1 MOSFET parameters used to evaluate the rms noise, see equation (1.7)

is still possible to outline a generic device. The device substrate is generally either quartz or glass, onto which an array of narrow metal conductors is photolithographically defined. The next stage is to deposit an insulating layer on top of this, and to define an etch mask for exposing both the electrode recording site and the bonding pads from which connection are made to external recording equipment. After etching through the insulating layer and removing the mask, the device is bonded to a printed circuit board and the centre of the pattern isolated within a glass ring to contain the cell culture.

The resolution of the photolithographic process is determined by the wavelength of the light used, and for ultra-violet light is generally 1-2μm. This allows an electrode density in excess of 100 electrodes/mm^2 for 100μm^2 recording sites. Obviously the higher the electrode density the more visual information is lost, because cells are generally viewed with light transmitted through the substrate and the electrodes are normally opaque. The possibility of such large electrode densities offers a high probability of a cultured cell attaching on or near an electrode. It is also possible for larger cells to be individually positioned on electrodes by manipulation with micropipettes, and therefore obtaining suitable cell/electrode contact is not a serious limitation.

This type of device design and fabrication allows relatively low cost mass production to be attained, given the initial high investment in equipment. Control over all the geometrical and material parameters is possible to a far greater extent than with more conventional devices and techniques (achieving a reliable and repeatable glass microelectrode tip is notoriously difficult for example), increasing the scope for systematic design procedures.

To date only limited use has been made of multi-electrode arrays *in vitro*, due to the lack of availability of fabrication facilities to neurobiological groups. Table 1.2 details the recordings that have been made, and includes those recordings obtained from electrically active chick embryo cardiac myocytes for completeness.

The first successful recordings made using planar microelectrode arrays, were indeed obtained from a confluent layer of chick embryo cardiac myocytes (Thomas 1972). These cultures have the double advantage that recordings of extracellular action potentials can be verified by observing simultaneous mechanical contractions, and that suitable culture conditions are relatively simple. As such they are a suitable cell type to use when in the initial design stages of neuronal recording electrodes (Connolly et al. 1990), as well as for studies in their own right (Israel et al. 1984). Over the last two decades work has been extended to recording initially from intact mollusc ganglia (Gross 1979) and then to dissociated neuronal cell cultures. Both vertebrate (Pine 1980)(Gross and Lucas 1982)(Gross, Wen, and Lin 1985)(Oliver et al. 1986) and invertebrate (Tank, Cohan, and Kater 1986)(Regehr, Pine, and Rutledge 1988) neurons have been successfully cultured and monitored for periods of several weeks. These studies have generally concerned cell types that have previously proved to be successful in work concerning conventional intracellular microelectrodes, and for which culture conditions are already well defined. The variety of cell types used however, makes the comparison of the results obtained with different patterns difficult.

The success of these devices can generally be gauged in terms of the signal to noise ratio (S/N) achieved in detecting extracellular action potentials. Although simply the occurrence of an action potential

Author	Cell type	Electrode surface	Electrode surface area	Electrode impedance	Cell-electrode contact	Recorded amplitude
Thomson (1972)	chick embryo myocardial sheet	platinum black	50μm2 (groove)	0.5MΩ		0.02-0.25mV
Gross (1979)	Helix Promata intact ganglia	laser deinsulated gold	100μm2	2-4MΩ	no	3mV
Pine (1980)	rat SCG's	platinum black	80μm2	0.1-1MΩ	yes	300μV
Gross (1982)	mouse spinal chord neurons	laser deinsulated gold	100μm2	6MΩ	yes	350μV
Israel (1984)	chick embryo myocardial sheet	platinum black	225μm2	160KΩ	yes	0.5-5mV
Gross (1985/86)	mouse spinal chord neurons	electrolytically deposited gold	100μm2	500KΩ	yes	250-650μV
Oliver (1986)	cerebellar neurons				yes	200μV
Tank (1986)	Helisoma neurons		75μm2			200-700μV
Regher (1988)	Helisoma neurons	platinum black	150μm2	500KΩ	yes	400μV-2mV
Dow (1989)	Lymnaea Stagnalis neurons	platinum black	100μm2	0.1-1MΩ	yes	100-500μV

Table 1.2 Previously reported recordings from cultured cells, using microfabricated extracellular electrode arrays

could theoretically be detected with any value of S/N greater than 1, the presence of spike like noise during recording makes this insufficient in practice. In addition information is often required on the shape of the signal both in order to relate it to the transmembrane potential (first derivative, second derivative etc) and to identify which cell type it arises from.

Minimum noise levels are limited by (a) thermal noise (Johnson noise) in the electrode/biological interface due to the thermal motion of electrons, (b) by flicker noise occurring at the same interface and by (c) device noise in the amplifiers (Stremler 1982b). In addition there will always be a certain amount of electrostatic noise produced by electromagnetic radiation in the atmosphere, and of biological noise from other electrically active neurons in the vicinity. These latter two contributions can be substantially reduced by both screening the recording set up in a faraday cage, and by differentially recording from two identical neighbouring electrodes. Both the electrodes will be subject to the same electrostatic and biological noise, and hence subtracting one signal from the other should leave only the signal generated by an active cell over one electrode. Noise levels typically remain around 5-20μV, and often reach 50μV depending on the particular electrode design. Thus with the minimum noise levels relatively fixed, it is important to maximise the signal amplitudes to maximise the signal to noise ratio.

From Table 1.2 it is apparent that recordings from large invertebrate neurons produce noticeably larger signals than those from smaller vertebrate neurons. An invertebrate neuron that could be individually extracted from the ganglia would be between 25-100μm in radius, while a vertebrate neuron may be only 5-10μm in radius. A rough comparison of the signal amplitudes for each would suggest that it varies in proportion to the cell radius, as suggested by equation (1.6).

Although such simple calculations as those previously detailed seem to provide reasonable values for extracellular potentials, they ignore the effects of cell attachment to the electrode. Cell adhesion is always critically dependent on the electrode surface properties, and an inspection of the surfaces used in table 1.2 shows that only a few have proved to be successful. Most notably platinum black coated electrodes have been preferred to smooth metal electrodes. It is known that the electrolytic deposition of platinum from a solution also containing lead acetate, leads to the formation of a microrough surface coating known as platinum black. Similar effects are caused by the electrolytic deposition of gold. The increase in surface area leads to a decrease in the electrode resistance and an increase in capacitance, producing a fall in the total impedance (Geddes 1972). A similar effect occurs upon the electrolytic deposition of gold.

The explanation generally given for requiring a reduction in impedance, is that the associated electrode noise is also reduced. This noise is normally dominated by thermal noise[#] which is proportional to the square root of the real part R of the electrode impedance

$$v_{noise} = \sqrt{4KTRB} \qquad (1.8)$$

[#] Flicker noise at the electrode-electrolyte interface is negligible in comparison (≈0.2μV), given the extremely high capacitance existing across it (≈1nF). See equation (1.7)

where T is the absolute temperature and the other symbols are as given previously. As an example consider a typical gold microelectrode which has an impedance of 6MΩ, that reduces to 500KΩ after platinisation. Assuming a constant phase angle of -45°, the thermal noise before and after platinisation will be 20μV and 5.9μV respectively (with a recording bandwidth B of 10KHz). A reduction of only 16μV is not greatly significant, with the continued presence of electrostatic noise with a similar or greater amplitude. This would suggest that electrode impedance should be a relatively minor factor (certainly for invertebrate neurons), as far as the improvement in noise levels are concerned, in determining the suitability of an electrode for extracellular recording. Comparison of the electrode impedances in Table 1.2 shows the wide variations that have been successfully used.

If the limited electrode noise is not a major factor in determining signal quality, what other improvements could electroplated electrodes provide that would explain the success obtained with them? Consider an electrode with impedance Z_e connected to an amplifier with an input impedance of Z_{in}. If the potential at the solution side of the electrode is v_e, then the potential across the input terminals of the amplifier is

$$v_{amp} = v_e \left[\frac{Z_{in}}{Z_{in} + Z_e} \right] \qquad (1.9)$$

Typically the input impedance for FET amplifiers exceeds 10GΩ, but is usually reduced to about 50MΩ by the stray capacitance of connecting leads. Given this value and assuming the impedance given for an unplatinised electrode above, from (1.9), approximately 90% of the signal applied to the electrode would appear across the input of the amplifier. For the case of the platinised electrode this would increase to 99%.

A 10% improvement in the recorded signal amplitude, although worthwhile, would probably still not account for the success of electroplated electrodes. It is also worth noting that in many other ways plated, and especially platinised, electrodes are inferior to the more stable smooth electrodes. Rough surfaces are more susceptible to 'flaking' and clogging by organic material, leading to corresponding changes in their electrical properties, and the increases obtained in S/N ratios would have to be substantial to compensate for these.

It is worth considering the only recordings obtained with relatively high impedance (2-6MΩ) electrodes, fabricated by laser deinsulation of gold conductors (Gross 1979)(Gross and Lucas 1982). The signal amplitudes obtained with these are comparable to those obtained with electroplated electrodes, despite the difference in impedance. Deinsulation by laser occurs when the beam is focussed on the underlying metal causing its surface to vaporise, blowing off the insulation above it. Such an aggressive method will almost certainly result in a slight roughening of the surface through redeposition of gold and insulating material, though it may not necessarily alter greatly the impedance from that of smooth evaporated gold electrodes. It may be that the surface topography formed bears similarities to that of electroplated electrodes, and it is this feature that is a requirement for successful recordings, and not the electrical properties. The electrode surface is likely to be a critical factor in all the reported recordings from cultured cells, as all the best case recordings come from cells adhering directly onto the electrodes.

Table 1.3 compares the methods described above for recording the electrical activity of cultured neurons.

Recording method	Attribute						
	Unlimited multisite recording	Record from an enclosed culture	Electrical stimulation	Unconstrained cell placement	Induced damage	Record transmembrane potential	Maximum continuous duration
Intracellular microelectrode	No	No	Yes	Yes	Yes	Yes	<1 hour
Patch clamp electrode	No	No	Yes	Yes	No	No	a few hours
Potentiometric optical probes	Yes	Yes	No	Yes	Yes	Yes	<30 minutes
MOSFET devices	Yes	Yes	No	No	No	No	unlimited
Extracellular electrode arrays	Yes	Yes	Yes	No	No	No	unlimited

Table 1.3 The main advantages and disadvantages of the recording methods discussed above.

1.4 ADDITIONAL USES OF PLANAR METAL MICROELECTRODES

The previous discussion has concentrated on the use of planar metal microelectrodes only in recording from cultured cells. Their properties are of interest however, in a much wider range of uses and devices.

It is obvious that of all the recording techniques outlined above, the only possibilities for the comprehensive recording of signals *in vivo* are either MOSFET type devices, or extracellular electrode arrays. As has been mentioned the study of neural networks is also being carried out *in vivo*, where the latest generation of recording devices take the form of planar electrode arrays mounted on mechanically strong probes (Pickard 1979)(Drake et al. 1988). These probes have a sharpened tip which penetrates into the nervous tissue allowing recording of multi-site neuronal activity. The requirements of these extracellular electrodes are similar, though probably less severe than for those used in culture, due to the larger signals that will exist *in vivo*.

In addition to such probes, there is the parallel development of devices intended for the long term recording and stimulation of both individual neurons and of nerve fibres, with a view to replacing the function of areas of damaged nervous tissue (Edell 1986). Such multielectrode devices must possess all of the properties of those used in network analysis, but must also be stable over a period of many years and must be capable of applying chronic stimulation currents to tissue.

The availability of microfabrication technology has also allowed the miniaturisation of many previously bulky sensing devices. In the particular area of biosensors where detection relies on amperometric, conductimetric, and potentiometric measurements at an electrode/biological interface (Turner, Karube, and Wilson 1987)(Schmid 1988) this offers the opportunity for both integrating multi-analyte devices with the appropriate electronics, and of developing *in vivo* sensors. Biosensors which rely on the local conductivity changes produced by cells in their local environment have been described (Kell, 1987), in addition to those that observe bacterial growth as changes in the conductivity of the medium (Hause, Komorowski, and Gayon 1981).

1.5 THE PRESENT WORK

The work described in this thesis forms part of a larger project aimed at developing a means to study small neural networks, with a view to obtaining a greater understanding of the functioning and structure of nervous systems. This is to be achieved through the controlled growth of dissociated neurons on microstructures fabricated using integrated circuit manufacturing technology. The transducing elements which allow the multi-site recording of neuronal action potentials are based on the planar microelectrode arrays already discussed.

It is clear that to date only limited success has been achieved with such devices due both to a lack of knowledge of what it is possible to record, and to the lack a rigourous approach to electrode design. With regard to the first of these deficiencies the previous section has outlined methods of estimating extracellular fields, and has applied them to the specific cases of axons and cell bodies on a scale which is realistic when considering cultured neural networks. The equations outlined clearly demonstrate the dependence of the extracellular potential on parameters such as the transmembrane current, the transmembrane potential, and the conductivities of the intra and extra-cellular regions.

One parameter, the tightness of the cell-electrode adhesion (related to the extracellular conductivity), is considered in chapters 3 and 4. The importance of this factor is first demonstrated by means of a simple calculation, and is followed by the consideration of a practical and reliable means of quantifying its value. This method, involving the monitoring of the electrode impedance over a time period consistent with cell attachment and growth, is demonstrated with the use of certain permanent cell lines. Initially large planar electrodes which could accommodate up to 100 spread cells were used to illustrate the necessity for an adequate control, with later results being obtained with only a single cell being present on a planar microelectrode.

These studies reveal the dependence of cell-electrode electrical 'tightness' on the electrode surface, and inference can therefore be taken on the relationship between recorded extracellular potential and the electrode surface. Specifically microrough surfaces such as platinum black and plasma etched gold are shown to greatly improve electrical tightness.

Chapter 5 considers the effect of extracellular boundaries on the extracellular potential. In order to incorporate complex three dimensional boundaries, use is made of a modified finite element method nominally designed for thermal analysis. Using this method, and modelling the neuron as a simple sphere on which a uniform action potential is generated, it is shown that recessing the electrode at the base of a groove (with high depth to width ratio) in which the cell is confined can significantly increase signal amplitudes. Other electrode geometries such as replacing the groove with a pit and the use of a grounded 'screening' electrode are also analysed.

For the case of an electrode in a groove, these results are verified by the testing of a range of groove depths with both micropipette injected current and with embryonic chick myocardial cells. The use of the former confirms the trend of increasing electrode potential with increasing groove depth, as does the latter where extracellular action potentials are recorded from small cells groups with amplitudes of up to 150μV.

CHAPTER TWO

MATERIALS AND METHODS

CONTENTS

2.1 INTRODUCTION

This chapter deals with the devices and techniques with which the results detailed in the following four chapters were obtained. It starts with a description of the design and fabrication methods for the two classes of electrodes utilised, that is the multi-cell large electrode pattern and the single cell microelectrode arrays. Two impedance measurement methods are outlined, one of which allows multiple measurements without impedance limits and the other which is only capable of single channel measurements of up to 1MΩ.

Cell culture techniques are given for the cell lines and primary neuronal and myocardial cells used, along with a description of the method by which extracellular recordings were obtained. A brief description is also given of specimen preparation for electron microscopy.

2.2 FABRICATION OF LARGE ELECTRODE DEVICES

Impedance measurements were performed in two systems, the first being based on an arrangement similar to that previously described for the observation of multiple cells in culture (figure 2.1a) (Giaever and Keese 1984). This device was fabricated by the evaporation of gold through a copper mask, which was held in contact with the base of a 60mm diameter polystyrene tissue culture petri dish. The gold pattern thus produced consisted of four measurement electrodes and one large area 'return' electrode. The measurement electrodes were insulated to within a fraction of a millimetre of the tip with a glass coverslip, sealed down with wax. The area left exposed had an area of approximately 0.1mm^2. A small area at the opposite end of the electrodes was also left exposed, allowing electrical connections to be made to the electrical circuit. These connections were then sealed over with more wax. The large area electrode shown

in figure 2.1(a) was left completely exposed, with an electrical contact also being made to it. Cell cultures were maintained inside the entire petri dish.

This device was modified here (figure 2.1b) to allow the use of a control electrode in experiments, and to prevent the wire connectors from being submerged in the culture medium. As above, gold was deposited in an interlocked metal evaporation unit which had been evacuated by rotary and diffusion pumps, to a pressure of approximately 3×10^{-5}T. In this system, tungsten boats which contain the metal (gold in this case) are electrically heated, melting and then evaporating it evenly in all directions. The controllability and uniformity of the thin films produced are both excellent, with the thickness chosen to be 500Å. Bees wax was used to seal down the coverslip in this case, with the final area of the exposed measurement electrodes being typically 200×700μm. This varied somewhat (±20%), depending on the particular mask used and on the contact obtained between it and the base of the petri dish.

The central portion of the petri dish (Falcon, UK), including the four exposed electrode tips and the major portion of the return electrode, was confined within a 1cm inner diameter glass cloning ring (holding ~0.5ml). This was sealed around the edges with sylgard resin (Dow Corning, UK), and a thin track of vacuum grease (Dow Corning, UK) was laid along a diameter running between the two central measurement electrodes. By fitting a section of porous cellulose nitrate membrane (pore diameter of 0.2μm) into this track, the ring could be divided into two with two electrodes on either side. Thus cells could be confined to grow on one side only, whilst any changes occurring in the medium were common to both. No break up in the gold electrodes was observed, despite repeated and continuous use. Figure 2.2 shows a photograph of the finished dish.

Platinisation of the measurement electrodes was carried out using a standard platinising solution consisting of 1g platinum chloride, 80mg lead II chloride, in 100ml distilled water (Geddes 1972), with a constant current passed through a 100KΩ series resistor. The exact amplitude and duration of this current was varied in order to alter the surface roughness of the electrode (see section 3.3.1). Certain gold electrode patterns were exposed to an oxygen plasma, created in a Plasmatech RIE80, in order to

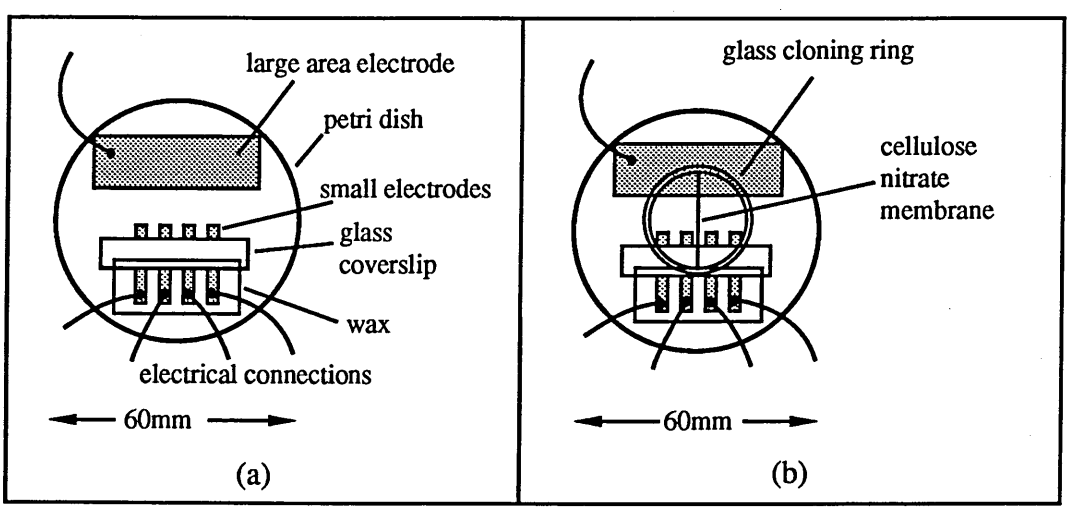

Figure 2.1 (a) Multi-electrode device designed by Giaever et al, with the entire dish being filled with solution. (b) Modification to allow the use of a control electrode, separated from the cell containing side by the cellulose nitrate membrane. In this device only the central area contains solution.

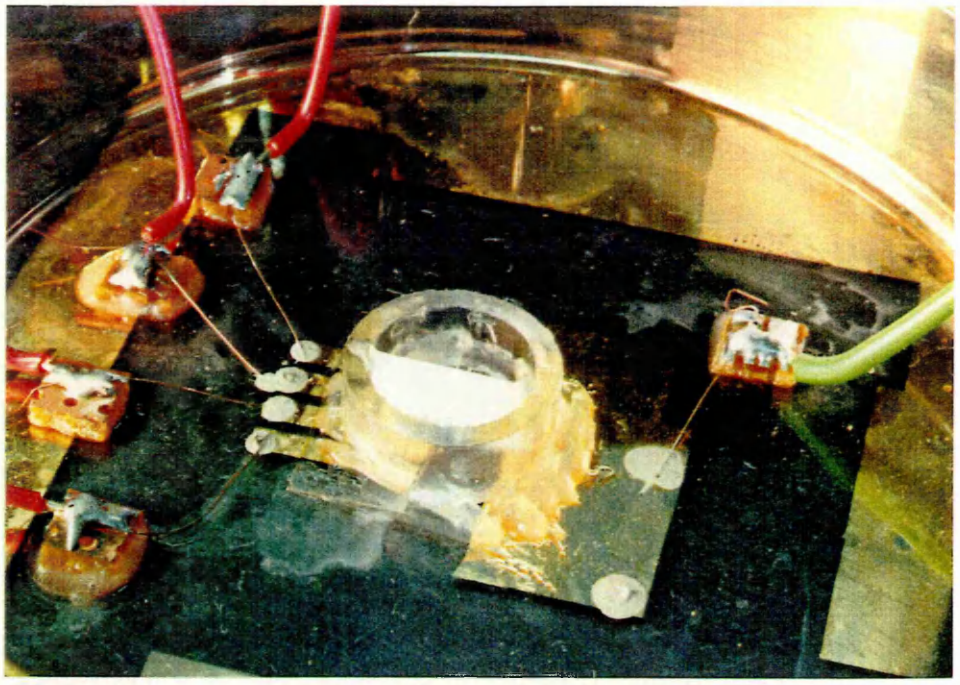

Figure 2.2 Photograph of the completed large electrode device, with two electrodes on either side of the cellulose nitrate membrane.

investigate the effect on electrode impedance and cell attachment. Again the etch conditions were varied depending on the surface requirements (again see section 3.3.1).

2.3 FABRICATION OF MICROELECTRODE DEVICES

The second type of electrode used for both impedance measurements and for the recording of electrical signal generated by cells, possessed an exposed area several orders of magnitude less than those described above. In order to make measurements on only a single cell, microelectrode arrays were fabricated with exposed measurement sites of 200μm^2 or less (Connolly et al. 1990). The resolution required for these devices precludes the use of the fabrication method described above, and instead must involve the techniques employed in the manufacture of semiconductor devices (Corporation 1979)(Zambuto 1989), which are typically of a similar or even smaller scale. Crucial stages in the fabrication process, that is sample cleaning and photolithography, were carried out in specially designated 'clean' cabinets with air filters reducing dust levels to less than 10 particles/m^3. These were themselves located within a clean room designed to reduce dust levels to 1000 particles/m^3.

2.3.1 Device design

Figure 2.3 illustrates the design of a microelectrode array consisting of 64 individual microelectrodes. The overall dimensions of the array are 19×17mm, centred on a substrate of 25×20mm. Each individual conductor had a width of 10μm, an interelectrode spacing at the centre of the pattern of 10μm, and was typically 600Å thick. The fan out was designed to allow connections to the electrodes at the large, rectangular 'bonding pads', each having dimensions of 1.0×0.2mm. Also included in the design were a large area triangular electrode (approximate area of 50mm^2), and an additional 10μm wide straight electrode. The surface of these devices was coated with an insulator of variable thickness, and a further step used to expose both the bonding pads and the electrode measurement sites.

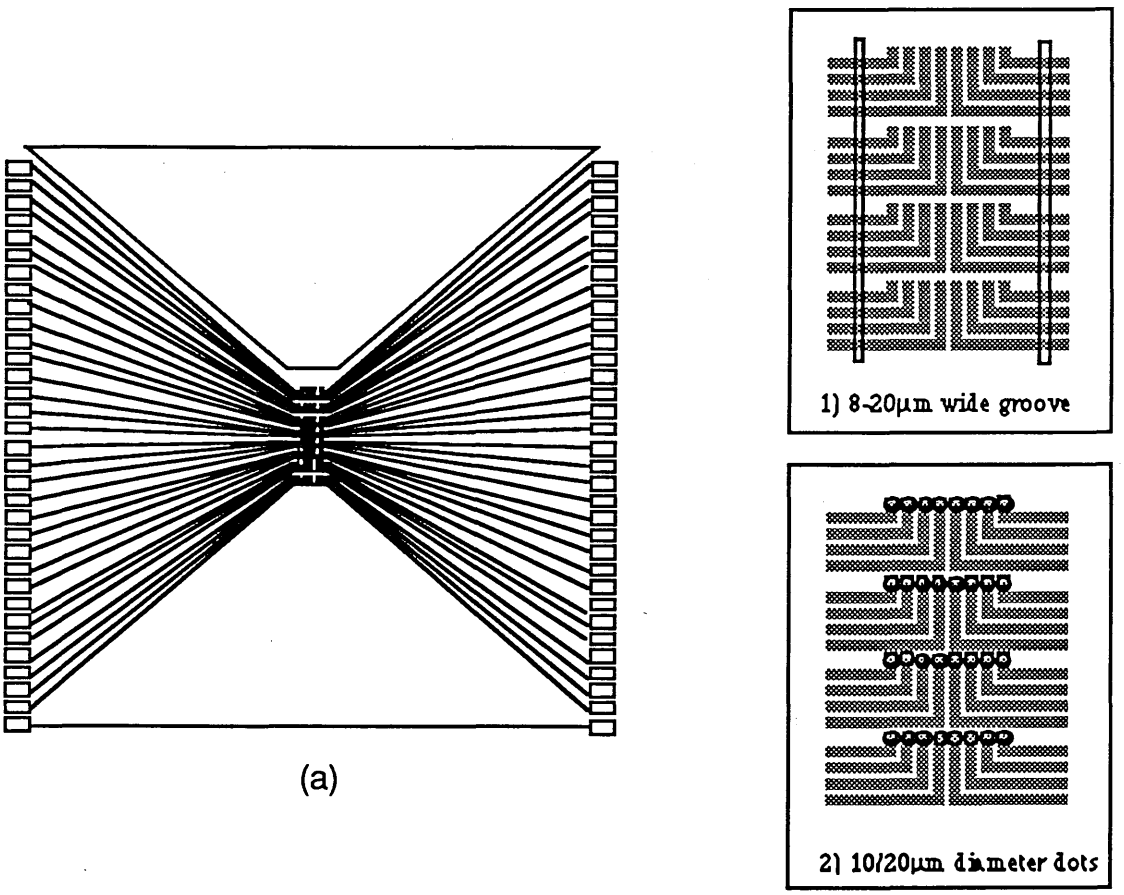

Figure 2.3 (a) Layout of the 64 microelectrode array, defined in gold on a glass substrate allowing connection to 32-way printed circuit boards on both sides. The large area triangular electrode at the top could be used as a reference electrode, whilst the straight electrode at the bottom could be used as a control (see text). (b) The two configurations used for exposing the active electrode sites through the overlying insulation.

Figure 2.3(b) shows the two variations which have been produced. The upper illustration shows the grooved pattern in which an 8-15µm wide groove running perpendicular to the electrodes, exposed sites varying in area from 80-150µm^2. The interelectrode spacing could be varied by shifting the groove outwards towards the bonding pads. The grooves extended down from the centre to expose at least one site on the straight 'control' electrode. Below this is shown an alternative design in which the tips of each conductor are exposed only by a dot of either 5 or 10µm in diameter.

Final electrode devices were mounted on a printed circuit board (PCB) with the layout illustrated in figure 2.4. The bonding pads on the patterns were connected to the corresponding PCB track by a fine gold wire, ultrasonically bonded at either end. The central portion of the device, containing the centres of the electrode, was enclosed within either a 1cm inner diameter glass cloning ring, or a 1×0.5cm glass box. This latter arrangement allowed the inclusion within the culture area of the lower control electrode, which could be exposed by the same groove used to expose the central array. The surrounding area, including the gold bonds, were then coated with sylgard in order to prevent both damage to the device and the leakage of culture medium. Although the large triangular electrode could be used as a reference electrode if the

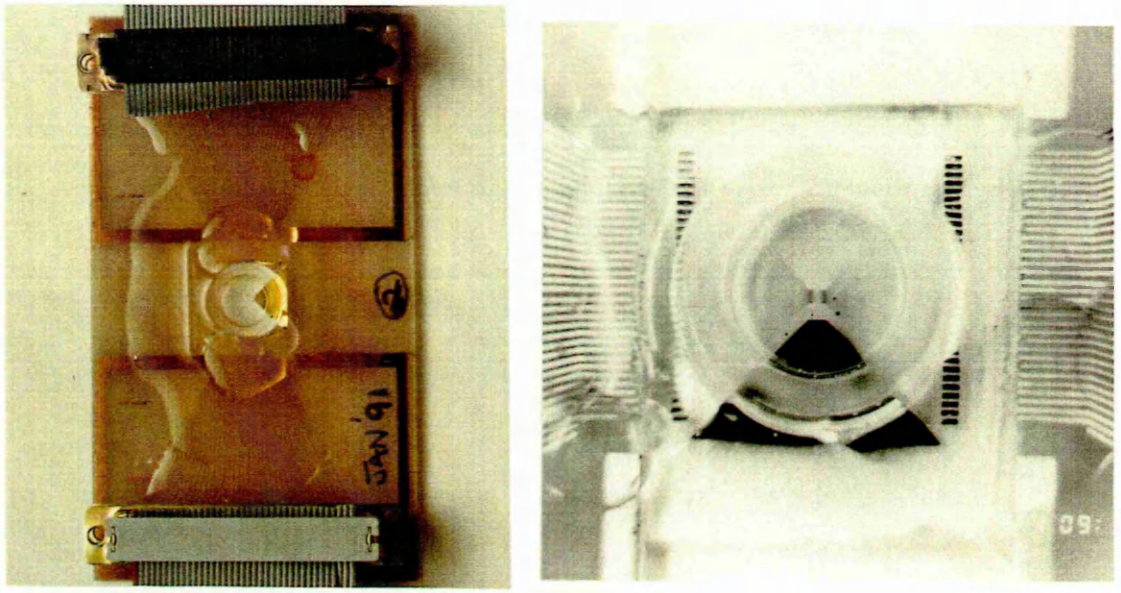

Figure 2.4 Photograph showing the final device, with the electrode pattern being connected to a PCB on either side. The centre of the pattern is confined within a glass ring into which the solutions are placed.

insulator above it was also removed, it was more common to use a platinum wire, attached to the PCB and dipped into the solution, for this purpose.

2.3.2 Fabrication procedures

Microelectrode arrays were fabricated according to the above specifications using the following procedures, which are illustrated in figure 2.5.

(1) Cleaning (figure 2.5a)

The substrate for electrode arrays was a glass microscope slide (BDH Laboratories, UK) cut into 2.5×2cm squares. These sections were thoroughly cleaned with a four step process. {I} Vigorous scrubbing with detergent and thorough rinsing in RO (reverse osmosis) water, {II} a 5 minute ultrasonic clean in first trichloroethane, {III} secondly in methanol, and {IV} finally in acetone. Samples were rinsed in RO water, blown dry with compressed air, and baked at 90°C for a period exceeding 10 minutes in order to remove any remaining moisture.

(2) Resist spinning and exposure (figure 2.5b-d)

A coating of photoresist (a photosensitive polymer, Shipley S1818), filtered through a 0.45µm pore size paper filter, was then poured onto the surface of the glass substrate which was immediately spun up to a speed of 4000rev/min for 20 seconds. This throws off the excess resist leaving a relatively even layer approximately 1µm thick. Samples were baked in a fan assisted oven at 90°C for 30 minutes in order to drive off the resist solvent.

The mask through which the electrode pattern was exposed, was manufactured (GU Dept. Electronics and Electrical Eng.) to the appropriate specifications by a process of photoreduction, the final mask bearing a negative image of the desired electrode pattern etched in a chrome film on its surface. The chrome side of the mask was brought into contact with the resist coated face of the glass sample using an automated mask aligner, and was exposed for 6 seconds to ultraviolet light. S1818 is a positive resist (with a non-toxic

solvent), which means that on exposure to UV light it becomes soluble to the appropriate developer (a weak alkali), producing a positive image of the mask. The exact exposure and development times are determined using a series of test samples. In this case, using Shipley Microposit developer, a suitable development time was found to be 75 seconds.

(3) Metalisation (figure 2.5e-f)

The developed resist pattern provided a mask through which metal could be evaporated, in order to produce the electrode pattern. This process was carried out in an interlocked metal evaporation unit by electrically heating metal filled holders, at a pressure of 3×10^{-6}T.

Gold (Au) was chosen to form the conductors, since it combines durability in a saline environment with biocompatibility and low resistivity. Gold however, will not adhere to glass on its own, peeling off almost immediately. In order to overcome this a thin coat (100Å) of nickel/chrome alloy (90%/10%) was first evaporated, as it will adhere well to glass and gold in turn will adhere to it (a suitable alternative to NiCr proved to be a layer a titanium of similar thickness). A 500Å layer of gold was then evaporated on top of the NiCr.

Soaking the devices in acetone for approximately 15 minutes, with gentle agitation, leads to the dissolution of the resist which is present under the metal layers. The metal is thus 'lifted off' everywhere, except where it is in direct contact with the glass substrate, i.e. in the exposed electrode pattern. After rinsing in RO water and blowing dry, there remained only the NiCr/Au electrode pattern on the glass surface. Due to the non-directionality of the evaporation process however, it is possible that the sidewalls of the resist mask could also become coated with metal as is illustrated in figure 2.6. This can lead to poor lift off, with the metal conductors acquiring 'tails' along their edges.

This problem could be substantially reduced by splitting the 30 minute resist bake in step (2), into two 15 minute bakes with a 15 minute chlorobenzene soak in between. The chlorobenzene is blown directly off the samples without rinsing. This additional step causes a hardening of the resist surface (Mimura 1986), and upon exposure and development produces an undercut resist profile. Evaporated metal will then lie only on the surface of the substrate and not on the sidewalls, producing well defined metal patterns. A short ultrasonication during lift off also helped in removing any remaining tails.

(4) Insulation and etching (figure 2.5g-h)

Several different types and combinations of insulating layers have been utilised depending on availability, required thickness, and durability. The preparation of these materials is detailed below. Sandwich insulators could generally be obtained simply by applying each material in turn, following the same procedures as for single layer preparation.

Silicon Nitride

Silicon nitride (Si_3N_4) was deposited by a plasma enhanced chemical vapour deposition (PECVD) process (P.D.80, Plasmatech) (Hollahan and Rosler 1978)(Reinberg 1979), using a silane-ammonia-nitrogen gas mixture. This process is carried out using essentially the same machine used to etch the

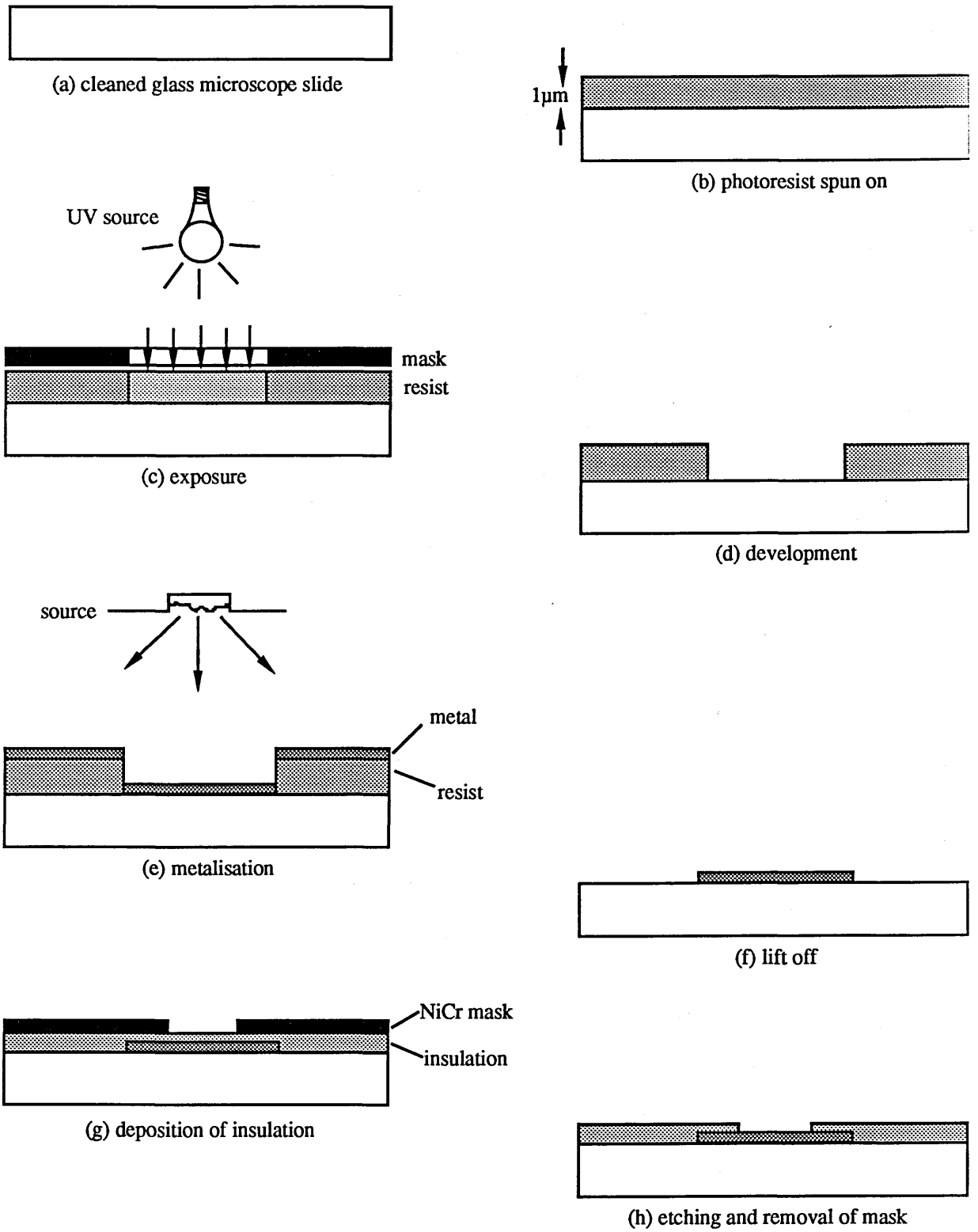

Figure 2.5 The main steps involved in the fabrication of microelectrode arrays.

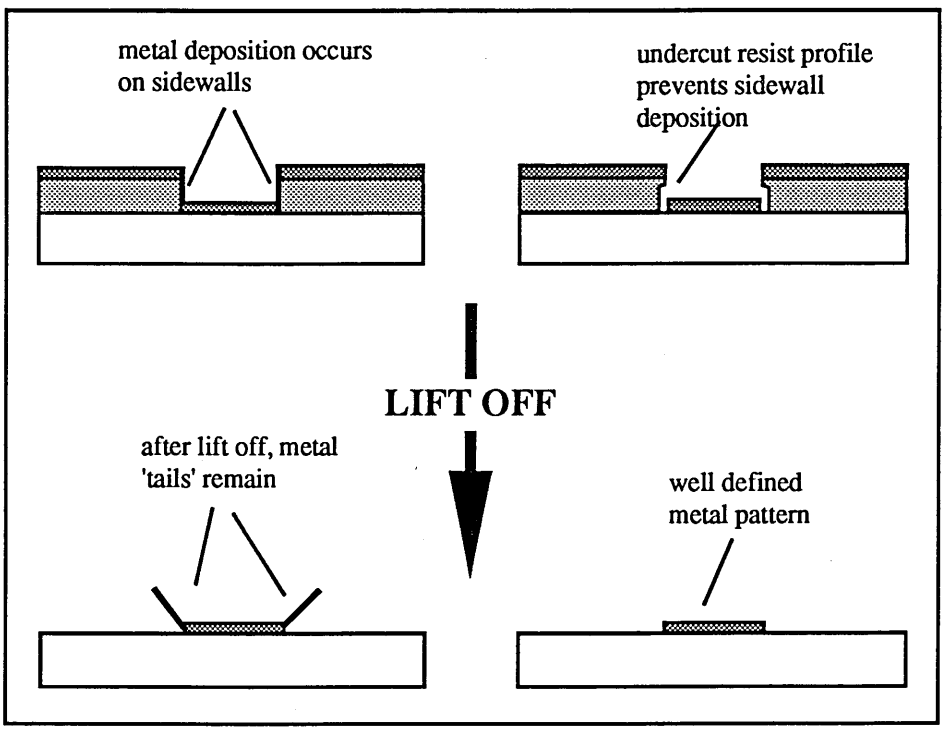

Figure 2.6 Metal deposition on the resist sidewalls can occur due to the uniform metal evaporation process, leaving metal tails after lift-off. This could be prevented by a 15 minute chlorobenzene soak in the middle of the resist bake, producing an undercut resist profile.

insulating material (see below), only with the RF power applied to the upper electrode. The deposition chamber was first evacuated to an appropriate backing pressure, and the gas mixture fed through at the required flow rate. The application of a RF field (13.6MHz) across the chamber causes the gases to ionise by high energy collisions, creating a plasma. The basic reaction occurring in the chamber is

$$3SiH_4(g) + 4NH_3(g) \rightarrow Si_3N_4(s) + 12H_2(g)$$

resulting in the uniform deposition of Si_3N_4 over the inside of the chamber. Exhaust gases are burnt off before release into the atmosphere.

The parameters which determine the film thickness are the gas flow rates, the chamber pressure, the RF power, and the deposition time. Normally the chamber pressure was held to 350mT, with gas flow rates for Si_3N4, NH_3, and N_2 set to 10, 40, and 100sccm^{-1} (standard cubic centimetres per minute) respectively. The RF power supplied was 20W (with no DC bias). Si_3N_4 forms a glossy coating on the surface of the electrode pattern, which can be up to ~3μm in thickness. Exceeding 3μm however, produced cracking in the films due to uneven stresses. The maximum deposition rate, which still produced a suitable film, was around 70Å.min^{-1}.

A further requirement of any insulating layer is that it should be possible to selectively etch through it in order to expose the active electrode sites for measurement purposes. Etching of Si_3N_4 was carried out using a reactive ion etching (RIE) process (Sugano 1985), in a RIE80 machine (Plasmatech, UK).Figure 2.7 shows a diagram of such a reactive ion etching system. This is similar to the system used for PECVD, with a RF generated plasma producing ions which will react with the exposed Si_3N_4. In this case C_2F_6 was introduced into the chamber, resulting in the generation of free radicals such as CF_3 and CF_2, which react with the Si_3N_4 to produce gaseous products, e.g.

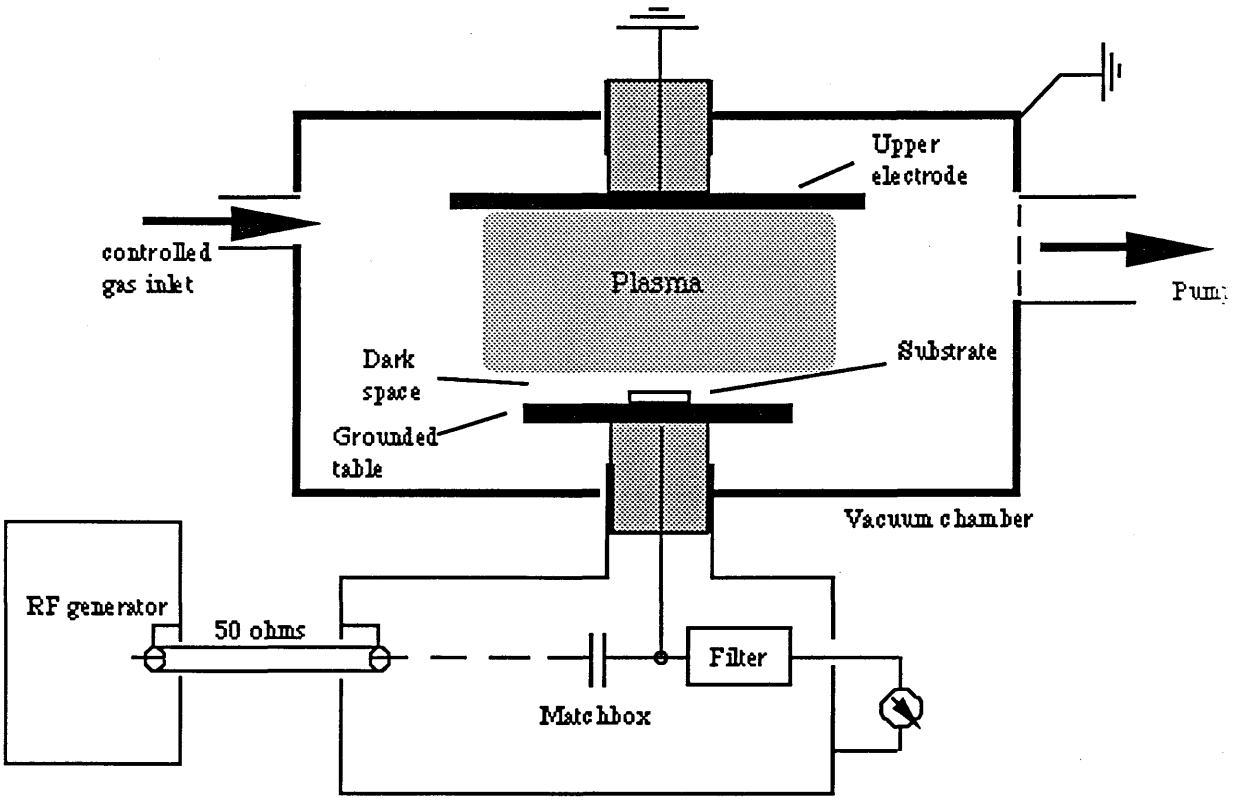

Figure 2.7 Reactive ion etching is carried out in a low pressure chamber, with a RF field applied between the lower and upper electrode plates. This creates a plasma containing ionised species which will react with the substrate to produce gaseous waste products. These ions are accelerated across the dark space to the substrate, giving anisotropic etch profiles

$$CF_x + Si_3N_4 \rightarrow SiF_y + CFN$$

On its own this chemical reaction would produce an isotropic etch characteristic as is the case with 'plasma etching'. The presence of a dc bias in the chamber however, causes the reaction to occur predominantly at the base of the unmasked area, and not at the sidewalls (a dc bias is not present during deposition, and hence this process remains isotropic). This directional etching tends to produce almost vertical sidewalls, although some slight undercutting can be observed. A gas flow rate of $20sccm^{-1}$, a chamber pressure of 16mT, and an applied RF power of 100W, produced a dc bias of 400V with an etch rate of approximately 500Å/min.

S1818 will act as a suitable etch mask for relatively thin layers of Si_3N_4, as it etches only slowly in C_2F_6. After spinning the resist onto the surface of the insulating layer, the appropriate pattern (one of the two configurations shown in figure 2.3b) was exposed using the procedure outlined above. After etching, the mask can be removed simply with a short soak in acetone.

One notable drawback of this etch process, is that as the directionality is increased so the specificity is decreased. That is to say that the kinetic energy with which the ions are endowed, tends to produce physical etching of materials other than that for which the chemical reaction is designed. Deterioration of the photoresist mask in this way was not a problem provided that it was sufficiently thick, but damage to the

electrodes could occur given the difficulty in judging precisely when all the Si_3N_4 has been removed. Gold, being a relatively soft metal tends to be rapidly etched, and hence care must be taken in determining the etch time.

It is possible to deposit a further layer of NiCr on top of the gold whilst depositing the electrode pattern. This can be removed with a wet etch once the reactive ion etch has removed all of the exposed insulator, thus preventing damage to the underlying gold. It was found however, that this caused a bubbling of the metal pattern to occur during the high temperature (300°C) deposition of the Si_3N_4, and lead to the break up of the insulation layer. Consequently the accurate determination of the etch time was preferred as a method of preventing etch damage to the gold electrodes.

Before the mask was removed, it was necessary to verify that the metal electrodes had been fully exposed. Variations in the thickness of the insulation meant that it was not always possible to time the etch exactly, and samples had to be removed from the chamber and examined under a microscope. When observed under a reflection microscope fitted with Nimarsky differential phase contrast, electrodes with a remaining residue of insulating material covering them appeared patchy, with colour variations over the surface. Completely clear electrodes however, appear to be a uniform colour. It was also possible to check the resistance across the bonding pads using a Hewlett Packard semiconductor parameter analyser (model 4145A). Two fine tungsten probes were rested on the surface of a bonding pad, and a low resistivity (<30Ω) between them was taken as an indication that the insulator had been completely removed. Unfortunately, the tip diameter and the sensitivity of the micromanipulators did not allow the exposed electrodes to be similarly tested.

Polyimide

The basic PIQ-4200 polyimide (Hitachi, FRG), which is marketed as a highly moisture resistant insulating varnish, was used to produce insulating layers of 3-6μm in thickness. The procedure for depositing this insulator was as follows (Hitachi product data sheet).

(1) Samples were first heated to a temperature of 250°C to drive off residual moisture.

(2) An adhesion promoter (Hitachi, FRG) was then spun on to improve the adhesion of the polyimide. The spinner speed was 2000rev/min for 40 seconds. Samples were baked at 250°C for 30 minutes. This is believed to deposit a fine layer of aluminium oxide on the substrate, to which the polyimide will attach strongly.

(3) The surface was then coated with a layer of PIQ-4200 (pre-warmed up to room temperature) and the samples spun at 1500-2500rev/min for 40 seconds. They were then baked at 100°C for 1 hour, 200°C for 30 minutes, and finally 350°C for 1 hour, so that the material was completely imidised.

(4) Oxygen plasmas are suitable for the rapid etching of most organic polymers including polyimide. No simple reaction can be written which describes completely the mechanisms producing the etch, but two possibilities are

$$2(n+1)C + O_2+ + nO_2 \rightarrow 2(n+1)CO$$

$$(m+1)C + O_2+ + mO_2 \rightarrow (m+1)CO_2$$

Obviously many other reactions are occurring involving the molecules, atoms, and ions in the plasma, and the carbon and other materials in the polymer. The etch conditions using the plasmatech RIE80

were as follows: a flow rate of 20sccm^{-1}, a chamber pressure of 13mT, and an applied RF power of 100W. This produced a dc bias of 390V and an etch rate of 280Å/min.

(5) It is obvious that photoresist on its own will not provide a suitable etch mask for use in an oxygen RIE, as it will itself be rapidly etched being an organic polymer. A more suitable mask was produced by the evaporation of a layer of NiCr on top of the polyimide, which could be patterned photolithographically with the desired etch pattern. NiCr was observed to be sputter removed at the rate of approximately 10Å.min^{-1} in an oxygen plasma (the exact rate depending on the etch conditions), and hence 500Å was an appropriate mask thickness for polyimide films which were less than 14μm thick. After completion of the polyimide etch, the remaining NiCr mask was removed by a wet etch in a 4:1 solution of HCl and water.

Later devices required a thicker insulating layer (5-20μm), which was provided by a slightly different type of polyimide, PIQ-6700 (Hitachi, FRG). This procedure differed in points (3), (4), and (5) above. These were amended as follows:

(3) The experimentally obtained film thickness against spinner speed is shown in figure 2.8, after coated samples were put through a three stage baking process, each stage lasting 60 minutes. The first at 150°C, the second at 200°C, and the third at 350°C. Spinner speeds below 1500rpm however, lead to films which appeared charred and blackened, and which were useless for observing cell cultures on. In order to produce films in excess of 10μm therefore, it was necessary to build up multiple layers of polyimide, with each layer requiring the complete baking process. The devices required to date have used a maximum of two layers of PIQ-6700.

(4) Due to the thickness of these films, etching with the RIE80 would have required an inordinately long time and would have lead to severe damage of the etch mask. A suitable alternative was provided by an electron-cyclotron resonance reactive ion etcher (ECR, Plasmatech, UK), which was capable of increasing the etch rate by a factor four. This machine uses a microwave power source to generate the plasma, with the RF power extracting it into the sample chamber and creating the dark space above the sample itself. This leads to a higher ion flux towards the surface for a given RF power (relative to the

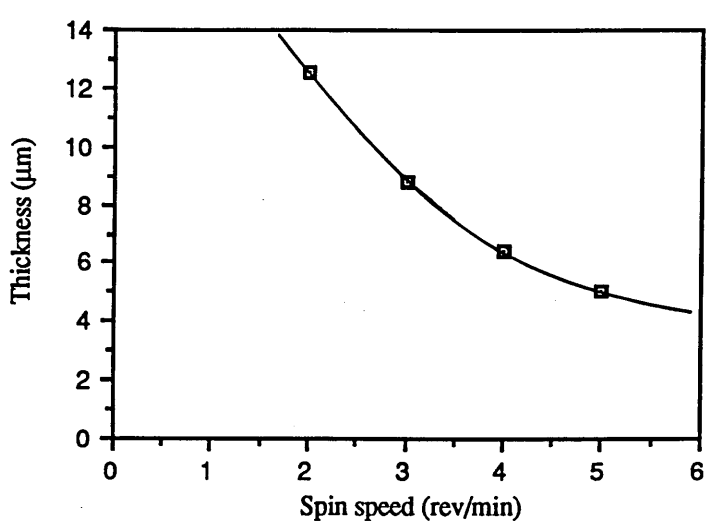

Figure 2.8 The thickness of Hitachi PIQ-6700 polyimide insulating varnish produced at a variety of spin speeds. The values shown are those obtained after the films have been baked as described in the text.

RIE system outlined above), with a consequently lower dc bias. A faster etch rate is thus achieved in addition to a lessening of the mask damage. The etch parameters consisted of an oxygen flow rate of 30sccm^{-1}, microwave power of 298W, RF power of 100W, producing a dc bias of only 222V and an etch rate of 0.32μm.min^{-1}.

(5) It was found necessary to replace the NiCr with aluminium (Al) as the mask material, in order to ensure that it survived the etch intact. A tough layer of aluminium oxide forms on the surface of the aluminium extending the lifetime of the mask. Approximate thicknesses of 0.2μm were used. This was then patterned photolithographically, using a wet etch consisting of 80% orthophosphoric acid, 5% nitric acid, and 15% water.

2.4 IMPEDANCE MEASUREMENTS

Impedance measurements were made using two different systems. The first enabled measurements to be made in the range 0-10MΩ, whilst the range of the second was 0-1MΩ.

2.4.1 Voltage division method

For experiments requiring the simultaneous monitoring of both an active cell bearing electrode and a control electrode, or for the measurement of impedances in excess of 1MΩ, a voltage division method was used. This involved the measurement of the potential dropped across the electrode by the passage of a constant current. Figure 2.9 illustrates diagrammatically the circuit used for monitoring electrode impedance in the case of the large electrode dish described in section 2.1, where it is desired to observe the impedance of one electrode on either side of the cellulose nitrate membrane.

The impedance presented by the dish consists of the summation of the small electrode/electrolyte interface impedance, the resistance through the culture medium, and the impedance of the large return electrode/electrolyte interface (for theory of electrode double layer, see section 3.2.1). As electrode impedance is proportional to area, that of the small electrode would be more than 100 times that of the large electrode. Also given that the resistivity of the medium is negligible in comparison (~500Ωcm), a measurement of the impedance between both large and small electrodes provided an approximate measure of only the small electrode impedance. Measured changes in impedance therefore, effectively reflected only changes occurring at the small electrode interface.

Considering figure 2.9, a 100mv, 1KHz electric field was applied across each arm of the measurement circuit, which consisted of a resistor R_s, in series with the electrodes. If the value of the resistor is significantly greater than the magnitude of the impedance of the electrode, then the current through each arm will be approximately $0.1/R_s$, and will remain constant despite relatively small variations in electrode impedance. The magnitude of this impedance could be determined from a measurement of the potential drop across the electrode, and is given by,

$$|Z| = R_s / \sqrt{\left(\frac{|v_{in}|}{|v_o|}\right)^2 - 2\left(\frac{|v_{in}|}{|v_o|}\right)\cos\phi + 1} \qquad (2.1)$$

where v_{in} is the amplitude of the 100mv, 1KHz input signal, v_o is the amplitude of the potential drop across the electrode and ϕ is its phase angle. Since v_{in} was typically 10 times larger than v_o, the second

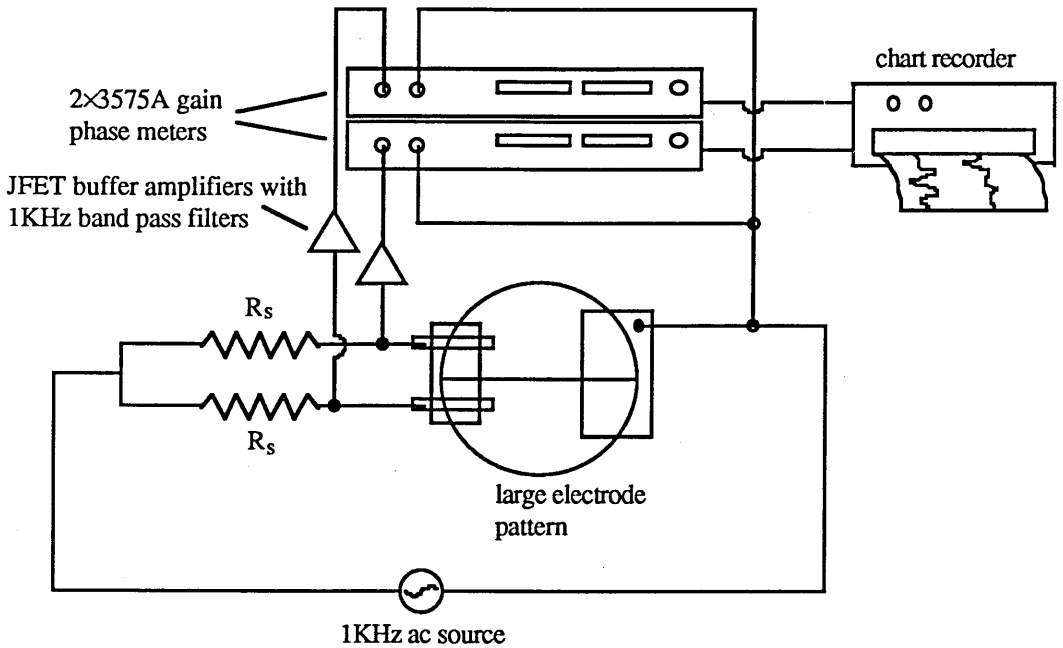

Figure 2.9 Two channel impedance measurements could be made by measuring the voltage drop across the electrodes when a known current was driven through them. This current was maintained at a constant level by choosing a value of series resistor R_s much greater than the electrode impedance.

and third terms in the denominator can, to a first approximation, be neglected and (2.1) simply reduces to

$$|Z| = R_s \frac{v_o}{v_{in}} \qquad (2.2)$$

Typically R_s was chosen so as to be at least a factor of five greater than the electrode impedance. In the case of low frequency measurements on microelectrodes, where the impedance could exceed 30MΩ, this was not practical, and equation (2.1) had to be determined in its full form in order to evaluate the impedance correctly.

The potential drop across the electrodes (v_o) was measured using two Hewlett Packard gain-phase meters (model-3575A) with an input impedance of 1MΩ at 1KHz, and with output to a multipen chart recorder. It should be noted that v_o is actually the voltage drop across the electrodes in parallel with the input impedance of the gain-phase meters, and would lead to erroneous measurements unless a ratio of greater than say 10:1 was maintained between them. That is to say that if the electrode impedance exceeded 100KΩ, then the measured potential drop would not provide a true value of the electrode impedance. For the larger electrodes (except when making low frequency measurements), whose impedance did not exceed 20KΩ, this did not present a problem. For microelectrodes however, which often had impedances well in excess of 1MΩ, it was necessary to increase the input impedance of the gain phase meters to a suitable value, by introducing unity gain buffer amplifiers at their inputs. These were based on JFET (352) op amps, and are shown in figure 2.9. Although the specified input impedance of such a buffer amplifier is in the GΩ range, the stray capacitance of the input leads and between the tracks on which it was mounted reduced this to only a few MΩ unless care was taken. By soldering inputs directly onto the appropriate legs of the JFET op amp, and by reducing the lengths of connecting leads to only a few centimetres it was possible to maintain the input impedance above 50MΩ, allowing impedance measurements of up to 5MΩ to be made.

A serious problem with noise also occurred when attempting to make high impedance measurements with very low currents (required in order to maintain current densities within the linear region characterised in figures 3.14 and 3.15), and it was found necessary to incorporate a band pass filter into the buffer amp in front of the gain phase meters. This was designed to have a centre frequency of 1KHz and a bandwidth of less than 100Hz, and reduced noise levels sufficiently to allow the full range of impedance measurements up to 5MΩ with currents as low as 5nA.

2.4.2 Automatic impedance measurements

Continuous impedance measurements of up to 1MΩ on a single electrode were made using a Hewlett Packard impedance analyser (model 4192A). This allowed direct measurements for samples connected across its input terminals, over a frequency range of 5Hz-13MHz. A fixed potential was applied across the electrodes, not the constant current used above, and was variable between 5mV and 1V, with automatic filtering and capacitive compensation provided.

A measured impedance could be displayed either in terms of its magnitude and phase angle, or in terms of its resistive and capacitive components. The resistive and capacitive components could in turn represent either the series or the parallel equivalent circuit. These three possible configurations are shown below in table 2.1. It is clear that the series and parallel representations are completely interchangeable, and by equating the real and imaginary parts of both,

$$R_s = \frac{R_p}{1+(\omega C_p R_p)^2} \qquad (2.3) \qquad \frac{1}{(\omega C_s)} = \frac{\omega C_p R_p^2}{1+(\omega C_p R_p)^2} \qquad (2.4)$$

Although the series or parallel representation of electrode impedance is arbitrary, it is often of intuitive value to select one in preference to the other. In general the results described in later chapters rely strongly

Lumped	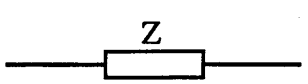	$Z= \lvert Z \rvert \angle\phi$
Series	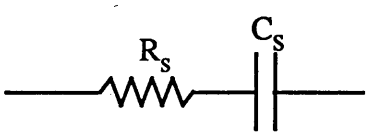	$Z=R_s-j(1/\omega C_s)$
Parallel	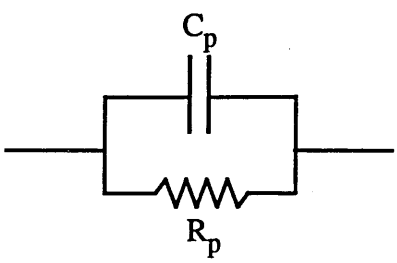	$Z= \frac{R_p}{1+(\omega C_p R_p)^2} - j \frac{\omega C_p R_p^2}{1+(\omega C_p R_p)^2}$

Table 2.1 The complex electrode interface impedance can be represented in terms of either its series or parallel equivalent circuit.

on the series representation, as this better demonstrates the additive nature of cell attachment to an electrode.

2.5 CELL CULTURE

2.5.1 Device preparation for cell culture

Between experiments devices were thoroughly cleaned to remove both debris and attached organic matter. This involved first detaching any remaining cells with a trypsin/versene mixture as detailed below. This process will also remove most of the adsorbed proteins. Samples were then soaked in a weak detergent solution for a short time to remove fragments of the lipid membrane, and were then rinsed thoroughly with de-ionised water. Prior to further use, the samples were thoroughly sterilised in a 70% ethanol solution. In the case of devices used for primary cell cultures it was generally necessary to pre-coat surfaces with adhesion proteins. The full details of these treatments are given below, in the appropriate sections.

Several cultured cell types have been used in this work, and the culture conditions are outlined below. First, details of the two cell lines used are given, followed by those for primary cell types including the dissection procedures.

2.5.2 Baby Hamster Kidney

The Baby Hamster Kidney (BHK-C13) cell line is a permanent fibroblast cell line, which forms a confluent monolayer in culture. Cell lines are effectively immortal, being able to divide indefinitely, and their use eliminates the need for animal dissection. This ease of availability is accompanied by relatively simple culture conditions and by the ease with which sterility can be maintained.

Cells were cultured (Clark et al. 1987) in Hepes-buffered Glasgow-modified Minimum Essential Medium (GMEM, Gibco, UK) supplemented with 10% calf serum, 10% tryptose phosphate broth, 3mM glutamate, 100 unit ml^{-1} penicillin, 100µg ml^{-1} streptomycin, and 2.5µg ml^{-1} amphotericin-B (this medium is commonly called HECT-Hepes Eagle Calf serum Tryptose phosphate). Stocks were maintained in tissue culture flasks, and cell suspensions obtained by the detachment of the cells with 0.05% trypsin in 0.2 mg ml^{-1} EDTA at 37°C for 5 minutes. Trypsinisation was stopped by the addition of growth medium and the cells washed by centrifugation and resuspension in growth medium at the required innoculum density.

In order to view these cells on surfaces which neither reflected nor transmitted significant amounts of light, it was first necessary to stain the cells with a fluorescent dye. This procedure involved the use of the live/dead viability/toxicity assay (Molecular Probes Inc, USA), which relies on the enzymatic hydolysis of calcein-AM (by intracellular esterase) to calcein, which is highly fluorescent. A stock solution of 5mM calcein-AM in dry dimethyl sulphoxide (DMSO), was used to prepare a working solution of 0.5µM calcein-AM in tissue culture grade phosphate buffered saline (PBS). After rinsing the medium off the cell cultures with several washes in PBS, the working solution was added and the cultures incubated at 37°C for 10 minutes. Following this the solution was poured off, and stained cells were then observed using the Nikon microphot microscope with a fluorescent lamp attachment.

2.5.3 Madden-Derby Canine Kidney

The Madden-Derby Canine Kidney (MDCK) cell line (McRoberts, Taub, and Saier 1981) is also a permanent cell line, but of the epithelial type. Cells were maintained in a basic growth medium (Clark et al. 1990) of Dulbeccos-modification of Eagles Minimum Essential Medium supplemented with 10% foetal calf serum, 10% tryptose phosphate broth, 20mM Hepes, and the amounts of glutamine and antibiotics outlined above. Cultures were maintained in the laboratory and prepared for use in a similar manner to that described for the BHK cells. Due to the tight nature of the intercellular junctions in MDCK monolayers however, detachment of cells takes considerably longer (up to 30 minutes). The action of the trypsin was stopped by centrifugation and resuspension in growth medium.

2.5.4 *Lymnaea stagnalis*

The *Lymnaea stagnalis* snails (Blades Biological, UK), a pond mollusc, were maintained in a freshwater tank kept at room temperature. Fed on a diet of lettuce they attained a weight of 2-3g before use. Cell culture medium (Wong, Martel, and Kater 1983) consisted of 50% L-15 medium, 50% snail salts[#], supplemented with glutamine and antibiotics. In order to obtain neurite outgrowth it was normally necessary to incubate the medium with one brain per ml for at least 48 hours. This ensured the presence of the necessary growth factors in the culture medium.

Before dissection, the shell was removed using fine scissors and the snails soaked in a 20% solution of ethanol in order to sterilise the exterior. After rinsing in hepes saline snails were pinned out on a sylgard coated dish containing culture medium, and an incision made from the top to the bottom of the manifold. This allowed the gut to be exposed, around which is located the brain. By cutting both the gut where it exits at the rear of the brain and nerve fibres holding the brain in place, the brain could be removed along with the buccal ganglia which are located approximately 1mm in front of it.

The brain and buccal ganglia were then pinned out with fine dissection pins in a second sylgard (Dow Corning, US) coated dish, and covered with pronase-E (Sigma, UK) made up to $1mg.ml^{-1}$ in culture medium. This enzyme treatment partially digests the ganglionic sheaths containing the neurons and the connective tissue between them. If the treatment was too long then cells tended to rupture on removal, and if it was too short they tended not to come out cleanly and did not attach to the culture dish. The optimum time was found to be about 1 hour at room temperature. The action of the enzyme was stopped by rinsing with medium containing 3% foetal calf serum, and replacing this with non-serum containing medium. Under a low power dissection microscope (×10) it was possible to isolate individual neurons from the ganglion, using fine tungsten needles with a tip diameter of 10μm. Glass micropipettes with a tip diameter slightly larger than the selected cell were then used to suck up the cell, and transfer it to the electrode pattern. All viable cells attached almost instantaneously, although it is not true that all attached cells remained viable.

Lymnaea neurons have only been cultured on the 64 electrode array patterns having a polyimide surface. Results suggest that the best preparation of this surface is to briefly expose it to a butane gas

---

[#] Snail salts were made up with; 40mM NaCl, 17mM KCl, 41mM $CaCl_2$, 15mM $MgCl_2$, 50mM Hepes, to pH 7.3.

flame for 1-2 seconds. This has the effect of creating additional surface charge and making the surface hydrophilic (Lucas, Czisny, and Gross 1986). Patterns were then covered in concanavalin-A (Sigma, UK) made up to 2mg.ml^{-1} in distilled water, and incubated at 37°C for a minimum period of 1 hour. This was rinsed off with distilled water followed by culture medium. After measurements had been made, cells were removed by rinsing with distilled water, and the patterns prepared for further use with a brief soak in detergent followed by sterilisation in ethanol.

2.5.5 Chick embryo cardiac myocytes

Cardiac myocytes were obtained from 6-10 day old chick embryos by the following procedure (Fange, Persson, and Thesleff 1956).

The embryos were removed from the eggs under sterile conditions and placed in a petri dish filled with Hanks-Hepes saline. After easing away the surface tissue, fine forceps were used to remove the heart, which lies on the left side of the chest (in the younger embryos this organ is more exposed, with a lack of significant surface tissue). The hearts thus obtained were then placed in a second dish containing fresh Hanks-Hepes saline.

After obtaining as many hearts as required (approximately 5 hearts were required to completely cover a 1cm^2 area), the majority of the saline was removed from the dish, and the hearts cut into fine pieces with dissecting scissors. This suspension was then added to a universal container and 3ml of 0.05% trypsin in 0.2 mg ml^{-1} EDTA was added. This was then aggressively triturated with a fine pasteur pipette and incubated at 37°C for 7 minutes. During this period the heavier fragments settle at the bottom whilst the smaller fragments and single cells remain in suspension. The supernatant was removed after this period and added to a universal containing 5ml of 199 growth medium (see below) and 5ml of Hanks-Hepes saline. This process of trituration, trypsinisation, and removal of the supernatant, was repeated for between 3 and 5 times, until all the fragments had been broken down. The suspension was centrifuged at 2000revs/min for 5 minutes, and the pellet of cells resuspended in fresh medium. Any remaining fragments were further broken down by forcing the solution through a fine sterile hypodermic needle.

The growth medium for this cell type was 199 medium made up as follows. 113ml of Eagles sterile water supplemented with 0.4ml ×10 199 concentrate (Gibco, UK), 10ml foetal calf serum, 10ml chick embryo extract, 100 unit ml^{-1} penicillin, 100µg ml^{-1} streptomycin, and 2.5µg ml^{-1} amphotericin-B. 17.2ml of a low potassium salt solution was also added. This was prepared as a 5× concentrate, made up as follows; 6.7g NaCl, 0.16g NaH_2PO_4, 0.09g KCl, 2.2g $NaHCO_3$, 0.9g glucose. These were dissolved in 190mls of distilled water, and the pH lowered to 5.5 by the addition of a few millilitres of concentrated HCl. 0.184g of $MgCl_2$ and 0.12g $CaCl_2.2H_2O$ were dissolved separately in 10ml of distilled water. These two solutions were then added together whilst stirring. This was diluted by a factor of five before addition to the 199 medium, with the final pH being brought up to physiological pH (indicated by the cherry red colour of the indicator contained in the 199 concentrate) by adding a small volume of sodium bicarbonate.

At this stage the remaining suspension contained a number of cell types, but with myocytes and fibroblasts making up the vast majority. In order to remove the fibroblasts, a differential adhesion was carried out which involved placing the cell suspension in a culture flask (gassed with a 5%CO_2/95%air mixture) and incubating at 37°C for 1 hour. This time period was insufficient to allow the myocytes to

attach but allowed the majority of the fibroblasts to attach and spread. The solution could then be removed and contained a relatively pure suspension of cardiac myocytes. Such suspensions could be kept in a refrigerator for several hours before application to the electrode patterns.

Electrode patterns were prepared for cell culture by sterilisation with ethanol, followed by incubation at 37°C with poly-l-lysine (made up as 1ml in 25ml of hepes saline) for 1 hour. This was rinsed off with Hanks-Hepes saline before the introduction of the cell suspension. Cultures were sealed in an air tight box, filled with 5%CO_2/95%air mixture, and incubated at 37°C.

2.6 SAMPLE PREPARATION FOR SEM EXAMINATION

In the course of this work it proved necessary to carry out scanning electron microscopy on a variety of devices and surfaces. The substrates involved, either glass or polystyrene, are prone to a build up of surface charge during examination unless they are first coated with a thin conducting layer. As such all specimens were coated with a thin layer of gold palladium (approximately 100Å thick) immediately prior to examination. This process was carried out in an Emscope SC500 sputter coating unit.

In order to view cells on patterned substrata, these were first fixed in 2.5% gluteraldehyde in phosphate-buffered saline (PBS) at 37°C for 15 minutes, and were then stored at 4°C for 12 hours. After rinsing in PBS samples were postfixed in 1% osmium tetroxide in distilled water for 1 hour, and subsequently rinsed in PBS. The samples were then rapidly quenched in liquid nitrogen-cooled liquid propane and were placed in a pre-cooled stage of a modified high vacuum coating unit (Edwards High Vacuum, UK) which was held at -80°C and at 10^{-6}Torr for 16 hours. Re-warming was at a rate of $10°C.hour^{-1}$ to 25°C after which the samples were sputter coated with gold palladium as described above.

2.7 SURFACE PROFILOMETRY

In addition to the examination of electrode surfaces by scanning electron microscopy, roughness could be directly quantified with the use of a Tallystep profilometer (Rank Hobson-Taylor, UK). This device detects the movement of a fine tipped stylus (by the inductive motion through a coil) which is tracked across the sample surface, and is capable of measuring vertical depths to a practical resolution of approximately 10nm. The maximum vertical deviation which can be measured is 10μm. Results of single track scans were recorded on chart recorder paper.

2.8 CURRENT INJECTION VIA GLASS MICROPIPETTES

In order to simulate a cell action potential using injected current, glass micropipettes with tip diameters of <2μm were produced using a standard microelectrode 'puller'. A glass tube of diameter 1.2mm with a fine inner capillary tube, is held fixed at one end with the other being held in a clamp which can be withdrawn at a controlled rate. The central portion of the tube passes through an electrically heated wire coil. As this section begins to melt, the clamped end is pulled slowly out until the diameter of the central section is sufficiently fine. A final sharp pull breaks the tube in two leaving two symmetrical microelectrodes with tapered tips. This process is completely automated with the parameters pre-set. In order to reduce the tip impedance however, the tip diameters were increased to between 3 and 5μm by

breaking off the ends under a microscope. Unfortunately this meant that it was impossible to produce identical tips to allow experiments to be repeated exactly. Electrodes are then filled to within a millimetre or so of the tip with 3M potassium chloride (KCl) solution, using a fine syringe. The final length to the tip is filled by capilliary flow along the inner tube.

Completed electrodes were inserted into a holder, also filled with 3M KCl, inside which a silver chlorided wire was mounted. One end of the wire protruded from the holder, to allow connection of the current source. Using a micromanipulator with freedom of movement in all directions, micropipettes were lowered onto the electrode until contact was made. They were then raised by approximately 0.5μm. In all measurements the electrode devices were covered with hepes saline, with the reference electrode being a length of platinum wire dipped into the solution.

In order to record the potential of the metal microelectrode, the appropriate pin on the 32-way connector was connected to a Gould Univeral amplifier via a Gould pre-amplifier. In addition a 1KHz band pass filter was used to reduce the noise further. Noise remained a problem however, given the proximity of the supply leads and the micropipette to the metal microelectrode and its connectors, and could be reduced to only around 10μV. Initial measurements were made using electrodes at the base of an 8μm wide groove with a depth of either 0.4μm, 14μm, or 28μm.

2.9 RECORDING OF CELL ACTION POTENTIALS

The action potential recordings detailed in chapter 6 were recorded extracellularly from embryonic chick cardiac myocytes, cultured on a variety of microelectrode arrays. Devices were removed from the incubator and immediately placed on the stage of a high power inverted microscope. This allowed the simultaneous observation of cell contractions and the recording of extracellular action potentials. Recording was carried out using a Neurolog amplifier and filter system, together with an extracellular preamplifier. A maximum

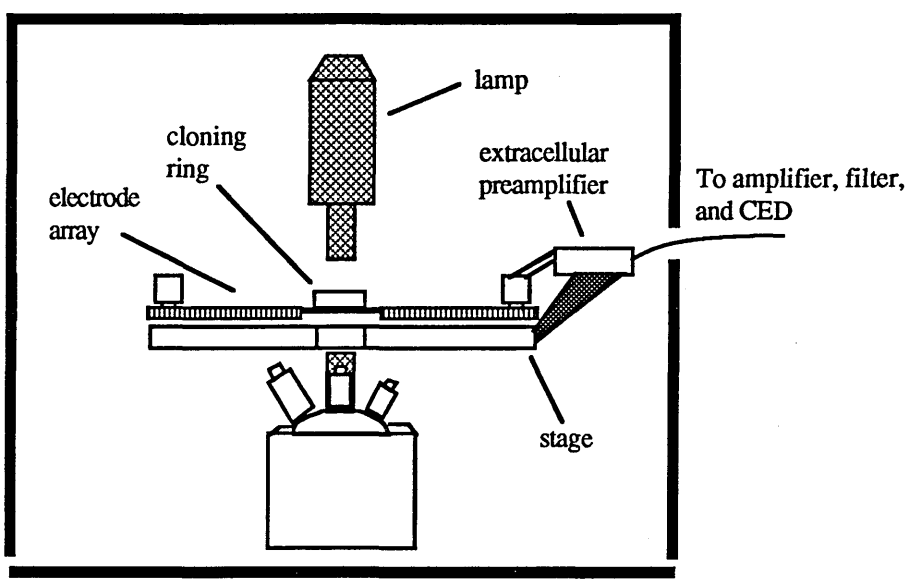

Figure 2.10 Set up for recording extracellular action potentials. The electrode array was screened inside a foil coated box with access for external connections. The microscope and preamplifier were contained inside a shielded hood.

overall amplification of 20,000 was possible, with filtering variable between 0.1Hz and wide band. The preamplifier was mounted directly on the microscope stage, with the microscope contained within a faraday cage in order to reduce noise levels to a minimum. Figure 2.10 illustrates this recording set-up. A fan heater was used to maintain the temperature in the cage above 25°C.

Data was stored using a programmable multi-channel analogue to digital converter (CED, UK) fitted with 8 megabytes of RAM (massram). This device can capture single channel data at a maximum sampling frequency in excess of 20KHz, with the data retrieved at a slower rate by the controlling PC. For further postprocessing and hard copy data was downloaded to a Nicolet oscilloscope. Digital filtering and signal averaging were used to 'clean up' recorded signals.

CHAPTER THREE

CELL-ELECTRODE ATTACHMENT AND AN INTRODUCTION TO IMPEDANCE MONITORING

CONTENTS

3.1 INTRODUCTION

3.1.1 Influence of cell to substrate adhesion on the extracellular potential

Sophisticated equipment and techniques are readily available which allow extracellular signals to be recorded and analysed, allowing their almost undistorted capture in terms of amplitude and waveform (given the signal distortion produced by the electrode). In attempting to improve further on existing signal to noise ratios, it is therefore necessary to concentrate on improving signal amplitudes at the cell-electrode interphase itself. In order to consider how this may be possible it is helpful to return to the calculations detailed in section 1.2.2, which describe the dependence of the extracellular potential, Φ_e, on (in the case of equation (1.6)) the transmembrane current density J_m, the cell radius ρ, the distance b from the cell centre, and the extracellular conductivity σ_e. That is,

$$\Phi_e = \frac{\sigma_e J_m b^2}{\rho}$$

It is clear that increasing the transmembrane current density will also lead to an increase in the extracellular potential. However the maximum deviation of this factor is dependent on the properties of the cell membrane, and as yet it is not possible for this to be artificially increased. The cell radius for a given cell type obviously cannot be increased, although it is possible to select larger cells such as invertebrate neurons in order to generate larger signals. The importance of the third factor noted above, that of the cell to electrode distance, does not deserve serious consideration at present (except in so far as unwanted signal pick-up is a problem) as it is reasonably practical to locate cells directly above planar electrodes (as has been the case for the vast majority of published recordings). Thus in considering how the extracellular signal amplitude can be increased above the often inadequate levels previously observed, it is necessary to concentrate on decreasing the value of the extracellular conductance from the cell to ground.

In section 1.2 this was considered as the conductance from the cell to some reference electrode, through a uniform volume conductor. It would be difficult to simply decrease the conductance of the extracellular fluid, as this is determined by the concentrations of the various components required to

produce healthy cell cultures. It should be clear however that the presence of artificial boundaries in the vicinity of the cell and the electrode can also produce the required decrease in conductivity. This is illustrated in figure 3.1a, which shows a scanning electron micrograph of a neuron obtained from the frontal hemisphere of an eight day old chick embryo. After 4 days in culture the cell body appears to be strongly attached to the microelectrode, and is surrounded by a mass of neurites belonging both to itself and to other neighbouring cells. As such the flow of current around the cell, particularly at the cell-substrate interphase, will be significantly restricted.

Whilst chapter 5 will deal with the effect of confining the cell within deep grooves and pits as a means of increasing signal amplitudes, this and the following chapter will concentrate on the importance of the attachments formed between the cell and the electrode.

In order to demonstrate the effect of the cell to substrate adhesion on the extracellular potential, as a first approximation the current flowing into (and out of) the cell body during an action potential can be assumed to flow entirely through either two points. The first representing the upper surface and the second the lower surface. Given that the voltage dependent ion channels are evenly distributed on both surfaces, the current densities will be identical, say J_m. The total current into the upper and lower surfaces therefore will be J_m multiplied by the upper surface area, S_u, and the lower surface area, S_l, respectively.

An equivalent circuit representing this situation is illustrated in figure 3.1b, where the current is drawn through impedances representing the extracellular region. The resistance into the upper surface consists only of that presented by the bulk solution, represented by R_s in figure 3.1b. A typical value for this resistance, given a cell radius of 5μm, is 16KΩ (see section 3.3.2). The current flowing into the lower surface, in addition to flowing through R_s, will have to pass through the additional impedance presented by the closeness of the cell-substrate contact consisting of a parallel resistance, R_c, and capacitance, C_c. Current is taken to flow out through the extensive network of processes. Also shown in figure 3.1b is an amplifier which would be connected to the electrode directly underneath the cell. The current drawn by the amplifier is assumed to be negligible in the calculations below.

This representation obviously involves a number of simplifying assumptions, the most important of which are:

(1) That the current flowing through the upper and lower cell membrane is treated 1-dimensionally and flows through a single lumped impedance. This allows a simple equivalent circuit to be constructed, and hence simplifies the complex 3-dimensional problem which would otherwise exist. If only an indication of the relationship between the extracellular potential at the outer membrane surface (where it will be greatest) and the extracellular impedance is required, this approximation is reasonable (as will be seen from a comparison of the results obtained with experimentally obtained data).

(2) That the current flow is uniform over the entire soma membrane, and close contact with the substrate does not affect this. It has been shown that there is a relatively high density of voltage dependent channels in the upper soma membrane (Catterall 1984), but it has not proved possible to identify the corresponding distribution at the membrane-substrate junction. The inaccessibility of

(a)

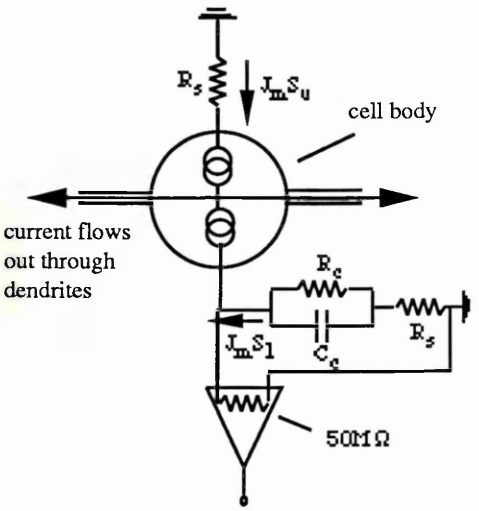

(b)

Figure 3.1 (a) A scanning electron micrograph of a chick cerebral hemisphere neuron, cultured on a planar microelectrode array. Underneath the cell is 10x10μm extracellular electrode, indicated by the arrow. Current flow into the lower surface of the cell will be restricted by the closeness of the cell attachment to the substrate, and (b) illustrates this constriction using an equivalent circuit. The high input impedance of the amplifier relative to R_c (<1MΩ) and C_c (negligibly small), suggests that the entire fixed membrane current $J_m S_l$ will flow through R_c.

this region makes techniques such as patch clamping and autoradiography impossible, although investigations may be possible by attaching fluorescently labelled specific toxins to the channels and making use of confocal scanning microscopy to look at the plane of the interphase region.

There would appear to be no reason however, why channels should be excluded entirely from the lower membrane surface (neural cells *in situ* are generally in close contact with neighbouring cells, but still exhibit membrane excitability), although it is probable that functioning channels will not be present at the regions of closest approach of cell to substrate (focal and close contacts) where bonds of attachment are formed (25% of the lower surface area, see section 3.1.2).

(3) That the impedance through the cell/substrate interphase region is substantially less than the input impedance of the amplifier. This ensures that all the current flowing into the lower membrane surface can be taken to flow through the interphase region from sources within the medium (see figure 3.1b). Given that the input impedance of a good JFET based amplifier can easily exceed 50MΩ (taking into account the reduction produced by the stray capacitance of the input leads and connectors), most of the transmembrane current will be drawn from either the reference electrode or from the dendrites, if the seal impedance is significantly less than 50MΩ. The situation existing at the cell-electrode interphase can

at best be likened to a loose patch clamp (see section 1.3.2) where seal impedances in the region of 1MΩ are obtained, justifying this assumption.

In order to further simplify the equivalent circuit, the capacitive component of the cell-substrate interphase impedance will also be neglected. The validity of this assumption is demonstrated by the results presented in chapter 4, where the variation in the resistive and capacitive components of the cell-electrode impedance with time are presented.

Given the equivalent circuit of figure 3.1b (ignoring C_c), it remains to estimate both the transmembrane current density and the cell-substrate seal resistance. If only the amplitude of the extracellular action potential is required, it is appropriate to choose the peak value for J_m, which is typically about 10pA/μm^2 inward (see section 5.4). For a cell of radius 5μm, this model suggests a potential at the upper surface of the cell of approximately 25μV. If a value for the seal impedance similar to that obtained in a loose patch clamp is assumed, i.e 1MΩ, the maximum potential obtained at the lower surface of the membrane would be 1.5mV.

Despite the simplicity of this approach, it serves to illustrate the possibly large effect that the cell/substrate interphase can have on the extracellular potential. To date, suggestions of how to improve the electrical 'tightness' of this junction have concerned physical methods of pressing the cell onto the electrode or vice versa. These include applying suction through a channel located beside the electrode, and restricting cell growth in a semi-enclosed pit thus forcing the cell down onto the electrode (Regehr 1988). Little attention has been given however, to improving the strength of cell adhesion to electrodes in order to increase the extracellular potentials. The following section discusses several means that have been used to study the structure of cell-substrate adhesions, and the process involved in their formation.

3.1.2 Processes and observation of cell-substrate adhesion

Cellular adhesiveness both to other cells and to extracellular matrices, plays a major role in developmental processes and in the stability of tissue (Harris 1973)(Middleton 1982). The displaying of similar cell properties *in vitro* is well known and has been intensively studied, most notably the adhesion of cultured cells to artificial extracellular substrata. The exact procedure for cell adhesion and the final state arrived at depends on the specific cell type involved, but it is possible to outline at least four basic steps (figure 3.2) (Grinnel 1978).

(a) Cell adhesion depends on the particular chemical and physical structure of the substratum, and also on the nature of any proteins which may adsorb to it. These proteins may be adsorbed prior to the addition of the culture medium containing cells, may be present in the medium (containing serum), or may be microexuded by the cells themselves.

(b) Before adhesion can occur, the cell must first come into close contact with the substrate. Since cells carry a net negative surface charge (due to a coat of short chain carbohydrates called oligosaccharides)(Keeton 1980), as do most substrates, there is often an initial electrostatic barrier to this contact. This may be overcome by cytoplasmic microextensions penetrating the barrier and bringing the cell surface close enough to allow adhesion to proceed.

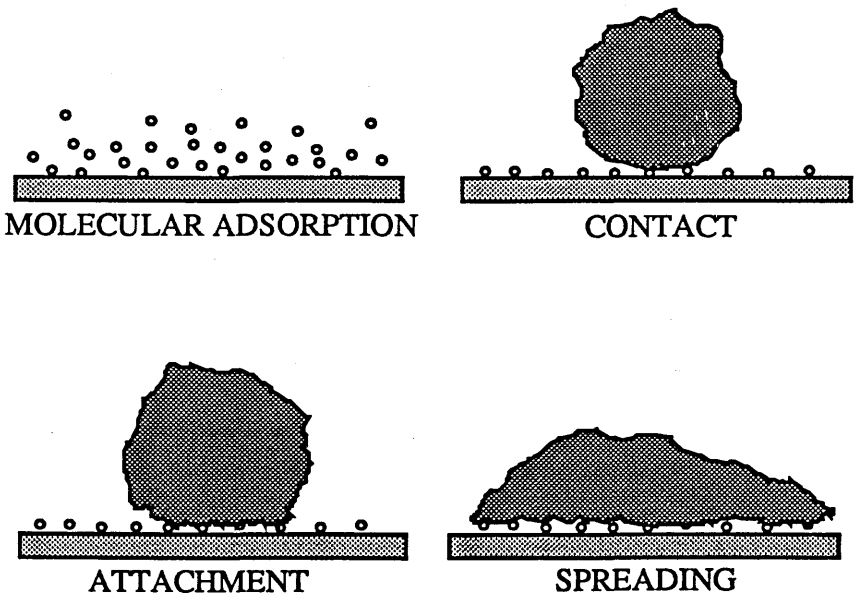

Figure 3.2 Four steps leading to cell adhesion (see text, steps (a) to (d))

(c) Upon contact, bonds of adhesion form between the two surfaces. While bonds to a protein free substratum are non-specific, those to protein coated surfaces appear to be specific ligand-receptor interactions.

(d) At this stage there is observed a reorganisation of the cell cytoskeleton, with the appearance of protruding extensions known as filipodia. These become attached to the substratum and cause a general spreading of the cell. In the specific case of neuronal adhesion, it is at this point that neurite extension will occur.

Little is known of the precise nature of the neuron-substrate interphase, and what is known has generally been inferred from the numerous studies concerning cultured fibroblast cells. The use of transmission electron microscopy (TEM) on vertical sections through fixed fibroblast cells, has identified two types of adhesion sites (Heath 1982). The first, known as focal contacts, are approximately 0.25-1μm wide and up to 10μm long and typically approach the surface to within 15nm. The second type are known as close contacts and approach only to around 30nm. Close contacts are much larger in area than focal contacts, and the focal contacts generally lie within close contact regions.

The use of TEM is limited as it offers only a 2-dimensional image of a cell-substrate section, and can only be performed on fixed cells. The chance of artifacts occurring is also alarmingly high, as the morphology of the cell may be seriously distorted by the fixing process. An alternative method is offered by interference reflection microscopy (IRM) (Curtis 1964), which offers a 'contour' type picture of the lower cell surface. An IRM image is generated (Verscheuren 1985) by the zero order interference of light reflected from the substrate-medium and cell-medium interfaces. Reflection at the latter interface causes a $\lambda/2$ phase shift in the reflected light (in order to prevent energy transfer across a nonconducting to conducting boundary), and hence for regions where the membrane is very close to the substrate ($\ll\lambda$ or $\ll$15nm) the light will interfere destructively producing a dark region. As the membrane moves further away from the substrate towards 100nm for green light ($\sim\lambda/4$ giving a total path difference between the beams reflected from the two interfaces of $\lambda/2$) the image will become progressively lighter.

IRM images of fibroblast cells suggest that only a fraction, 1/4-1/3, of the lower surface of the membrane adheres to the substratum (at either focal or close contacts) with the remainder being 100nm or more above it. The areas of tightest adhesion, the focal contacts, predominate at the extended edges of the cell. These edges are known as lamella and are extended to facilitate cell motion and spreading. Similar results have been obtained with tandem scanning reflected light microscopy (Paddock 1989), where light can be focussed onto a single plane. In addition, recent studies involving scanning electron microscopy (SEM) of the underside of fibroblast (Nil 8) monolayers on fibronectin (Singer, Kazazis, and Scott 1989) (where samples are prepared by etching away the glass substrate), have demonstrated that there is a time lag between cell spreading and the development of focal contacts of approximately 1hr.

IRM studies have also shown (King, Heaysman, and Preston 1979) that the distance between the substrate and the unattached regions of the lower cell membrane, can be increased by decreasing the electrolyte concentration of the medium (similar observations have been made using scanning acoustic microscopy (Grattarola et al. 1988)). This observation is important as it suggests[#] that electrostatic forces play an important role in cell adhesion, beyond merely facilitating initial contact between the cell and electrode.

It is clear that the degree and nature of cell adhesion is extremely dependent on the physical and chemical structure of the substratum. It has been observed that to facilitate fibroblast adhesion a surface must have a minimum negative charge density (at least 5 negatively charged groups per $100Å^2$ (Maroudas 1973)), which is a condition equivalent to the wettability of the surface. Polystyrene is a substratum of low wettability and does not generally support cell adhesion, but can be converted to do so by either wet chemical etching (Martin and Rubin 1974) or by exposure to an oxygen glow discharge (Amstein and Hartman 1975). Such processes endow the plastic surface with the required charge density by producing dangling carboxyl groups (COO^-), and make them the most commonly used substrata for cell culture. This observation appears to contrast with the assertion above, that a negatively charged substrate will repel a like charged cell. It would appear however, that the carboxyl groups must be present in order that adhesion proteins either on the cell surface or in the medium can form the necessary bonds.

Certain cell types, notably many permanent cell lines, are capable of adhering to such substrates in the absence of both adsorbed surface proteins and of serum in the growth medium. Spreading occurs from the initial point of contact and is believed to be due to cells secreting appropriate microexudates. For a variety of cell types however, including primary neurons, this 'passive' adhesion is not possible and although cells may initially attach they remain rounded. To promote spreading and neurite outgrowth either medium containing serum, adsorbed proteins, or both are required. Adhesion under these conditions, known as 'active' adhesion, occurs initially through microprotrusions and is thought to be through specific membrane bound receptors for the adsorbed proteins.

A number of adsorbed proteins which enhance cell adhesion have been identified, with each affecting different cell types differently. The criterion generally used in selecting a suitable surface adhesion molecule for neuronal cultures is that it should promote neurite outgrowth, although again a number are available

[#] The repulsion forces between similarly charged surfaces increase in range as the concentration decreases.

with the success depending on the neuronal cell type involved (Rauvala et al. 1989). Little attention appears to have been given to the effect of these proteins on the ultrastructure of the adhesions formed by the cell body, while the attachment of the growth cone to the substratum has received considerable attention (Bray 1979). This tends to be firmly anchored as would be expected, since it is the leading edge for the neurite extension. The neurite itself is usually anchored only at discrete points along its length.

Physical influences on cell attachment and adhesion involve the relative smoothness of the substratum. The influence of macroscopic surface topography has been described in section 1.3.1, where cell morphology may be controlled to a large extent by the incorporation of regular features into the substratum. A second factor concerns the degree of micro-roughness of the surface, where microroughness may be considered to consist of irregularly spaced features with dimensions of 1μm or less. There is little conclusive evidence of the effect that this has on cell adhesion, due to the difficulty in obtaining optical microscope images of the cell-substratum interphase and the lack of any TEM studies. Two previous studies have suggested that 'adhesion' (quantified by the number of cells which attach within a given time, as compared to a control area) is increased by chemically smoothing polystyrene surfaces (Curtis et al. 1983), and that plasma roughened surfaces do not significantly increase adhesion (Clark et al. 1987). In addition it has been suggested (Curtis and Clark 1990) that the formation of focal contacts is a result of surface roughness, or dirt.

It has been indicated that these studies used the rate of cell attachment and spreading as their measure of cell adhesion. As such is not possible to say that the strength of attachment (and the tightness of the cell-substrate seal) will be similarly affected by roughness. Indeed the opposite may be true, with the increased total area of the cell making focal contacts with the substrate, leading to a substantially stronger attachment. Circumstantial evidence for this may exist, arising from studies into the effect of microroughening the surface of surgical implant materials (both metal and plastic) (Banks, Weigand, and Babbush 1976). In this work, implants were roughened prior to implantation by ion beam bombardment, producing surface features of around 1μm. Results suggested that thrombus attachment is stronger to such surfaces than to smooth surfaces of similar materials. As the basis of thrombus formation is in its nature similar to that of cell attachment in culture, all be it involving a number of cell types and serum components, this would suggest that cells in culture may attach more strongly to similarly roughened substrates.

Returning to the situation of a neuron located above a planar metal microelectrode where a tight cell to electrode seal is required, it would be helpful if the ultrastructure of the interphase could be visualised. This would need to be achieved in real time, as the above discussion makes clear the dynamic nature of the adhesion process which is fundamental to cell growth and motion. For large invertebrate neurons which typically overgrow the electrodes the seal will be formed mainly around the surrounding insulating material, and adhesion in this area could be observed optically (e.g. IRM). Smaller vertebrate neurons however, tend to lie wholly over electrodes which are commonly roughened with either electroplating or some other method, and which precludes the use of optical techniques to view the adhesion plane.

The monitoring of electrode impedance has been suggested and demonstrated (Giaever and Keese 1984) as a method for observing cultured cells in real time, and may overcome many of the problems

encountered with optical methods. In this original study a low frequency (4KHz) electric field was applied across a planar gold electrode, onto which certain fibroblast cell lines were able to attach. By maintaining a constant current, the impedance of the electrode/cell 'sandwich' could be approximated from measurements of the potential drop across it. The size of electrodes chosen in this earlier study were approximately $3\times10^{-4}cm^2$, allowing somewhere in the region of 100 spread cells to be present on it in a confluent monolayer. The two fibroblast cell lines studied were WI-38 and WI-38/VA-13.

Slowly varying impedance changes were observed, and were identified with initial cell attachment, spreading, and overall cell density. In addition smaller, more rapid fluctuation were apparent and were attributed to the brownian like motion of attached cells on the electrode surface (Giaever and Keese 1986). No adverse effects due to the applied field were observed on cell development.

Although these results may appear to be predictable, the lack of an appropriate control leaves them open to question. It is possible that significant impedance changes could be due to the modification of medium conductivity and ionic constituents by cell metabolism, or to electrode 'poisoning' by adsorbed proteins and other organic molecules. A suitable control would require the monitoring of the impedance of a second electrode exposed to the same medium and environment as that in the cell culture, but with cell adhesion prevented.

Allowing for such a control electrode it would appear possible to extend this technique of impedance monitoring to allow single cell observation, by scaling down the electrode dimensions to those of the cell. This would require electrode areas of around $100\mu m^2$, introducing significantly higher impedances and also difficulties in microscopically observing the attachment of cells to electrodes. It is easy to see however, that electrode arrays designed for making extracellular recordings will also perform as impedance monitoring electrodes. That is to say that whilst recording is in progress from an electrically active cell, it would be possible to simultaneously (perhaps alternately) observe the state of the cell adhesion.

The following section briefly describes how the electrode-electrolyte impedance arises, in order that changes in this impedance due to cell adhesion and motion may be correctly attributed. Obtaining an understanding of the fundamentals of the electrode-electrolyte interphase will also aid in clarifying how extracellular action potentials are acquired by planar metal microelectrodes.

3.2 ELECTRODE IMPEDANCE IN SOLUTION

3.2.1 Principles of the electrode double layer

The situation pertaining at the interphase between a metal and a biological electrolyte is both extremely complex and only partially understood. Generalisation is difficult due to its critical dependence on both electrode surface and concentration of individual ions and molecules in the electrolyte. It is known however, that there is a redistribution of charged particles on either side of the interphase, resulting in the development of both an electric field and a complex impedance.

There exist a variety of models to represent this charge distribution, each designed to explain experimentally observed results. The simplest, and first, is known as the Helmholtz model. This is

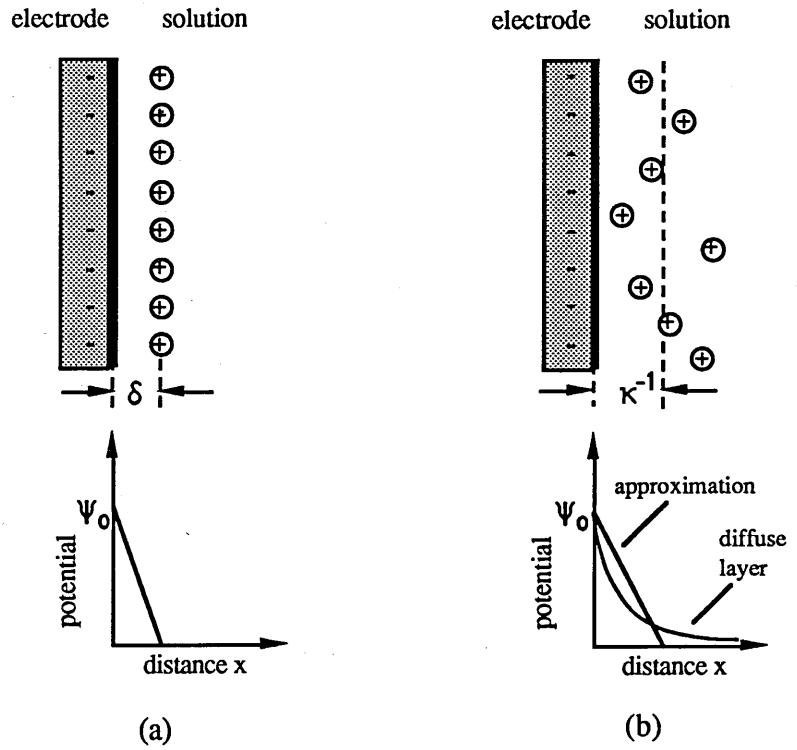

Figure 3.3 Two models representing the electrode-electrolyte interphase. (a) shows the Helmholtz model, where two planes of equal but opposite charge face each other at a distance δ. The charge on the electrode is produced by a migration of electrons from the metal surface, whilst that in the solution consists of physically adsorbed anions. The potential distribution across this layer is linear. (b) In the Gouy-Chapman model the fixed layer on the solution side is distributed by thermal agitation, producing an exponential potential distribution.

illustrated in figure 3.3(a), and regards the interphase as a plane layer of charges (excess adsorbed ions) in the solution, facing a plane layer of charges of opposite sign on the electrode. The separation δ, of the charge layers is somewhere in the region of 0.5nm, or several atomic radii. Such a charge distribution is equivalent to a parallel plate capacitor across which some potential will exist. This will vary linearly across the double layer of charge (hence the name 'double layer' which is often used as a generic term for all electrode-electrolyte interface models), and is also shown in figure 3.3(a). If the potential at the surface of the electrode is ψ_0, then the potential at some distance x from the surface, for $0<x>\delta$, is given by

$$\psi_x = \psi_0(1 - (x / \delta)) \qquad (3.1)$$

At a finite temperature however, the fixed charge layer represented on the solution side of the Helmholtz model would suffer a certain amount of diffusion due to thermal agitation. This is taken into account in the Gouy-Chapman model (figure 3.3(b)) where a diffuse charge layer exists on the solution side of the interphase, and the potential distribution across it decays exponentially, i.e.

$$\psi_x = \psi_0 \exp(-\kappa x) \qquad (3.2)$$

Here κ represents the reciprocal of the effective thickness of the diffuse ionic layer. This distance is best represented as the plate separation of a capacitor which could effectively replace the charge layer in terms of its passive electrical properties. For a simple electrolyte containing only one species of cation and anion, κ^{-1} can be shown to be inversely proportional to the square root of the bulk ionic concentration, n_0. This suggests that the electrode capacitance of the Guoy-Chapman model, C_G, will be proportional to the square root of the concentration (Bockris and Reddy 1977b),

$$C_G \propto \sqrt{n_o} \qquad (3.3)$$

In reality the situation existing at the interphase will be infinitely more complex than either of these two models suggest. The electronic charge on the electrode will be balanced by a combination of solvent dipoles, solvated cations, and unsolvated ions. This is illustrated in figure 3.4, where directly opposite the electrode is the 'primary hydration sheath', consisting of a layer of partially oriented solvent dipoles. Also present in this layer are a few contact adsorbed anions. The remainder of the electronic charge is balanced by the presence of a secondary hydration sheath, and by solvated cations whose centres on average lie on a plane known as the outer Helmholtz plane#. In addition to the adsorption of ions to the electrode surface it is also possible for large organic molecules to adsorb, increasing the complexity of the situation even further. Whatever the exact situation pertaining at the interphase, there exists across it an extremely high field.In equilibrium, i.e. with no externally applied electric field, this field gives rise to a potential known as the reversible potential, V_{rev}.

A necessary aspect of all the above models is that no charge transfer across the double layer can occur in either direction. That is to say that altering the potential difference across the interphase will result only in changing the charge in the solution near the metal. This would imply that the electrical behaviour of this interphase is purely capacitive, and that no ohmic leakage resistance corresponding to ionic discharge is present. Electrodes satisfying this condition are known as 'ideally polarisable', and include both mercury and platinum under certain bias conditions. The majority of electrodes in solution however, do allow the limited transfer of charge across the interphase giving rise to electrochemical reactions at the surface. The rate of these reactions is dependent on several factors, the most important of which are:

(a) the adsorption of reactant ions at the metal surface;

(b) the activation energy of the reaction at the surface;

(c) the presence of adsorbed intermediates and reaction products;

(d) the potential difference existing across the interphase.

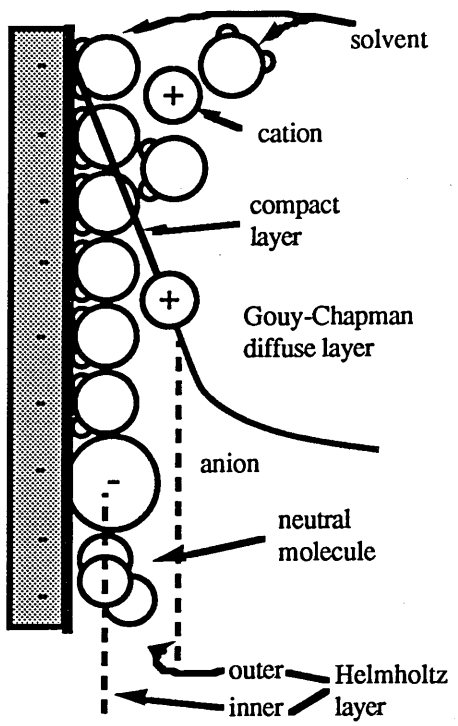

Figure 3.4 General representation for reactant adsorption at the double layer.

The rate of reaction is directly proportional to the current flowing across the interphase, and can therefore be measured in terms of amps.cm^{-2}. Electron transfer across the energy barrier presented by the

Due to the smaller radii of anions compared to cations, they tend to lack a primary hydration sheath of their own. This allows them to find their way into the primary hydration sheath of the electrode, whilst the cations are obstructed by their closely bound solvent dipoles.

electrode-electrolyte interphase, is subject to the the laws of quantum mechanics, i.e. electrons can tunnel through the barrier with energies less than the barrier height. It is therefore possible for net current flow to occur even at very small deviations from the reversible potential, V_{rev}. The dependence of current density on this deviation from V_{rev}, known as the overpotential η, is expressed by the Butler-Volmer equation (Bockris, Bonciocat, and Gutmann 1974)

$$i = i_o\left\{\exp\left[\frac{(1-\beta)F\eta}{RT}\right] - \exp\left[-\frac{\beta F\eta}{RT}\right]\right\} \qquad (3.4)$$

where β is a symmetry constant, i_o is the exchange current, and the other symbols are as previously given. The exchange current is that current which flows equally in both directions across the interphase when the net current is zero. For very small values of overpotential, i.e. $\eta \ll RT/F$, the exponential in (3.4) can be expanded and taking only the first two terms in $e^x \approx 1+x+...$ valid for small values of x, gives after rearranging

$$\eta \approx \frac{RT}{F}\frac{i}{i_o} \qquad (3.5)$$

Thus for small overpotentials, <10mV, the overpotential is proportional to the net current, i.e. the electrode has a constant resistance of $(RT/F)i_o$, known as the 'faradaic' resistance.

The passing of a direct current across the electrode/electrolyte interphase will occur via the faradaic resistance. Under an alternating electric field however, there will be a delay in charge transfer due to the finite time in which reactions will occur. To the external circuit this delay, or phase lag, appears as a capacitance (known as a pseudo or faradaic capacitance) in parallel with the faradaic resistance (Grahame 1952)(Bockris and Reddy 1977a). The total faradaic impedance is itself in parallel with the double layer capacitance discussed above[#] . These three components combine to produce a complex impedance that behaves unlike any conventional passive electrical component. In order to correctly attribute changes in this impedance to cell activity, it is necessary to be aware of any non-linearities in its behaviour under an applied a.c. field.

It is generally assumed that the double layer capacitance is independent of both current density and frequency (being purely a function of the electrode surface and the electrolyte ionic concentrations), though this is certainly not true of the faradaic impedance. Increasing the frequency will give ions that have donated or received charge less time to diffuse away from the metal surface before the electrode polarity is reversed. This will cause an increase in the concentration of reactant species at the interphase, and hence the resistance will decrease with increasing frequency. The faradaic capacitance will increase with frequency, due to the increasing charge at the electrode surface for a given potential, i.e. C=Q/V.

In order to determine the behaviour of the electrode impedance as the current density is varied, it is helpful to examine the Butler-Volmer equation (3.1). From this it would appear that at low current densities the resistance is approximately constant (3.2), but as the current density is increased further the potential will increase only slowly (as the log of the current density) which is equivalent to a decreasing resistance. The Butler-Volmer equation however, takes no account of the difficulty that reactive species

[#] The double layer capacitance is a true capacitor in that no actual charge transfer is involved when ac current flows through it. This is unlike the faradaic capacitance which is due to the finite time in which faradaic current can flow via some electrochemical reaction.

have in diffusing from the bulk electrolyte to the electrode surface where they can receive or donate electrons. At low current densities supply will meet demand, but at very high densities the rate at which charge can be transferred will be severely limited resulting in an increased electrode resistance. This diffusion related impedance effect will be superimposed on that suggested by the Butler-Volmer equation, with the overall characteristic depending on the current densities at which each becomes dominant. This would be revealed by the current versus voltage behaviour of electrodes.

It has already been stated in section 1.3.2 that a low impedance electrode is often sought for recording purposes, in order to reduce both the proportion of the extracellular signal dropped across it and the thermal noise generated by the real part of the impedance. For such recording purposes the frequency spectrum is fixed by the time course of the action potential (approximately centred around 1KHz), so the fact that the impedance decreases with increasing frequency is of no great importance. The current density will be extremely low, tending towards zero, due to the high input impedance of the amplifier and the electrode impedance will lie within the linear region noted above. The only techniques remaining therefore to reduce the impedance are either chemical or physical electrode modifications. It is often difficult to distinguish between these as employing one will generally affect the other.

Physical modifications involve increasing the electrode surface area by either adding or removing material from the surface, creating a microrough surface. This does not have a significant effect on the overall electrode dimensions, and will not therefore lead to the reduction in the recorded signal that would arise from merely increasing these dimensions (due to the averaging of signals from both close to, and distant from the cell). The two most common methods of 'additive' microroughening, involve the electrolytic deposition of silver chloride and of platinum (Geddes 1972). The former, whilst only reducing the impedance by around a factor of 3, is often employed due to the stability both in terms of impedance and dc potential that silver chlorided electrodes exhibit. Platinisation on the other hand is capable of reducing electrode impedances by more than three orders of magnitude, whilst the reduced impedance demonstrates a marked instability over time. The exact magnitude of the reduction depends both on the platinising current, and on the solution in which the platinum is dissolved. It is found that the optimum conditions involve the use of a solution of platinum chloride containing lead acetate, which results in a flaky black deposit often termed platinum black. Whilst microroughness is believed to arise from both a crystalline growth and from the amplification of protrusions (Barkey, Muller, and Tobias 1989a)(Barkey, Muller, and Tobias 1989b), it is not clear why platinum black proves so successful.

In situations where current is being passed through an electrode in order to measure an impedance, for example that of a cell suspension, it is important to be able to distinguish this component from that impedance contributed by the electrode-electrolyte interphase. Unless care is taken it is possible to overestimate the changes in impedance occurring if, in this example, a rising cell suspension impedance causes a reduction in current density which in turn leads to an increase in the interphase impedance. Measurements should therefore be made at a reasonably constant current density, preferably within the region where the impedance is constant with current density, i.e at low current densities. In addition impedances measured at different frequencies should not be compared, unless a note is made of the general trend in frequency characteristics.

3.2.2 Possible modifications resulting from cell adhesion

The use of electric fields to monitor biological systems is now widespread, often involving the measurement of the impedance presented by some material, suspension, or solution. The two basic measurement regimes are polarographic (dc or slow pulse) and sinusoidal (ac) (Gabrielli 1990). Use of the former is limited due to the reaction products which may form at the electrode, affecting as they will both the electrode and the biological entities. The use of a sinusoidally varying field overcomes this problem in general, and allows the determination of the complex impedance presented by the electrodes in series with the bulk phase. In order to relate this impedance to that through which the transmembrane current will flow, it is only necessary here to carry out measurements at a fixed frequency. It is worth noting however, that important information can be gained from the characteristic variations in impedance with frequency (known as impedance spectroscopy), concerning dispersions caused by dielectric material (Kell 1987).

If it is hoped to detect cell adhesion to an electrode as a change in the measured impedance, it is worth considering what possible interactions may be involved. The most obvious is that suggested by Giaever and Keese to explain their results, and involves the blocking of the current path between the planar electrode and the larger reference electrode. This treats the cells as simple insulators which would add a resistive component in series with the measured electrode double layer impedance.

There are however more complex models which may involve the interaction of the cell membrane charge and the double layer. It has been made clear that the electrode impedance arises from the charge layers which arise at the interphase, and that any redistribution or any change in composition there, would undoubtedly alter the impedance. Considering that the double layer charge penetrates into the solution by less than 1nm, and that the closest approach of the cell membrane is around 15nm at areas of focal contact (accounting for only a small fraction of the lower membrane surface) it seems unlikely that there will be any dramatic effect on the double layer via this mechanism.

A further possible influence could be the changing ionic environment in the vicinity of the cell. The double layer models (equation 3.3) suggested that the interphase capacitance is inversely proportional to the ionic concentration in the bulk solution. This only considered of course a simple system containing a single anion and cation, but it is certain that the capacitance in more complex systems will exhibit a similarly complex dependence on the ionic concentrations. It is also certain that the resistance presented by the electrode-electrolyte interphase will also vary non-linearly with concentrations. As such any alterations in the ionic constituents in the vicinity of the cell, may, if significant, result in changes in the measured impedance.

3.3 EXPERIMENTALLY DETERMINED ELECTRODE PROPERTIES

3.3.1 Surface modification by electrodeposition

Before studying more closely the electrical properties of the electrode devices with which it is desired to observe cell attachment and activity, the electrode surfaces were viewed using a scanning electron microscope. Sample preparation is detailed in section 2.6.

Figure 3.5(a) shows a portion of the surface of an evaporated gold electrode of overall dimensions 0.2×0.7mm, at a magnification of 100,000 times. Shown in figure 3.5(b) is the surface of the polystyrene substrate onto which the electrodes are deposited. A granular structure of similar texture is apparent on both, and is almost certainly due to the gold palladium which is sputtered onto the surface prior to examination (100Å thick). This suggests that the texture of the gold electrode surface itself is of a similar or smoother texture than that observed in these micrographs.

The surface of two platinised electrodes of similar dimensions are shown in figures 3.6(a) and (b). The platinising current density used in preparing the first was $9mA.cm^{-2}$, whilst that in the second was $15mA.cm^{-2}$. In both cases the duration of the platinisation process was 30 seconds. The dependence of surface roughness on the plating current is apparent, whilst the effect of the plating duration was observed to be less significant. For example the plating of an electrode at $9mA.cm^{-2}$ for 60 seconds did not result in surface texture greatly dissimilar to that obtained after 30 seconds. Figure 3.7 shows the surface of a gold plated electrode, again at a magnification of 100,000 times. The plating current density used in this case was $15mA.cm^{-2}$, for a duration of 30 seconds. The largest feature size obtained (in the region of 100nm) is similar to that produced by the higher platinising current, whilst the features themselves appear to be smoother and less crystalline.

Figure 3.8 shows a SEM of the surface of a large gold electrode which had previously been subjected to an oxygen plasma etch for a duration of 5 minutes. The RF power of 100W produced a DC bias of 300V with a gas flow rate of $20sccm^{-1}$. A comparison with the unaltered gold electrode shown in figure 3.5(a) suggests that this process does little to alter the physical surface of the gold.

Considering now the microelectrodes (10×10μm) fabricated with a combination of photolithography, metalisation, and reactive ion etching, figures 3.9(a) and (b) show SEMs of an unaltered evaporated gold and a platinised electrode respectively. The platinising current used was $416mA.cm^{-2}$ applied for 10 seconds. It proved impossible to plate these microelectrodes with current densities similar to those used to platinised the large electrodes already described, requiring as it would, current magnitudes of below 21.6nA. This observation is in accordance with those of Robinson (Robinson 1968), as is the threshold current density of around $400mA.cm^{-2}$. This phenomenon is believed to arise from the rate at which the volume immediately surrounding the electrode will be depleted of the plating metal ions, which will be significantly faster than the rate at which the ions can either drift or diffuse into it from the bulk solution. It is not therefore possible to produce a platinum black deposit similar to that shown in figure 3.6(a) using a constant current (although it may be possible to achieve this with a short pulsed current), and only a very rough deposit can be obtained.

3.3.2 Impedance versus frequency

Large electrodes - 0.2×0.7mm

The magnitude of the impedance, |Z|, versus frequency characteristic for an evaporated gold electrode of dimensions 0.2×0.7mm, is shown in figure 3.10(a). Also included are the results obtained after the electrode had been platinised with a constant current of 50μA for 30 seconds, i.e. a current density of $15mA.cm^{-2}$. Figure 3.10(b) plots the corresponding values of the phase angle for both types of electrode. These characteristics were obtained with a constant current density of $0.714mA.cm^{-2}$, a value chosen

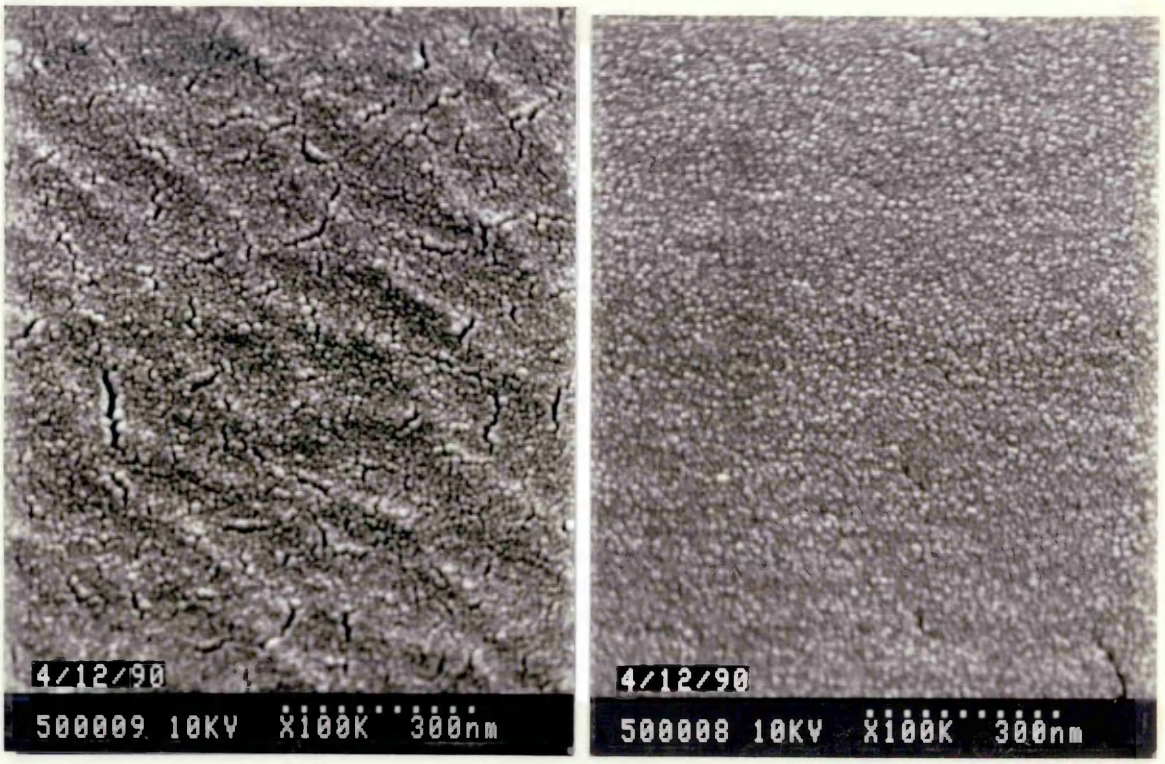

(a) (b)

Figure 3.5 Scanning electron micrographs of the surface of (a) an evaporated gold electrode, and (b) the polystyrene dish, at a magnification of 10^5. Both surfaces were coated with a 100Å layer of gold palladium.

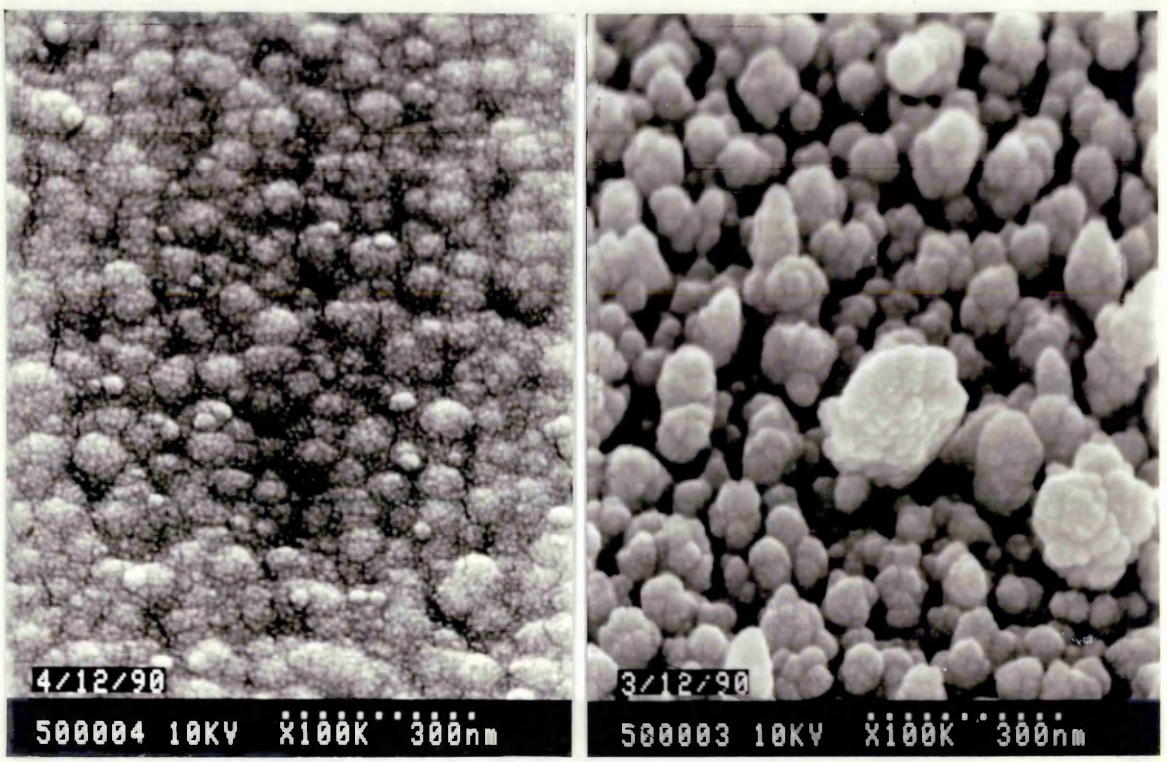

(a) (b)

Figure 3.6 Scanning electron micrographs of platinised electrodes, with plating current densities of (a) 9mA.cm^{-2} and (b) 15mA.cm^{-2}.

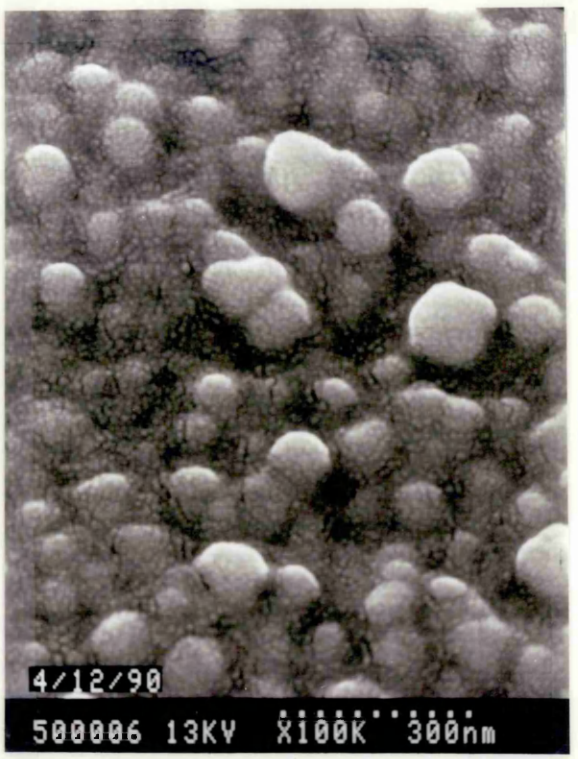

Figure 3.7 SEM of a gold plated electrode, prepared using a current density of 15mA.cm^{-2}. The magnification is 10^5.

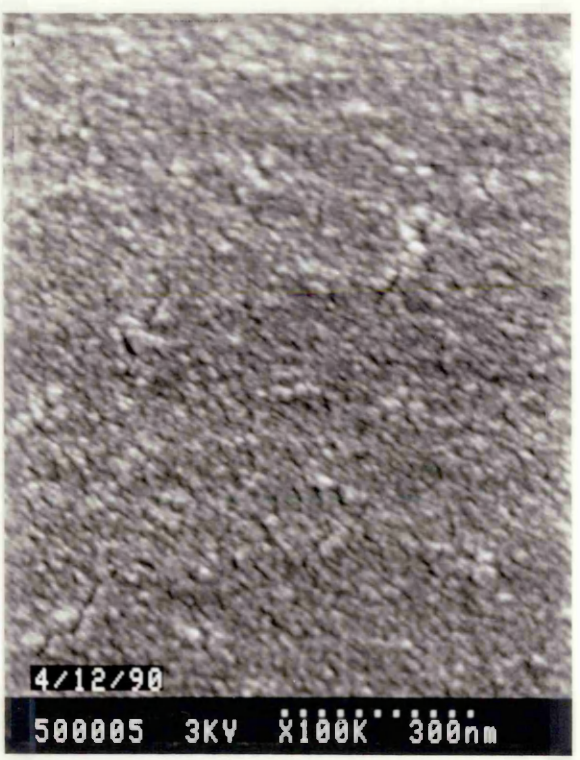

Figure 3.8 SEM of an electrode previously subjected to an oxygen plasma etch. See text for details. The magnification is again 10^5.

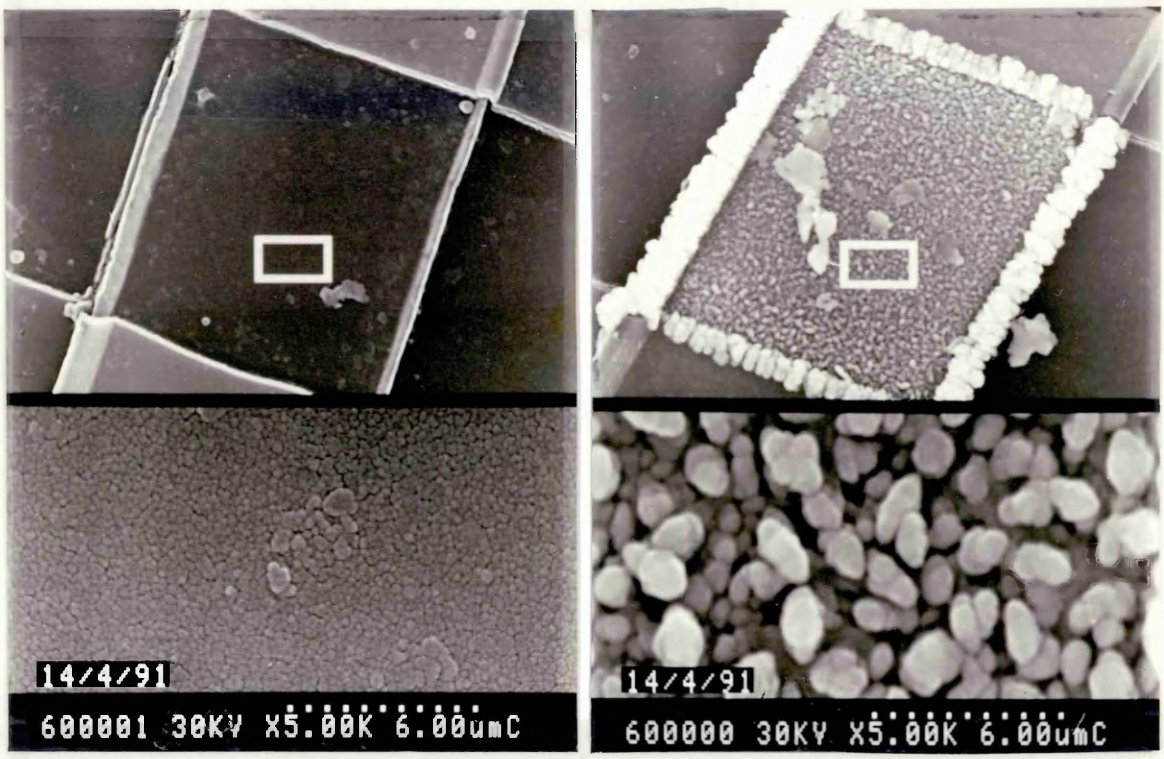

(a) (b)

Figure 3.9 SEM 's of the surface of (a) unplatinised and (b) platinised microelectrodes. The magnification is 10^5.

because it is similar to that which flows during a transmembrane action potential ($10pA.\mu m^{-2}$ or $1mA.cm^{-2}$, see section 5.4). As such it is unlikely to induce cell damage.

At low frequencies the impedance is observed to increase sharply with decreasing frequency for both the platinised and the unplatinised electrode, with the magnitude of the impedances at 1KHz being 1.44KΩ and 9.37KΩ respectively. This low frequency behaviour of the electrode impedance is well explained by the theory given in section 3.2.1. That is that the resistance will decrease and the capacitance will increase as the frequency increases, due to charge being unable to diffuse away from the surface. At a sufficiently high frequency however, 10KHz in the case of the platinised electrode, the impedance of the electrode double layer drops below the impedance presented by the bulk solution which is almost completely resistive and frequency independent. The measured high frequency impedance will therefore be this 'spreading resistance', having a phase angle near zero. This is true for both platinised and unplatinised electrodes (at high enough frequencies), with the value being mainly dependent on the electrode area. These results agree well with the previously reported characteristics for similarly sized electrodes (Geddes 1972).

Measurements made on the platinised and unplatinised electrodes at 1MHz produced impedance values around 0.65KΩ for both, with the phase angle being near zero as expected. This value can be compared with that calculated for a hemispherical electrode of radius r_e (0.25mm), as shown in figure 3.11 (Robinson 1968). The resistance of a thin hemispherical shell of radius r and thickness dr of specific conductivity σ is

$$dR_s = \frac{dr}{2\pi\sigma r^2} \qquad (3.6)$$

Integrating from r_e to infinity gives

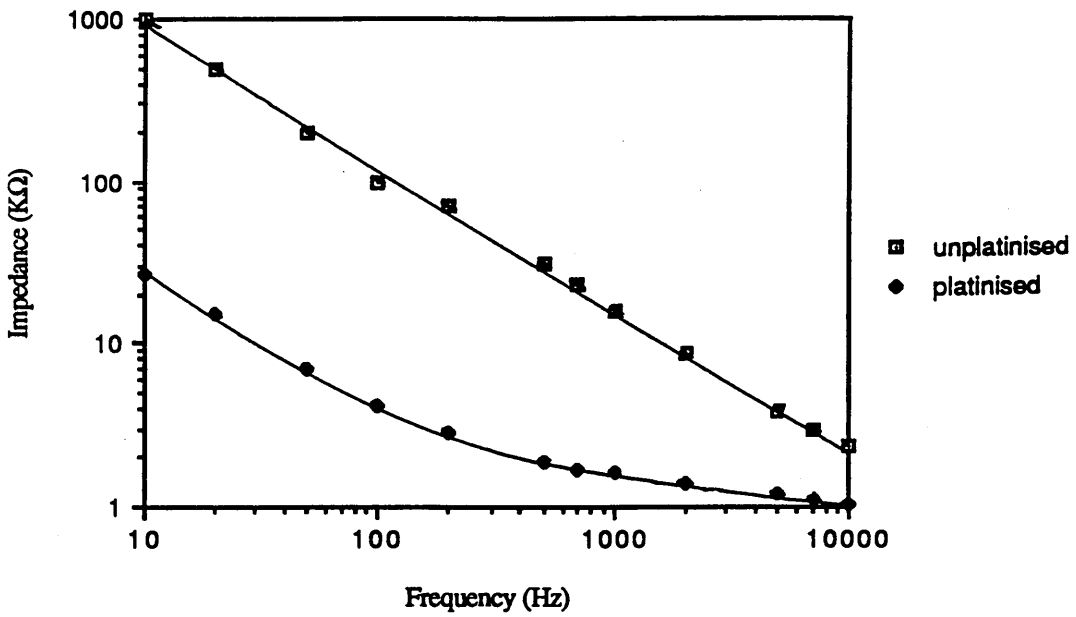

(a)

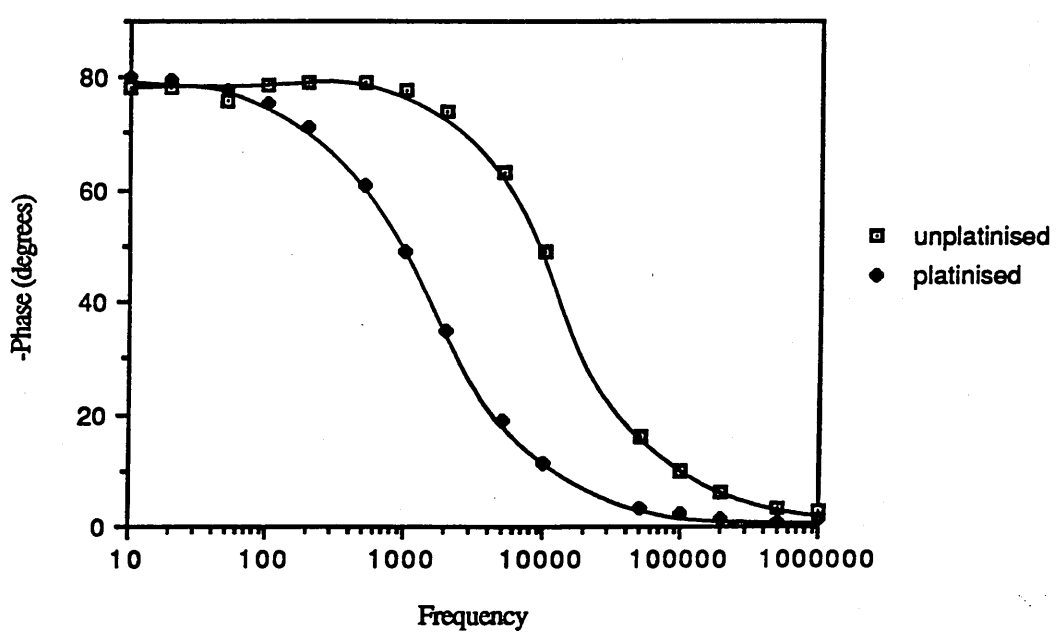

(b)

Figure 3.10 (a) Impedance versus frequency and (b) phase angle versus frequency, for 0.2x0.7mm gold electrodes in saline.

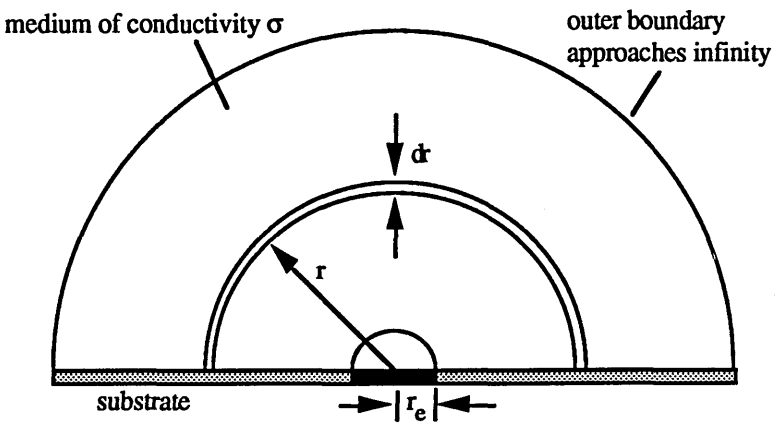

FIGURE 3.11 In order to estimate the spreading resistance from the electrode to ground, a planar electrode can be approximated as a hemispherical electrode of radius r_e.

$$R_s = \int_{r_e}^{\infty} dR_s = \frac{1}{2\pi\sigma r_e} \qquad (3.7)$$

Using a value of $0.02 S.cm^{-1}$ for the resistivity of saline (Geddes and Baker 1967), R_s is approximately 318Ω. This compares well with that value obtained experimentally at high frequencies for these electrodes. In addition it suggests that at much lower frequencies the spreading resistance presented by the bulk solution is negligible in comparison to the electrode impedance.

Microelectrodes - 10×10μm

The results of a typical impedance versus frequency measurements made on 10×10μm microelectrodes are shown in figure 3.12a, whilst figure 3.12b shows the corresponding variation in the phase angles. Plots are given for both a smooth gold electrode and a platinised electrode, where the platinising current was 0.25μA passed for 10 seconds (a current density of $0.2 A.cm^{-2}$). Measurements were made with a constant current of 42.5nA, i.e. a current density of $42.5 mA.cm^{-2}$. Although this current density greatly exceeds that used in the above measurements and that which flows during an action potential, it was required in order to maintain a suitable signal to noise ratio when measuring the potential drop across the electrode, whilst minimising the complexity of the screening and recording procedures.

The trend is similar to that observed above for the larger electrodes, with the impedance for both the unplatinised and platinised microelectrodes increasing rapidly once the frequency drops below approximately 1KHz. The magnitudes of the impedance at 1KHz for the unplatinised and platinised electrodes are 4.78MΩ and 201KΩ respectively. The phase angle drops from around 70° to almost 0° at high frequencies for the platinised electrode, whilst that of the unplatinised electrode drops only slowly from a value of 60° at 10Hz.

From the value obtained for the impedance at high frequencies (1MHz), the spreading resistance can be estimated at approximately 10KΩ. This compares with a value calculated from equation (3.6) for a 5μm radius hemispherical electrode of 16KΩ. Again this value is negligible in comparison with both the platinised and unplatinised electrode impedances at low frequencies.

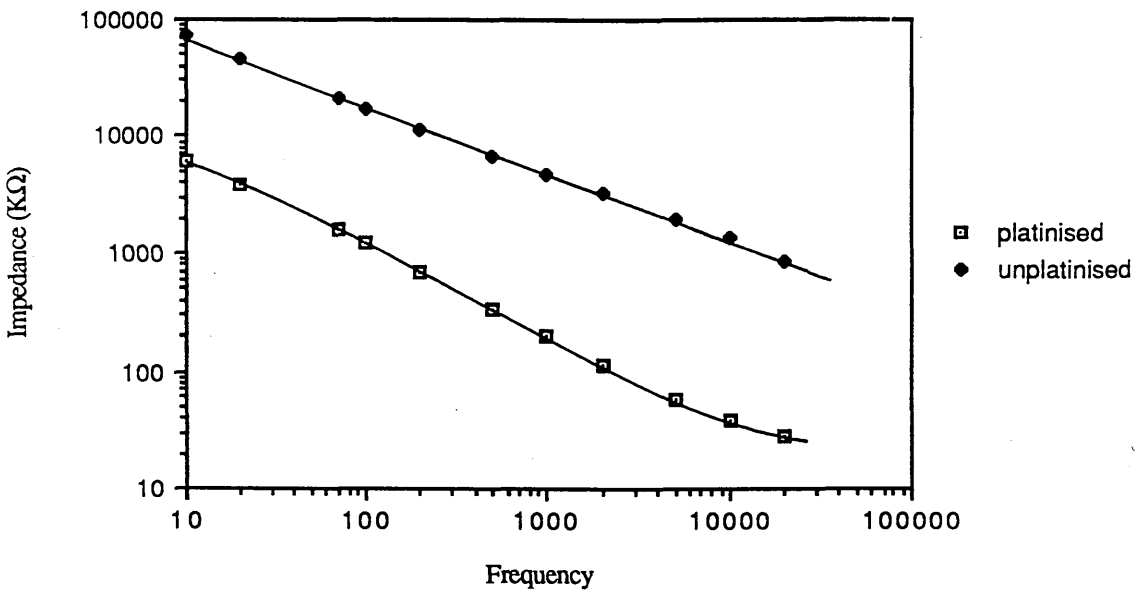

(a)

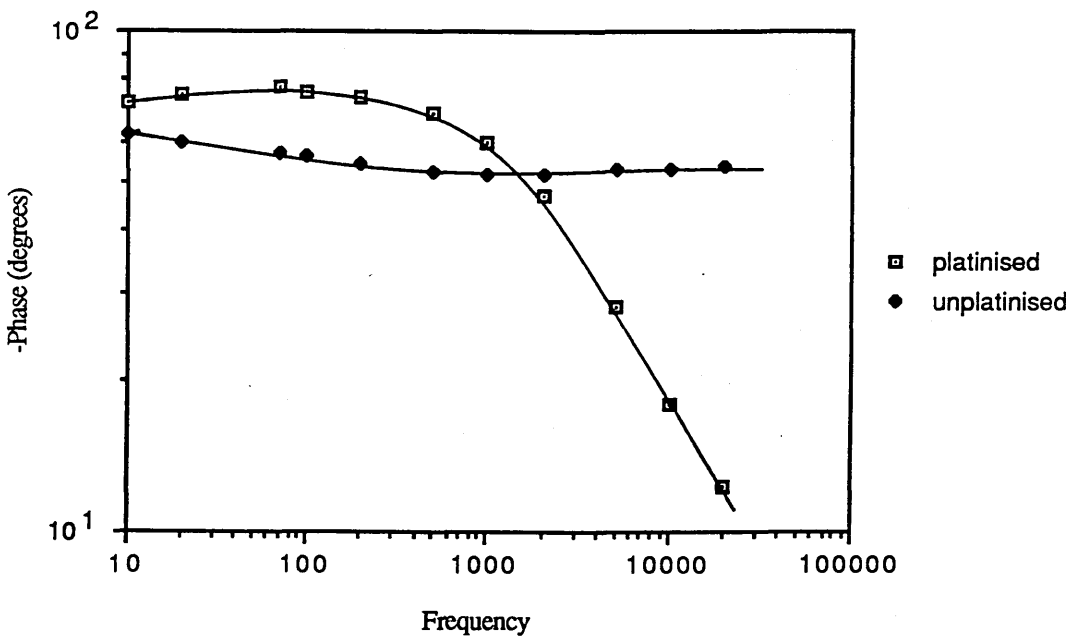

(b)

Figure 3.12 (a) Impedance versus frequency and (b) phase angle versus frequency, for 10x10μm microelectrodes in saline.

Selecting an appropriate measurement frequency

In choosing an appropriate frequency at which to make impedance measurements, it is necessary to consider the applicability of any results obtained from impedance measurements, to the recording of extracellular action potentials. Given that it is required to relate the measured electrode-cell impedance to that impedance through which the transmembrane current must flow during an action potential, it would be appropriate to make measurements at or around the centre frequency of the action potential. This frequency, and also the signal bandwidth, is dependent on the particular cell type concerned. For example figure 3.13(a) and (b) show an intracellular and extracellular action potential respectively, recorded from a leech Retzius cell[#] . Extracellular recordings were carried out using a bandwidth from dc to wide band, and digital filtering was then used to remove 50Hz noise (using a 48-52 Hz notch filter). Figure 3.13(c) shows the frequency spectrum of the extracellular signal obtained using the fast fourier transform (Stremler 1982a) facility on a Nicolet 4094 digital oscilloscope.

Considering figure 3.13(b), the centre frequency of the action potential can be approximated from its duration, i.e. 5mSecs. This suggests a centre frequency of around 200Hz. Inspection of the fourier transform illustrated in figure 3.13(c), suggests that the bulk of the frequency components lie between 0 and 500Hz (the very low frequency components, below 60Hz, are obscured by the 50Hz peak and the impulse function at 0Hz), and are centred around 275Hz. It is important to note that the recorded extracellular signal will not be an exact representation of the true extracellular action potential, as it is certain to be distorted by both the electrode and by the amplification and recording procedure.

Examination of extracellular recordings from other neuronal cell types, allows similar approximations of the centre frequencies to be made from the action potential duration (where data, from which the fourier transform could be obtained, was not available). In the case of cells from the pedal ganglion of the pond snail *Lymnaea stagnalis*, signals tend to be slower by up to an order of magnitude with estimated centre frequencies of 20Hz. Extracellular action potentials generated by vertebrate neurons on the other hand are generally substantially faster than those of invertebrate neurons, having centre frequencies of up to 1KHz.

It has already been stated that recordings with excellent signal to noise ratios have frequently been obtained from invertebrate neurons, due to their large diameters. In order to suggest how to improve recording techniques and devices concerning vertebrate neurons therefore, it is desirable to concentrate on observing cell induced impedance changes in the region of their 1KHz centre frequency. Considering the electrode impedance versus frequency characteristics shown in figures 3.10(a) and 3.12(a), it appears fortuitous that at 1KHz the magnitude of the impedances are relatively small (increasing sharply at lower frequencies). The frequency is also low enough to prevent the impedance being dominated by the spreading resistance of the solution (~650Ω for the large electrodes and ~16KΩ for the microelectrodes), which may prevent the detection of cell attachment via impedance measurements.

[#] Provided by R.J.A. Wilson, Dept. Cell Biology, The University of Glasgow.

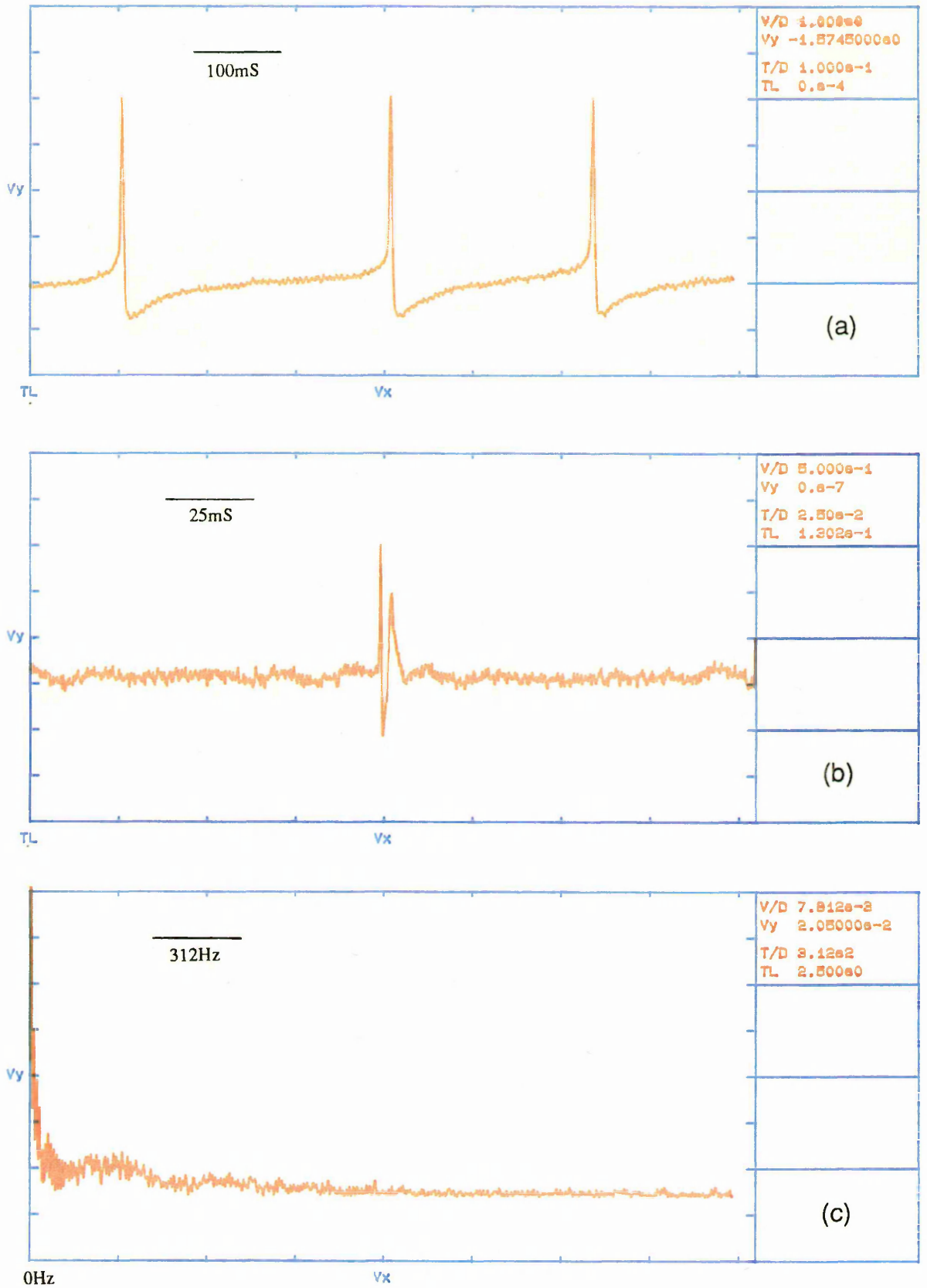

Figure 3.13 (a) Intracellular recording obtained using a glass microelectrode, from a leech retzius neuron, and (b) the corresponding extracellular recording. (c) shows the frequency spectrum of (b), obtained by fourier transform.

3.3.3 Impedance versus current density

Large electrodes - 0.2x0.7mm

The non-linear properties of electrode impedance with regard to current density have been introduced in 3.2.1 above, with the suggestion that impedance measurements be made in the low current density region where the electrode impedance remains constant. Using a 1KHz supply and a constant current source the behaviour of electrode impedance was observed over a range of densities around that used in earlier cell impedance measurements by Giaever et al, i.e 3.3mA.cm^{-2}. Figure 3.14 illustrates the results obtained for both the unplatinised and platinised large electrodes described above.

It is apparent that for both electrodes the variation over at least an order of magnitude is minimal, and if impedance measurements are made around the centre of this range small variations in current density will have a negligible effect on the results. Geddes (Geddes 1972) observed only a 20% decrease in both the resistive and reactive impedance components (for a silver electrode of area 0.157cm^2) when the current density at 1KHz exceeded 10mA.cm^{-2}, which lies beyond the range of the above measurements and which would hence appear to be consistent over this measurement range. The measured phase angle remained relatively constant throughout measurements.

This result is particularly important if the HP 4192A impedance analyser is used to monitor electrode impedance (section 2.4.2), as in this system a constant voltage is applied across the sample and the impedance determined from the resulting current density. If a potential is selected which allows the current density to lie in the centre of the above region, the impedance would have to change by a factor of at least five before electrode effects become important. This potential will obviously depend upon the impedance of the electrode under observation, but was typically chosen to be in the range 5-20mV for these large electrodes.

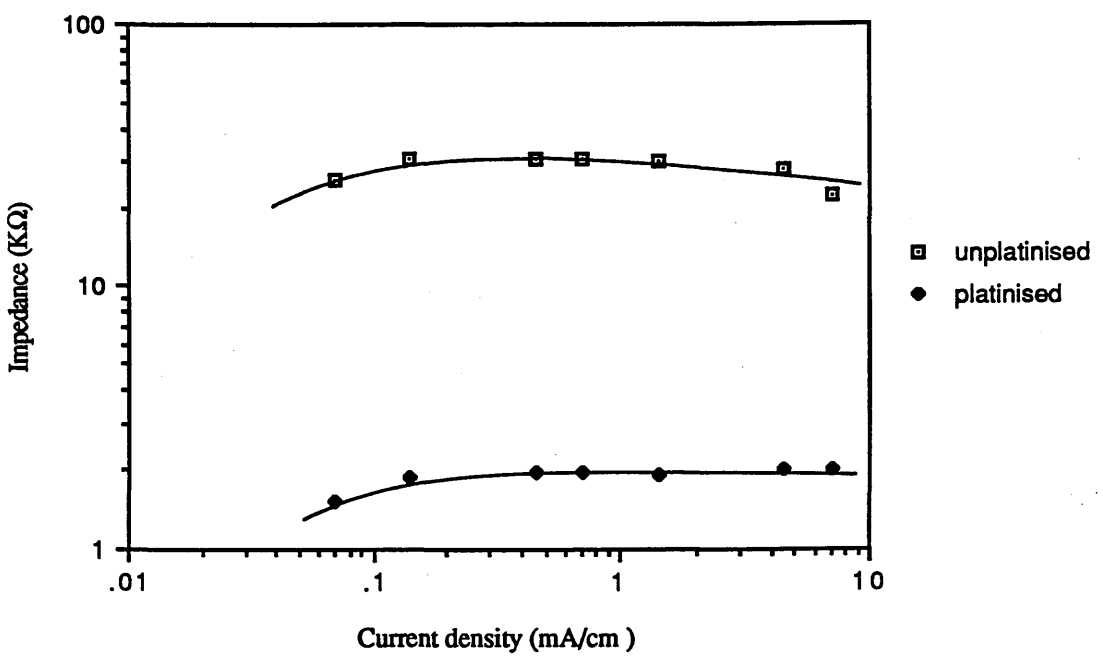

Figure3.14 Impedance versus current density for 0.2x0.7mm electrodes in saline.

The voltage division method (section 2.4.1) used as an alternative method of impedance measurement, utilised a 100KΩ series resistance to limit the current. With an applied 1KHz signal having an amplitude of 100mV, a constant current density of 0.7mA.cm^{-2} was achieved.

Microelectrodes - 10×10μm

Figure 3.15 shows the impedance versus current density characteristics for both the unplatinised and platinised microelectrodes also described above. Again the frequency was maintained constant at 1KHz over the measurement range (3.3mA.cm^{-2} to 330mA.cm^{-2}). This range was chosen to ensure that the potential drop across the electrode could be detected with a sufficiently high signal to noise ratio. Results for the unplatinised microelectrode demonstrate an almost constant impedance over the range, whilst that of the platinised microelectrode begins to decline significantly above approximately 100mA.cm^{-2}. The phase angles remained approximately constant over the entire range. In order to maintain the current densities within the linear region, all the subsequent impedance measurements made using these electrodes involved a current density of 42.5mA.cm^{-2} (with potentials being selected to maintain a similar current density when using the HP impedance analyser)

3.3.4 Impedance versus time

It is known that the impedance of metal electrodes can deteriorate substantially with time, with the greatest changes occurring with (a) new electrodes, (b) upon immersion, (c) and after vigorous treatment such as cleaning. Platinised electrodes tend to be more susceptible to this deterioration than more stable smooth metal electrodes such as gold electrodes, due amongst other factors to their inferior mechanical strength.

The variation in the impedance of a 100μm^2 platinised microelectrode is shown in figure 3.16, recorded over the 30 hours directly following platinisation. Measurements were made in hepes saline with a current density of approximately 42.5mA.cm^{-2}. Over this time period the magnitude of the impedance increases from 80 to 150KΩ, whilst the phase angle increases from 62° to 72° (capacitive). Almost 80% of both the magnitude and phase changes have occurred within the first 10 hours, with a levelling off after this time. This effect is not caused by any irreversible reactions occurring due to the applied electric field, as the impedance of adjacent platinised electrodes showed similar increases between their initial and final impedances, with measurements only being taken at these two points. Changes could be due to a number of factors including the detachment of some of the platinum black, or the formation of insoluble compounds on the electrode surface. The latter effect is the most likely explanation as this would tend to insulate the electrodes hence increasing the phase angle, whereas a reduction in surface area due to detachment would leave this relatively constant.

Allowing platinised microelectrodes to dry and observing the impedance after reimmersion, produced changes of between 50 to 200% in relatively new electrodes. The resulting impedance tended to remain more stable than that of freshly platinised electrodes however, and was still substantially less than their unplatinised impedance. Such electrode impedance fluctuations with time were less pronounced with the larger platinised electrodes showing only a marginal increase with time, probably being due to the lower overall impact of platinisation on the impedance.

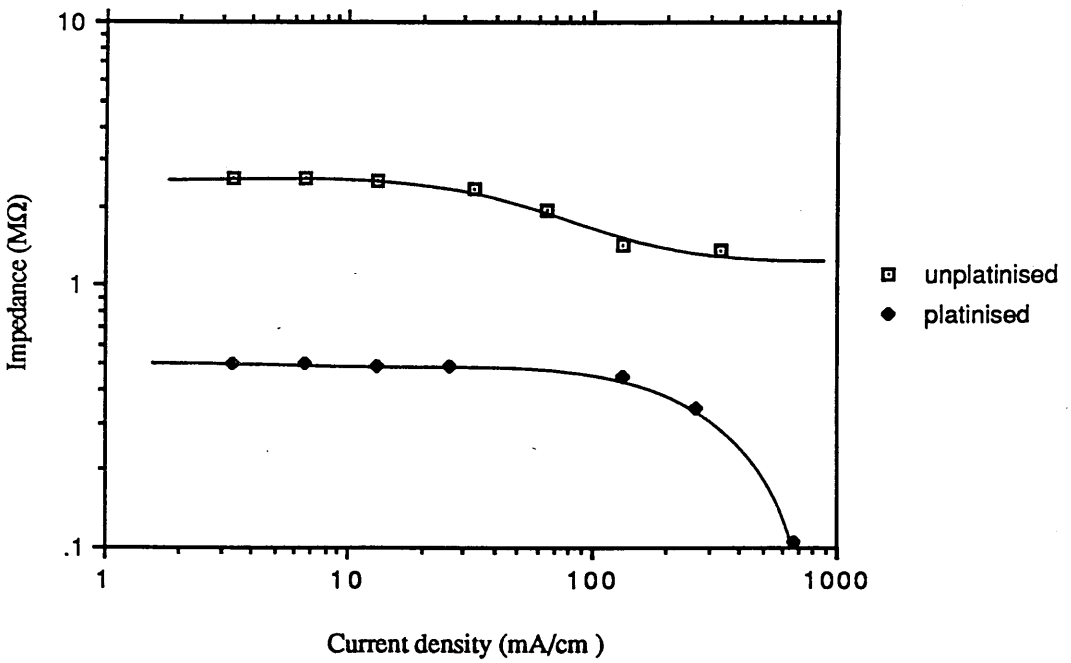

Figure 3.15 Impedance versus current density for 10x10μm microelectrodes in saline.

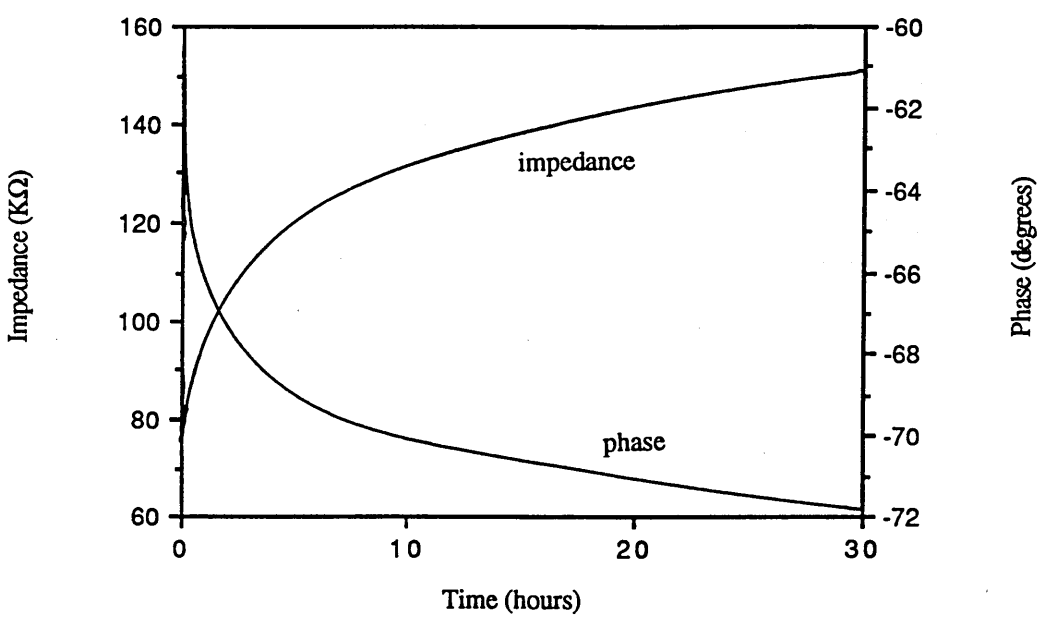

Figure 3.16 The variation in the impedance of a freshly fabricated, platinised microelectrode with time after immersion in saline.

These effects are of considerable concern here, given that it is hoped to observe fluctuations due to cell activity which will occur over a similar time scale. The effects can be minimised firstly by soaking electrodes in saline (or culture medium) for long enough to allow the impedance to reach a near equilibrium value, and secondly by comparing results with those from a control electrode. The use of a control electrode is not ideal as no two platinised electrodes can ever be the same due to the random and uneven nature of the platinisation process. It can indicate in general however, whether or not the electrode impedance is stable enough to allow fluctuations in the overall impedance to be attributed to cell activity.

Such control electrodes were incorporated in devices and were in all cases identical in size and material to the actual 'cell monitoring' electrodes. Although attempts were made to ensure that the initial impedances of both electrodes were as close as possible, slight variations were inevitable due to the platinisation process. These were not considered important however, as only the general trends were compared, and not the absolute values. A semi-permeable membrane (cellulose nitrate) with a pore size of 0.2μm was used to separate the control electrode from the cell measurement electrode (fabrication details are given in sections 2.2 and 2.3). This allowed cells to be confined on the measurement side only, whilst still maintaining equal concentrations of ions and molecules in both.

It is apparent that impedance changes in such a control electrode will not only be due to any subsequent alterations to the platinum black surface, but will also arise from factors such as temperature fluctuations, protein adsorption, and changes in ionic concentration (due to cell metabolism). It could be argued that these are intrinsic factors in the determination of the electrode-cell junction, and should therefore not be eliminated from measurements. This may be true in the case of a single isolated cell on an electrode, but when it is required to monitor the activity of a cell amongst many hundreds or even thousands of others it is important to be able to distinguish bulk effects from local effects. For this reason a control electrode was not only included in measurements with platinised electrodes, but also with those made using smooth gold electrodes which exhibited little or no variation in their intrinsic double layer impedance.

The use of a control electrode was only disregarded after non-local factors were shown to be minimal, and when use was made of the HP 4192A impedance analyser to split the impedance into its in phase and

characteristic	electrode type			
	macroelectrode		microelectrode	
	unplatinised	platinised	unplatinised	platinised
electrode spreading resistance				
-calculated	650Ω		16KΩ	
-measured	318Ω		10KΩ	
typical impedance at 1KHz	9.37KΩ	1.44KΩ	4.78MΩ	201KΩ
maximum current density at which impedance remains linear	>10mA.cm^{-2}	>10mA.cm^{-2}	>1000mA.cm^{-2}	100mA.cm^{-2}
time for impedance stabilisation	immediate	<2 hours	immediate	<12 hours

Table 3.1 Summary of planar metal electrode impedance properties.

quadrature components. This was necessitated by the limitation of single channel recording when using this system. Table 3.1 summarizes some of the important points detailed above.

Given that impedance variations due to non-linear electrode properties can be minimised sufficiently, it should be possible to detect cell attachment to planar metal electrodes. The following chapter describes the results obtained to date with a variety of cell types, using both macro and micro-electrodes.

CHAPTER

FOUR

CELL-ELECTRODE IMPEDANCE MEASUREMENTS

CONTENTS

4.1 INTRODUCTION

Chapter 3 introduced the concept of observing the cell-electrode interface by means of a continuous impedance measurement. This method should allow quantifiable results to be obtained, which in turn will enable the comparison of a number of parameters which determine to some extent the nature and 'strength' of the attachment formed between cell and electrode, for example cell type, electrode surface, and a number of environmental factors.

It has already been pointed out that previously reported work involving such impedance measurements was concerned with monitoring the growth of fibroblast cells in culture, on a planar gold electrode which was large enough to accommodate approximately 100 spread cells. Such a system, although it is concerned with more than a single cell, provides a suitably straightforward means to investigate some of the factors detailed above, and may therefore provide certain information on the neuron-electrode interface which is of primary interest here. In addition it will allow the introduction of a control electrode to evaluate the influence of factors such as temperature, cell metabolism, and protein adsorption, in producing impedance changes and will ensure that any changes due specifically to cell attachment can be correctly attributed. There are also advantages to be gained by initially continuing with the use of a fibroblast cell line, notably their ease of culture and the considerable knowledge which exists concerning their adhesion to artificial substrata.

This chapter therefore begins by describing the results obtained with a system based upon that used by Giaever and Keese, but substantially modified to include a control electrode which allowed the monitoring of background impedance changes. The comparison of fibroblast attachment to several electrode surfaces including evaporated gold, plated gold, platinum black, and plasma etched gold is considered. Experiments using an epithelial cell line are then discussed, in order to demonstrate the significant differences which exist in the effects produced by different cell types.

Given that these results indicate that cell attachment and activity can be detected using electrode impedance monitoring (with an appropriate electrode surface), experiments are extended to allow for the first time, the observation of a single, identifiable cell possessing a cross-sectional area of less than $200\mu m^2$. This involves the use of a suitably scaled microelectrode, and utilises both fluorescence microscopy and time lapse video to confirm observations. Again fibroblast cells are used to demonstrate the success of this technique, which is particularly suited to the detection of the rapid movements which these cells exhibit. Preliminary results are then presented concerning the attachment of neurons extracted from the brain of the pond snail *Lymnaea stagnalis*, which are large enough to be positioned mechanically over the microelectrode.

Due to the nature of the experimentally obtained impedance variations, where the behaviour with time is a function of unique cell activity and electrode properties, only typical examples for each electrode and cell preparation are given, i.e. it is not possible to produce averaged results. In this case typical means that the given result exhibits similar trends, in terms of the amplitude and period of variations, to a series of experiments where the total number, n, is indicated.

4.2 LARGE AREA ELECTRODE-CELL IMPEDANCE MEASUREMENTS

4.2.1 BHK fibroblast cell line

The impedance of the large area electrodes, the design and fabrication of which are described in section 2.2, were monitored for a period of up to several days following the introduction into one side of the dish of a suspension of BHK fibroblast cells. Cultures could be observed periodically (or continuously if required) using a microscope enclosed in a perspex box, the inner ambient temperature being maintained at 37°C±2 (dependent on the prevailing room temperature) by a thermostatically controlled heater. Cells growing on smooth gold electrodes could be observed using both reflection and phase contrast objectives due to the relative transparency and smoothness of the evaporated layer. Those on gold plated electrodes however could only be viewed using reflection objectives, as the increased electrode thickness prevented light transmission, whilst in order to view cells growing on the surface of a heavily platinised electrode it was necessary to fluorescently stain the cells and to observe them using a fluorescence microscope. Fluorescent microscopy and impedance monitoring could not be carried out simultaneously, as the short working distance of the objective (<1mm) required the removal of the cloning ring and hence of the bulk of the culture medium.

Plain gold electrodes

Initial measurements concerned unaltered evaporated gold electrodes with an area of approximately $0.14mm^2$, using the additional large area electrode as the return electrode for the applied 1KHz ac field (see figure 2.9). The current density was maintained constant at $0.7mA.cm^{-2}$. Figure 4.1 shows a series of phase contrast micrographs at a magnification of ×150, taken at intervals after the introduction of 0.3ml of a suspension of BHK cells into the dish, at a density of $3\times10^5 cells.ml^{-1}$. After 15 minutes the majority of cells have settled onto the electrode but have not spread to any significant degree. 15 minutes later somewhere in the region of 20% of the cells show signs of spreading, although the total number of attached cells has remained unchanged. Within 2-3 hours the majority of cells are well spread with electrode coverage increasing. The final micrograph shows a confluent cell layer after 10 hours in culture. A comparison of the morphologies of cells growing on the surface of the electrode and on the adjacent

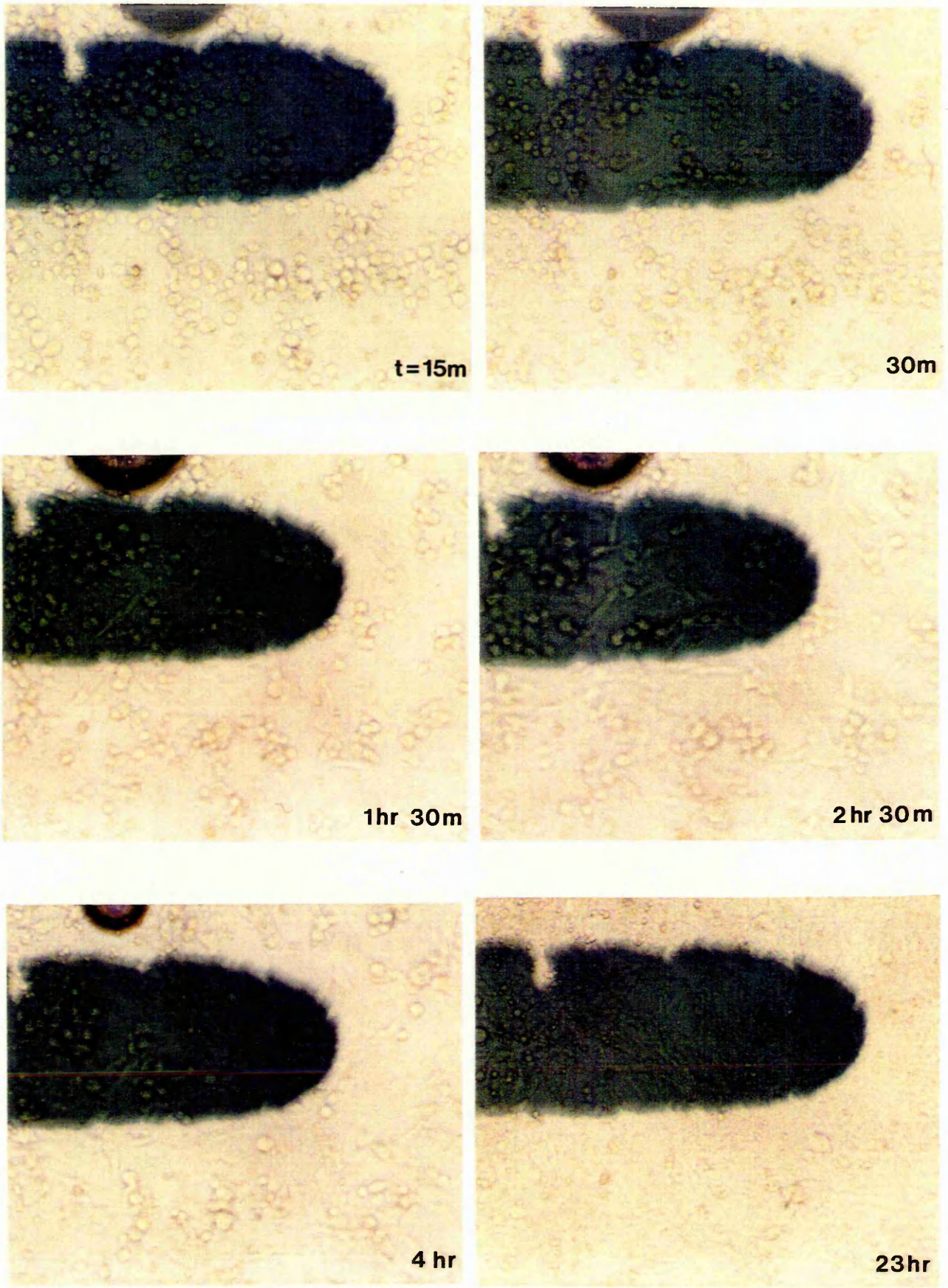

Figure 4.1 Phase contrast micrographs showing initial attachment, spreading, and multiplication of BHK fibroblast cells on a gold electrode. The magnification is x150.

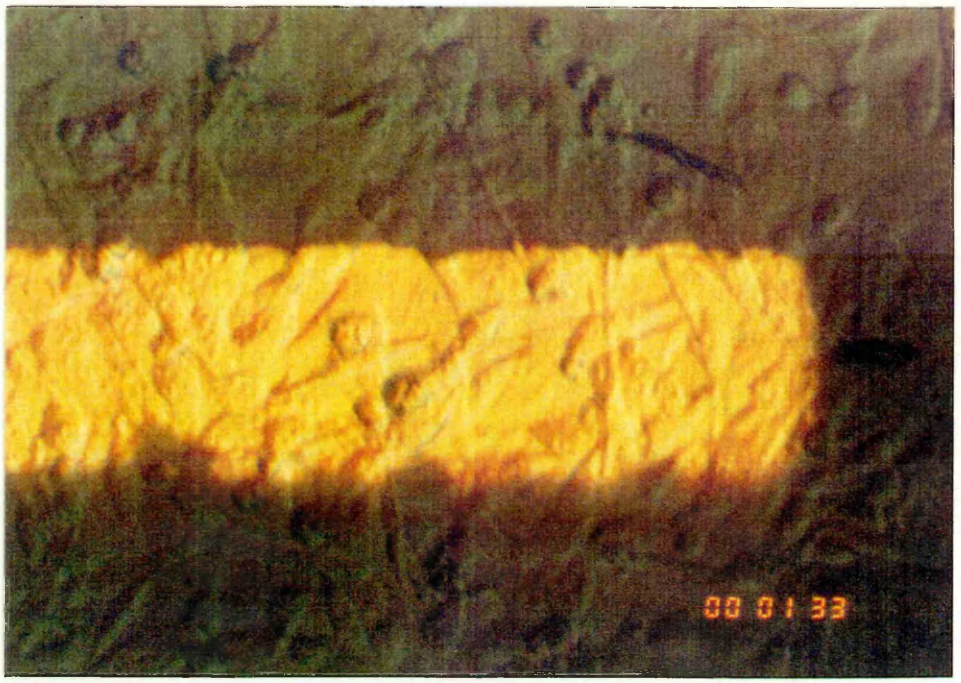

Figure 4.2 Reflection micrograph showing BHK fibroblast cells on a gold electrode. The magnification is ×140.

uncoated polystyrene region suggests no observable differences, indicating both that gold acts as a suitable substrate for cell culture and that the applied electric field produces no adverse affects on cell development. Figure 4.2 shows a micrograph taken using a reflection microscope, at a magnification of ×140, of the same electrode and confluent cell culture.

Figure 4.3 shows the typical variation in the magnitude of the impedance on both the cell measurement and control electrodes (n=8), from the time after the initial introduction of the cell suspension into the cell measurement side (the control side being simultaneously filled with a similar volume of fresh HECT medium). In this and the following experiments the quantity of cells introduced (0.3ml at a density of 10^6cells.ml^{-1}) was greater than that used in obtaining figure 4.1, and was sufficient to result in a confluent cell layer within 3-4 hours. This ensured that the maximum rate of change of impedance possible, would be achieved. All impedance values are normalised against the initial values for each electrode in order to allow a more straightforward comparison of results.

The first point of note from figure 4.3, is the fall occurring in the impedance of both electrodes over the first 15 minutes. This is due to the temperature of the dish and its contents rising from room temperature to 37°C, after being placed in the incubator. If the dish and suspension are warmed separately to this higher temperature prior to innoculation, the fall is substantially reduced or eliminated. After this period, when the dish has reached the equilibrium temperature, the impedances level out at approximately 95% of their initial value (following a slight rise and fall). Over the following 11 hours the behaviour of the impedance of the measurement electrode varies little from that of the control, with the former decreasing by 5% whilst the latter remains nearly constant. The corresponding phase angles exhibited practically no variations over the measurement period. Repeating this experiment a number of times resulted in the impedances drifting at similar rates, although not always in the same directions.

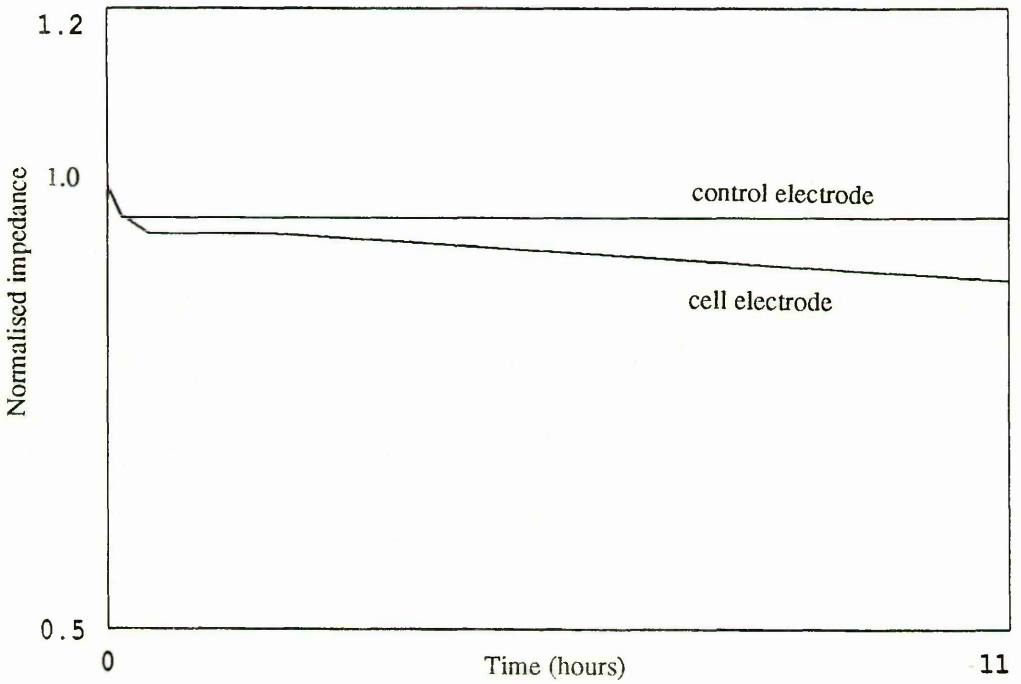

Figure 4.3 The variation in impedance (normalised against the initial electrode impedance) with time for BHK cells cultured on a smooth gold electrode with dimensions 0.2x0.7mm.

Figure 4.4 Reflection micrograph showing normal cell development of BHK cells on a lightly platinised electrode. Magnification is x140.

These results provide no conclusive evidence to suggest that cell induced changes in the measured impedance are occurring, with the variations between control and measurement electrodes being minimal. There are certainly no significant fluctuations occurring at the times when cell attachment and initial spreading commence (within 2-3 hours of seeding), when the greatest changes might be expected. The slow drifts observed ($<100\Omega.hour^{-1}$) are consistent with those noted above for electrodes immersed only in a simple saline solution.

It is unlikely that this result is due to current leaking through the cells as BHK's exhibit extremely high membrane resistances, typical of biological cell membranes, of the order of $10^5\Omega.cm^2$ (Cassaleggio et al. 1985). Comparison with the successful observations made by Giaever and Keese, whose electrode preparation and measurement method were almost identical, suggests that the strength of adhesion of BHK cells to gold when compared to WI38 and WI38/VA-13 is relatively weak. It was suspected at this point that surface roughness may play a role in cell attachment, and as the most common electrophysiological technique used to increase roughness is the deposition of platinum black, the attachment of BHK cells to electrodes modified in this way was studied.

Platinised electrodes

Both control and measurement electrodes were platinised with a constant current of 13μA (a current density of $9mA.cm^{-2}$) passed for 60 seconds, which resulted in reducing the impedance from approximately 20KΩ to between 3 and 6KΩ. This produced a light deposit of platinum on which cells could still be easily observed using reflection microscopy (figure 4.4). The cells appeared to develop normally on these electrodes and initial attachment, spreading, and confluence occurred over a similar timescale to that noted above.

The resulting variation in electrode impedance (n=6) is shown in figure 4.5, for the 12 hour period following innoculation with the cell suspension (the cell density and volume being identical to that used above). After the initial fall in impedance due to the temperature rise, it remains relatively stable on both electrodes with a drift of less than $30\Omega.hour^{-1}$. After comparisons between the results obtained for both the control and cell measurement electrodes, and between these results and those obtained above, there again appears to be no evidence of cell induced changes. This experiment was repeated several times, after platinising electrodes with a similar current density for periods of up to 3 minutes. Observation of the electrode impedances upon the introduction of a cell suspension, failed to demonstrate any cell induced fluctuations.

Electrodes of similar area were then platinised with the higher current density of $18mA.cm^{-2}$, for 30 seconds. Impedances were reduced by at least one order of magnitude from that of the unplatinised electrodes. This produced a black, optically opaque deposit on which cells could not be observed unless they were first fluorescently stained (see section 2.5.2). Figure 4.6 shows the cell distribution over the electrode, and was obtained using a double exposure. The first exposure used transmitted light to show clearly the electrode, whilst the second involved fluorescent light to show the position of the cells. Cell densities are similar both on and off the electrode, and in addition the cell density on the electrode is observed to increase at a similar rate to that on the adjacent polystyrene, suggesting normal cell development.

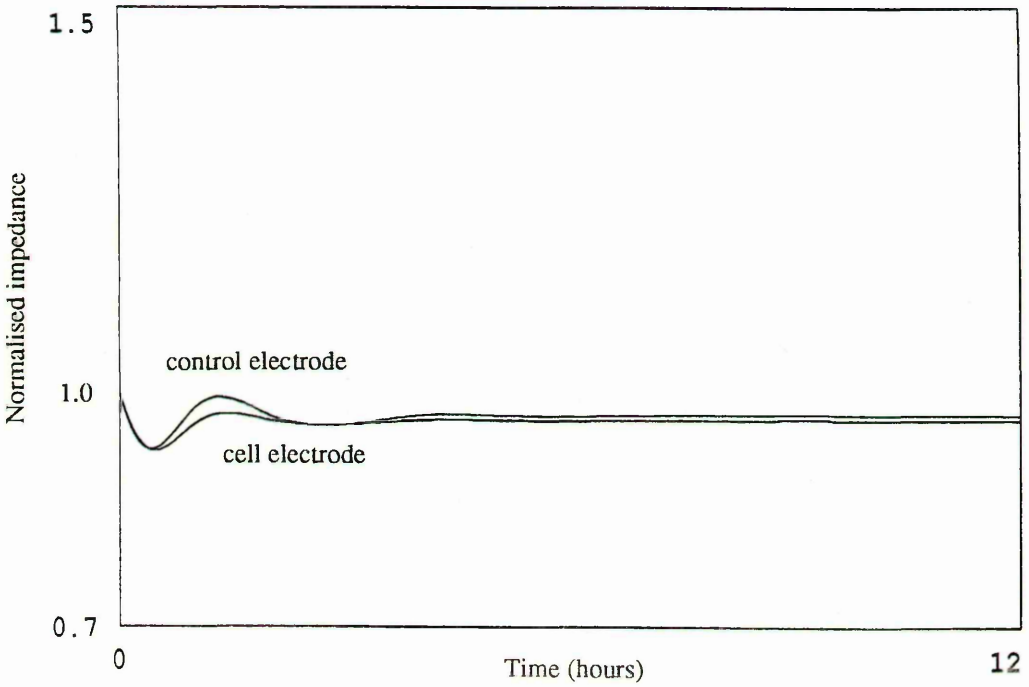

Figure 4.5 The variation in the normalised impedance with time for BHK cells cultured on a lightly platinised gold electrode with dimensions 0.2×0.7mm.

Figure 4.6 In order to observe BHK cells growing on heavily platinised electrodes, they were first fluorescently labelled and then viewed under a fluorescence microscope.

Figure 4.7a shows the variation in the cell measurement and control electrode impedances over an initial period of 10 hours. It is immediately obvious that the impedance of the cell measurement electrode begins to increase markedly after only 15-30 minutes. The rate of increase accelerates rapidly (to a maximum rate of $2.4K\Omega.hour^{-1}$), before the impedance reaches a plateau at 1.7 times the initial value of the impedance. This change is not reflected on the control electrode where a drift of about $180\Omega.hour^{-1}$ continues over the entire measurement period. Repeated experiments (n=8) involving this and other identically prepared electrode patterns, produced similar rises involving a near doubling of the initial impedance over a similar time scale. This time (15 mins to 4 hours) corresponds well with the time at which cells are observed to attach and spread most prolifically (figure 4.1).

In order to identify which mechanism is responsible for this impedance change, it is helpful to split it into both its resistive and reactive components. Whilst it has previously been shown (section 2.4.2) that the series and parallel equivalent representations may be used interchangeably, the series model is intuitively more helpful as will be outlined later. Figure 4.7(c) shows both the series resistive and reactive components for a typical experiment (n=4), and it is clear that the rise in impedance is due almost entirely to an increase in the series equivalent resistance, with the change in the out of phase (reactive) component during this period being less than 10% of the resistive change.

It has been noted that the initial cell suspension density used in obtaining the above results (10^6 $cells.ml^{-1}$), was sufficiently large that once the initial cell attachment and spreading was completed a confluent layer of cells existed. Reducing the cell density to below approximately $3\times10^5 cells.ml^{-1}$ (figure 4.1), results in an initial layer of spread cells with significant gaps between them. As the cells are not contact inhibited, they are able to divide until these gaps are filled. This produces a more gradual rise in the impedance, until eventually it again levels out at approximately twice the initial value. Thus the rate of rise is an excellent indicator of cell density, as is the magnitude of the rise.

A second important feature of these results, in addition to the initial rising impedance due to cell attachment and spreading, are the fluctuations that occur both during and following cell attachment. Figure 4.7(b) shows a portion of 4.7(a) with an expanded time scale. The maximum amplitude of the fluctuations depends to a large extent on the initial density and the time after seeding, decreasing as the available space is filled by spread cells. It seems clear that these fluctuations are due both to cell locomotion across the electrode, and to the process of cell division which involves cells rounding up and occasionally lifting off. Both of these processes will occur to a greater extent in relatively sparse cell layers, decreasing as confluence is reached. In general the fluctuation as a fraction of the total impedance is relatively small (<5%), due to the averaging effect of a large population of cells. That is to say that perhaps only one or two cells that are present on the electrode are dividing at any one time with the overall effect on the impedance being minimal, and that cell motion is largely random and hence for a large cell population the effect is averaged out.

These observed impedance variations, both the fluctuations and the large initial rise, for BHK's cultured on a heavily platinised electrode, are similar to those observed by Giaever and Keese for WI-38 fibroblasts cultured on smooth gold electrodes. This latter cell line was not available in our laboratory to allow a direct comparison for different electrodes, but it is apparent that the effectiveness of adhered cells in

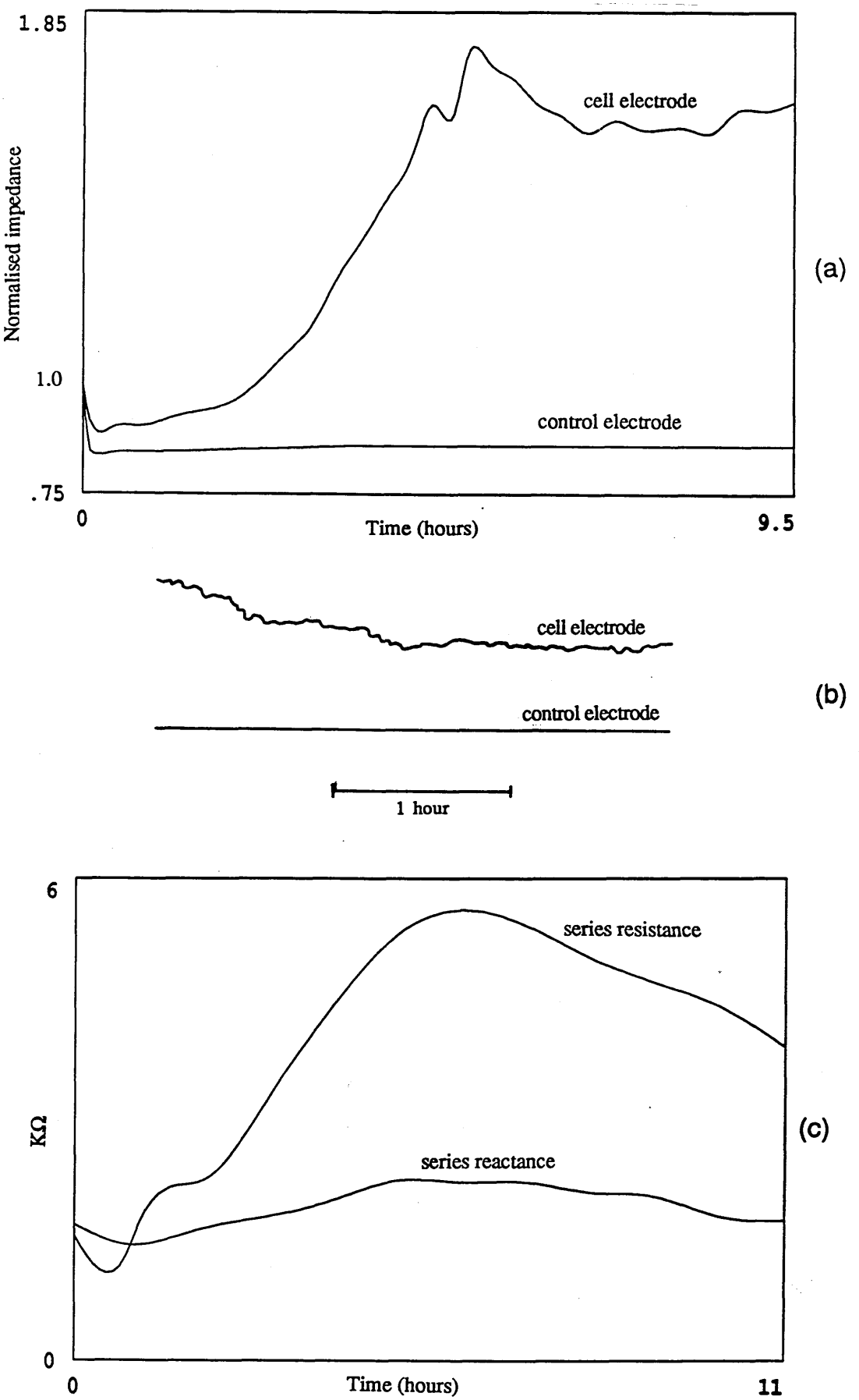

Figure 4.7 (a) The variation in the normalised impedance with time for BHK cells cultured on a heavily platinised gold electrode with dimensions 0.2x0.7mm. (b) a section of (a) displayed with a faster time base, and (c) the reactive and resistive components of the measured impedance (not the same experiment shown in (a) and (b).

blocking the electrode current is dependent on the electrode surface and on the cell type. Considering the effects produced by electrode platinisation, it would appear that the cause of the cell induced impedance changes is due to physical and not chemical changes produced on the electrode surface. This is clear from the differing results obtained with the light and heavy platinum deposits. Although both will have similar surface chemistry, a comparison of the scanning electron micrographs shown in figures 3.6(a) and (b) indicates the vastly differing surface roughnesses which they possess. In order to further clarify the importance of this factor in cell adhesion two additional electrode surfaces were investigated, namely electroplated gold, and plasma etched gold.

Gold plated electrodes

Figure 3.7 demonstrates that by electroplating these large electrodes with a current density of 15mA.cm^{-2} for 30 seconds, it was possible to produce a surface texture similar to that achieved with high current density platinisation. Whilst spread cells could not be observed easily using phase contrast on this surface, reflection microscopy did show that cell development on these electrodes followed a normal time scale (figure 4.8). Figure 4.9 shows the variation in impedance upon the introduction of BHK cells into one side of the dish (n=6), and follows a similar trend to that observed with the heavily platinised electrode. The maximum deviation in impedance occurs after approximately 16 hours and is of magnitude 0.6KΩ, or 40% of the equilibrium (at 37°C) electrode impedance.

Plasma etched gold electrodes

In an attempt to produce a microrough gold electrode surface by a subtractive, rather than additive process, electrode patterns were subjected to a 5 minute oxygen plasma etch under the conditions given in section 3.3.1. Scanning electron microscope examination however (figure 3.8), suggests that there is little physical alteration to the surface.

Figure 4.10 shows the variation in impedance with time, with both cell and control electrodes having been exposed to the same etch conditions. Again there is a significant rise in the impedance of the cell measurement electrode compared with that of the control, within 1 hour of seeding. This is followed by the fluctuations which were characteristic of cell activity on the platinised and gold plated electrodes. Although this experiment has only been carried out a small number of times (n=3), it suggests that other mechanisms, apart from surface roughness (unless roughness is increased at a scale below the resolution of the SEM examination process), may be involved in determining the response of the measured impedance to cell adhesion.

Before discussing further the significance of these results in terms of the strength of cell adhesion to an electrode, it is necessary to demonstrate that care must be taken in applying conclusions to different cell types. This is done by considering the extreme example of the growth of a confluent monolayer of MDCK epithelial cells on unaltered gold electrodes identical to those described above.

4.2.2 MDCK epithelial cell line

MDCK cells were maintained as described in section 2.5.3, and were introduced into one side the multielectrode device at a density of 5×10^5cells.ml^{-1}. Figure 4.11(a) shows a typical plot (n=6) of impedance versus time after the introduction of 0.15ml of the MDCK cell suspension into the cell side of

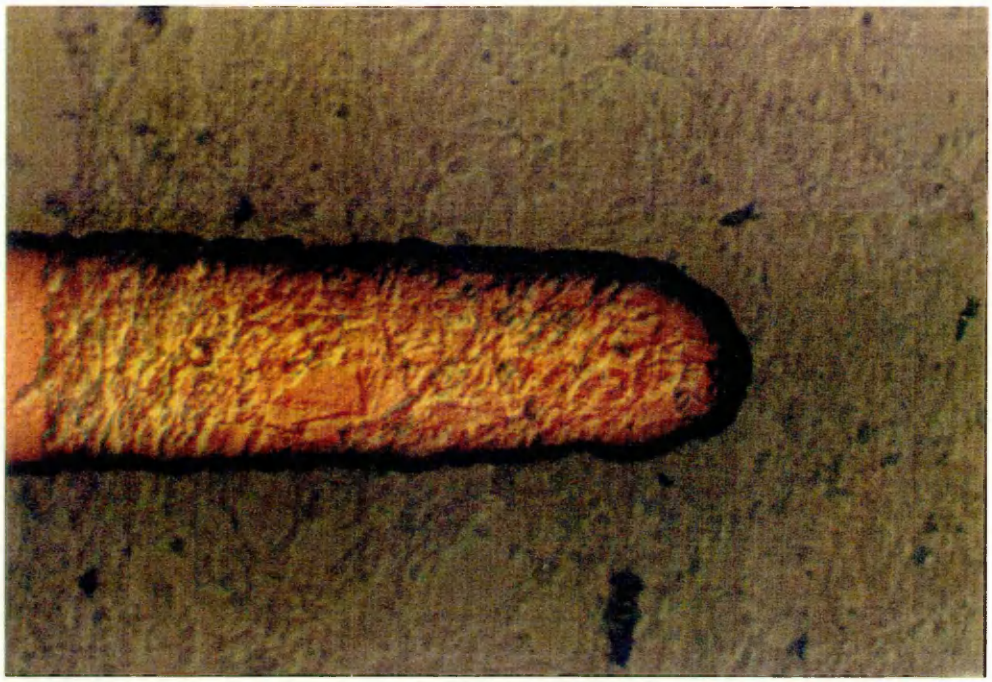

Figure 4.8 Reflection micrograph of BHK cells on a gold plated electrode. The magnification is ×140.

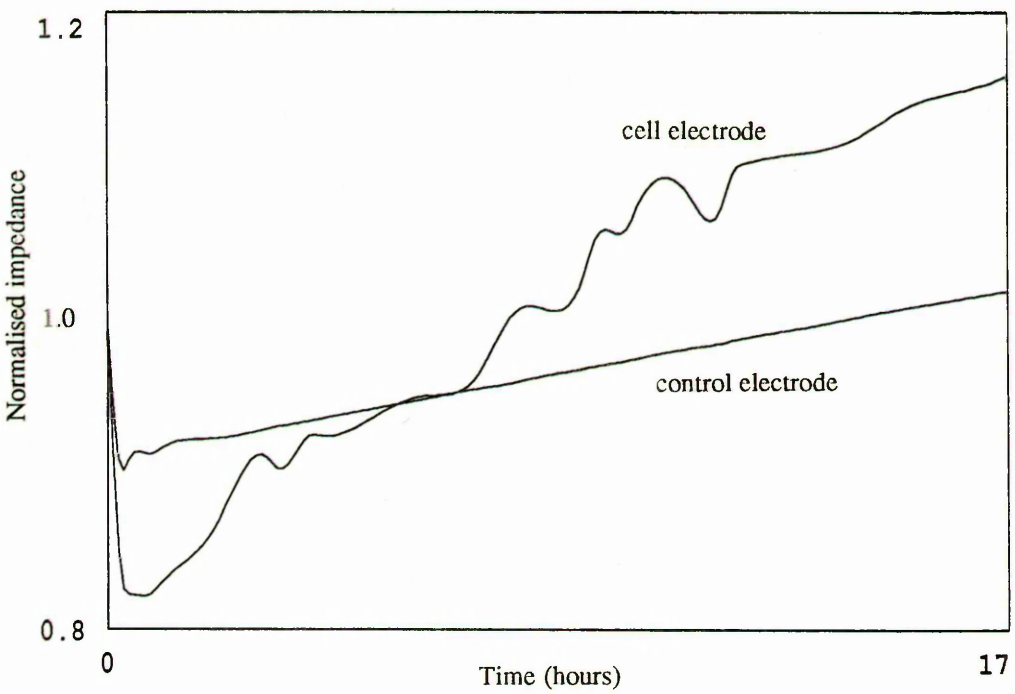

Figure 4.9 The variation in the normalised impedance with time for BHK cells cultured on a gold plated electrode with dimensions 0.2×0.7mm

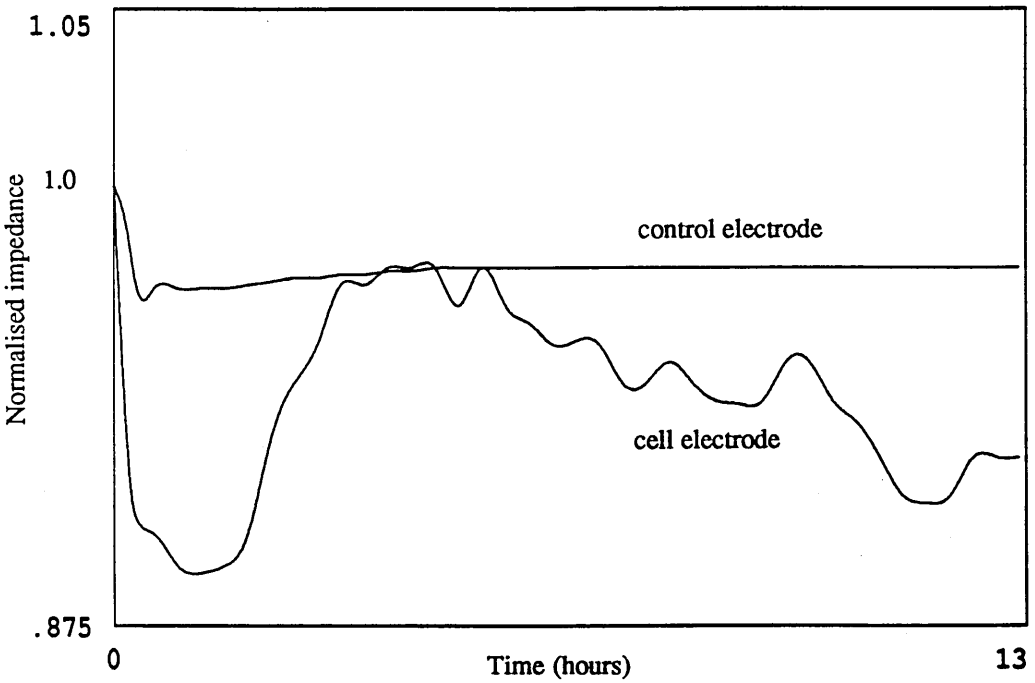

Figure 4.10 The variation in the normalised impedance with time for BHK cells cultured on a gold electrode with dimensions 0.2x0.7mm, previously subjected to an oxygen plasma etch.

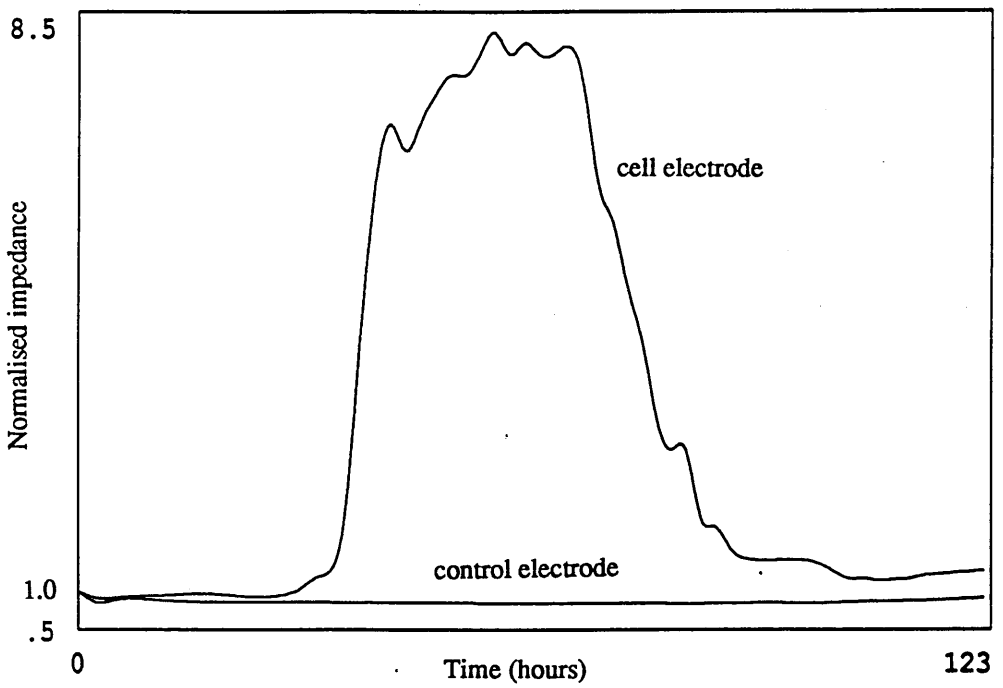

(a)

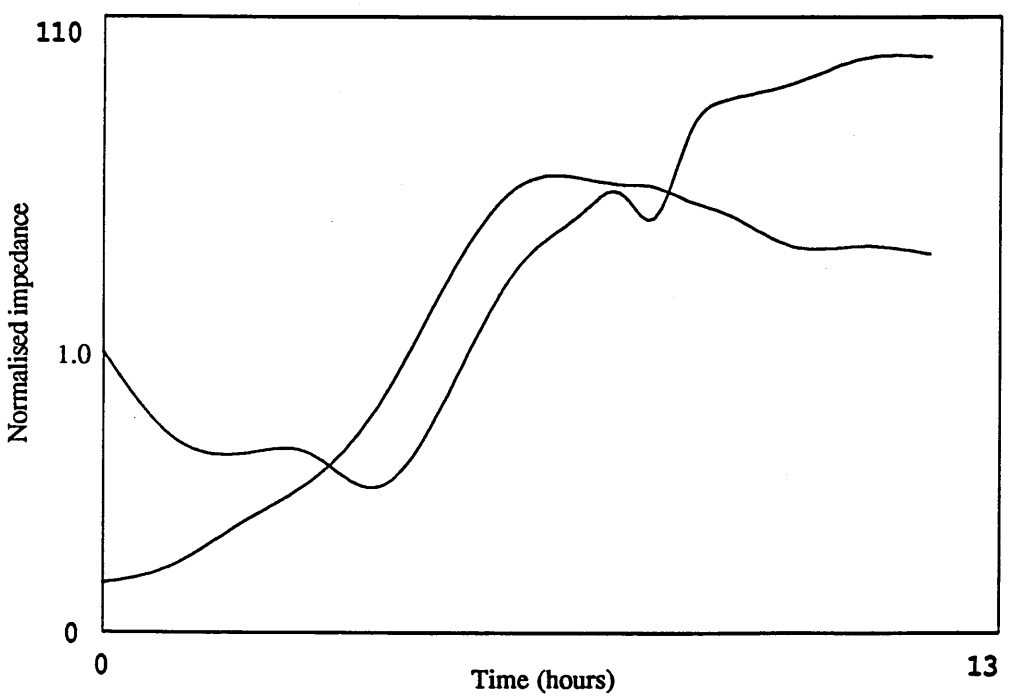

Figure 4.11 (a) The variation in the normalised impedance with time for MDCK epithelial cells cultured on a gold electrode with dimensions 0.2×0.7mm (b) The resistive and reactive changes occurring during a similar experiment.

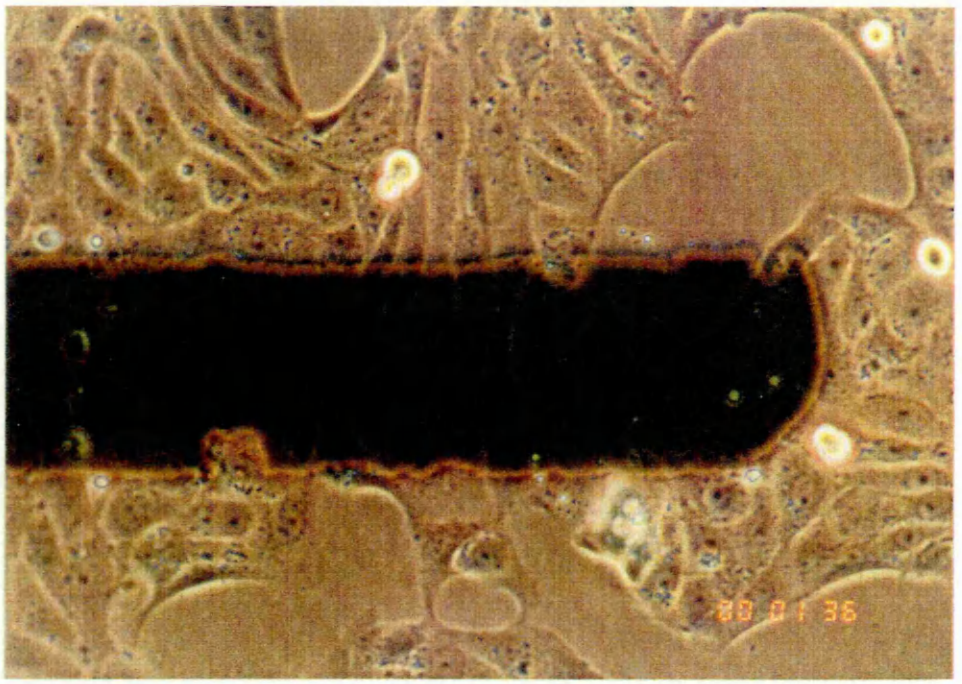

Figure 4.12 Phase contrast micrograph of MDCK cells cultured on a gold electrode with an applied field. The magnification is x150.

the pattern, and of a similar volume of fresh medium into the control side. After 35 hours there is a rise in the impedance of the cell measurement electrode by a factor of more than 7, over a period of only 1 hour. Following the initial rise the impedance remains relatively high until approximately 65 hours, when it returns almost to its original value.

Figure 4.12 shows a phase contrast micrograph of a confluent layer of MDCK cells cultured on an unmodified gold electrode. It is obvious that these cells differ greatly in morphology from fibroblast cells, and unlike fibroblasts they tend to form tight monolayer sheets which are relatively impenetrable to a variety of ions. It is this property which is responsible for the enormous rise occurring in the impedance, and probably not the effect of individual cell-electrode contacts. This is suggested by the negligible change in impedance over the first 35 hours, despite the substantial cell attachment and spreading that occurs within this period. It is not until the cells join together in a sheet that the impedance reacts very quickly.

Splitting the impedance into its series resistive and reactive components (figure 4.11b) shows that unlike the BHK induced impedance changes, the reactive component contributes significantly to the overall impedance rise (note that figure 4.11b was obtained from a different experiment than 4.11a). This is to be expected as the significant capacitance of the MDCK cell layer (C_{MDCK}) will be in series with the electrode capacitance (C_{el}), hence reducing the overall measured capacitance (C_{tot}). That is,

$$C_{tot} = \frac{C_{el} \times C_{MDCK}}{C_{el} + C_{MDCK}} \qquad (4.1)$$

The capacitance of the electrode without the cell layer, from figure 4.11b, after reaching thermal equilibrium is approximately 19.7nF. With the formation of a confluent layer this falls to a value of 9.7nF after 12 hours. From equation (4.1) the capacitance of the cell monolayer can be approximated as 6.5nF which, given that the electrode area is $0.14mm^2$, produces a capacity of $4.6\mu F.cm^{-2}$. If the cell

monolayer is considered as a continuous double sheet of cell membrane (consisting of an upper and lower membrane) as is illustrated in figure 4.13(a), the capacitance will have a value of one half of that of a single membrane layer. Given that membrane capacitance is typically around $0.8\mu F.cm^{-2}$ (Davey and Kell 1989), this suggests a bilayer impedance of $0.4\mu F.cm^{-2}$, which is substantially below that measured here. The discrepancy is almost certainly due to the membrane not being a uniformly flat surface, consisting in fact of a great many folds. Increasing the effective surface area would produce a rise in the capacitance per unit area, and comparing the experimental and theoretical values would indicate that this must rise by a factor of 11.5.

Surprisingly there appears to have been no previous measurements made of the capacitance across an MDCK epithelial cell sheet (given that they are a widely used and studied cell type). Measurements have been made (Gonzalez-Mariscal et al. 1985) however, of the capacitance between two neighbouring cells which were both penetrated by intracellular electrodes. The measured capacitance had a value of 45.1pF, indicating that each cell possessed a capacitance of 90.2pF. An epithelial cell may be modelled as a cylinder of height 5μm and radius 7μm, hence possessing a surface area of $836\mu m^2$ (figure 4.13(b)). A membrane capacitance of $0.8\mu F.cm^{-2}$ would suggest a cell capacitance of 6.7pF. Comparing this value with the 90.2pF obtained experimentally, the increase in surface area due to membrane folds must be nearly 13.5, which agrees well with that obtained above.

The resistance presented by the MDCK cell layer is simply added in series with the electrode resistance, and hence has a value of 57.6KΩ or a resistivity of $80.6\Omega.cm^2$ after 12 hours. This compares well with values which have previously been obtained by growing cells on filter paper ($80\text{-}140\Omega.cm^2$ (Taub and Saier 1979)), separating two immersed electrodes.

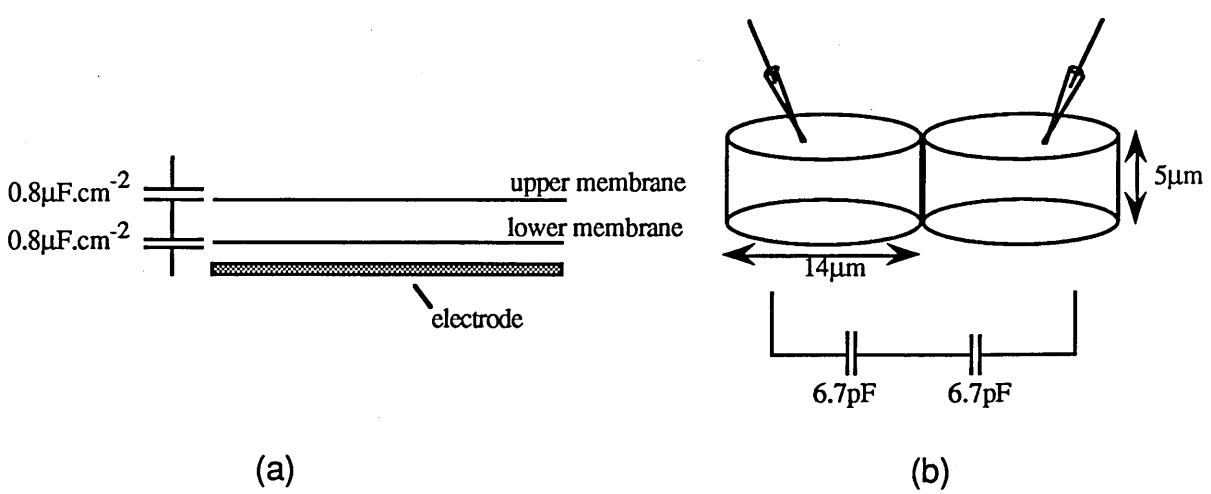

Figure 4.13 (a) An MDCK monolayer can be approximated by two continuous layers of membrane, each having a typical capacitance of $0.8\mu F.cm^{-2}$, giving a combined capacitance of $0.4\mu F.cm^{-2}$. (b) By approximating an MDCK cell as a cylinder of appropriate dimensions, the capacitance between two neighbouring cells may be approximated. Comparison with experimental data allows an estimation of the true cell surface area to be made.

4.2.3 Discussion

The results obtained above have clearly demonstrated that electrode impedance measurements can act as a sensitive detector of cell attachment and activity. It is also clear however, that care must be taken to eliminate or compensate for additional factors. Variations in temperature for example, can lead to fairly significant changes in the impedance, with both the resistance and the reactance observed to fall with increasing temperature (a rise in the temperature from 21°C to 37°C typically gives rise to a 5% reduction in the impedance). Consideration of equation (3.2) which was derived from the Butler-Volmer equation, suggests that for low values of overpotentials (<10mV) electrode resistance should increase proportionally with temperature. This discrepancy may be explained by the process of the diffusion of reactive species to the electrode from the bulk solution, where the diffusion flux is proportional to the temperature (Bockris and Reddy 1977c). This is seen from the relationship which describes the steady state diffusion flux J_i, down a concentration gradient c_i, i.e.

$$J_i = - BRT\frac{dc_i}{dx} \qquad (4.2)$$

where B is an undetermined phenomenological constant (related to ionic mobility), R is the gas constant, and T is the temperature in Kelvin. If electron transfer across the electrode is diffusion limited, it is this temperature dependence which will dominate the reaction, and will result in a resistance which decreases with increasing temperature. This suggests that even at the relatively low over potentials used in these experiments, electron transfer is diffusion limited.

Temperature effects can easily be minimised by maintaining cultures at a constant temperature. The variation in the incubator temperature over the duration of experiments was less than 1% (after the initial warming period), with the resulting impedance variation being of similar size. These are obviously insignificant when compared to the cell attachment induced changes. Significant drifts in the impedance of electrodes were observed however, which were due neither to temperature nor cell attachment. There exists three main possible explanations for this phenomenon.

(1) Protein adsorption onto the electrodes from the serum which is contained in the growth medium. It may be possible to determine the significance of this, by varying the serum concentration of the medium, although this itself is known to alter the cell adhesion process.

(2) The changing ionic concentration of the medium due to cell metabolism. This could alter both the conductivity of the medium and the impedance of the electrode double layer. Preliminary investigations have shown that refreshing the medium at regular intervals can sometimes reduce the drift rates, but the results are far from consistent.

(3) Electrode surfaces had not stabilised completely. This was pointed out in the previous chapter, where the variations in electrode impedance were observed (using serum free saline).

Without further studies it is impossible to identify which of the above is/are responsible for electrode drifts, but it is apparent that care must be taken in attributing them to cell activity given that control and cell measurement electrode impedances can drift at differing rates.

It is important at this point to note that, in the case of BHK fibroblast cells, the results presented thus far do not demonstrate with absolute certainty that the impedance changes resulting on cell attachment, are a definite indicator of cell adhesion (although they can undoubtedly be correlated with cell attachment). They may be due for example, to ionic fluctuations occurring in the vicinity of the cell, or to interactions

between the cell membrane charge and the electrode double layer. The latter explanation has already been questioned due to the exceedingly small distance which the double layer penetrates into the solution (0.5nm), when compared to the relatively large distance from the electrode to the majority of the lower cell membrane surface (100nm). The effect of ionic concentration variations in the vicinity of the cell-electrode gap cannot be ruled out however, as equations (3.3) and (4.2) indicate that the double layer capacitance and the diffusion limited current density will be sensitive to the ionic concentrations.

Considering the change observed mainly in the series resistive component of the heavily platinised electrode impedance upon cell attachment, this could be viewed as the resistance of the cell monolayer adding on top of the electrode-electrolyte series resistance whilst leaving the series reactive component almost unaltered. Cell spreading would increase the resistance even further (as was observed). The impedance change can however be represented as a variation in the parallel resistive and reactive components due to the local change in ionic concentrations. Later results concerning instantaneous impedance changes resulting from the placement of individual neurons tend to favour the physical blocking of current as the correct mechanism.

Whilst both evaporated gold and lightly platinised electrodes produce no impedance changes upon cell attachment, roughened electrodes of the same material produce clear rises in impedance over times which correspond to the occurrence of cell attachment and spreading. Figure 4.14 shows the surface profiles of all the electrode surfaces used above, and confirms the differing roughnesses of each (obtained using a Tallystep profilometer as described in section 2.7). There would appear to be little corroborating evidence to date for the effect of roughness on cell adhesion, due to the problems already pointed out concerning the visualisation of the interface by optical microscopic techniques, except for the limited evidence of improved thrombus attachment to micro-roughened implants. It should however be possible to quantify adhesion by using mechanical shear forces, commonly applied via a rapidly flowing solution (Weiss 1961).

Given the impedance changes observed upon the attachment of BHK cells to plasma etched electrodes, it is clear that factors other than roughness are important in determining the state of cell adhesion and activity. In this particular case it is again not immediately apparent what effect the plasma has on the gold surface which induces the impedances changes. Two possibilities are either a roughening of the surface which is below the resolution of the SEM, or a modification of the surface charge (3.1.2 described how adhesion to plastic surfaces is improved by exposure to an oxygen plasma).

It may be the case that neuronal adhesion will exhibit a similar dependence on roughness (and also on plasma exposure, though this is left to future studies), and that the amplitude of extracellular signals can be increased by modifying the electrode surface. Before this can be verified, it is necessary to extend measurements to microelectrodes, and to verify that the attachment of single cells can be observed. Whilst the experiments carried out using the MDCK epithelial cell line were useful in demonstrating the different results that may be obtained with different cell types (albeit with an extreme example), it is appropriate to continue with the BHK fibroblast line as these cells tend to remain isolated in culture i.e. they don't form intercellular junctions.

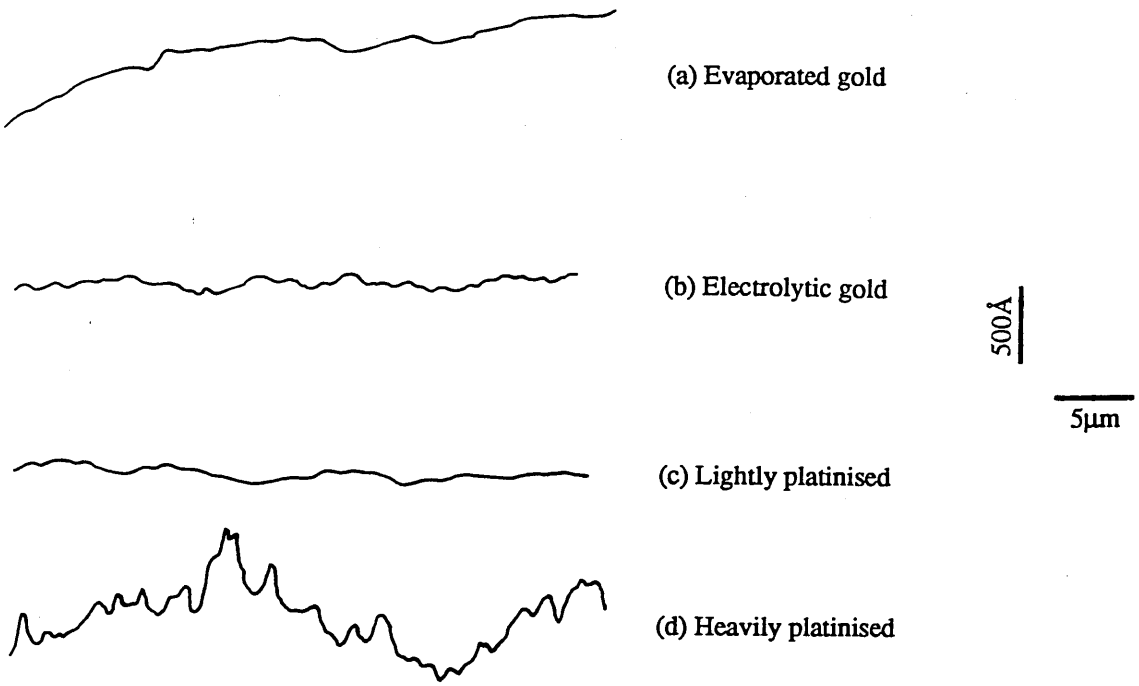

Figure 4.14 Surface roughness profile of the electrodes used for impedance measurements. These were obtained using a Tallystep profilometer.

4.3 MICROELECTRODE-CELL IMPEDANCE MEASUREMENTS

In the process of extending the above technique to allow the study of the neuron-electrode interphase, which is hidden from more conventional techniques, the effect of BHK cell adhesion on the impedance of both smooth gold and platinised microelectrodes was monitored. The results indicate that it is possible to to detect single cell attachment and activity, and that development is unaffected by the large electric fields required.

4.3.1 BHK fibroblast cell line

Microelectrode arrays fabricated according to the procedures detailed in section 2.3, were used in the following series of experiments. Electrodes were exposed by etching a 10μm wide groove through the insulating layer, this being either silicon nitride (~2μm thick), polyimide (PIQ-4200, ~4-5μm thick), or a sandwich of polyimide on silicon nitride. This created 10×10μm 'active' electrode sites exposed to the cell culture medium.

Initially silicon nitride was the chosen insulator due to its mechanical strength and its durability in a saline environment. Early experiments with confluent BHK cell cultures however, produced cells aligned in the direction of the electrode conductors, i.e. perpendicular to the groove. The length of the polarised cells exceeded the width of the grooves, and it was probable that they were straddling the grooves and were not making contact with the electrodes. Examination of Figure 4.15, which shows a SEM of a cross-sectional cut through one of these Si_3N_4 insulated patterns, makes clear the reason for this somewhat unexpected alignment.

After the exposure and development of the photoresist, the metal layers are evaporated onto the surface forming the electrode conductors after lift-off. Due to the layout inside the evaporator, the metal is evaporated at a slight angle and tends to coat one of the resist sidewalls (obviously the chlorobenzene soak process does not completely overcome this problem, see section 2.3.2). After lift off there remains a tail along the length of one side of the conductors, becoming amplified with the deposition of 2μm of silicon nitride. Although these ridges are relatively small, the effect of 32 converging electrodes (on each side) is enough to swamp any guidance produced by the groove and to align the cells perpendicular to it, especially in a confluent cell monolayer.

Two techniques were available which could eliminate this unwanted effect, the first being the removal of the metal tail by modifying either the resist profile or the position of the evaporation source with respect to the patterns. Neither of these methods proved successful, and a second method was used which involved the use of a further insulating layer of polyimide. This is a viscous liquid which is spun onto the device, and which produces a relatively planar surface with excellent step coverage. In this way the underlying ridges are masked, with plasma enhanced reactive ion etching again used to expose the electrodes. Using such patterns cells were found to align well, in and adjacent to the grooves. The width of the grooves was such that only one cell could lie across the width of the groove, and hence only one or two cells (head to tail) could lie over an electrode. Although polyimide on its own will acts as an adequate insulating material its mechanical strength is very poor, with the surface being prone to scratch damage. For this reason the polyimide was usually deposited on top of a previously prepared layer of silicon nitride. Thus whilst the silicon nitride prevented the unwanted exposure of the conductors by scratching, the polyimide produced the necessary surface planarisation. In order to expose the active electrode sites, a two process etch was required, the first being an oxygen etch of the polyimide layer followed by a C_2F_6 etch of the nitride.

BHK cells cultured on these patterns appeared to attach and develop normally both on the polyimide surface and in the grooves. Imaging cells in the groove did prove difficult however, as phase contrast microscopy is most suitable for observing cells on planar substratum and not when in proximity to sharp steps.

All measurements were carried out with a 1KHz ac field, and a constant current density of approximately $32mA.cm^{-2}$. This value far exceeds that used to monitor the impedance of cells growing on the large electrodes ($0.7mA.cm^{-2}$), but does lie within the linear region (impedance versus current density) shown in figure 3.15. Such a large current density was required in order to maintain a reasonable signal to noise ratio in the detection of the potential drop across the electrode (for signal levels below 1mV, noise levels started to become significant). It was not anticipated that this would in any way affect cell growth, or cause irreversible electrode damage.

Plain gold microelectrodes

Control electrodes were separated from the cell side of the dish by the cellulose nitrate membrane described previously. Of the 64 electrodes located on the cell side only one was monitored at any one time, for comparison with the control electrode. Under the applied field (see above) the impedance of the gold electrodes ranged from 3-5MΩ. Figure 4.16 shows the impedance versus time for both the cell

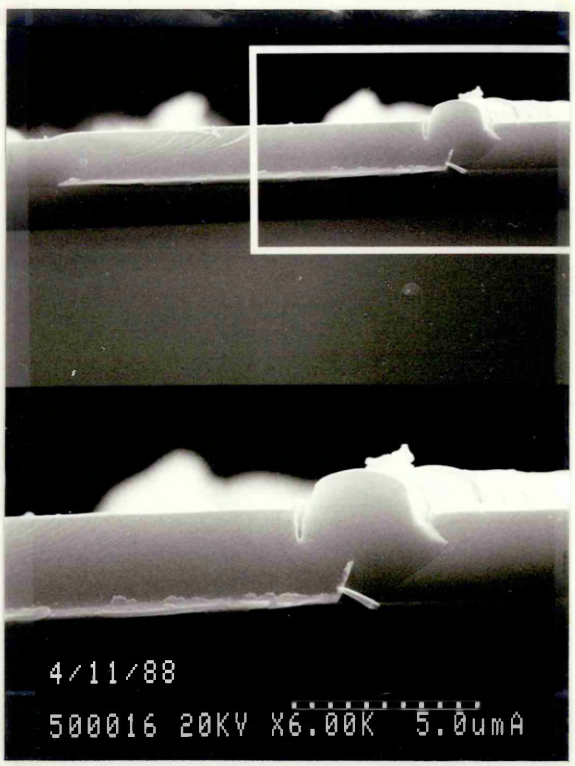

Figure 4.15 Scanning electron micrograph of a microelectrode, showing the electrode 'tails' which remain after lift-off. These often caused cells to allign themselves across the groove.

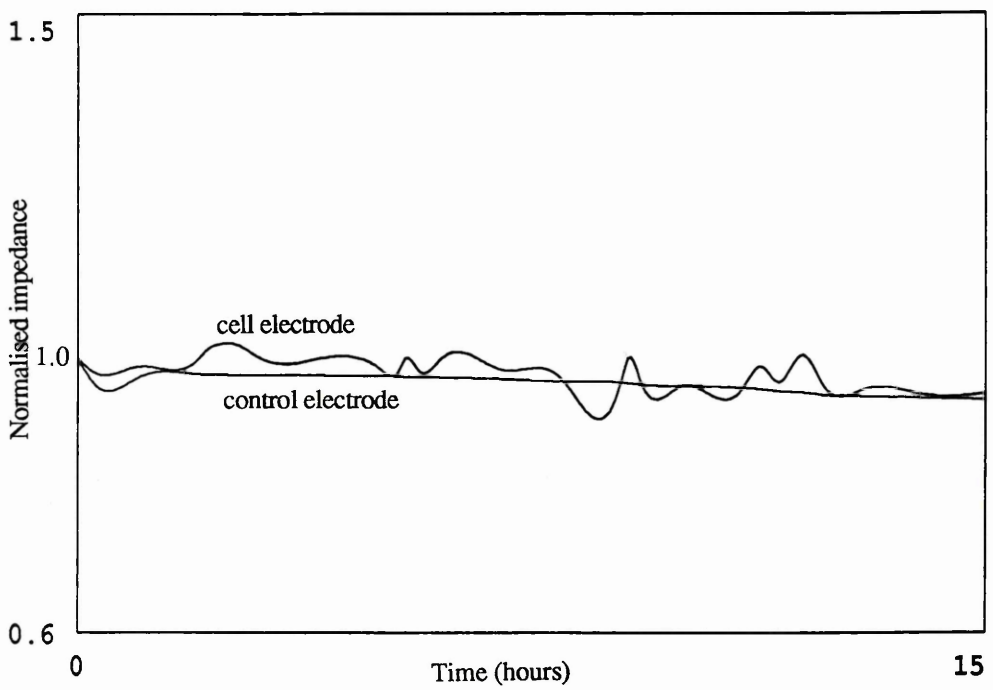

Figure 4.16 The variation in the normalised impedance with time for BHK cells cultured on a 10×10μm gold microelectrode.

measurement and control electrodes, immediately after the inoculation of 0.3ml of a BHK cell suspension, with a cell density of 4.10^5cell.ml^{-1}. It is apparent that there are some fluctuations occurring in the impedance of the cell side electrode compared to that of the control electrode, but these are of relatively small amplitude both in magnitude and as a fraction of the total measured impedance. The presence of cells around and on the cell side microelectrode was noted microscopically during the experiment. It should be noted that the results obtained with different electrodes show some variations, often with no indication of impedance changes.

This variability may be due to the slightly different durations for which the electrodes are exposed to the plasma etch, during their fabrication. After etching through the insulating layer, it is inevitable that the surface of the electrodes will be exposed to the plasma for a short time. If this time is sufficient to produce the changes which were observed with the large electrodes after etching, then the surface may be more suitable for cell adhesion. Electrode surfaces exposed for only short times will probably remain almost unaffected.

Platinised microelectrodes

Obviously the next step would be to reproduce the platinised surface which proved successful with the large electrodes. It is not possible to exert a similar degree of control in the platinisation of microelectrodes, due to the greater influence of diffusion limits (see section 3.2.1). The two levels of platinisation used with the large electrodes, 9 (which showed no resulting impedance changes) and 18mA.cm^{-2} (which produced an impedance rise upon cell attachment), would require currents of 10.8 and 21.6nA respectively. It did not therefore prove possible to investigate the impedance response of 'lightly platinised' microelectrodes to cell adhesion, and only results obtained with heavily platinised electrodes are described below.

After platinising the cell measurement and control electrodes with identical currents, impedance measurements were made with the same 1KHz, 32mA.cm^{-2} constant current. Despite the identical electrode preparation there remained slight differences in the impedances of the two electrodes, generally between 20 and 50%. Figure 4.17a shows the variation in impedance with time over the 14 hours following inoculation with the cell suspension (0.3ml at 4×10^5cells.ml^{-1}). Whilst the control electrode impedance remains stable, that of the cell measurement electrode proceeds to fluctuate greatly almost immediately after thermal equilibrium is reached.

It has previously been noted that a volume of 0.3ml and a density of 4×10^5cells.ml^{-1} is sufficient to produce an almost confluent layer of spread cells within 1-2 hours, and that there is therefore a high probability that a cell will settle onto the selected microelectrode within this period. Even if no cell initially attaches to it, it is almost certain that within a short time a cell will move on top of it given the high degree of motility that fibroblasts exhibit. The maximum rise observed in figure 4.17a is approximately 50% of the initial impedance reached at thermal equilibrium. The largest fluctuations also return the impedance at some points to within a fraction of its initial value. This would be expected as the averaging effects of many cells, observed with the large electrodes, will not occur and the attachment and motion of the single cell would exhibit a proportionally greater effect.

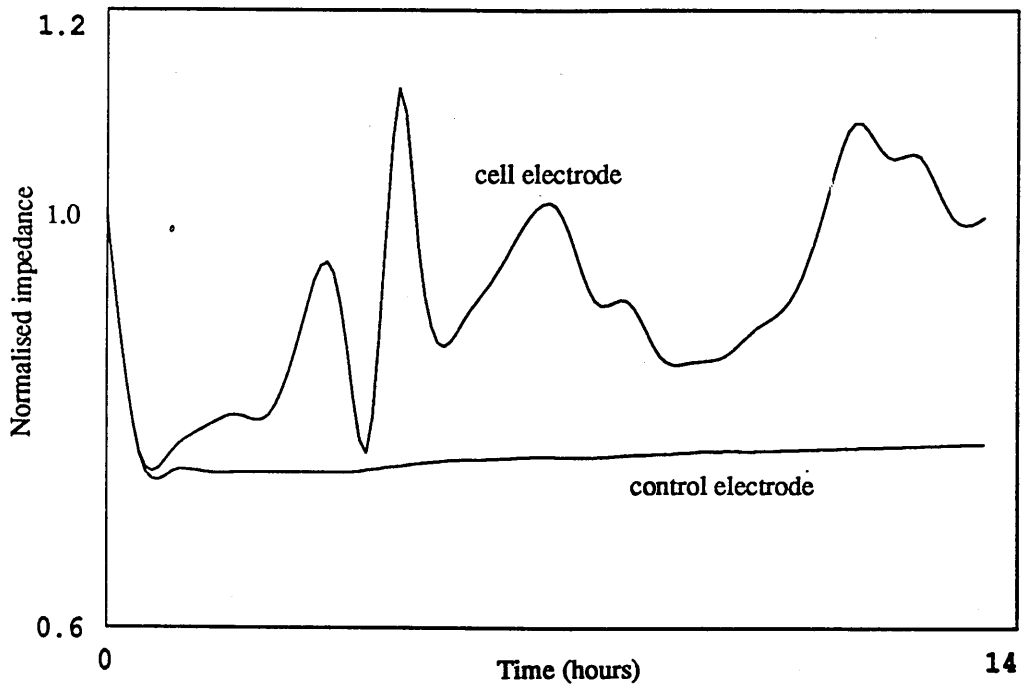

(a)

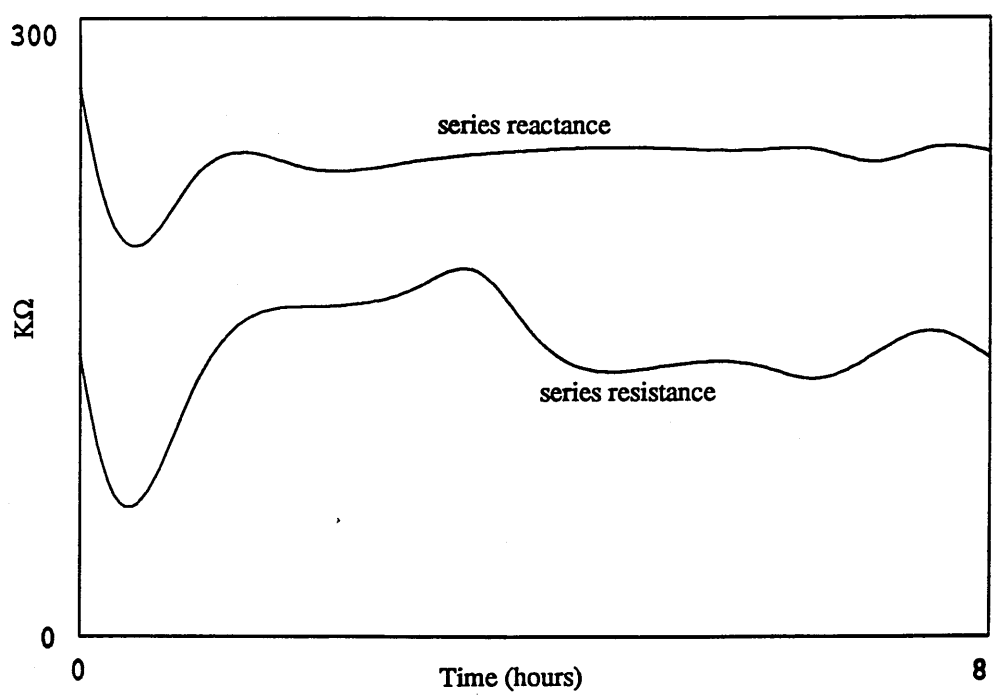

(b)

Figure 4.17 (a) The variation in the normalised impedance with time for BHK cells cultured on a 10x10μm platinised microelectrode, and (b) the changes occurring in the resistive and reactive components for a similar experiment.

As has been described previously, it is possible to fluorescently stain cells in order to observe them more clearly. Correlation of cell activity with impedance changes using this method however, has proved difficult due to both the rapid bleaching of the dyes and to the extremely short working distance required by the microscope objective. Bleaching severely limits the total cell exposure time to less than one minute, insufficient for either time lapse or single shot, periodic, observation, whilst the working distance (less than 1mm) required, means that the dish is insufficiently filled with medium, resulting in significant impedance changes due to evaporation (constantly emptying and refilling the dish would also give rise to corresponding impedance fluctuations). To date, only single micrographs of cells on electrodes have been obtained, with impedance monitoring carried out until the staining and photographing process, and terminating after this point. Figure 4.18 shows a fluorescent micrograph of a BHK cell on a microelectrode, after a rise in impedance of 20KΩ had been observed.

Figure 4.17b shows the variation in the resistive and reactive components of the impedance, for a similar experiment. It is apparent again that the variation in impedance is almost entirely due to an increase in the series resistance, with only a slight corresponding variation in the reactive component. In an attempt to estimate the purely resistive change produced by a cell in close proximity to a microelectrode, the model shown in figure 4.19 was considered. This assumes that the increasing resistance is due to the constriction of current flow through the tight gap between cell and electrode, and not to any double layer interactions. Considering the lower surface of the cell to be perfectly flat and completely insulating (and possessing identical dimensions as the electrode, a×bμm), the boundary condition at the upper surface of the gap is that no current may flow in the z direction, i.e. $d\Phi/dz=0$, at $z=0$. In addition the boundary at $z=c$, is the microelectrode which is held at some potential V_0. The remaining four sides represent the paths through which the current flows into the bulk solution and are effectively grounded. In order to calculate the resistance through the electrode to ground, given the voltage V_0 on the electrode, it is

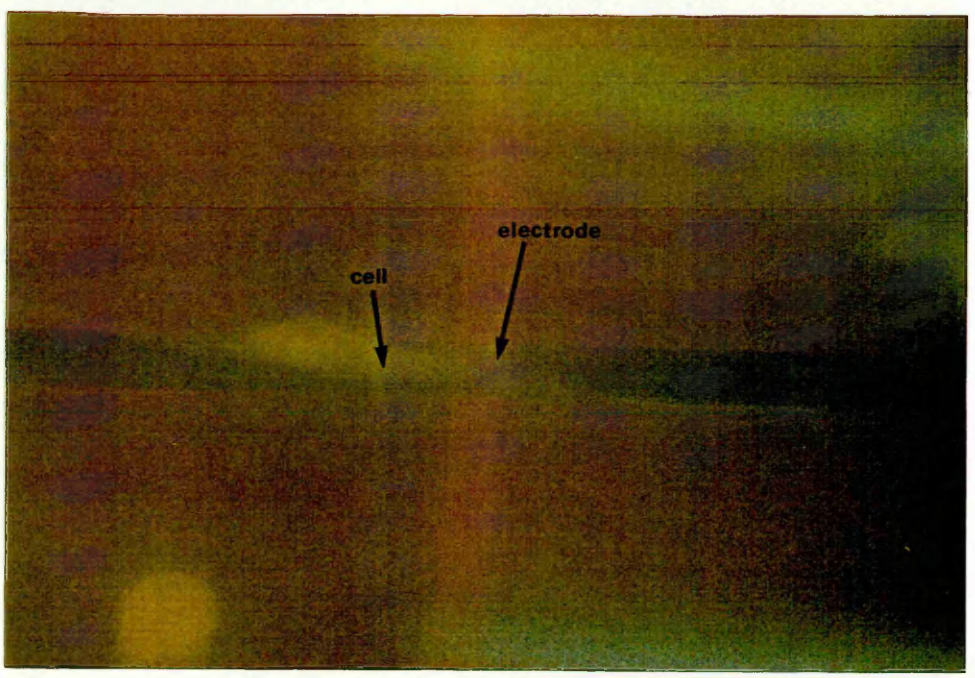

Figure 4.18 Fluorescent micrograph of a BHK fibroblast spread over a microelectrode.

necessary to evaluate the current flowing across the electrode into the solution. This requires the solution of Laplace's equation

$$\nabla^2\Phi = 0$$

in three dimensions.

The solution (see appendix I) gives the resistance, R, as

$$R = \frac{1}{\sum_n \sum_m \frac{-64ab\sigma}{(mn\pi^2)^2} \tanh Pc} \qquad (4.3)$$

where σ is the conductivity of the medium, a b and c are the dimensions of the gap in the x y and z directions. The denominator is a doubly infinite summation over the constants m and n, which can have any positive, odd value.

Figure 4.20 plots the variation in resistance with increasing cell-electrode separation distance, for electrode dimensions of 10×10μm, and a medium conductivity of 0.00333S.cm^{-1}. This indicates that for large separation distances (>100nm), the effect on the overall measured impedance will be of a similar order to the impedance drifts which are observed during measurements. For very small gaps (<5nm) the effect starts to become significant, when compared to an electrode impedance of 100KΩ to 1MΩ. These values for small separation distances are of a similar order to those measured experimentally with the heavily platinised electrodes, and may suggest that the bulk of the lower cell membrane is pulled into a much closer contact than is the case with gold electrodes. If these values are approximately correct, they also bring into question previously estimated values for cell-substrate separation distances as discussed in section 3.1.2.

These results can only be a crude approximation to the situation pertaining at the interphase, where the lower cell surface is certainly not uniform consisting as it does of focal contact, close contacts, and membrane folds. Equation 4.3 also indicates that significant changes in the ionic concentration, leading to changes in the conductivity of the gap region, may also produce large changes in the measured impedance.

Attempts have been made to correlate impedance fluctuations with cell attachment and motion observed with time lapse video. As has been noted, good phase contrast images are difficult to obtain due to both the blackness of platinised electrodes and the proximity of the sharp sidewalls of the groove. It has only been possible to observe the attachment and motion of cells close to the electrode being monitored, and to follow them as they apparently move over the electrode where they then disappear from view. The likelihood of observing a cell responsible for an increase in the impedance is greater with very low density cultures, and this has allowed some major impedance fluctuations to be attributed to single cells moving onto and off of the microelectrodes. It has not been possible to say whether any of the smaller changes are due to changes in cell morphology, or to cell division, but these remain likely possibilities.

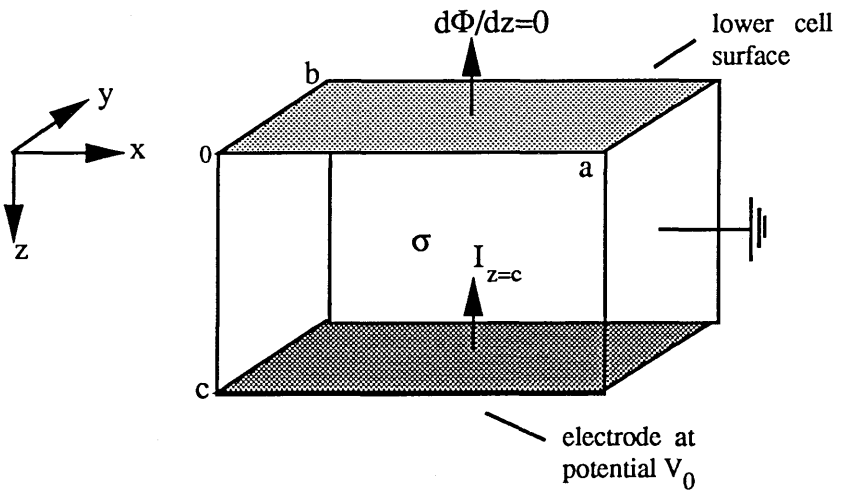

Figure 4.19 To estimate the additional resistance due to the narrow cell electrode gap, it is necessary to solve Laplace's equation for this region. The lower cell membrane, considered to be insulating, is a distance c above the electrode which has dimensions axb. The conductivity of the medium filling the gap is σ. All four sides exposed to the bulk solution are effectively connected to ground.

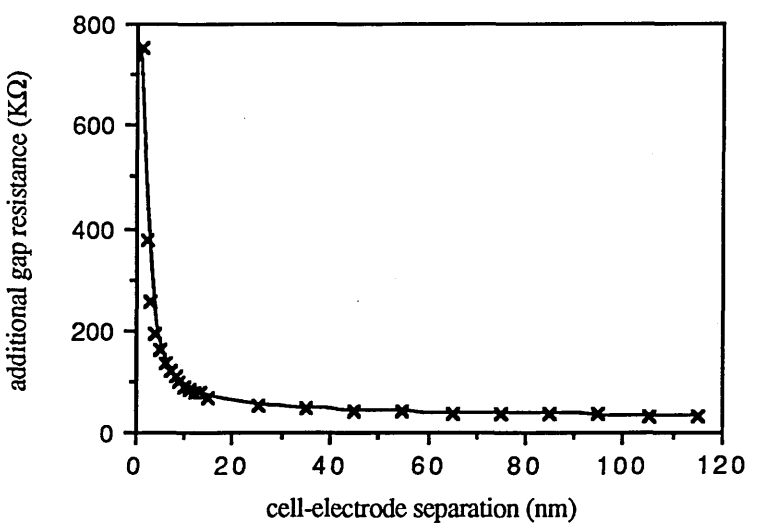

Figure 4.20 Resistance presented by the cell-electrode gap, as obtained from (4.3)

4.3.2 *Lymnaea stagnalis* neurons

It is now clear that the attachment and motion of a single fibroblast cell can be observed by the technique of continuous electrode impedance monitoring. It is obviously envisaged that studies should be extended to allow the process of neuron-electrode attachment and adhesion to be quantified. This would clarify the effects of surface roughness in this specific case, and would also allow the dynamic nature of the adhesion process to be monitored.

A variety of neuronal cell types were available for study, including vertebrate and invertebrate neurons. The former were neglected at this stage due to the difficulty in placing small neurons accurately on a microelectrode (neuronal cells are post mytotic, i.e. they no longer divide, and exhibit little motility in culture. It is therefore critical that initial attachment to the microelectrode occurs), and to the difficulty in obtaining an electrically excitable culture. Of the latter type, neurons from the pond snail *Lymnaea stagnalis* were already being cultured and recorded from in our laboratory. These neurons can show prolific outgrowth under suitable conditions, and their relatively large size (100-200μm in diameter) allows their accurate placement over electrodes (see section 2.5.4 for culture and placement techniques).

The multielectrode devices used in these studies differed from those described above, in that the active electrode sites were not exposed by a groove, but by 10μm diameter dots at the end of each conductor. Impedance measurements however, were made under identical conditions. It was observed that in order to obtain any response to cell attachment, the electrode had to be platinised to the extent that the platinum entirely filled the dot, as shown in figure 4.21. Under these conditions, the rise in the resistive component of the impedance was typically of the order of 5%. For example an electrode with initial resistance of 46KΩ, rose to 51KΩ upon cell attachment, over a period of less than 1 minute. The corresponding rise in the reactive component was typically less than 0.2% (e.g. 93KΩ to 93.2KΩ).

Neurons were extracted from a variety of the brain ganglia, but consistent cell outgrowth was difficult to achieve (a rare example of successful outgrowth is shown in figure 4.22). As such it did not prove possible to observe the electrode impedance with an attached and spread cell. This problem seemed to be due to the unsuitability of the polyimide surface, and to the difficulty in adequately cleaning it after re-use. This was in contrast to the relatively successful cell growth achieved on polystyrene tissue culture plastic. It was however possible to measure the changes which occurred in electrode impedance upon the initial attachment of cells, which were dropped onto their surfaces. This attachment, although not resulting in cell spreading and outgrowth, was relatively strong, and it required vigorous agitation to dislodge the cells from the electrodes. It is probable that adhesion at this stage is due to the electrostatic attraction between the charged cell surface and the concanavalin A coated substrate.

It is probable that these results owe more to the size of the neurons involved, than to any process of adhesion. This phenomenon was not observed with the smaller BHK cells (<10μm in diameter), with the impedance rising only once the cells had begun to spread. The time scale over which the change occurs also seems to preclude any adhesion mechanism, other than the relatively fast electrostatic attraction already indicated.

Figure 4.21 Scanning electron micrograph of a 10μm diameter dot microelectrode, used to detect neuronal attachment. This was only possible when the dot was completely filled with platinum black.

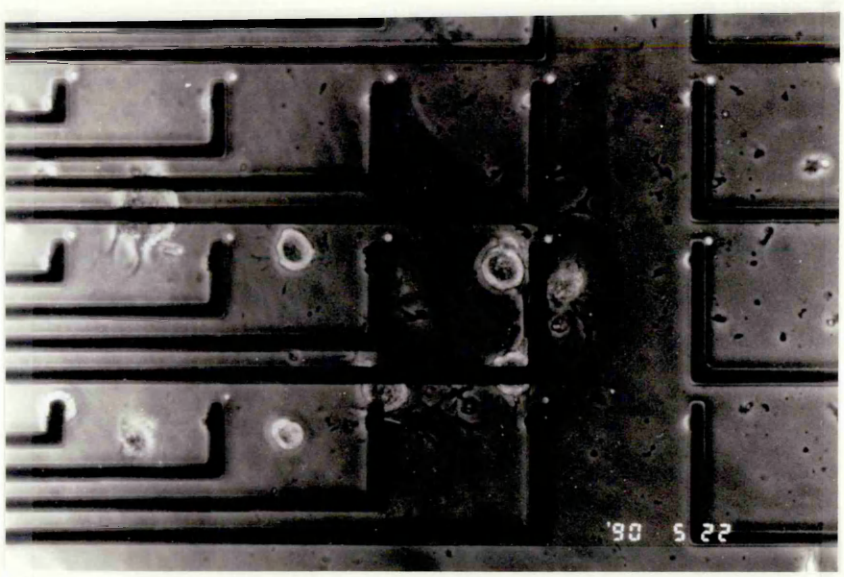

Figure 4.22 Phase contrast micrograph illustrating a rare example of outgrowth from *Lymnaea stagnalis* neurons after 48 hours in culture.

4.3.3 Discussion

Considering now the results obtained with both fibroblasts and neurons cultured on microelectrodes, it still remains open to question what exactly is being observed during impedance measurements. From the limited evidence it would appear however that the impedance rises are due to a physical blocking of the current by the cell membrane, and not to some ionic changes in the locality of the cell. Whatever the mechanism involved, be it the complete blocking of certain portions of the electrode or the 'squeezing' of the current path into a small area between cell and electrode, the measured impedance can be directly related to that through which the transmembrane current must flow during an action potential (see figure 3.1b). That is to say that a large measured impedance suggests a relatively tight cell-electrode seal, and consequently will lead to a relatively high extracellular signal.

The impedance fluctuations in the case of BHK cells attached to platinised microelectrodes (and the lack of activity observed with smooth gold microelectrodes), tends to confirm the conclusions drawn from the experiments carried out with the larger electrodes, regarding cell attachment to roughened surfaces. In addition it has been possible to correlate directly, cell attachment and motion with the electrode impedance changes.

4.4 CONCLUSIONS

It is now clear that continuous electrode impedance measurements allow the detection of cell attachment and activity, on a scale varying from confluent cell monolayers to single cells. It is therefore a powerful technique in the study of cell adhesion to artificial substrates, allowing access to an interphase region which is often hidden from conventional microscopic methods. Perhaps its greatest advantages are its ability to monitor in real time and to produce no obvious cell damage. Used in conjunction with the electron microscopic examination of cell-electrode sections (both horizontal and vertical), it may be possible to answer many fundamental questions concerning the time course of cell adhesion and the effects of the substrate surface properties.

Cell impedance measurements may also allow the effects of a variety of pharmacalogical agents to be quantified. One example is the effects on cell motility produced by cytochalasin B and its solvent dimethyl sulfoxide (Me_2SO). The former is thought to immobilise cells with the latter acting as a solvent for cytochalasin B, restoring motion. This effect on a confluent cell layer has previously been detected as a cessation and restoration of impedance fluctuations by Giaever and Keese (Giaever and Keese 1984), but the extension to microelectrode and single cell studies would surely allow a clearer determination of the link between the drugs, cell motion, and impedance, due to the greater sensitivity offered.

Regarding the results obtained with the MDCK epithelial cell line, it was shown that the formation of a tight cell sheet, or epithelium, produced a very large impedance rise. Studies are already underway into the penetration of these sheets by neutrophils, which it is hoped to detect as a sharp fall and rise in impedance.

The application of impedance measurements has already demonstrated the improved cell-electrode seal obtained using roughened electrodes, with both electrolytically deposited gold and platinum producing a suitable surface. Of these it is believed that gold will produce the more suitable electrode due to its

superior mechanical strength. Although it has only been possible to date to monitor the long term adhesion of a single BHK fibroblast cell, it would appear possible to obtain similar results with a suitable neuronal cell type. Neurons from *Lymnaea stagnalis*, given suitable culture conditions and substrates, should prove suitable and in addition will allow the simultaneous recording of extracellular action potentials. This experiment would prove the link between signal amplitude and electrode impedance, and would also confirm the effect of electrode surface roughness.

CHAPTER FIVE

FINITE ELEMENT ANALYSIS OF ELECTRODE GEOMETRY

CONTENTS

5.1 INTRODUCTION

Chapter 1 introduced the concept of using the extracellular conductance as a means of increasing the potential surrounding an electrically active cell. In chapters 3 and 4 this was shown to be possible by improving the strength of cell adhesion to, and around, the electrode. This chapter considers the effect of the presence of the electrode and insulating boundaries themselves, with the use of the relatively novel technique (in biological applications) of finite element analysis.

Section 1.2.2 briefly described several methods previously used in the calculation of extracellular fields around both axons and cell bodies. These were generally analytical methods, which developed expressions relating the extracellular potential to either the transmembrane potential or the surface potential. Only limited consideration has been given to the effects of extracellular boundaries on electrically active cells, with one example concerning the potentials existing within a nerve trunk surrounded by a highly resistive tissue sheath (Clark and Plonsey 1968). Figure 5.1(a) illustrates this simple case of a single axon located within such a cylindrical sheath, with the sheath being modelled by a distributed resistive and capacitive network. This allows both the interstitial (within the sheath) and external potentials to be evaluated, given that the conductivities for both regions are known.

In a similar approximation to that used in obtaining the extracellular potential around a single axon in an infinite, homogeneous volume conductor, the transmembrane action potential can be simulated by the summation of three appropriately chosen Gaussians (see section 1.2.2). For an axonal radius of a=60μm, a nerve trunk radius of b=300μm, and a distance from the origin to the axon centre of R_s=150μm, the maximum extracellular potential existed at the axon surface and was shown to be approximately 1500μV. This is almost a 20-fold increase in the maximum potential for an axon in an infinite volume conductor. The magnitude of this increase illustrates the importance of including extracellular boundaries into calculations, and suggests the significant role that they may play in increasing the signal to noise ratios of recorded signals. In order to consider the effects of more complicated boundaries however, such as the

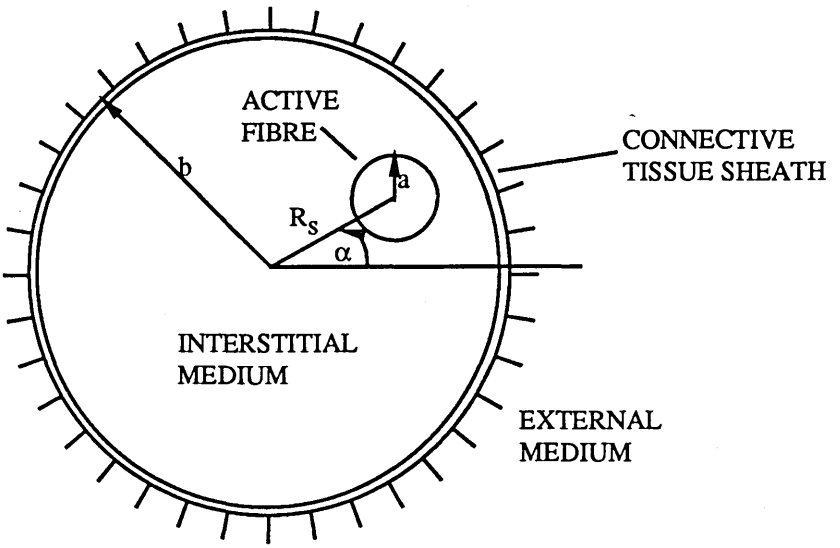

(a)

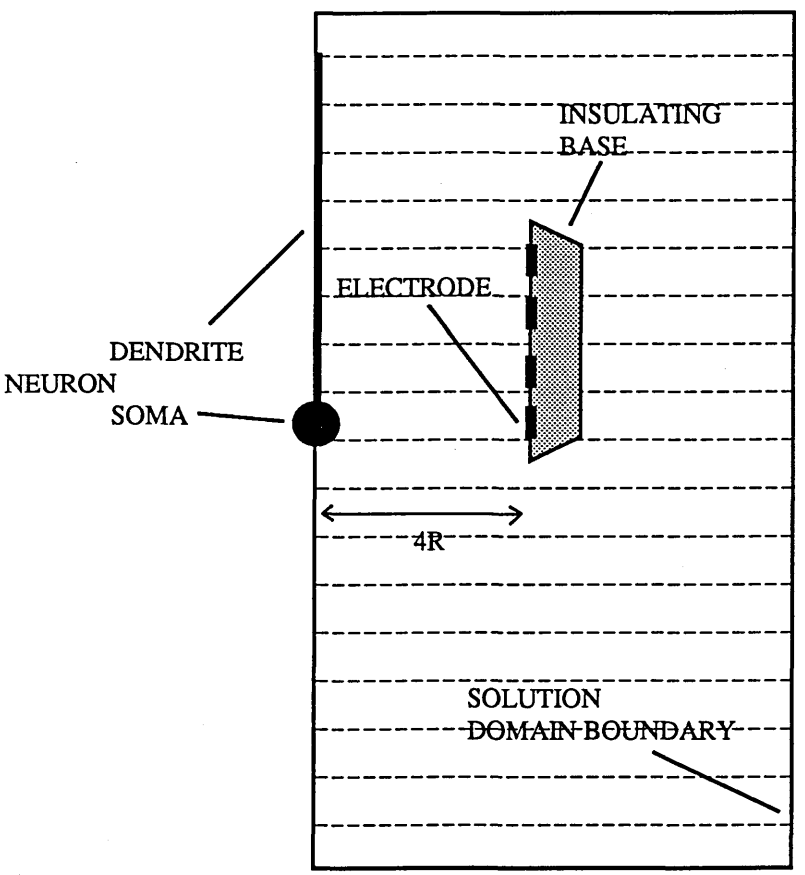

(b)

Figure 5.1 Two models previously used to consider the effect of extracellular boundaries on the extracellular potential. (a) Clark et al evaluated the extracellular potential generated by a single axon contained within a tissue sheath, whilst (b) Drake et al considered the perturbing effect of a multi-electrode probe on the field around a single neuron with a lumped dendritic process.

electrodes themselves, it is necessary to employ numerical field solution methods which generally require to be carried out on computer. These boundaries may be a mixture of straight, spherical, or curved types, and not simply the cylindrical type in the nerve sheath problem.

The perturbing effect of a multielectrode probe penetrating into nervous tissue on the extracellular potential has been approximated (Drake et al. 1988) using one such numerical method, the finite difference method. This problem considered a neuron located in a volume conductor, with the insulating base of the probe being located a distance of a few soma radii from the cell (figure 5.1(b)). One boundary condition consists of the membrane surface potential calculated using the Rall model (see 1.2.2), with the other presumably being an assumed zero potential a long distance from the cell. For a soma radius of 20μm the potential at a distance of 80μm was found to be 225μV without the inclusion of the electrode base. With this included the potential at the same point, i.e at the surface of the probe facing the cell, where the electrode would be located, increased to 325μV. This increase is due to the restricted current flow in the vicinity of the electrode probe, and despite the relatively large distance between cell and electrode is still seen to be significant.

This analysis again illustrates the importance of considering the location of the cell with respect to the electrode and also the precise electrode geometry. For the case of neurons cultured on a multielectrode array the cells will necessarily be in contact with the substrate, and for the case of optimum recordings will be directly above the electrodes. It would be expected from above that the increase in potential at the surface will be substantial, over that for a cell suspended in a volume conductor. Of potentially greater significance however, would be any increases due to partially enclosing the cell in a groove or a pit, where the extra insulating boundaries may further restrict the current flow. Such a problem, involving an electrically active cell in close proximity to geometrically complex electrodes, has not previously been considered, although several authors have solved the inverse problem. That is the ability of extracellular electrodes to stimulate, by current injection, neighbouring cells and nerve fibres (Rattay 1988)(Rubenstein et al. 1987)(Veltink, Van Alste, and Boom 1988). These calculations have generally involved relatively straightforward geometries, and have been carried out semi-analytically.

In order to solve the problem of irregular shaped cells with square or rectangular electrodes, a number of simplifications must still be introduced even after allowing for computer based numerical solutions. In order to assess which would be appropriate, and also to allow the appropriate analysis method to be selected, it is worth outlining the type of field problem involved in terms of boundary conditions and material properties.

Figure 5.2 illustrates a typical situation of a cell located above the base of an electrode pattern, which would be an insulator with metal electrodes embedded into it. The solution domain would be that volume V, contained above the substrate and within the distant region set to zero potential by the reference electrode. As only the extracellular field is required in this particular case, a further boundary is formed by the outer surface of the cell membrane. The maximum biological frequency of interest in this problem being in the region of 1KHz (since the duration of the fastest action potential is approximately 1mSec) it is possible to neglect inductive and capacitive effects in the medium, and to treat it as purely resistive. If in addition propagation delays in the transmission of the electric field from source point to field point are

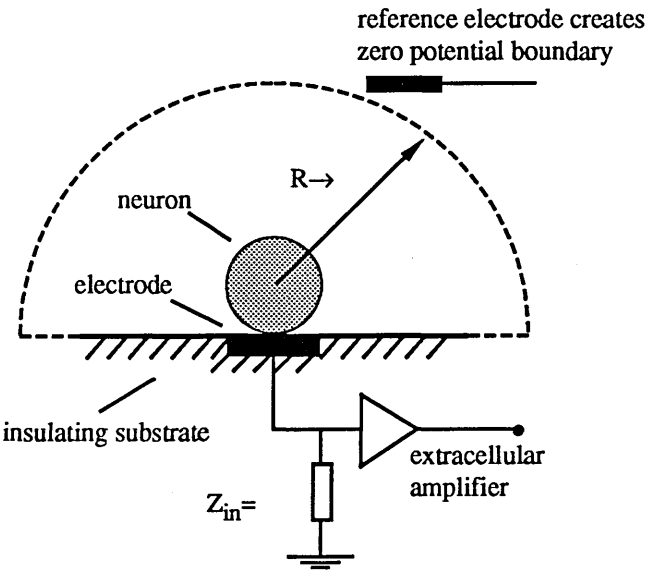

Figure 5.2 For a neuron situated directly above a planar microelectrode, the outer boundaries consist of the insulating substrate and the distant zero potential created by the reference electrode.

neglected, the problem can be considered to be quasi-static (Plonsey 1969). That is to say that the potential field at any point in time is dependent on only the conditions pertaining at that instant, and not on the field existing either before or after it. For such a field existing in an ohmic conductor the current density $\underline{J}$, is proportional to the electric field $\underline{E}$ through conductivity σ siemens per metre (S/m)#

$$\underline{J} = \sigma \underline{E} \tag{5.1}$$

and is derivable from a scalar potential, so

$$\underline{J} = -\sigma \nabla \Phi \tag{5.2}$$

For a stationary (i.e. time invariant) current, continuity requires that the net flow of charge out of any closed region be zero since there cannot be a build up or decay of charge within the region in the steady state. This can be written as

$$\oint_S \underline{J} \cdot dS = 0 \tag{5.3}$$

or in differential form

$$\underline{\nabla} \cdot \underline{J} = 0 \tag{5.4}$$

Substitution of (5.2) into (5.4), gives

$$\nabla \cdot \nabla \Phi \Rightarrow \nabla^2 \Phi = 0 \tag{5.5}$$

This is known as Laplace's equation, and defines the potential uniquely within a bounded region given the appropriate boundary conditions. Making use of Green's theorem

$$\int \left(\Phi \nabla^2 \psi - \psi \nabla^2 \Phi \right) dV = \int (\Phi \nabla \psi - \psi \nabla \Phi) \cdot dS \tag{5.6}$$

where in this case Φ is the above scalar potential and ψ is defined as $1/|\underline{r}|$, where $\underline{r}$ is the distance vector between the field point and the source point. The left hand side of (5.6) represents an integral over the entire volume V of the bounded region, whilst that on the right hand side represents an integral over the surface of the bracketed term in the direction normal to the surface. It can be shown that given (5.5), (5.6) reduces to

For theory of static electric fields see for example Panofsky and Phillips, 1962

$$\Phi(x_\alpha) = \frac{1}{4\pi}\int\left(\Phi\frac{r}{r^3} + \frac{\nabla\Phi}{r}\right)\cdot dS \qquad (5.7)$$

Equation (5.7) defines the potential at any point x_α within the volume V, given the potential and its divergence over the surface. From (5.2) it is clear that the divergence can be specified in terms of the normal component of the current density on the surface. Also given that Φ and $\underline{J}.d\underline{S}$ cannot be independently specified over the surface, only either one or the other is required on any portion, and not necessarily both.

This indicates that in the bounded system with which we are concerned, that is a cell in a culture dish, either the potential or the normal current density on the entire surface must be known in order to calculate the potential within the extracellular medium. Going through each boundary in turn it is possible to show that this condition is easily achieved. Firstly, as the surface of the electrode device will be an insulator (excluding the embedded metal electrodes themselves) and no current can flow across this boundary, the normal current density there is zero. Some distance from the cell the potential will decay to zero due to the reference electrode, providing the remainder of the outer boundary. It will be shown later that the exact shape of this portion has little effect on the field distribution close to the cell providing that it is far enough away, and is chosen purely to simplify the calculation. The final boundary is the outer surface of the membrane, through which flows the transmembrane current. It is clear that it must be this current that is used as the boundary condition, as this is the fixed quantity unlike the surface potential whose variation is what is under investigation.

Given that the boundary region is split up into these three regions, the insulating base, the distant zero potential surface, and the cell membrane, what method can be used in order to solve (5.7) (or alternatively (5.2) and (5.4))? Clearly, given the complicated nature of the boundaries analytical methods must be excluded if an at all realistic solution is to be obtained. The most commonly used computer based method is known as the finite difference method (Adey and Brebbia 1983)(Smith 1978), and relies on using the approximation that the potential at the centre of a very small cube is the average of the potential at the centre of the six faces. A regular mesh is created throughout the solution domain and expressions are written relating the potential at each node (including the boundary nodes) to their nearest neighbouring nodes. These can then be assembled into a matrix which can be solved to obtain the node potentials. Although this method allows complicated distributions of boundary conditions to be included, the boundaries themselves must be linear in order to fit the regular shaped mesh into it. A second method, known as the finite element method, overcomes this limitation, but generally requires increased computational power. This technique is described briefly in the following section.

5.2 THE FINITE ELEMENT METHOD: THEORY

The finite element method (FEM) is powerful computational tool that has been widely used over the past 20 years to solve complex structural engineering problems (Reddy 1984)(Strasa 1985). Although this area remains the main user of FEM, it is now also gaining wide acceptance in areas such as thermal analysis and electromagnetics.

The basic idea behind the FEM is to divide the structure, or region being studied into a large number

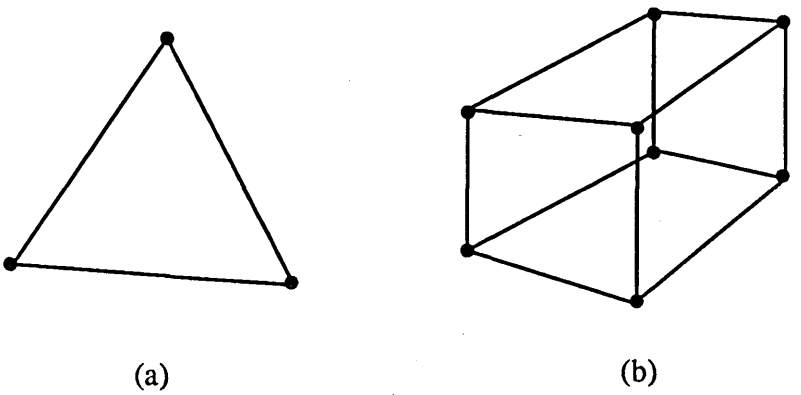

Figure 5.3 (a) A typical two-dimensional element having three corner nodes and (b) a quadrilateral element used to construct three-dimensional models.

of finite elements which may be one, two, or three dimensional. A popular element chosen for two-dimensional analysis is the triangle, whilst three-dimensional analysis often uses quadrilaterals (figure 5.3). If it is required to find for example, the potential distribution over the plate shown in figure 5.4a for a given plate material, specified boundary conditions, etc, there is obviously an infinite number of points in the plate and hence an infinite number of temperatures to be determined. If a closed form analytical solution to Laplace's equation (or in the more general case, Poisson's equation) existed, this would allow the temperature to be computed at any of these points because the solution is expressed as a mathematical function of the coordinates x and y {in the form $T = F(x,y)$}. The irregular geometry of the plate in figure 5.4a however, precludes such a closed form solution.

Instead of requiring that the potential be determined at every point in the plate, the FEM determines only the potential at a finite number of nodes, that is at the element vertices. A solution to Laplace's equation is obtained using the 'variational method' to solve the integral equation, utilising interpolation functions such as low order polynomials to approximate the potential field. Using the condition that both the potential and its first derivative (i.e. current density) must be continuous at each node, and given suitable outer boundary conditions, it is possible to evaluate the coefficients of the interpolation functions.

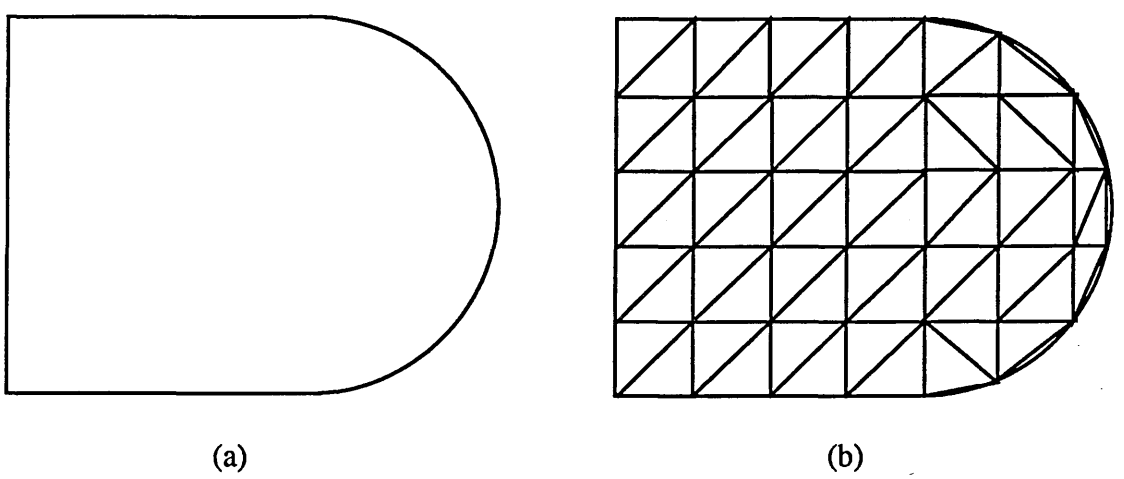

Figure 5.4 For the case of even a moderately complex geometrical shape (a), a closed form analytical solution is often difficult, or impossible to obtain. By dividing this region into a large number of simple finite elements an overall solution may be constructed from the solutions obtained for each element.

This method is illustrated by means of an example, in appendix II.

The procedure for obtaining a finite element solution may be summarised as follows.
(1) Discretisation of the domain into a collection of finite elements, with both the elements and nodes being consecutively numbered (as shown in figure 5.4b).
(2) Derivation of the individual element matrices.
(3) Assembly of the element matrices to form a matrix for the entire domain.
(4) Imposition of the boundary conditions and solution of the problem at the nodes.
(5) Display of the results in tabular or graphical form.

The accuracy of a finite element solution depends mainly on the discretisation of the domain, the overall number of nodes, and the approximation functions chosen for each element. Due to the flexible nature of the elements, and the fact that they can be mixed, e.g. prism and tetrahedral, it is possible to fit the model accurately to the domain, even around tightly curved boundaries. Increasing the number of elements and nodes, whilst improving the accuracy, also increases the solution time by a disproportionate amount. There is generally a point at which the improvement in accuracy is minimal compared to the increasing solution time however, and this is normally found by a stepwise refinement in mesh size. Finally, the approximation functions are generally linear polynomials, with the solution accuracy improving as the degree increases. It is generally difficult however to fit polynomials of high degree to complex shaped elements, and these are generally restricted to either linear or quadratic.

5.3 SOFTWARE: PATRAN AND ABAQUS

Whilst the development of the FEM has been hampered historically by the numerically intensive calculations required, the present generation of personal and mainframe computers has produced numerous and widely available software packages (Cendes 1989). As noted above their main area of application is in structural mechanics and thermodynamics, and as such most packages are tailored for these areas. One such package was used in this analysis due to the analogy of thermal and electrical problems.

ABAQUS (Hibbit, Karlson, and Sorenson Inc.[#]) is a general purpose FEM solver which was run on an IBM 3090 mainframe computer. It is designed to solve, amongst others, the thermal field problem given by the equations[§]

$$\int_V \zeta U dV = \int_S \underline{q} \cdot d\underline{S} + \int_V R dV \qquad (5.8)$$

$$\underline{q} = -k\nabla\theta \qquad (5.9)$$

where ζ is the material density, U is the rate of increase of the internal energy density throughout the volume V, $\underline{q}$ is the heat flux across the surface $\underline{S}$ which encloses V, and R accounts for the increase in internal energy due to, for example plastic work or radiation coupling. θ is the temperature, and k is the thermal conductivity. In order to solve electrical problems the temperature can be identified with the electrical potential Φ, the heat flux with the current density $\underline{I}$, and the thermal conductivity with the electrical conductivity σ (Miller and Henriquez 1988). In the absence of capacitive and inductive effects the

[#] Made available under academic license
[§] Obtained from ABAQUS technical manual: Theory

internal energy term U, is identically zero, as is the term in R which has no obvious electrical equivalent in this situation. Equations (5.8) and (5.9) thus reduce to

$$\int_S \underline{J} \cdot d\underline{S} \Rightarrow \underline{\nabla} \cdot \underline{J} = 0$$

$$\underline{J} = -\sigma \nabla \Phi$$

which are identical to those already defined in (5.4) and (5.2). ABAQUS will therefore provide suitable solutions at the element nodes for electrical problems, providing that the units used are consistent. The boundary conditions in the initial configuration, i.e temperature and heat flux, are replaced by the electrical potential and the current density respectively.

ABAQUS accepts as input a data deck containing the numbered nodes and elements, and their coordinate location. It also requires the boundary conditions on the element faces (or nodes) which lie on the outer boundary, and the conductivity of the region within each individual element. This data is generated using the PATRAN (PDA Engineering) preprocessor running on a DEC VAX mainframe, which enables the three-dimensional construction of the problem domain to be made graphically and which then automatically creates the required number of elements and nodes. It is possible to reduce the number of nodes, and hence the solution time by taking into account any symmetry present in the model. Lines of symmetry coincide with electric field lines, and hence no current can flow normal to their surface. This is equivalent to creating a boundary condition on this plane of $\underline{J} \cdot d\underline{S} = 0$, and it is therefore possible to consider only one half of the model if one plane of symmetry exists (e.g. X=0), one quarter if two planes exist (eg, X/Y=0) etc. Once the solution is obtained for this region, the overall solution is obtained simply by mirroring it in the planes of symmetry.

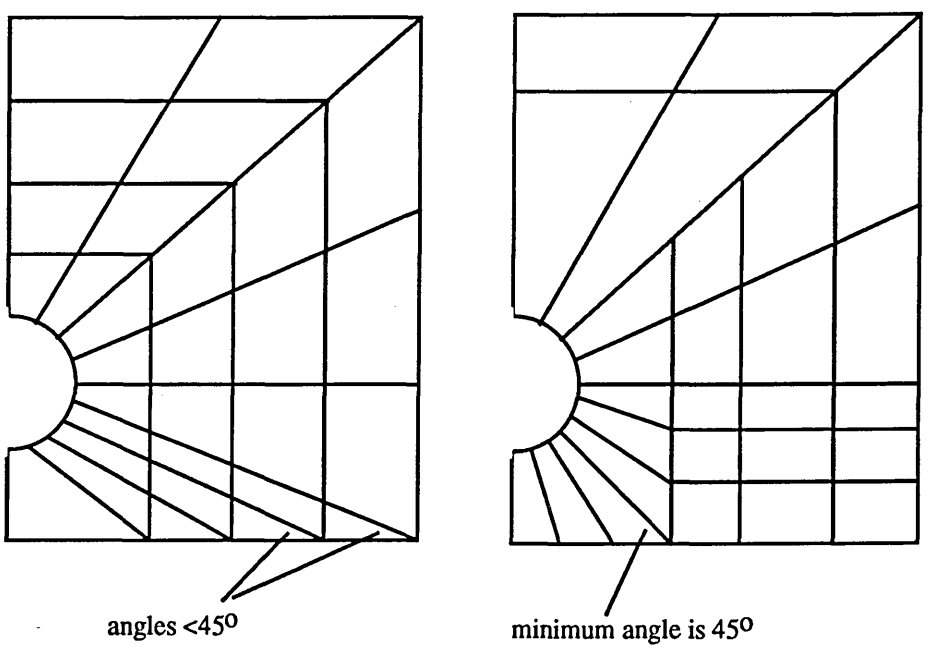

Figure 5.5 Section through an example model showing two different mesh configurations. In the left hand example the minimum element angle is less than 45°. This can cause errors due to the difficulty in generating appropriate approximation functions. Using the construction on the right, this problem is overcome.

A limitation on the type of elements from which models can be constructed, is that the angles which element faces make with each other should be greater than 45°. This is due to problems encountered in constructing suitable approximation functions for elements with faces making more acute angles than this. Figure 5.5 illustrates two different mesh configurations for a cell contained in a cube, in two dimensions (only one quadrant is modelled due to symmetry). The first (a) contains elements which do not meet the above condition, whilst the second (b) overcomes the problem by first creating an inner mesh which then connects to a looser outer mesh. After incorporation of the boundary conditions and element properties an interface package, PATABA, generates the ABAQUS input data. As noted above the time taken to obtain a solution depends mainly on the total number of elements and nodes from which the model is constructed, but was typically in the range 300 - 5000 central processing unit (CPU) seconds.

Solutions for either the electrical potential or the current, or for both, can be generated using ABAQUS. These are then returned to PATRAN for graphical display via the reverse translation interface, ABAPAT. The display style chosen in this case was a plot of the equipotential contours on cross-sections through the model, whilst individual node potentials could be extracted by the use of a cursor.

5.4 GENERAL FORMULATION OF PROBLEMS

The initial problem considered, that of a cell suspended in a volume conductor, consisted of a spherical cell at the centre of a cube of dimensions 200×200×200μm held at zero potential and representing the distant reference electrode. Neurons were modelled as spheres of radius 5μm, without associated dendrites or neurons and without any account taken of cell spreading. Although this morphology is an obvious oversimplification, it allows initial quantitative results to be obtained. The extracellular space contained a region of relatively high conductivity, $0.0033 S.cm^{-1}$ (resistivity = 300Ω.cm), representing the culture medium and occupying all of the solution domain. As already noted, capacitive and inductive effects were neglected in this region.

In order to determine a value for the current density flowing across the membrane during an action potential, it is necessary to employ several simplifying arguments. The first concerns the potential distribution around the soma during an action potential. The existence of voltage gated sodium channels in the soma has already been discussed, but what is not clear is how an action potential would spread around it. It may for example be initiated in the initial segment, spreading outward by local circuit action, or depolarisation may occur simultaneously over the entire region. Considering the former and assuming a rate of conduction similar to that observed in axons ($20m.Sec^{-1}$), it would take approximately 2μSec for the depolarisation to travel around the entire surface of a 10μm diameter cell. As the duration of a vertebrate action potential is typically greater than 1mSec, it can be assumed that the entire soma membrane would be at the same state of depolarisation. That is to say that this situation is identical to that existing if depolarisation occurred simultaneously over this region.

Figure 5.6 illustrates this ideal spherical cell, and shows a portion of the membrane represented by its equivalent distributed components. These are connected via resistances representing both the internal (R_i) and external (R_e) media resistivities. During an action potential, the membrane capacitance C_m is charged and discharged by ionic currents flowing through the voltage gated channels. A typical value for C_m is $10^{-2} pF.\mu m^{-2}$ (Barnes and Hu 1977) and given that it charges from -70 to +30mV, the total charge required is

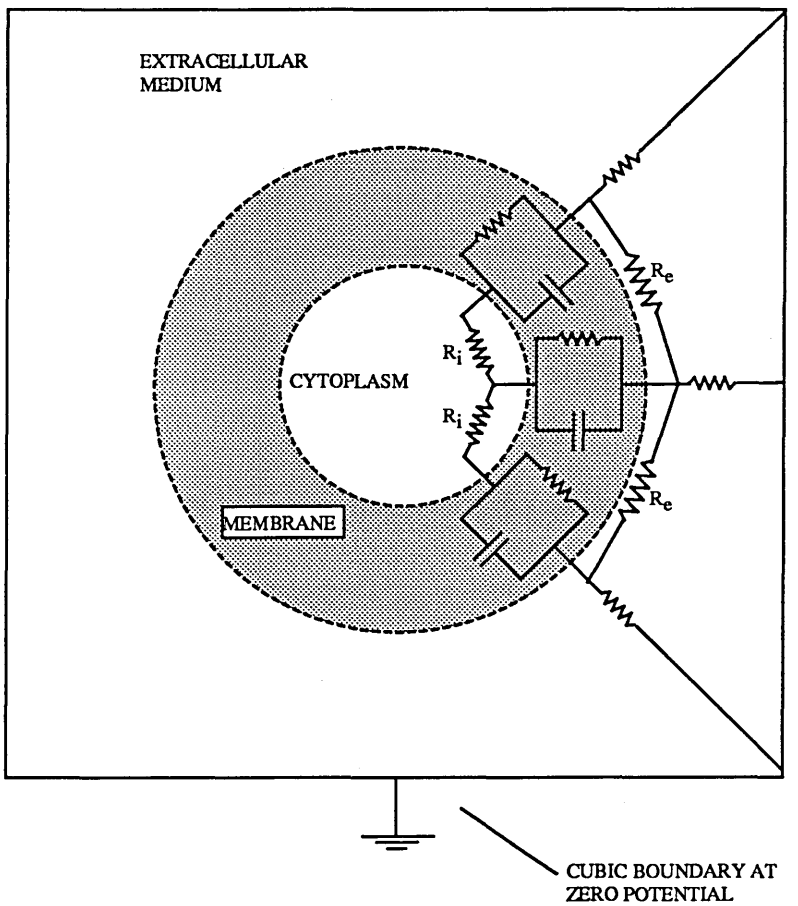

Figure 5.6 A distributed component model of a cell surrounded by a volume conductor. A grounded reference electrode in the conductor is represented by a cubic boundary, some distance from the cell. If the entire membrane depolarises simultaneously, all the transmembrane current is drawn through the resistors R_b.

$$Q = C_m \times V_m = 10^{-15} C.\ \mu m^{-2} \qquad (5.10)$$

This is supplied by the inward sodium current which flows for about 100μSec, so the inward current density is

$$|J| = \frac{Q}{t} = 10pA.\ \mu m^{-2} \qquad (5.11)$$

It is clear that if the state of depolarisation is identical across each membrane portion, then no current will flow through either R_i or R_e, but will be drawn through the high conductivity extracellular medium (represented by R_b) from the zero potential cube, and will enter the cell along the normal. As this situation is quasi-static, the peak extracellular potential will correspond with the peak transmembrane current density. Given that it is this peak signal amplitude which is of most interest for recording purposes, all the following calculations were carried out at this point in the action potential.

The incorporation into the problem of an electrode mounted on an insulating substrate was achieved by the specification of the zero normal current density condition. Electrodes were considered only as a region of high conductivity ($5S.cm^{-1}$) embedded in the substrate, with their surfaces exposed to the medium. The lower boundary condition thus became the interface between the substrate and the medium, and between the substrate and the electrode (figure 5.2). In any real situation the electrode would be connected to a high impedance amplifier which would draw negligible current, hence the reasoning behind

surrounding the lower surface of the electrode with the insulating substrate. The effect of the exposed metal beneath the cell will be to average out the potential existing above it, since the entire surface must be at the same potential.

In order to clarify this reasoning it is helpful to return to the thermal analogy given by (5.8) and (5.9). The cell can be considered as a source of heat which raises the temperature in the surrounding medium, including that above the electrode. Due to the finite conductivity of the medium there is a decay in this temperature away from the cell membrane. The conductivity of the electrode is very much higher than that of the medium (1500 times) and so the temperature will tend to equalise across its surface. In addition no heat can flow out from the electrode to the 'amplifier', and so the base is isolated by the insulator.

5.5 RESULTS AND DISCUSSION

5.5.1 Cell in a volume conductor: Comparison with a simple analytical calculation

The first case analysed using this method, was that of a spherical cell in a volume conductor. This is the most common situation for such calculations, and allowed comparison with a simply derived analytical approximation. Figure 5.7a illustrates this model, with the cell at the centre of a grounded cube. The dimensions are as stated above and are also included in the diagram. Symmetry on the X, Y, and Z axis would have required only one octant to be included in the analysis, but in order to allow comparison with later models two were included (2 and 6 in figure 5.7a inset, that is the octants at the back right). Figure 5.7b demonstrates the same model generated using PATRAN.

Analysis was carried out on this model for successively increasing numbers of nodes and elements. Figure 5.8 shows the potential calculated at the cell surface (where the maximum potential exists) versus the number of nodes in the mesh. This is a slight distortion of the true model, since in the case of the finest mesh, the complexity was increased selectively only in the vicinity of the cell, as this was the area of major interest. Such selective enhancement provides a substantially improved solution in this area at the expense of only a marginal increase in solution time. The solutions are observed to converge in the region of 2000-3000 nodes. Figure 5.9a shows the equipotential contours on a cross-section through the Y=0 (and hidden X=0) plane of symmetry, superimposed on the finite element mesh. Also shown in figure 5.9b is the same contour plot with the mesh subtracted.

The peak extracellular potential, occurring at the membrane surface, is 143.3μV. This then decays away towards the zero potential cubic boundary (not shown). Close to the cell the equipotential contours form concentric spheres with a value approximately inversely proportional to the radial distance from the origin. Further out these become distorted by both the increasing crudeness of the mesh, and by the influence of the boundary. This latter effect will cause the contours to become less spherical and more cubic with distance.

If the cubic boundary is replaced by a spherical boundary of radius b=100μm, it is possible to calculate the extracellular potential at some radius R, exactly, using the definition of potential difference

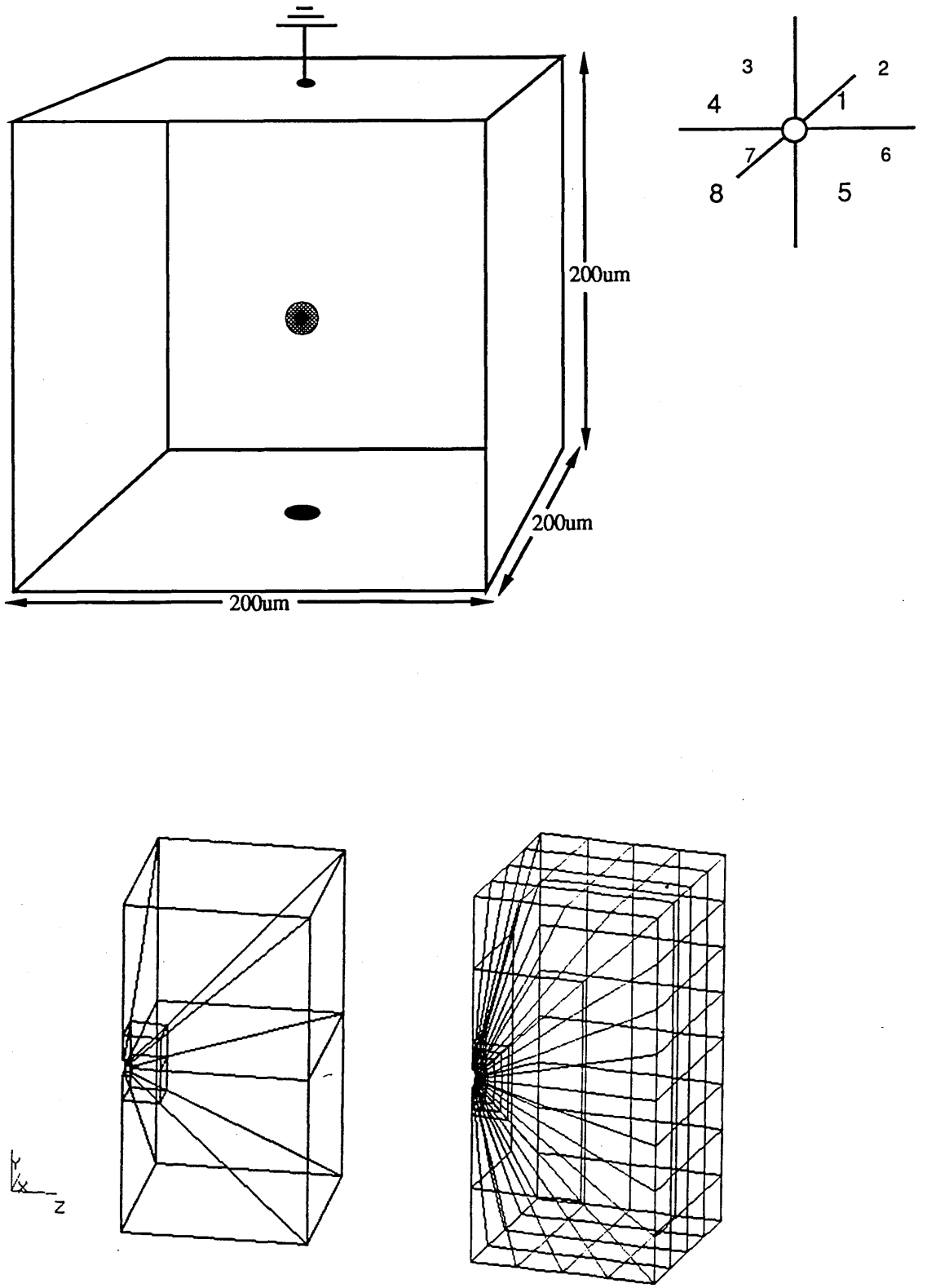

Figure 5.7 (a) The model constructed in order to simulate a spherical cell suspended in a volume conductor, showing the outer boundary condiitions and (b) the resulting mesh generated by PATRAN (only two octants are modelled due to symmetry).

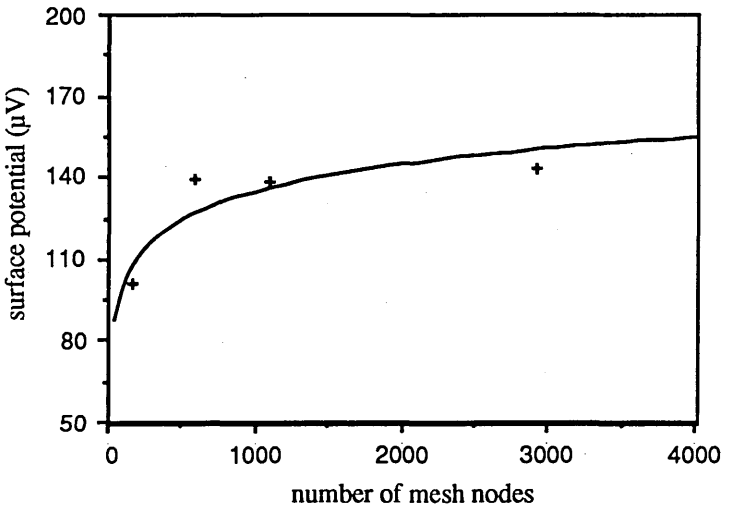

Figure 5.8 Potential at the surface of a spherical cell, located at the centre of a volume conductor, versus the number of ABAQUS mesh nodes.

$$\phi = -\int_{R}^{a} E \cdot dr = \frac{I}{4\pi\sigma}\left[\frac{1}{b} - \frac{1}{R}\right] \qquad (5.12)$$

from equation (1.6) the total current I, flowing into the cell is the membrane current density 10pA.μm^{-2} multiplied by the cell surface area 314μm^2. Thus the potential at the surface where R=b will be 142.5μV. A difference of only 0.5% exists therefore between the solution obtained analytically for the spherical boundary and that obtained numerically for the cubic boundary, for the region close to the cell. This similarity, including the 1/R decay, would be expected since the boundary is some distance from the membrane compared to the dimensions of the cell itself. Setting the outer boundary to infinity, from (5.12) the maximum potential increases to 150μV at the cell surface. Again, this difference is minimal and illustrates the marginal effect that the choice of outer boundary, representing as it does the grounded reference electrode, has on the solution.

It has already been stated that this cell morphology represents an ideal case, with specifically no regard taken of the neurites that would in reality emanate from the soma. It has also been suggested (figure 3.1) that a proportion, or all, of the current flowing into the soma may be transmitted out through the dendrites in a closed loop. This will have the effect of reducing the total current flowing towards the cell at increasing radial distance, which in the above calculation was maintained constant. In turn this will lead to a potential field distribution initially similar to figure 5.9, but falling off as less and less current flows. The effect has been estimated (Rall) to differ by less than 10% from the above calculation, at the cell surface. It would seem reasonable therefore not to include the effect the of the dendrites sourcing current in the interests of maintaining a simple model, and the effect of axons is similarly neglected.

5.5.2 Cell in proximity to a planar surface electrode

In order to quantify the effect of the electrode and its substrate on the extracellular field, a model similar to figure 5.10 was constructed. Again a 5μm diameter cell is suspended in a volume conductor, but in this case the lower boundary is formed by the insulating substrate with a metal electrode embedded in, the dimensions of the electrode being 11×11×1μm. The surface of the electrode lies in the same plane as that of the substrate. A line drawn perpendicular to, and through the centre of the electrode would pass

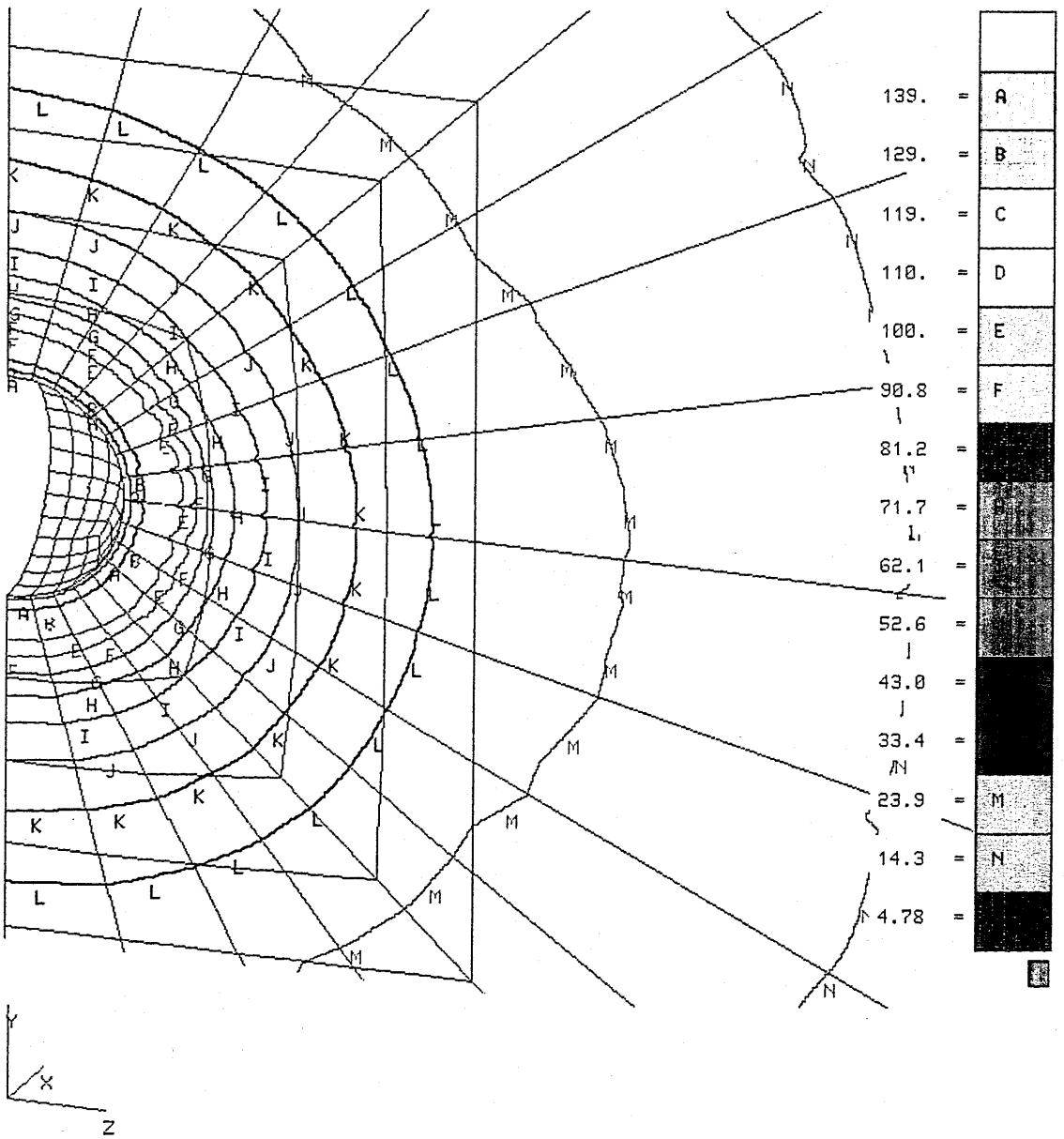

Figure 5.9 (a) Solution generated by ABAQUS for a cell at the centre of a volume conductor showing the finite element mesh.

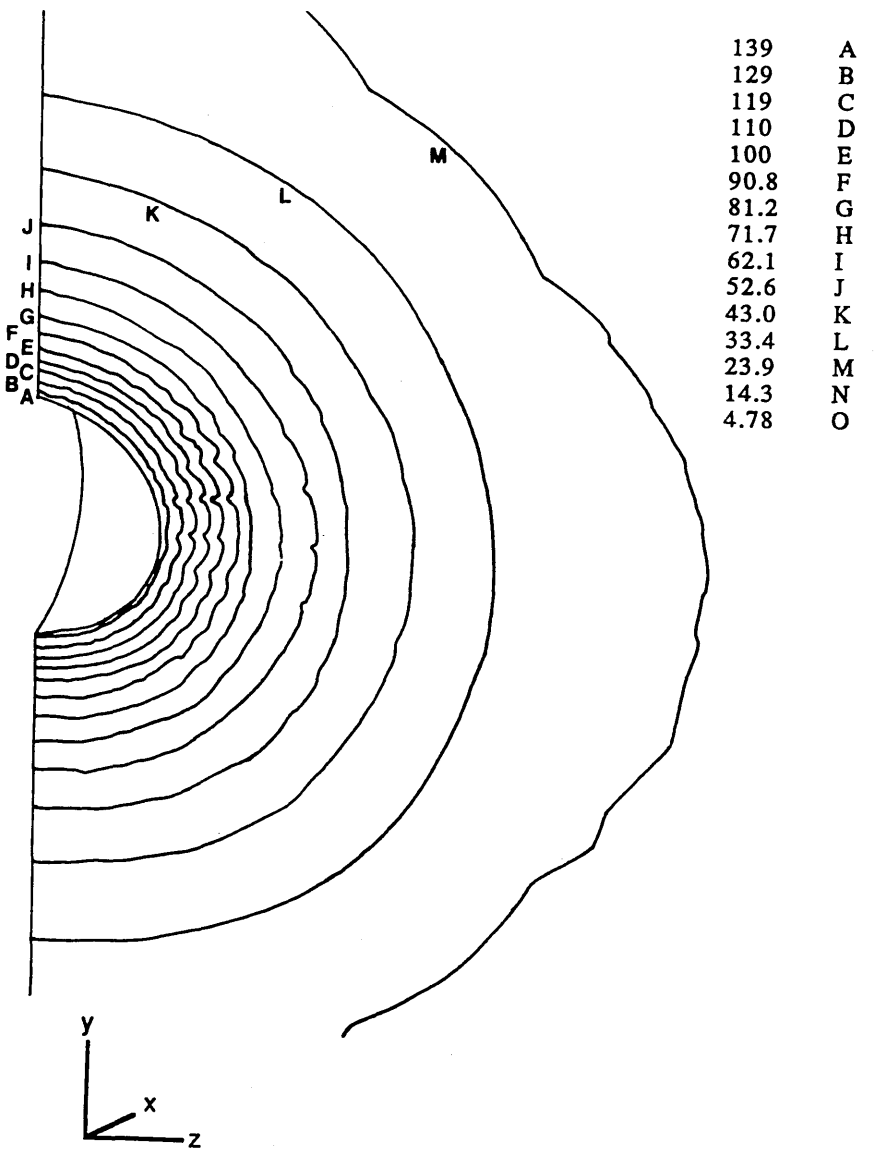

Figure 5.9 (b) As (a), only with the finite element mesh removed in order to allow the equipotential contours to be seen more clearly.

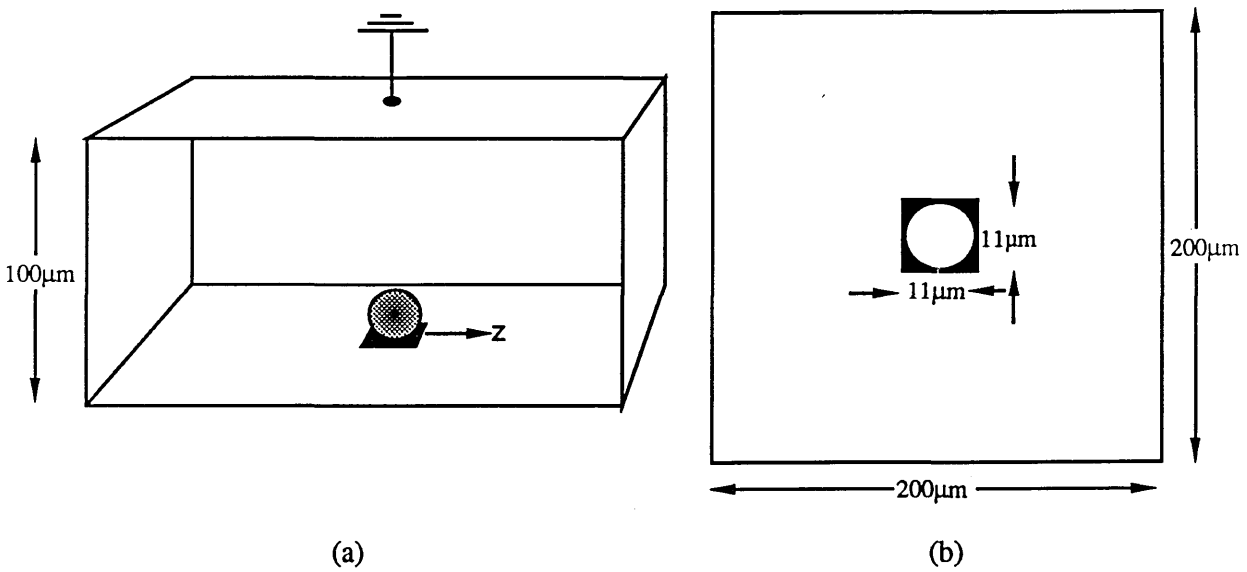

Figure 5.10 (a) Model constructed to allow the effects of an electrode embedded in an insulating substrate to be evaluated, and (b) the same in plan view.

through the centre of the cell, which is located at some variable distance above it. The zero potential boundary is located at the planes X/Y/Z=100μm, with symmetry at X/Z=0μm. Meshes were constructed from a similar number of nodes and elements to those used in the previous model, i.e ~2900 nodes and 500 elements.

FEM solutions were obtained for distances between the electrode and the closest part of the cell membrane of 15, 5, and 0.5μm, i.e. with the cell suspended above the electrode. Figure 5.11 illustrates the equipotential contours obtained for a 5μm separation on a cross-section through the X=0 (and hidden Z=0) plane. Again the contours exhibit a smooth, regular behaviour in the region close to the cell where the mesh is finest, but become distorted at greater distances. It is also clear that at the insulator-medium boundary the contours are perpendicular to the interface, equivalent to the specified boundary condition that the change in potential across the normal be zero. The potential over the surface of the electrode shows negligible variation (<0.01%), as would be expected for a material of such relatively high conductivity.

Figure 5.12 plots the variation in the electrode potential with cell-electrode separation distance. Also included are the potentials at the same coordinates without the electrode present (obtained above). The effect of the substrate is seen to be proportionally greatest at the largest separation distance, with a 100% increase over the previous model. This is of the same order of magnitude as the increase observed with the 2-dimensional analysis carried out previously (Drake et al. 1988) using the finite difference method. As the distance is reduced to 0.5μm however, an increase of only 38μV, or 30%, occurs. This is perhaps surprising, but illustrates that merely extrapolating the changes for various distances would prove erroneous.

The value of closest approach of cell and electrode (0.5μm) was chosen in order to represent the gaps that are generally present under a neuron adhering to a planar substrate. Although these are probably an order of magnitude less than the value used here, this allowed a much simplified mesh and in addition

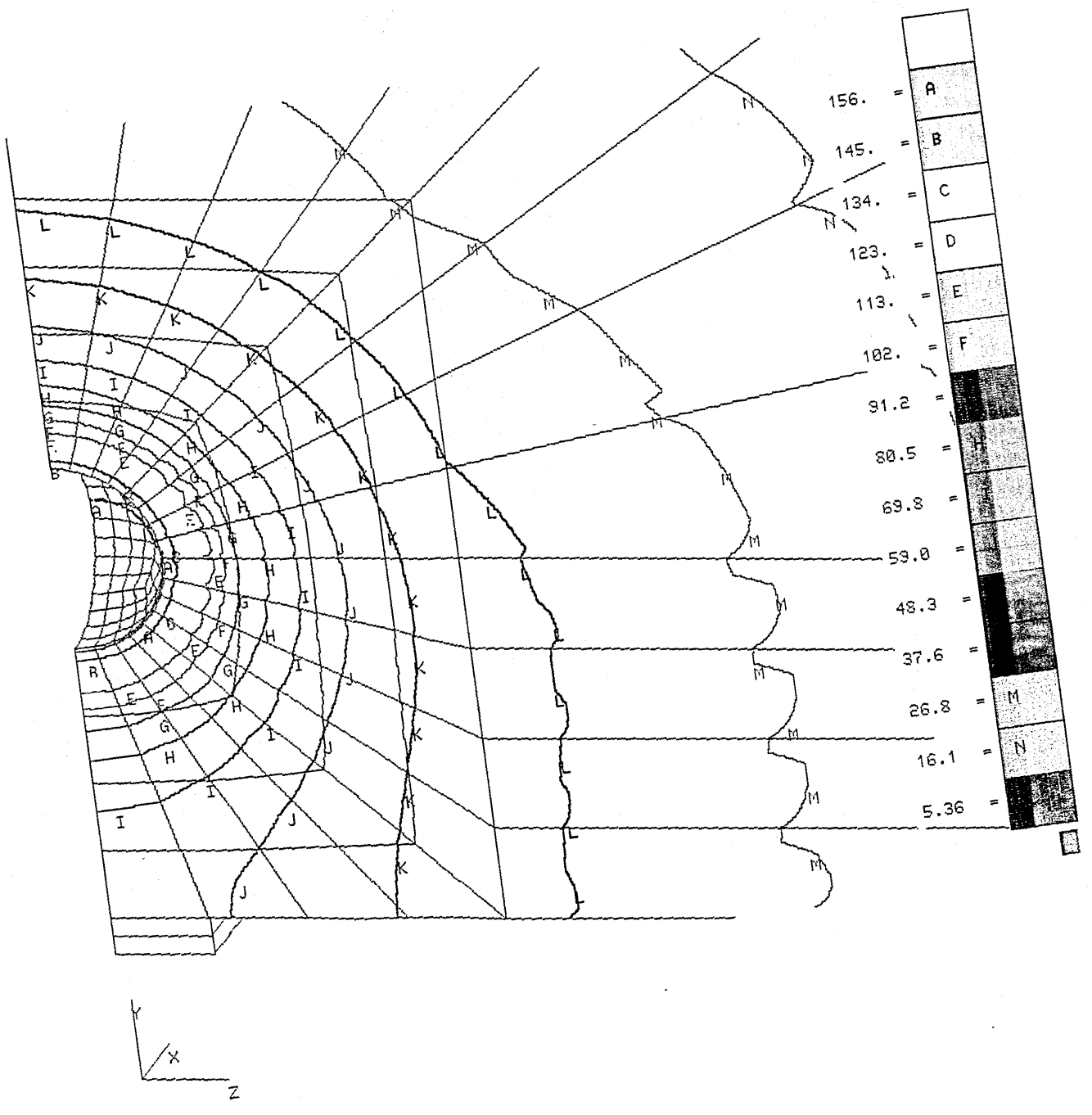

Figure 5.11 Potential field solution obtained for a cell located 5µm above a planar microelectrode.

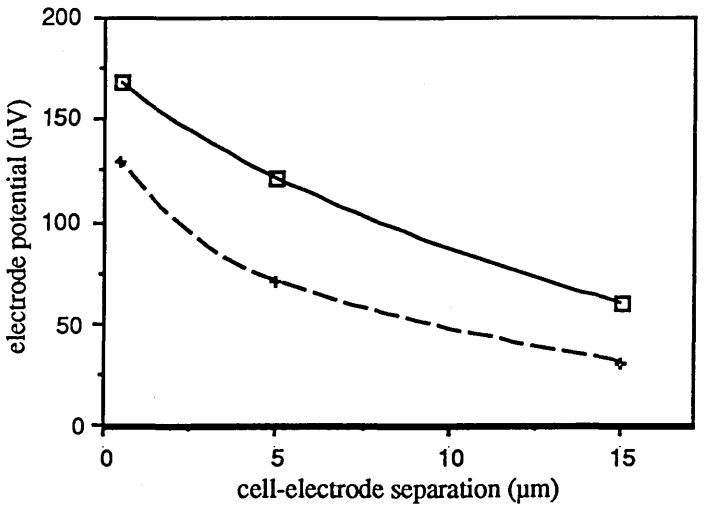

Figure 5.12 Variation in the potential at a planar electrode with distance below the cell (□). Also shown in the lower plot (+) is the corresponding distance potential variation for a cell suspended in a volume conductor (section 5.5.1).

would probably only have a marginal effect on the potential, given that the spherical cell can only make contact at a single point.

The increase in potential observed with the electrode being very close to the cell, whilst not in itself proving startling, suggests that bringing further insulating boundaries into proximity with the cell may produce a more significant result.

5.5.3 The effects of recessing both electrode and cell into the substrate

A survey of the appropriate literature suggests that all recordings made from both vertebrate and invertebrate neurons using multielectrode arrays, have involved the use of electrodes similar to those described above, i.e with the electrode surface being approximately flush with the substrate (± 2μm). This applies to both *in vitro* and *in vivo* devices. The use of deep pits with electrodes at their bases has been suggested (Regehr 1988) as a means of pressing the cell onto the electrode, but has not been demonstrated experimentally to date. It is the aim of this section to quantify the effects of recessing the electrode into the substrate on the extracellular potential, and hence to make suggestions on an appropriate electrode design.

The motivation for studying recessed electrodes comes both from the above results, and from the advances in device fabrication technology which makes the precise manufacture of electrode features possible. In particular the fabrication step involving the exposure of metallic conductors underlying an insulating layer, offers a simple means of creating an electrode whose recess depth depends on the thickness of the insulator. Figure 5.13 illustrates such an electrode configuration, where an electrode has been exposed by etching a groove through the above insulating layer. Such a device structure, in addition to possibly increasing the extracellular potential, will allow neurite outgrowth to be guided along the groove to other selected cells, as discussed in section 1.3.1. This situation was modelled using PATRAN for a groove width of 11μm, and electrode dimensions of 11×11×1μm. The electrode was located with its surface flush with the bottom of the groove, 0.5μm under a cell of radius 5μm. This also provided a

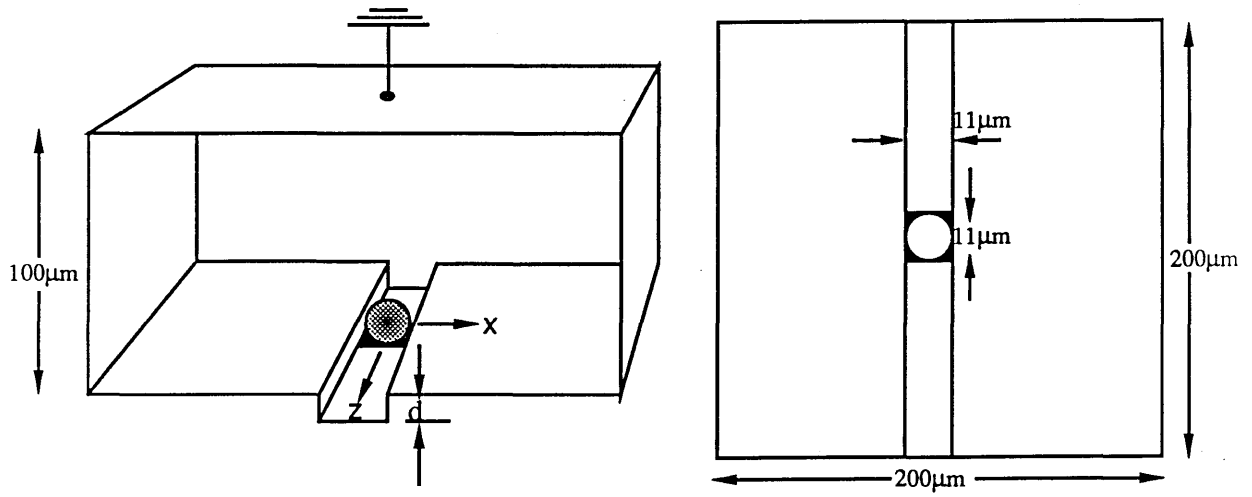

Figure 5.13 (a) Model showing a cell located in an 11μm wide groove, and directly above an 11x11μm electrode, and (b) the plan view.

0.5μm gap between the cell membrane and the sidewalls. Identical outer boundary conditions were applied to those detailed for the previous model.

Figures 5.14 and 5.15 show the equipotential contour plots for groove depths of 5.5μm and 22μm respectively, on cross-sections through both the X=0 and Z=0 planes (see figure 5.13). In both cases the maximum potential contour shown, marked A, is no longer directly under the cell but has shifted towards the portion of the membrane facing the edge, at the base of the groove. It is also clear that the magnitude of the potential has been increased within the groove and in the vicinity of the cell, whilst that in the surrounding areas has been only slightly affected. Figure 5.16 plots the potential existing at the electrode for groove depths varying from 2.75μm to 22μm, with a constant width of 11μm. Also included for comparison is the electrode potential obtained in the above analysis of a planar electrode (0.5μm cell-electrode separation), equivalent to a zero groove depth. A simple logarithmic curve can be fitted to this data, providing an expression relating the depth d to the electrode potential ϕ_e,

$$\phi_e = 74.1 + 311.5 \log(d) \qquad (5.13)$$

In the case of the deepest groove (22μm) the electrode potential has reached 512μV, compared to only 168μV for the planar electrode. This increase of over 200% represents a substantial improvement in the extracellular signal amplitude, and hence in the signal to noise ratio that would be achieved with such an electrode geometry.

It would be expected that confining the cell even more tightly would further increase the electrode potential. This is illustrated in figure 5.17 where the electrode is located at the bottom of an 11μm deep pit, with an 11x11μm square cross-section. The cell is therefore enclosed on five sides with only the upper surface remaining fully exposed to the medium. The FE mesh was constructed from over 5000 nodes and 900 elements, and the time taken to run the analysis exceeded 5000 CPU seconds.

Figure 5.18 shows the equipotential contours plotted on a cross-section through the X=0 (and hidden Z=0) plane. Again the contour defining the maximum potential has been displaced upwards slightly, but the potential of the electrode (which covers the entire base of the pit) has risen to 1164μV (1.164mV). It

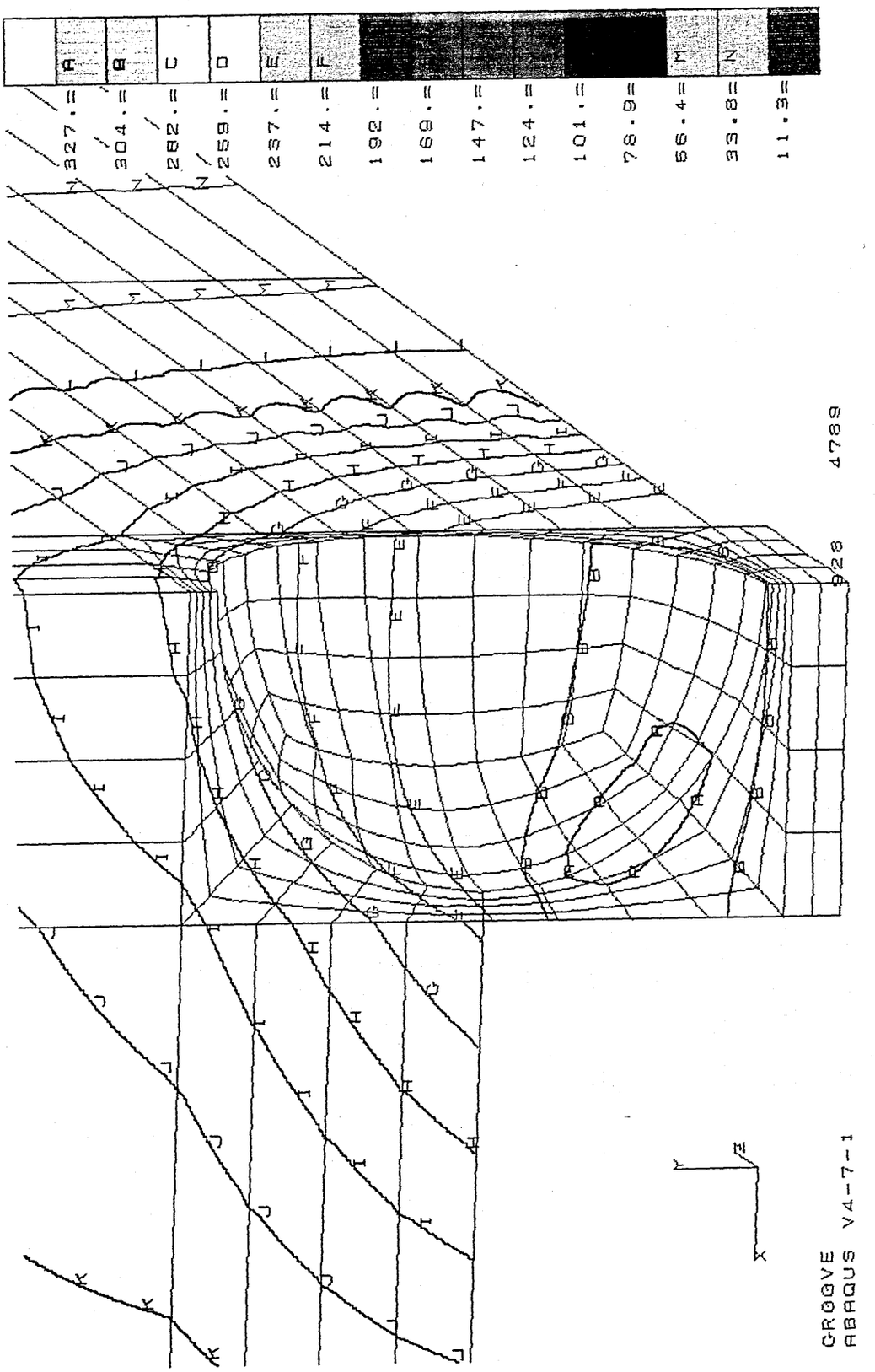

Figure 5.14 Potential field solution obtained for a cell in a 5.5μm deep groove.

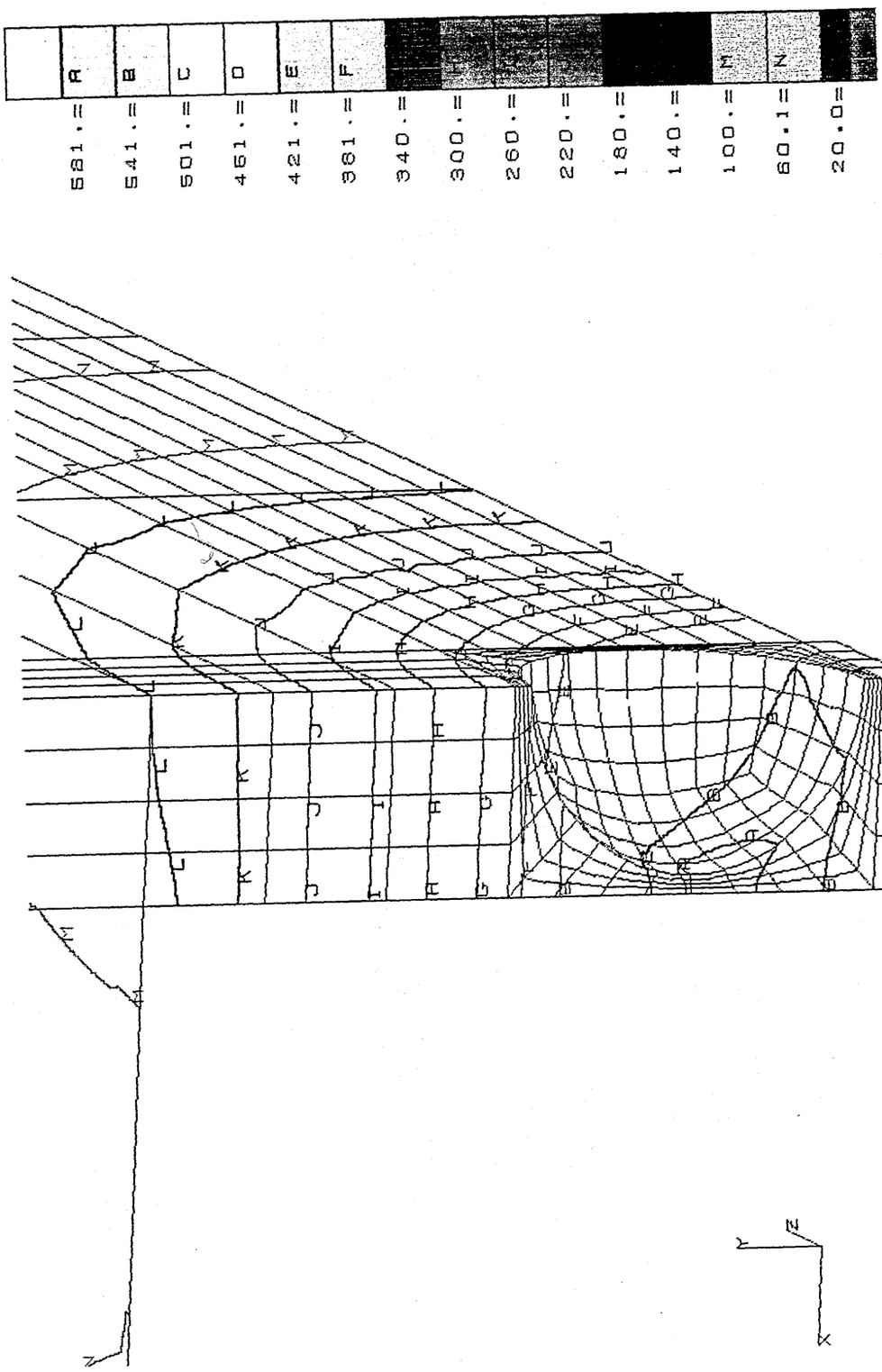

Figure 5.15 Potential field solution obtained for a cell in a 22µm deep groove.

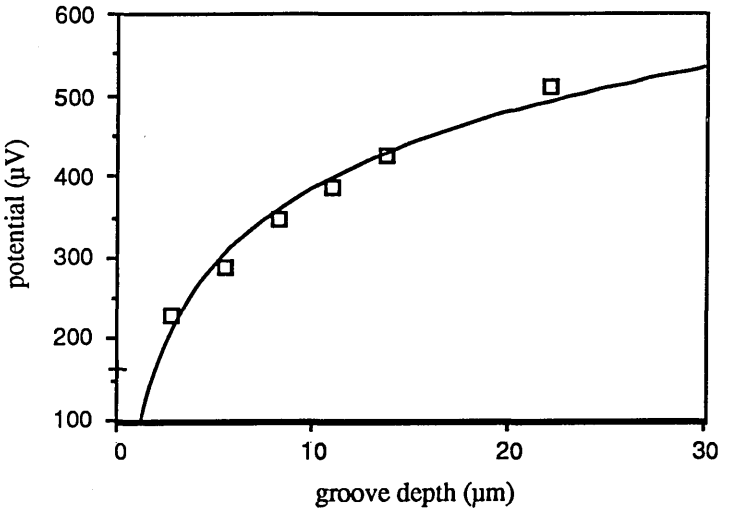

Figure 5.16 Electrode potential versus groove depth (❑) with a logarithmic curve fitted. Also shown is the electrode potential calculated with the cell located immediately above a planar electrode (+), calculated in section (5.5.2)

would be expected that the electrode potential would follow a similar pattern to that for an electrode in a groove with increasing recess depth, i.e. levelling off at large depths.

5.5.4 Signal pick-up from distant cells

The variations in electrode potential have been detailed above, for cells located directly above the electrode. It is also of interest however, to note the potentials present at some distance from the cell in order to estimate both at what distance it is practical to record extracellularly, and also what level of biological noise will be picked-up from additional cells surrounding the particular cell of interest.

Figure 5.19 shows the potential (extracted from the above contour plots) which exists on the surface of the insulating substrate at varying distances from the cell, for (a) a cell on a planar substrate, (b) a cell in an 11μm deep groove, and (c) a cell in an 11μm deep pit. Distances are measured from the vertical axis passing through the centre of the cell, and the directions are as indicated in figures 5.10, 5.13, and 5.17 respectively. It is important to note when considering the observed decay, that the potential at large distances from the cell will be slightly affected by the imposed zero potential boundary.

If the contributions from both thermal and electrostatic induced noise are assumed not to exceed 20μV, and that a signal to noise ratio in excess of 5:1 is required for adequate detection, then the magnitude of the extracellular potential must exceed 80μV. Considering figure 5.19(a) it can be estimated that for a planar electrode geometry, potentials in this region will lie within a circle of radius 16μm. Electrodes lying either wholly or partially within this area will, theoretically, be able to detect extracellular action potentials with a reasonable signal to noise ratio. It is more difficult to obtain similar results for recessed electrodes. For example, what signal will a recessed electrode detect from a cell which is on the substrate above it, or that is in an adjacent pit or groove? In order to solve these problems exactly it would be necessary to incorporate multiple electrodes and non-centred cells in the analysis, which would eliminate much of the symmetry utilised above and would lead to an enormous increase in solution time. From figures 5.19(b) and (c) it is possible only to gain a conservative estimate of the

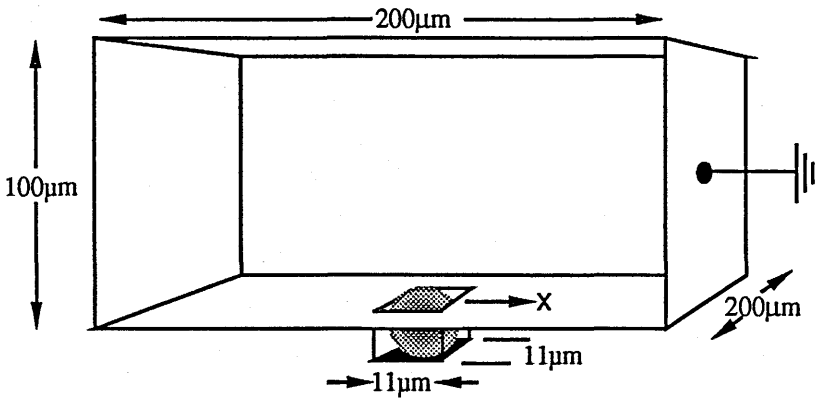

Figure 5.17 Model constructed to simulate a spherical cell located in a pit, with the electrode at the base.

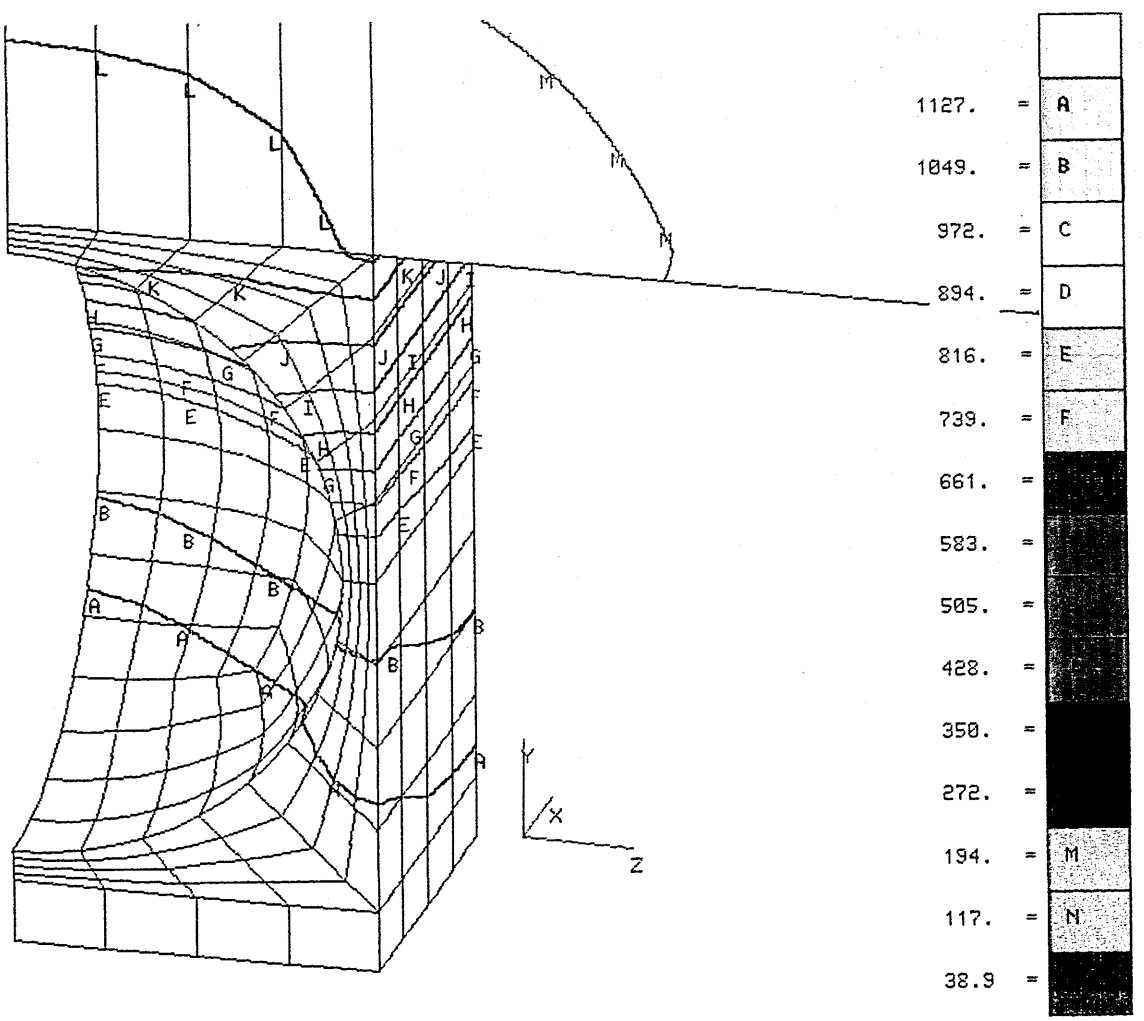

Figure 5.18 Potential field solution for a cell confined in an 11µm deep pit, with an 11x11µm square cross-section.

maximum recording distance, which would be reduced by the recording electrodes being recessed. This is again in the region of a 16μm radius circle around the cell. For the case of a cell in a groove but not directly above the electrode it is possible to be more precise, with a suitable S/N ratio being achieved within 30μm.

For recordings from cells directly over the electrodes, these figures also suggest how far additional cells must be from the electrode before overlapping signals are recorded. This is not a problem if the individual extracellular signals have a distinct waveform and if the amplitudes are large enough to be able to observe the differences, although this is not always the case. One method to reduce this unwanted biological noise is to incorporate a grounded screen around the electrode. This would be achieved by evaporating a further metal layer in the area surrounding the electrode, as illustrated by the shaded region in figure 5.20. Potentials generated by cells outwith the groove would decay very sharply due to this screen, but it would also be expected that the electrode potential of interest, beneath the active cell, would also be decreased. Such a model was analysed for an 11μm deep groove, and the electrode potential observed to fall to 276.5μV (from 388μV without the screen) whilst the field shape remained similar in the region beneath the cell. In order to assess the suitability of this electrode configuration fully, it would be necessary to offset this reduction in signal amplitude against the reduction achieved in noise levels.

5.6 CONCLUSION

The use of the finite element method has demonstrated that electrode geometry is an important consideration in the design and fabrication of microelectrode recording devices. This technique is well suited to considering the complex boundaries and material inhomogeneities encountered and is capable of calculating extracellular potentials with superb accuracy, given the appropriate boundary conditions. The main approximation made in deriving these boundary conditions, concerned the use of a uniform current density to describe the transmembrane action potential. Whether or not this is exactly the situation pertaining at the membrane surface, the general effect of the boundaries considered will remain the same.

Results suggest that significant increases in the extracellular potential can be achieved by recessing the cell and the electrode into the insulating substrate. Given the appropriate recess dimension, the increase could be as much as an order of magnitude. Present microfabrication methods however, will probably limit the application of these electrodes to smaller vertebrate neurons, given the difficulty in depositing and etching insulating layers which are sufficiently deep to accommodate invertebrate cell bodies. Bearing in mind that good signal to noise ratios are not difficult to achieve for these particular neurons, and that it is obtaining recordings from vertebrate neurons that presents the major problem to present electrode devices, this is not a serious restriction.

Recessed electrodes may also offer the opportunity to obtain recordings from single neurites, in particular from invertebrate neurites which can exceed 5μm in diameter. Such recordings have not previously been reported due to the small magnitude of the extracellular signals generated. It would be possible to record from both the cell body and from surrounding neurites recessed in grooves, which guide them away from the cell body. Finite element analysis could be used to estimate the signal which would be obtained from the neurites, using as a basis the model of an axon described in section 1.2.2.

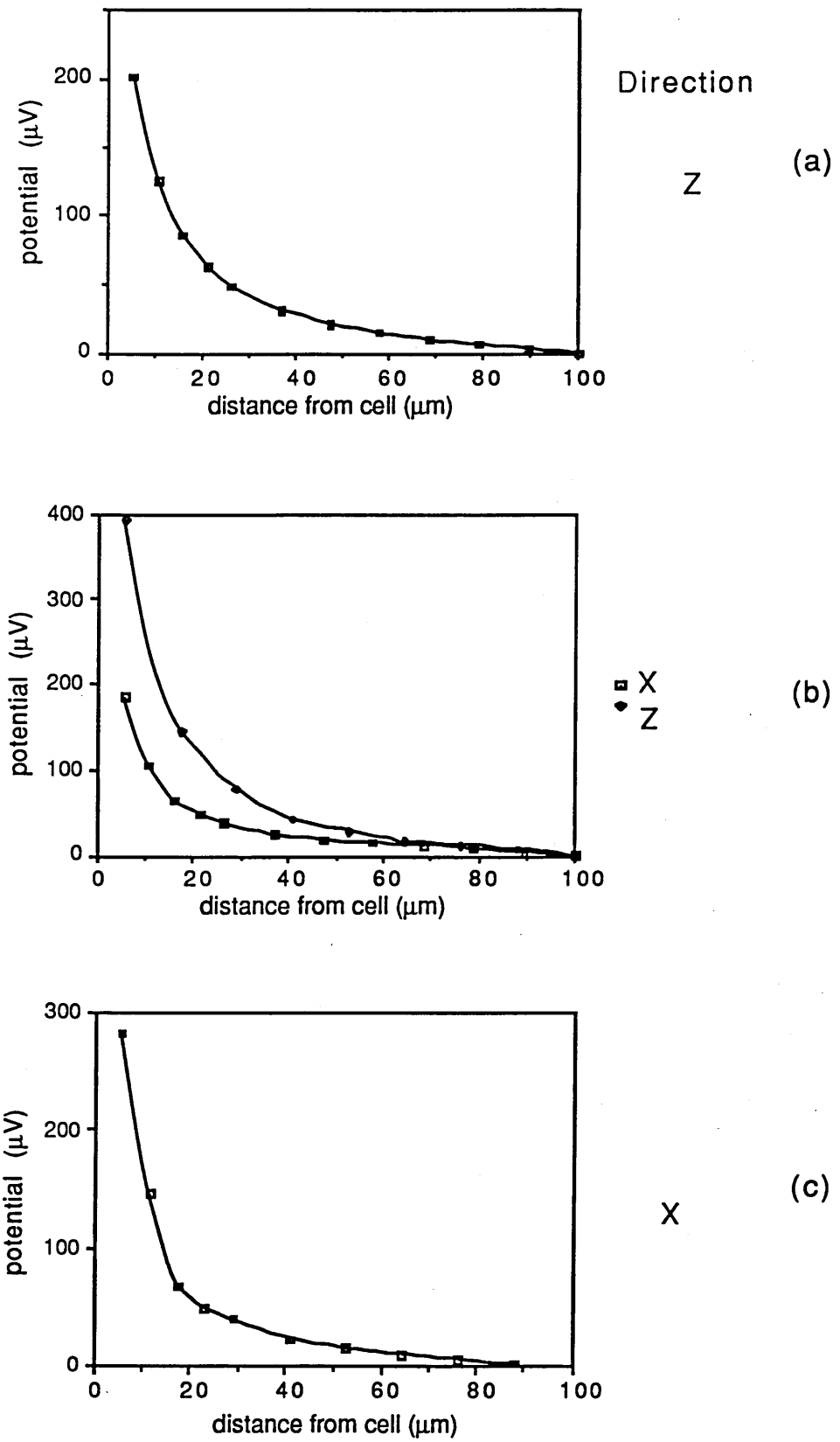

Figure 5.19 Potential decay with distance from the cell centres, as obtained from the above contour plots (values shown are those just above the substrate surface). (a) For a planar electrode, (b) for an electrode in a groove, both along the groove, and perpendicular to it, and (c) for an electrode in a rectangular pit.

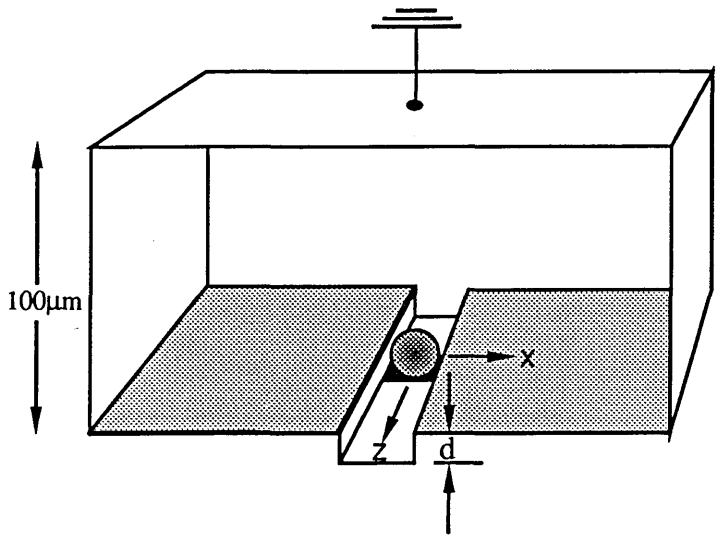

Figure 5.20 A finite element analysis solution was obtained for a cell in a groove, with the surrounding region of the substrate grounded (shown by the shaded region). In practice this region would be coated with metal during fabrication.

Chapter 6 attempts to experimentally verify some of the results described above using a variety of techniques, including current injection via glass microelectrodes, and the use of electrically active chick embryo cardiac myocytes.

CHAPTER SIX

EFFECT OF DEEPLY RECESSED ELECTRODES

CONTENTS

6.1 INTRODUCTION

The results described in chapter 5 suggest a number of electrode geometries which would increase the extracellular potentials around small vertebrate neurons, to an appropriate level for recording with planar microelectrodes. Although a number of such neurons have been comprehensively studied in culture by other researchers, at this time none was available for use in this work (chick cerebral hemispheres and dorsal root ganglion cells have been cultured, but attempts to record electrical activity have proved unsuccessful), with access only to large invertebrate neurons e.g. *Lymnaea stagnalis*. As has already been noted it is impractical to fabricate recessed electrodes with dimensions similar to that of these cells, and in order to verify the results of chapter 5, it was necessary to employ two alternative methods.

The first of these utilised a glass micropipette with a tip diameter of 2-5μm to inject a known current into the portion of a groove directly above the metal microelectrode, simulating in practice the finite element model. This test was used to gauge the effect of the parameters which were missing from the previous analysis, namely the electrode double layers, diffusion rates, and others such as concentration and diffusion. The second method involved embryonic chick cardiac myocytes to mimic the action potentials produced by neurons. These cells have the advantage that they are of a similar size to vertebrate neurons, are easy to culture, and their mechanical contractions are synchronised to action potential generation. They do however have several disadvantages, the most significant of which is that they tend to act in concert with neighbouring cells to form a beating sheet. These problems are discussed fully later.

The fabrication of grooved devices with depths up to, and in excess of 25μm was achieved with the use of multilayer insulators which provided both the necessary thickness and afforded a suitable degree of mechanical and chemical strength. An underlying layer of silicon nitride (~4000Å) prevented the unwanted exposure of the electrodes during use (by for example scratching with the glass micropipette) and was resistant to ion penetration and the resulting break up. A further layer of high moisture resistant polyimide varnish provided the depth and was easily etched using a recently introduced electron cyclotron resonance (ECR) reactive ion etching machine (see section 2.3.2).

6.2 ESTIMATION OF RECESS EFFECT USING MICROPIPETTE INJECTED CURRENT

A simple method of estimating the increased potential in the vicinity of a recessed microelectrode is to inject current, directly above the electrode, via a glass micropipette and to record the potential to which the microelectrode is raised. If the pipette tip is very fine compared to the dimensions of the groove and the planar electrode, it can be considered as a point current source. In the previous chapter, for a 10μm diameter cell, a peak transmembrane current density of $10pA.\mu m^{-2}$ was assumed. That is a total current of 3.14nA flowed into the cell. Hence injecting such a current through the micropipette it should be possible to simulate an electrically active neuron. An appropriate frequency to use would be 1KHz#, as this represents the approximate centre frequency of a vertebrate neuronal action potential. Section 2.8 details the method used to produce and manipulate micropipettes, in addition to describing the recording set-up. Figure 6.1 shows a micropipette manipulated into a position directly above a planar metal microelectrode, exposed by a groove.

Attempts to detect the potential produced by an injected current of around 3nA (the current suggested above) proved unsuccessful, with signal amplitudes being below the noise levels. Only with substantially larger currents could relatively clean signals be detected. Figure 6.2 shows the potentials obtained with two different micropipettes, one having a tip diameter of approximately 4μm (A) and the second of 2μm (B), the injected current being 100nA. It is obvious that the potentials generated with the larger tipped micropipette are significantly greater. Before considering the reason for this, it is worth estimating what potential would be expected in this situation. For a point current source in a uniform volume conductor (ignoring the extracellular boundaries), the potential at some radial distance ρ is given by (equation 5.12, for b at infinity)

$$\phi = \frac{I}{4\pi\sigma\rho}$$

The conductivity of saline, σ, is significantly greater than the previously quoted value for culture medium ($0.0033S.cm^{-1}$) and was taken as $0.02S.cm^{-1}$ in this instance. Thus at a distance of 0.5μm, a potential of 3.9mV would be expected. Only the closest point of the metal electrode to the micropipette is 0.5μm away however, with the farthest point being 5μm away. At this distance the potential would drop to 795μV, while the true electrode potential should lie somewhere between these two values. If the boundaries are included, as in chapter 5, the electrode potential would be shown to be significantly increased. This suggests significantly greater potentials than were observed experimentally during current injection (figure 6.2). It is probable that this discrepancy is due to the micropipettes, given the variations already described, the tips of which were broken off in an uncontrolled fashion.

Comparison of the theoretically obtained results (figure 5.16) with those above however, confirms the importance of recess depth in determining the electrode potential. Regarding the magnitude of the potentials calculated and recorded, it is unclear whether the discrepancy is due to deficiencies in the model or to inconsistencies in micropipette manufacture and its 'likeness' to an electrically active cell.

Using a function generator it was possible to produce simulated action potentials which could be fed through the micropipette. It was more difficult however, to filter detected signals than was the case with the single 1KHz frequency, where a simple band pass filter proved sufficient.

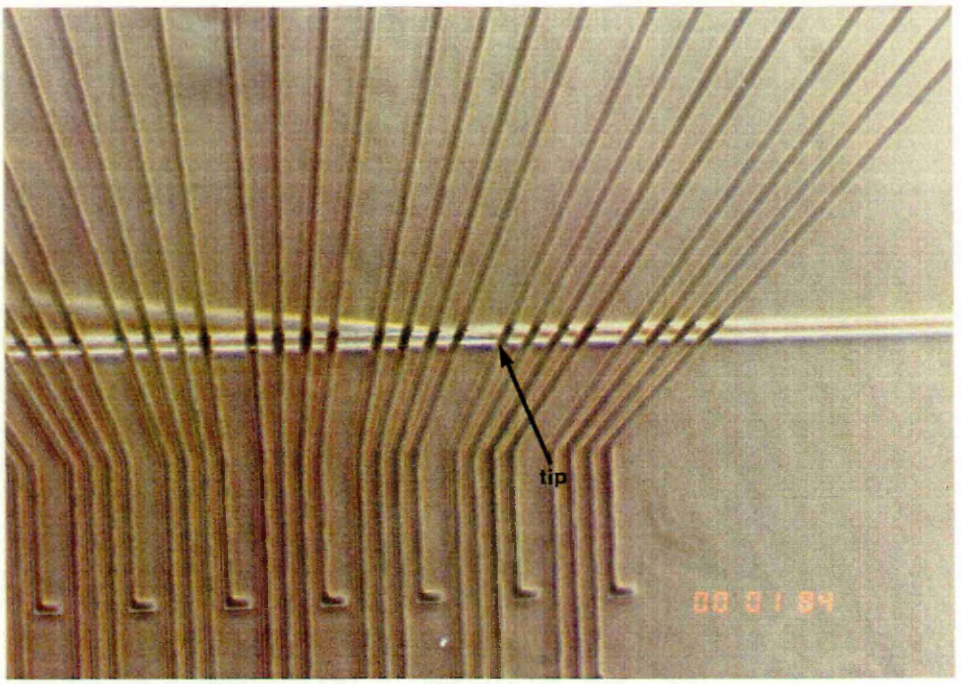

Figure 6.1 Micrograph showing a glass micropipette poised over a metal microelectrode. The electrode potential was recorded during current injection via the pipette.

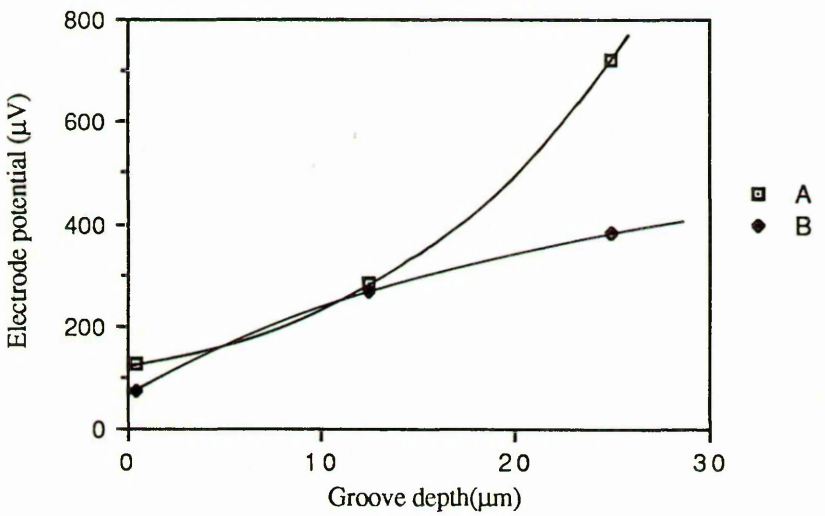

Figure 6.2 The electrode potentials obtained whilst injecting a fixed current (100nA) through a fine tipped glass micropipette, positioned in the groove directly above the electrode. Averaged results (n=10) are given for three different groove depths, and for two different micropipettes A and B.

6.3 RECORDINGS FROM CHICK CARDIAC MYOCYTES

6.3.1 Properties of cultured cardiac myocytes

Although electrode testing using micropipette injected current is appropriate for initial inspection, in the final analysis electrically active cells must be utilised. As has been stated in the introduction to this chapter a suitable vertebrate neuronal cell type was unavailable, and instead it was decided to use chick cardiac myocytes as a substitute. The mechanism of action potential generation in cardiac myocytes is similar to that in neurons, although the type and relative contributions of the ions involved differ (Manning and Akuja 1969). Sodium is replaced by calcium as the depolarising ion in myocytes, and a delay in the closing of the calcium channels causes the action potential to have a characteristic plateau as shown in figure 6.3. Cardiac myocytes preserve their electrical excitability in culture given suitable culture conditions, which are detailed in section 2.5.5. One of the main benefits of using these cells as a method of testing electrode properties is that the mechanical contractions can be observed microscopically, and can be correlated with recorded potentials. This is fortunate as it eliminates the need for simultaneous intracellular recordings (which are in any case extremely difficult due to tip damage which would be caused during contractions).

In culture a confluent layer of cardiac myocytes will form a beating sheet, where depolarisation spreads from one cell to another. The junction between these cells can become very tight, effectively insulating the electrodes which lie beneath them. This has allowed very large potentials to be recorded using planar microelectrode arrays (see section 1.3.2, table 1.2). Obviously a cell sheet is not very similar to an electrically active neuron, but fortunately myocytes will also beat in smaller, more loosely connected groups, and occasionally individually (given that the initial plating density is sufficiently low). Of the previously reported recordings however, none were made from such small groups although this was attempted. This failure may be due to the unipolar method of recording, with the indifferent or reference electrode being a large plate, some distance from the recording electrode. Such a configuration tends to be very noisy compared to a differential recording, where the reference electrode is identical to the recording electrode and is only a short distance away. It may have been that the signals from small cell groups were too small to be detected. If this problem can be overcome, it should be possible to determine the effect of recessing the electrode using small groups. It should be noted at this point that for cells in a sufficiently deep groove, say >5μm, the discontinuity in the surface will prevent cells in the groove from forming a tight seal with their neighbours above them.

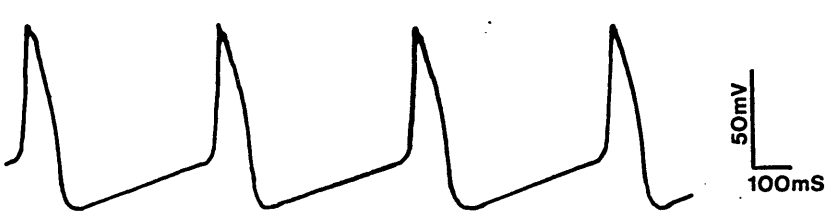

Figure 6.3 A typical intracellular recording from a cardiac myocyte.

6.3.2 Recorded extracellular action potentials

Electrically coupled cell sheets

All recordings from cardiac myocytes were made from 1-2 day old cultures, prepared as detailed in section 2.5.5. Microelectrode arrays identical to those used to detect single cell attachment by impedance monitoring were used in these experiments. In order to test both the electrode arrays and the recording equipment initial experiments concerned the well formed rhythmically contracting cell sheets. Only a very shallow groove (4000Å deep and 18μm wide) was used in this experiment in order to maintain the continuity of the sheet. Sheets extended over relatively large areas, covering a number of adjacent electrodes. As such it was necessary to use a distant microelectrode as the reference electrode, with the large area triangular electrode grounded. Noise levels tended to be high (typically 20μV) but still remained well below the signal amplitudes. Figure 6.4a shows a series of action potentials with an interbeat period marginally greater than 2 seconds. In figure 6.4b the time scale is expanded to show more clearly the waveform of one action potential. These were obtained from the electrode indicated in figure 6.5, where the chosen reference electrode is also indicated. The cell sheet can also be clearly seen in this micrograph.

The amplitude of the signals recorded in this case were in excess of 1.5mV which, along with the biphasic shape, is similar to the recordings previously reported. Care must be taken when selecting the filtering levels as this can significantly distort the recordings. In this recording the maximum available bandwidth was utilised, that is 0.1Hz to wide band (>50KHz). This was only possible due to the extremely large signal amplitudes. It should however be pointed out that the amplitude and in particular the waveshape varied significantly with time. This is not surprising as recordings were made at room temperature with the cultures rapidly cooling from the 37° incubation temperature, affecting the cells electrical behaviour. In fact cultured cells rarely continued beating (and generating action potentials) after around 30 minutes, given these conditions.

Small groups

Extracellular signals generated around small groups of cells will be much smaller than those underneath continuous cell sheets. As noted above the detection of these requires extremely low noise levels, in turn often requiring differential recording from two similar electrodes in close proximity. This requirement is easily met by using two adjacent array electrodes which have been platinised identically. Differential recording also has one other major advantage in this instance. That is that signals generated by distant cell sheets and clumps (a small number often remain after dissociation) will not be detected and mistaken for action potentials generated by small cell groups in close proximity. Signals will only be detected from active cells which lie significantly closer to one electrode than to the other.

Cells were cultured on the electrode patterns utilised in the current injection studies. These possessed grooves of width 8μm and of depths varying from 0.4μm to 25μm. It was found that although cells elsewhere on the substrate behaved normally, those in the grooves of depths greater than 5μm were never observed to beat. Recordings from these devices also failed to detect any rhythmic action potentials. There are several possible explanations for this behaviour. The first is that the cells are so tightly confined on either side that their ability to contract is reduced. The contraction of the cell cytoskeleton is a response to the influx of calcium during the action potential, but it is probable that the restriction of the former will have a knock on effect on the latter. A second explanation is the difficulty that the ions and other

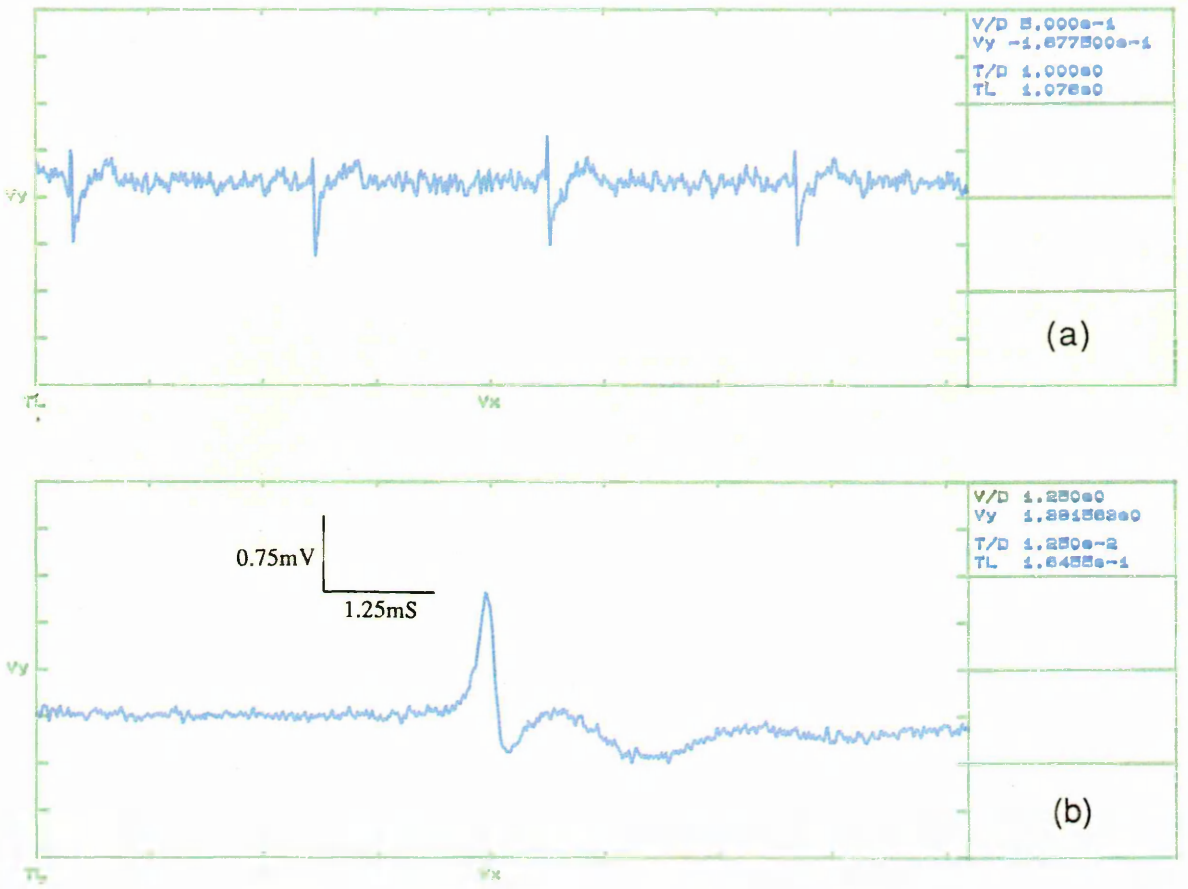

Figure 6.4 Recordings obtained from a microelectrode located under a rhythmically contracting cell sheet using (a) a slow time base and (b) a fast time base.

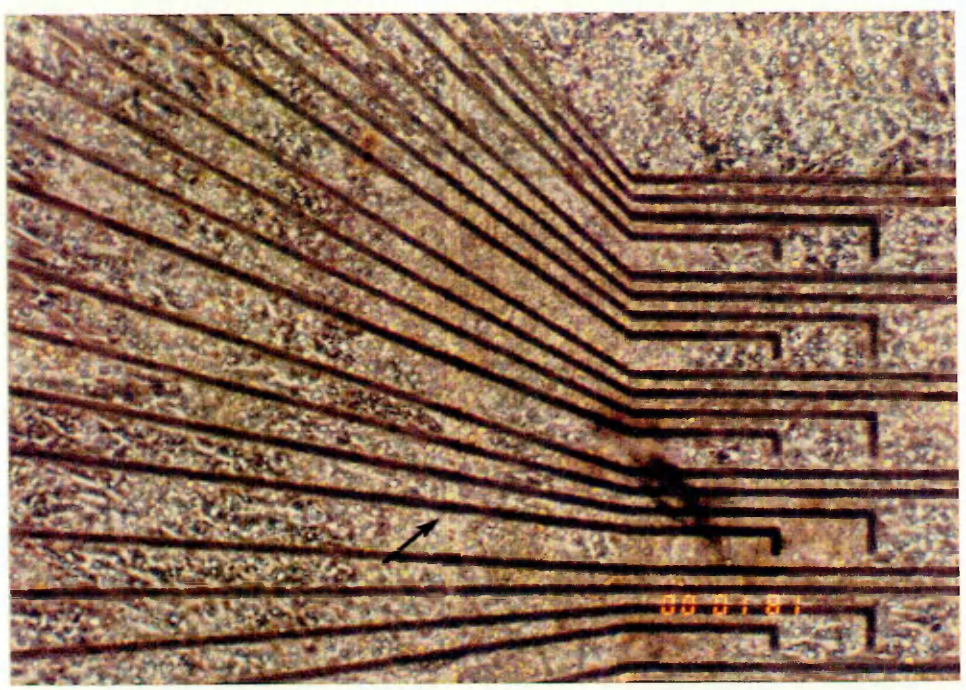

Figure 6.5 Micrograph showing cell sheet from which the recordings shown in figure 6.4 were obtained. The recording electrode is indicated.

components required for cell activity will have in diffusing into such a small space. It is possible that the cell will rapidly exhaust the supplies available in the groove, and that the electrical and mechanical activity will cease. This explanation is probably the least likely as the diffusion process is fast, relative to the firing rate (1 per second), and the confinement is similar to that in intact tissue where metabolites also have to diffuse through tiny capillaries.

This problem was overcome by fabricating devices with increased groove widths of 18μm. This allowed several cells, usually two, to lie side by side across it, hence increasing the freedom of movement and improving the diffusion of metabolites. Cells were observed to beat normally in these structures. This situation is obviously not ideal from the point of view of simulating the situation of a single neuron over a microelectrode, as recordings will be made simultaneously from several cells. The effect of the groove will also be weakened due to the reduced confinement of the potentials. It should be possible however to treat the cells overlying the electrode as a single entity providing that they beat in close synchrony.

Figure 6.6 shows a micrograph of a small group of cells overlying a microelectrode, exposed by a 4000Å deep groove. It can be seen that the cell overlying the electrode (indicated) is, from its rounded shape, a myocyte and not a fibroblast (which are present in significant numbers in the culture). This cell was observed to beat regularly and lay below a small group beating in synchrony. There appeared to be no beating cells either below or to the sides of it. Recordings were made differentially between this electrode and its neighbour, on which no beating cells were present. Figure 6.7a shows recordings obtained from these electrodes using a slow time base, with figure 6.7b obtained using a faster time base. The interbeat period in this case is constant at 1.08 seconds, whilst the approximate duration of the action potential is 8mS. The amplitude of the signal shown is 54μV, whilst the noise level is approximately 10μV.

Devices were fabricated with similar groove widths (18μm) but of depths between 5 and 28μm, where the insulation consisted of a layer of silicon nitride beneath a thick layer of polyimide varnish. Due to the depth of these devices it proved difficult to completely expose the electrode, indicated by the difficulty in depositing platinum black on the surface. Following the etch of the polyimide in an oxygen plasma it was possible to leave a residue of polymer on top of the silicon nitride. At this stage, as the electrodes (and the bonding pads) remained covered by the silicon nitride layer, the only way to judge whether the polyimide had been completely removed was by optical microscopic examination[#]. If the C_2F_6 etch of the nitride was carried out with this polymer remaining, the resulting deposit proved very difficult to completely remove. As noted the electrodes on such patterns proved difficult or impossible to platinise, although it was found that a short soak (<2 minutes) in concentrated sulphuric acid often removed the deposit. This did however cause a degradation of the insulating layer causing a reduction in the measured impedance of the electrode. In order to render some of the devices usable, silicone vacuum grease was applied over the surface to within 100μm of the groove, in order to reinsulate the electrodes. The current leakage through the remainder of the uncovered insulator appeared to be negligible (no significant reduction in the electrode impedance being observed), allowing the devices to be used for recording purposes.

[#] Examination using a scanning electron microscope is destructive, as the holder can only carry a sample of less than 5x5mm and the complete device size was approximately 2x2cm. Use of the Tallystep profilometer (see section 2.7) was also limited to steps of less than 10mm in height.

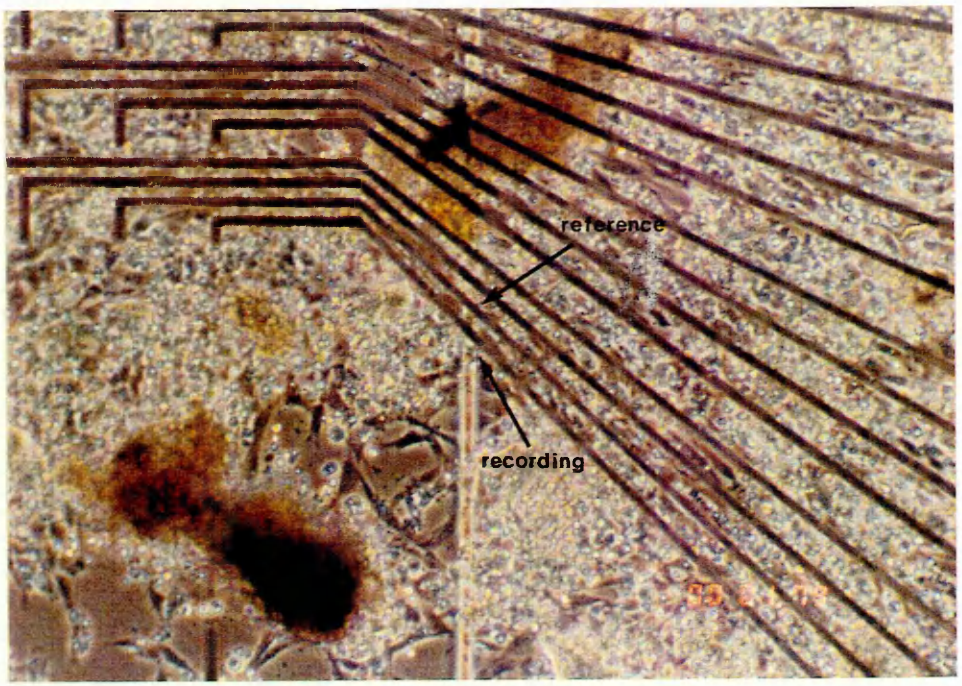

Figure 6.6 Micrograph showing the small cell group (indicated) from which the recordings shown in figure 6.7 were obtained. The groove depth in this device was 0.4μm.

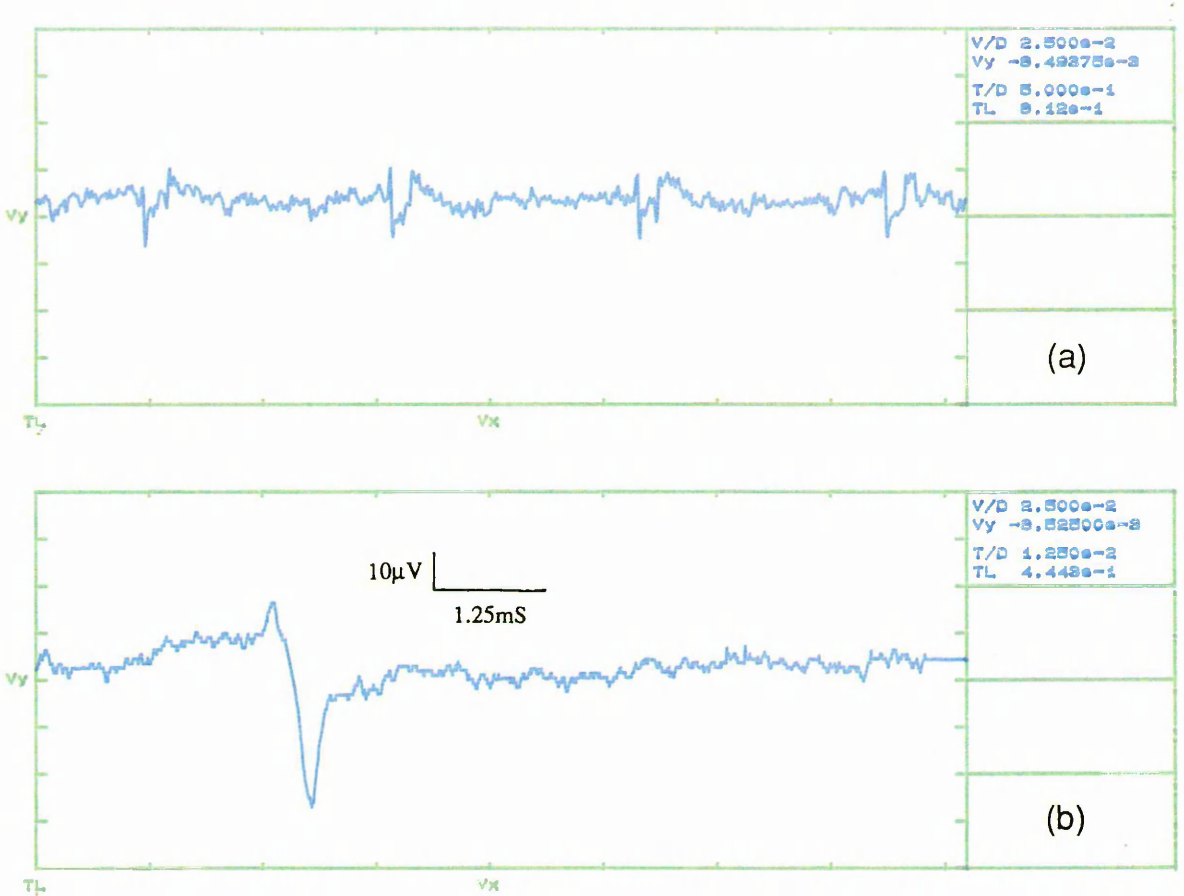

Figure 6.7 Recordings obtained from a small cell group, observed to be rhythmically contracting, over a microelectrode in a 0.4μm deep groove, (a) with a slow time base and (b) with a faster time base.

To date it has only proved possible to fabricate a 28μm deep groove, as shown in figure 6.8. Cardiac myocytes were plated onto the surface at a density sufficient to produce a confluent layer, but still low enough to prevent cells from accumulating on top of each other. Within 10 hours the strip of cells lying in the groove were observed to beat rhythmically for lengths of up to 1mm (figure 6.9a, where the interbeat period is 7 seconds). These cells were isolated from the cells on either side of the top of the groove, as could be seen from the lack of synchronised beating. Figure 6.9b shows a typical signal recorded from an electrode under such a cell strip, displayed using a slow time base. In this recording both the reference and the indifferent electrode were connected to the large exposed triangular electrode. The amplitude of this particular signal is 117.5μV, having a duration of approximately 4mS. Recordings have been made using a number of different electrodes (on the same device), and the variation in signal amplitude obtained with each has been small (<15μV).

6.4 CONCLUSION

These preliminary results, from both micropipette injected current and from cardiac myocyte generated action potentials, suggest that it may be possible to obtain significant increases in the amplitude of extracellular neuronal action potentials recorded by microelectrode arrays. Although the magnitude of the results obtained with the injected current are heavily dependent on the shape of the pipette tip, the trend observed when using the same pipette to inject current into devices with differing grove depths, shows that the metal electrode potential increases with grove depth. Precise control of the tip size and shape is important in future, if any conclusions are to be drawn about the signal amplitudes.

Cardiac myocytes provide a relatively simple to culture electrogenic cell type, with the useful property that mechanical contraction can be synchronised with extracellular recordings. The restriction of contractions by deep narrow grooves however, appears to lead to the loss of electrical activity. Contractions were only observed when the groove width had been considerably increased, to allow up to two cells to lie abreast. Results suggest that the use of the 28μm deep groove increases the signal amplitude by a factor of approximately two, over that obtained with the shallow groove. Comparison with the finite element results are difficult given the different dimensions of this device (having a wider groove), but again the trend of increasing potential with recess depth is suggested. It is important to note however, that although the recordings obtained using the deep groove were repeatable and consistent, that obtained using the shallow groove was only a single result (due to the difficulty in locating single cells or small cell groups over an electrode). The lack of a set of multi-electrode devices with a range of groove depths, has also proved a major obstacle to obtaining results which will verify the calculations outlined in the previous chapter.

The problems encountered with device fabrication, specifically obtaining complete electrode exposure, have proved to be severe given the difficulty in accurately measuring the etch depth. As such the yield of successful devices has proved to be extremely low.

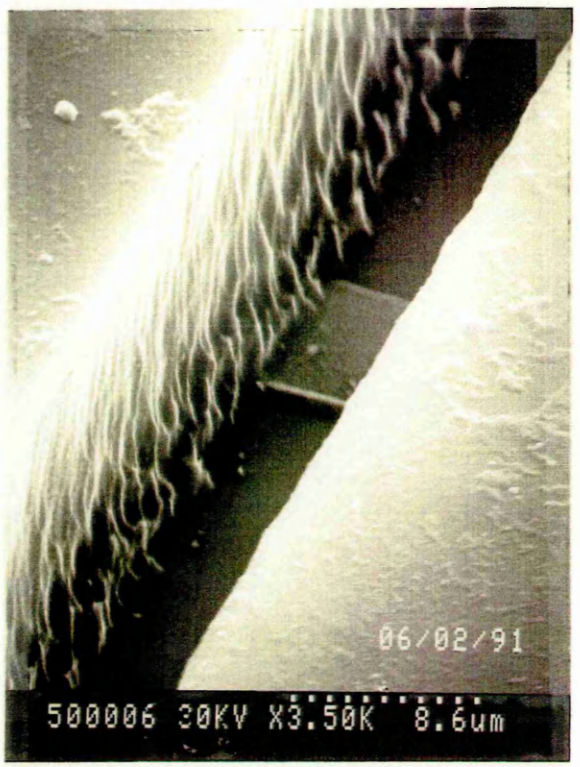

Figure 6.8 A scanning electron micrograph of a microelectrode array, with the electrodes exposed by a 28μm deep groove.

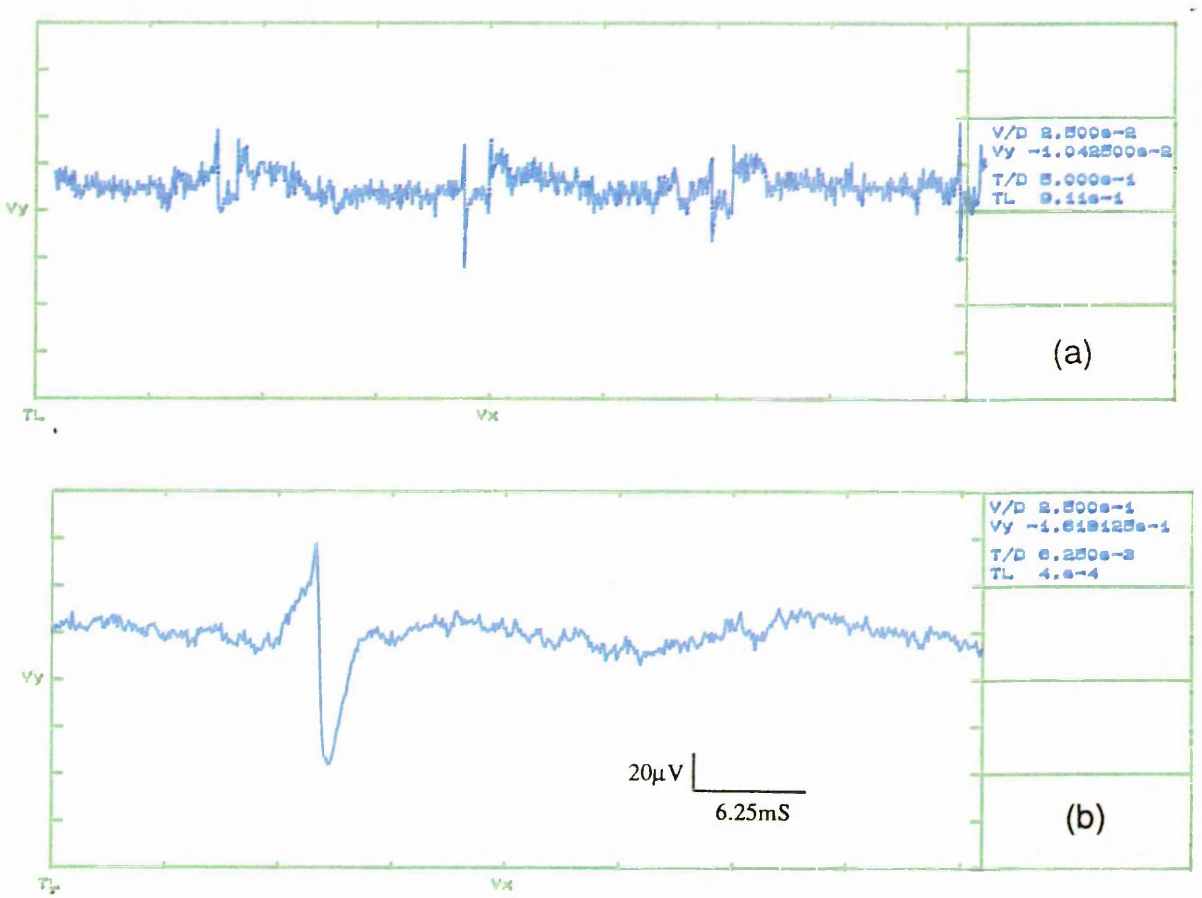

Figure 6.9 Recordings obtained from cells which were observed to be rhythmically contracting in a 28μm deep, 18μm wide groove. (a) with a slow time base, and (b) with a faster time base.

CHAPTER SEVEN

CONCLUSIONS

CONTENTS

7.1 ELECTRODE PROPERTIES

It has been demonstrated that the continuous monitoring of the impedance of a planar electrode in cell culture is a suitable method for the detection and study of both cell attachment and activity. The initial work of Giaever and Keese has been extended by the inclusion of a suitable control electrode, and latterly by the use of microelectrodes to increase the resolution of the system to allow the observation of single cells. Such work is crucial in order to allow the examination of the microelectrode-cell interphase, an understanding of which is required if the magnitude of extracellular action potentials is to be increased to an appropriate level. Before commencing with such studies however, it is important to ensure that non-linearities in the impedance of the electrode-electrolyte interphase do not lead to fluctuations which could be wrongly attributed to cell activity at the interphase. Although a study of the prevailing models of the double layer region suggests the trends which these non-linearities may display, the actual limits and regions within which the impedance will remain constant can only be obtained experimentally. As such the variation in the electrode impedance was observed against a number of variables, namely; frequency, current density, and time.

The variation of the electrode impedance with frequency is as predicted by the double layer models, increasing rapidly at lower frequencies. At high frequencies (>100KHz) it begins to approach the value of the resistance presented by the bulk solution (between the measurement electrode and the large return electrode), which is effectively independent of frequency. The value of this resistance, known as the 'spreading resistance', can be accurately predicted using the assumption that the planar electrode can be replaced by a hemispherical electrode of similar size. It is obvious that any measurements to monitor cell activity should be carried out at a single frequency, and in this case a frequency of 1KHz was chosen with the reasons being three-fold. Firstly, this frequency was high enough to ensure that the magnitude of the electrode impedances remained in all cases low enough to be measured with reasonable accuracy. Secondly, it was low enough to allow the impedance of the double layer to dominate the measured impedance, with the spreading resistance being negligible in comparison. This relied on the assumption that cell activity on the electrode would result in changes to the double layer impedance. Finally, as the major concern of this work is to improve the extracellular potentials recorded from cultured neurons, it is appropriate to choose a frequency near that at which action potentials themselves are generated. This is necessary so that the measured impedance bears a direct relationship to that through which the membrane current, flowing into and out of the cell during an action potential, must flow. In the case of vertebrate neurons, which are of

particular concern here due to the relatively small signals which they generate, action potentials are typically generated around a 1KHz centre frequency.

The experimentally observed behaviour of electrode impedance with current density was less characteristic and less predictable. Theory suggests that at low frequencies the impedance remains constant, but above some threshold will begin to decrease significantly. Measured impedances suggested little variation over a wide range of current densities however, with the only exception being the platinised microelectrode ($100\mu m^2$) whose impedance started to decrease above approximately $100mA.cm^{-2}$. In selecting a current density at which to carry out measurements it is important to remain within a region of constant electrode impedance, in order to ensure that any changes in the measured impedance (due to the interaction of cell and electrode) are linear. This is not a serious limitation given the noted experimental observations. A more important consideration is that the current density must be low enough so that no adverse affects are induced in the developing cells. A review of the literature would suggest that fields below $150mV.mm^{-2}$ will produce little observable difference in the behaviour of subjected cells, but a better guide is the current density which flows during a neuronal action potential. If current densities are kept below levels which produce such field strengths, there is little prospect of either cell damage and importantly, if neurons themselves are being monitored, little possibility of stimulating unwanted action potentials. A typical value for the peak current density flowing during an action potential is $1mA.cm^{-2}$. Such a value was chosen for use with the large multi-cell electrodes (0.2×0.7mm) and provided a suitable signal to noise ratio for the detection of the potential drop across the device (with the impedance being calculated from the potential drop). For the microelectrodes however, such a current density would result in a total current of only 1nA, i.e. a voltage drop of less than $100\mu V$ across the platinised microelectrodes. This value did not provide a sufficiently large signal to noise ratio, and instead the significantly larger current density of $32mA.cm^{-2}$ was used. Whilst this is probably sufficient to stimulate neuronal electrical activity, it did not produce an obvious deviation in the behaviour of Baby Hamster Kidney (BHK) fibroblast cells, which were used in initial experiments. Given an improved screening, filtering, and recording set-up, it should in the future be possible to reduce this excessive current density however, by up to one order of magnitude.

The variation of impedance with time due to non-cellular activity was investigated by monitoring the impedance of electrodes covered with a saline solution. It is important that these variations are minimised in order to increase the accuracy with which cell activity can be observed. It was found that impedances of freshly prepared electrodes tended to rise initially, with this effect being more pronounced with platinised electrodes. After approximately 12 hours in the case of the platinised electrodes, and within 1 hour for unplatinised electrodes, impedances tended to reach a steady value which remained constant so long as the electrodes were kept under solution. Allowing the electrodes to dry however, resulted in a significant change in the impedance upon re-immersion. Observing the impedance of neighbouring electrodes, one continuously and the other periodically, suggests that it is not the applied electric field which results in the rise in impedance as both varied at similar rates. Rather it is the adsorption, formation, or deposition of some insoluble compounds onto the electrode which is responsible. This conclusion is further strengthened by examination of the phase components of the impedance rise, which shows that it is chiefly the out of phase (capacitive) component which is responsible. This is consistent with the formation of a semi-insulating layer over the electrode. If the process were due to mechanical instabilities at the surface,

which is particularly possible with brittle platinum black coated electrodes, with material breaking away from the surface, both the in and out of phase components would change in a similar fashion leaving the phase angle unchanged. In order to reduce this time dependent behaviour to a minimum all newly prepared electrodes were soaked in a saline solution for a period exceeding 12 hours, before use. Also to prevent the deterioration of the electrode between uses electrodes were kept stored under de-ionised water.

7.2 IMPEDANCE MONITORING

The use of a control electrode in the experiments carried out here has illustrated the need to be careful in attributing measured impedance changes to local cell activity. Under culture conditions, in addition to the instabilities noted above, there will be changes due to the bulk effects of cell metabolism. In a dense culture it is possible for the ionic and molecular balance of the medium to change rapidly, resulting in spurious impedance fluctuations (changes in the contents of the medium in the gap between cell and electrode will obviously not affect the control electrode, and these are in any case important in determining the impedance of cell-electrode junction). Whilst it is not possible to remove these effects entirely it is possible to gauge their significance by observing the behaviour of the control electrode. This will also follow changes induced by factors such as temperature and protein adsorption. It is often possible however, to neglect the use of a control electrode if it is clear that the changes in impedance due to cell attachment and motion are significantly greater than any background fluctuations. This was occasionally necessary in this work, given the limitation of certain equipment to single channel operation.

Initial observations have been made concerning mainly cells of the Baby Hamster Kidney (BHK) fibroblast permanent line. Although these are significantly different from primary neurons in terms of morphology and electrical behaviour, they are relevant for study given the similarities in the adhesion processes of both. Unlike some other cell types, fibroblasts do not form inter-cellular junctions and each cell may be treated as a separate entity. They do exhibit however a high degree of motility in culture (a property which is perfectly suited to studies by continuous impedance monitoring) which is absent in neurons (excepting neurite outgrowth).

One concern which has been highlighted throughout this work, is the relationship between induced impedance changes and cell adhesion. This latter phenomenon has in the past been quantified by a number of methods including; the number of cells attaching to a substrate in a given time, the degree of spreading achieved also within a given time, and the shear force required to remove cells from the substrate. Here cell adhesion is defined as the the 'tightness' of the cell-electrode seal through which any transmembrane current must flow. As such the measurement of the impedance of this junction via an applied ac field is a direct measurement of cell adhesion as defined. It is unimportant, from the viewpoint of increasing the recorded extracellular potential, whether the improved adhesion is arrived at via more focal contacts, closer approach of the membrane to the electrode, a decrease in conductivity of the interphase region, or some other process. None the less, it is important from a cell biology perspective to attempt to understand this, perhaps obtaining new insight into adhesion mechanisms.

From the measurements made which resulted in cell induced impedance changes, it was shown that it was the series equivalent resistive component which contributed the bulk of the change. This suggests

firstly that there are no modifications occurring at the double layer, and that there are no significant changes to the ionic and molecular concentrations in the cell-electrode gap region, during and after cell adhesion. Either of these effects would surely result in a significant change in the measured capacitance. One of the few remaining alternative causes of the resistive change is that the cells present over the electrode significantly block the flow of current out from it. It was shown in section 4.2.3 that due to the exceptionally high cell membrane capacitance the measured capacitance would be unaffected by the presence of the cell, resulting in only a change in the resistive component.

It is clear from the results obtained with the larger planar electrodes that BHK fibroblast adhesion is dependent to a high degree on the surface of the substrate. Surprisingly no affect was observed upon the impedance of an unaltered evaporated gold electrode when these cells attached and spread, given that the attachment of WI-38 fibroblasts as observed by Giaever and Keese did produce a significant increase. This discrepancy could be due to a differing electrode preparation (unlikely, as the processes used were almost identical) or to the different adhesion processes of the two cell lines. If the later explanation is true, it further confirms the view that care must be taken in extrapolating the results to different cell types. A light deposit of platinum black onto the gold electrode surface again produced no observable impedance change upon attachment of BHK cells, whilst only marginally altering the surface texture. A heavier deposit of platinum, obtained by increasing the plating current density from 9 to 18mA.cm^{-2}, was observed to produce an extremely rough surface texture with a maximum feature size of approximately 100nm. Upon the formation of a confluent cell layer the impedance change produced was at its maximum almost 100%. Comparison of these results, i.e. those with the two differing levels of platinisation, suggest that it is not a modification of the surface chemistry which results in the successful response with the higher level, but that it is instead due to the increased roughness. This is further confirmed by the similar results obtained using the gold plated electrodes. Without further studies it is not possible to say whether the affect produced by the rough electrodes is to produce more focal contacts (as suggested by Curtis and Clark) or whether the entire lower surface of the cell is brought closer to the electrode.

The successful use of electrodes exposed to a plasma suggests that either a roughening of the gold surface is occurring which is below the resolution of the scanning electron microscope (determined by the sputtered gold palladium particle size, 10nm), or that some chemical alteration of the surface, possibly the generation of significant charged groups, is occurring. Either of these may also result in improved cell adhesion. This suggests, as is perhaps obvious, that there are more factors to consider when attempting to improve cell adhesion, than merely surface roughness although this is arguably the most significant.

This technique of impedance monitoring of cell activity offers a powerful method for the study of large cell populations. For example it is a clear indicator of both the health of a cell population and of the cell density. The ability to observe the behaviour of a single cell however, using thin film microelectrodes, offers perhaps the most exciting prospects.

Using a suitably sized planar microelectrode (<100μm^2) it has been possible to extend measurements to include single cell attachment, spreading, and motion. Given however, that the fabrication of devices requires the exposure of electrodes with a reactive ion etch, it is not possible to control the surface properties as precisely as could be achieved with the larger electrodes. Results obtained upon the

attachment and spreading of BHK cells to unplatinised electrodes remain variable, a fact probably due to the various durations for which the gold surface may be exposed to the etch. Consistent results were obtained after microelectrode platinisation with the high current densities required (in order to overcome the depletion boundaries adjacent to the electrode), producing a surface texture similar to that obtained with the heavily platinised large electrodes. The impedance fluctuations observed were consistent with the attachment and the movement onto and off of the electrodes of whole cells, with the impedance often returning to its initial value. In addition smaller fluctuations, both in amplitude and period, were present and in the lack of any contradictory evidence are believed to be due to modifications in the structure of the lower membrane, e.g. the formation and destruction of focal contacts, close contacts etc. Optical microscopic examination has been limited by the lack of either sufficient transmitted or reflected light by electrodes (particularly those which have been platinised). The use of time lapse video has allowed limited cell motion to be correlated with large impedance changes, but has not been able to relate changes to finer cell activities.

Considering the results previously reported concerning the use of planar metal microelectrodes to record from electrically active cells in culture, there is some evidence that electrode roughness is an important factor in determining signal amplitude. This would appear to be confirmed by the results presented here, but it is obviously desirable to observe the impedance response of neurons attached to microelectrodes, directly. To date, attempts to monitor the development of neurons from the snail *Lymnaea stagnalis* have proved unsuccessful, due to the inability to obtain consistent spreading and outgrowth. Whilst cells will occasionally exhibit such behaviour on areas of the devices not subjected to an electric field, it has never been observed of a cell over an active electrode. The lack of a rigourous survey has prevented the drawing of any conclusion regarding the injurious affects of such a field (this is possible, given the high current densities already noted).

7.3 MICROELECTRODE GEOMETRY

From the limited work published on the topic, and using intuition, it is clear that commonly used models for estimating the value of extracellular fields do not accurately represent the situation of a cell in close proximity to certain extracellular boundaries. It is clear that if these boundaries consist of substantial insulating regions, potentials in the local may be significantly increased (or decreased if the region of interest lies behind the insulating surface). Incorporating such boundaries into the design of microelectrode arrays, may lead to significant improvements in the signal to noise ratios with which extracellular action potentials can be recorded. Firstly however, it is important to develop and apply, rigourous and quantitative design and testing procedures.

The finite element method (FEM) is a numerically intensive solution method for all types of field problems, whose availability is now widespread. Although it is most often used in the solution of structural and thermal problems, its ability to analyse problems with complicated boundary conditions and material properties lend it to a wide variety of bio-electrical problems. As with all field solution methods however, the accuracy of the results is chiefly dependent on the validity of the boundary conditions involved (given in the case of FEM, a suitably fine mesh). In this instance the model used to represent the cell was an extreme approximation, that is an ideal sphere with uniform membrane depolarisation. The

calculated extracellular potentials are surprisingly realistic given this model, lying only slightly below the sort of values typically recorded. This difference is probably due to the inability to account for the close adhesion between cell and substrate, which is discussed elsewhere. The only other possible source of error lies in the failure to include time variant effects in the model, namely the double layer capacitance and the capacity of the medium, due to the excessive computation that such a model would require.

Given these approximations however, it was shown that for the case of a cell suspended in a volume conductor the FEM solution in the region close to the cell differed by only 0.5% from the easily obtained analytical solution. In order to achieve this accuracy, it was necessary to progressively increase the mesh size until the change in the potential values between consecutive solutions became negligible (less than a 2% change for a doubling in the mesh complexity). This iteration process was carried out for all models, and whilst in most cases analytical solutions were too complex to undertake, a degree of accuracy similar to that estimated for the cell suspended in a volume conductor was assumed.

Whilst the actual amplitudes of the extracellular potentials calculated using this method have proved to be extremely close to those experimentally reported values, giving some justification to the choice of current densities and depolarisation spread, it is in determining trends and relative values that it is of most use. It has been shown that positioning a planar electrode immediately below a cell will only increase the potential at the electrode (from that existing at the field point without the presence of the electrode) from 143 to 181μV. The most dramatic increases are obtained by recessing the electrode and the cell in a groove, where the depth of the groove begins to become comparable with the cell diameter. For example with a groove depth of 11μm the electrode potential rises to almost 490μV. Even more dramatic increases are obtained if the electrode is confined at the bottom of a pit with rectangular cross section.

These results demonstrate that it is possible to improve the design of microelectrode arrays by taking into account electrode geometry, with the only limitation being the practicalities of device fabrication.

It has been stated that appropriate testing procedures must be used in conjunction with design methods such as these, in order to verify the theoretical results (in which a number of assumptions have to be made). There is obviously no substitute for the use of primary neurons given their unique morphologies and electrical behaviour. In the absence of a suitable cell type it has been necessary to utilise two methods, which although far from ideal, have indicated that electrode performance can be improved by applying the results of the FEM analyses.

Constant current injection via a fine tipped, saline filled glass micropipette is a simple method of simulating an extracellular action potential. Although the magnitude of the recorded signals varied widely depending on the exact shape of the pipette tip, it was possible to compare different electrode devices by using the same electrode with each. This demonstrated the same trend, of increasing electrode potential with increasing groove depth, using the limited number of devices which have been fabricated. Fabrication has been a major problem due to the difficulty in etching through thick insulating layers to completely expose the electrodes. This has also limited studies using chick cardiac myocytes, which generate action potentials with a duration similar to that of vertebrate neurons. These cells have the advantage that mechanical contractions, observed under an optical microscope, can be used to verify the recording of

extracellular action potentials thus doing away with the need for simultaneous intracellular recording. Although both the electrical and mechanical activity of these cells appeared to cease in very narrow grooves (8μm), probably due to constriction by the sidewalls, recordings made from cells in wider grooves (18μm) again appear to indicate an increase in electrode potential with groove depth. These results are only preliminary, involving the comparison of a 0.4μm and a 28μm deep groove, and a more thorough parametric analysis will be required in order to confirm them.

7.4 GENERAL COMMENTS ON EXTRACELLULAR MICROELECTRODES

The relative advantages and disadvantages of thin film metal microelectrode arrays over other methods of recording from neurons *in vitro* have already been discussed. The long term monitoring capabilities offered by the former, when compared to the majority of these alternatives, is often offset by the relatively low signal to noise ratios which can be achieved. This is especially true of small vertebrate neurons which are of particular interest from both a neurophysiological and a medical point of view. It is apparent that if signal amplitudes can be improved to sufficient levels to allow not only spike detection, but also some degree of waveform discrimination, then extracellular microelectrodes offer by far the most promising technique.

The careful study of cell-electrode adhesion carried out here using continuous impedance monitoring, apart from implying the effect of surface roughness on signal amplitude, offers a method to raise signal amplitudes by studying numerous additional factors including, media, time in culture, and cell type. Together with the use of computer aided design (CAD) procedures and the ever more advanced fabrication methods available the prospects for the study of real neural networks are enormous.

The results obtained here also have implications for other areas including *in vivo* probes and implantable neural prosthesis. Particularly for the latter, the use of impedance monitoring will allow the adhesion of cells to be monitored over long periods of time, and may reveal how the electrodes deteriorate with time due to organic deposition and electrolysis. CAD techniques will prove useful in the design of the majority of bio-electronic devices where potentials are being either generated or detected.

7.5 FUTURE WORK

The application of impedance monitoring to the study of cell adhesion processes is clear. In order to further clarify the role of local ionic changes in the gap between cell and electrode several techniques may prove useful. Using cyclic voltammetry for example, where the current response to a slowly ramping voltage is obtained, it would be possible to obtain both the identity and the concentration of ions at the electrode-electrolyte interphase, allowing any significant fluctuations to be observed. Taking measurements at various frequencies would also indicate whether the impedance fluctuations are frequency independent, and therefore due mainly to changes in the cell-electrode gap as suggested. If this is indeed so, it may prove a more sensitive method of detection to use high frequencies (>100KHz) in order to observe cell activity. The extrapolation of results to 1KHz i.e. near the spectrum of vertebrate action potentials, would be unnecessary due to the frequency independence.

In order to correlate the observed impedance fluctuations more closely with cell activity, the optical imaging of cells must be improved. This would require firstly, longer working distance lenses than were available here, given that the electrodes used are almost completely opaque and a reflection microscope must be used. It is worth noting at this point that initial studies have been carried out using transparent indium tin oxide electrodes, replacing the gold electrodes used here. Problems have been encountered in ensuring that the electrodes are completely exposed, even for thin insulating layers, given that the electrodes cannot be clearly seen under a microscope. If the surface of the electrodes can be made suitable for impedance monitoring (obviously platinisation would cause a loss in optical transmission), cells could be clearly observed on the surface. In the absence of such transparent conductors, and given longer working distance lenses, the most suitable method of observation would involve the use of fluorescent dyes. Present dyes are limited to exposure times of only several minutes however, due to bleaching. If only periodic observations are made (time lapse photography) it may be possible to gain limited information on cell motion. Another possible, though more complex, method of observation would be confocal scanning microscopy of the cell, which provides high resolution 3-D images in almost real time.

From the point of view of obtaining information on how surface roughness affects cell adhesion, it would be useful to examine cross-sections of cell and substrate using either scanning or transmission electron microscopy. This would indicate whether roughness does indeed increase the occurrence of focal contacts, or whether other regions of the lower membrane surface are brought closer to the substrate.

With regard to the finite element models considered here, it would be interesting to consider the effect of groove structures on both axons and dendrites. Again a three dimensional model would be required, with the variable potential (as described by an approximation such as a gaussian summation) along the neurite membrane being specified. This could have implications for the design of neural prosthesis, in particular for structures designed for nerve regeneration.

Several primary vertebrate neuronal cell types present themselves as suitable for use in culture with the electrode devices described here, given suitable culture conditions. For example rat and mouse spinal chord are reported to exhibit spontaneous electrical activity after several days in culture. The simultaneous recording of action potential generation and of the cell-electrode impedance would provide direct information on the relationship between these two dependent variables.

BIBLIOGRAPHY

Adey, R.A., and C.A. Brebbia. 1983. Basic computational techniques for engineers. 118-136. London: Pentech Press.

Ahmed, Z. 1988. Expression of membrane currents in rat neocortical neurons in serum-free culture: I inward currents. Develop. Brain Res. 40 : 285-295.

Alberts, A., D. Bray, J. Lewis, M. Raff, K. Roberts, and J.D. Watson. 1983. Molecular biology of the cell. 1018-1034. New York & London: Garland.

Amstein, C.F., and P.A. Hartman. 1975. Adaption of plastic surfaces for tissue culture by glow discharge. J. Clin. Microbiol. 2 (1) : 46-54.

Arvanitaki, A., and Chalazonitis. 1961. Excitatory and inhibitory processes initiated by light and infrared radiations in single identifiable nerve cells (giant ganglion cells of *Aplysia*). In Nervous Inhibition. Edited by E. Florey. Toronto: Pergamon Press, Canada Ltd.

Banks, B.A., A.J. Weigand, and C.A. Babbush. 1976. Potential biomedical applications of ion beam technology. NASA Technical Manual NASA TM X-73512

Barkey, D.P., R.H. Muller, and C.W. Tobias. 1989a. Roughness development in metal electrodeposition I. Experimental results. J. Electrochem. Soc. 136 (8) : 2199-2206.

Barkey, D.P., R.H. Muller, and C.W. Tobias. 1989b. Roughness development in metal electrodeposition II. Stability theory. J. Electrochem. Soc 136 (8) : 2207-2214.

Barnes, F.S., and C.L.J. Hu. 1977. Model for some nonthermal effects of radio and microwave fields on biological membranes. IEEE Trans. Microwave Theory Tech. 25 (9) : 742-746.

Bockris, J.O'M., N. Bonciocat, and F. Gutmann. 1974. An introduction to electrochemical science. 63-66. London: Wykeham.

Bockris, J.O'M., and A.K.N Reddy. 1977a. Modern electrochemistry. 1026-1029. New York: Plenum.

Bockris, J.O'M., and A.K.N Reddy. 1977b. Modern electrochemistry. 722-732. New York: Plenum.

Bockris, J.O'M., and A.K.N. Reddy. 1977c. Modern electrochemistry. 293-296. New York: Plenum.

Bray, D. 1979. Mechanical tension produced by nerve cells in culture. J. Cell Sci. 37 : 391-410.

Britland, S.T., G. Moores, P. Clark, and P. Connolly. 1989. Patterning cell adhesion and movement on artificial substrata; a simple method. Proc. Anat. Soc. Gt. Brit. (18)

Cambiaso, A., G. Grattarola, S. Arnaldi, S. Martinoia, and G. Massobrio. 1990. Detection of cell activity via ISFET devices: modelling and computer simulations. Sensors and Actuators B1 : 373-379.

Cassaleggio, A., L. Marconi, G. Morgavi, S. Ridella, and C. Rolando. 1985. Current flow in a cell with non-linear membrane stimulated by an electric field. Bioelectro. & Bioenergetics 14 : 13-21.

Catterall, W.A. 1984. The molecular basis of neuronal excitability. Science 223 (4637) : 653-661.

Cendes, Z.J. 1989. Unlocking the secrets of Maxwell's equations. IEEE Spectrum (April) : 29-35.

Clark, J., and R. Plonsey. 1966. A mathematical evaluation of the core conductor model. Biophys. J 6 : 96-113.

Clark, J., and R. Plonsey. 1968. The extracellular potential field of the single active nerve fibre in a volume conductor. Biophys. J. 8 : 842-864.

Clark, P., P. Connolly, A.S.G. Curtis, J.A.T. Dow, and C.D.W. Wilkinson. 1990. Topographical control of cell behaviour: II multiple grooved substrata. Develop. 108 : 635-644.

Clark, P., P. Connolly, J.A.T. Dow, A.S.G. Curtis, and C.D.W. Wilkinson. 1987. Topographical control of cell behaviour: 1. simple step cues. Develop. 99 : 439-448.

Cohen, L.B., and B.M. Salzberg. 1978. Optical measurement of membrane potential. Rev. Physiol. Biochem. Pharmacol. 83 : 35-88.

Connolly, P., P. Clark, A.S.G. Curtis, J.A.T. Dow, and C.D.W. Wilkinson. 1990. An extracellular microelectrode array for monitoring electrogenic cells in culture. Biosensors 5 (3) : 223-234.

Corporation, Fairchild. 1979. Semiconductor & Integrated Circuit Fabrication Techniques. Reston Publishing.

Crick, F. 1982. Do dendritic spine twitch? Trends Neurosci. 5 : 44-46.

Curtis, A.S.G. 1964. The mechanism of adhesion of cells to glass; A study by interference reflection microscopy. J. Cell. Biol. 20 : 199-215.

Curtis, A.S.G., and P. Clark. 1990. The effects of topographic and mechanical properties of materials on cell behaviour. Crit. Rev. Biocomp. 5 (4) : 343-362.

Curtis, A.S.G., J.V. Forrester, C. McInnes, and F. Lawrie. 1983. Adhesion of cells to polystyrene surfaces. J. Cell Biol. 97 : 1500-1506.

Davey, C.L., and D.B. Kell. 1989. Low frequency dielectric properties of cell suspensions. IOP short meetings 21 : 51-62.

Drake, K.L., K.D. Wise, J. Farraye, D.J. Anerson, and S.L. Bemont. 1988. Performance of planar multisite microprobes in recording single unit intracortical activity. IEEE Trans. Biomed. 35 (9) : 719-732.

Droge, M.H., G.W. Gross, M.H. Hightower, and L.E. Czisny. 1986. Multielectrode analysis of coordinated multisite rythmic bursting in cultured CNS monolayers. J. Neurosci. 6 (6) : 1583-1592.

Eccles, J.C. 1964. Excitatory responses of spinal neurons. Prog. Brain. Res. 12 : 1-31.

Edell, D.J. 1986. A peripheral information transducer for amputees: long term multichannel recordings from rabbit peripheral nerves. IEEE Trans. Biomed. 33 (2) : 203-214.

Elbicki, J.M., and S.G. Weber. 1989. Ultrafiltration of human serum to determine the size of species that poison voltammetric electrodes. Biosensors 4 : 251-257.

Fange, R., H. Persson, and S. Thesleff. 1956. Elecrophysioligical and pharmacological observations of trypsin-disintegrated embryonic chick hearts cultured in vitro. Acta. Physiol. Scand. 38 : 173.

Fuchs, P.A., L.P. Henderson, and J.G. Nicholls. 1982. Chemical transmission between individual retzius and sensory neurons of leech in culture. J. Physiol. 323 : 195-209.

Gabrielli, C. 1990. Use and application of electrochemical impedance techniques. Slumberger Technologies. NTIS, 12860013.

Geddes, L.A. 1972. Electrodes and the measurement of bioelectric events. Wiley Interscience.

Geddes, L.A., and L.E. Baker. 1967. The specific resistance of biological material: a compendium of data for the biomedical engineer and physiologist. Med. Biol. Eng. 5 : 271-293.

Geselowitz, D.B. 1966. Comments on the core conductor model. Biophys. J. 6 : 691-692.

Giaever, I., and C.R. Keese. 1984. Monitoring fibroblast behaviour in tissue culture with an applied electric field. Proc. Nat. Acad. Sci. 81 : 3761-3764.

Giaever, I., and C.R. Keese. 1986. Use of electric fields to monitor the dynamical aspect of cell behaviour in tissue culture. IEEE Trans. Biomed. 33 (2) : 242-247.

Gonzalez-Mariscal, L., L. Borboa, R. Lopez-Vancell, G. Beaty, and M. Cereijido. 1985. Electrical properties of MDCK cells. In Tissue Culture of Epithelial Cells. Edited by M. Taub. 25-36. New York: Plenum Press.

Grahame, D.C. 1952. Mathematical theory of the faradaic admittance. J. Electrochem. Soc. 99 (12) : 370C-385C.

Grattarola, M., M. Tedesco, A. Cambiaso, G. Perlo, G. Gianetti, and A. Sanguineti. 1988. Cell adhesion to silica substrata. Biomaterials 9 : 101-106.

Grinnel, F. 1978. Cellular adhesiveness and extracellular substrata. Int. Rev. Cytol. : 65-144.

Grinvald, A., L.B. Cohen, S. Lesher, and M.B. Boyle. 1981. Simultaneous optical monitoring of activity of many neurons in invertebrate ganglia using a 124 element photodiode array. J. Neurophysiol. 45 (5) : 829-840.

Gross, G.W. 1979. Simultaneous single unit recording in vitro with a photoetched laser deinsulated gold multimicro-electrode surface. IEEE Trans. Biomed. 26 (5) : 273-279.

Gross, G.W., and J.H. Lucas. 1982. Long term monitoring of spontaneous single unit activity from neuronal monolayer networks cultured on photoetched multielectrode surfaces. J. Electrophysiol. Technol. 9 : 55-69.

Gross, G.W., W. Wen, and J. Lin. 1985. Transparent indium tin oxide electrode patterns for extracellular, multisite recording in neuronal cultures. J. Neurosci. M. 15 : 243-252.

Hadley, R.D., S.B. Kater, and C.S. Cohan. 1983. Electrical synapse formation depends on interaction of mutually growing neurites. Science 22 : 466-468.

Harris, A.K. 1973. Behaviour of cultured cells on substrata of variable adhesiveness. Exp. Cell. Res. 77 : 285-297.

Hause, L.L., R.A. Komorowski, and F. Gayon. 1981. Electrode and electrolyte impedance in the detection of bacterial growth. IEEE Trans. Biomed. 28 (5) : 403-410.

Heath, J.P. 1982. Adhesions to substratum and locomotory behaviour of fibroblastic and epithelial cells in culture. In Cell Behaviour. Edited by R. Bellairs, A. Curtis and G. Dunn. 77-108. Cambridge: Cambridge University Press.

Hermann, L. 1879. In Handbuch der Physiologie. Edited by L. Hermann. Leipzig: Vogel.

Higgins, M.L., M.N. Smith, and G.W. Gross. 1980. Selective cell destruction and precise neurite transection in neuroblastoma cultures with pulsed UV laser microbeam irradiation: an analysis of mechanisms and transection reliability with light and scanning microscopy. J. Neurosci. M. 3 : 83-99.

Hirono, T., K. Torimitsu, A. Kawana, and J. Fukuda. 1988. Recognition of artificial microstructures by sensory nerve fibres in culture. Brain Research 446 : 189-194.

Hodgkin, A.L., and A.F. Huxley. 1952. A quantitative description of membrane current and its application to conduction and excitation in nerve. J. Physiol. 117 : 500-544.

Hollahan, J.R., and R.S. Rosler. 1978. Plasma deposition of inorganic thin films. In Thin Film Processes. Edited by J. L. Vossen and W. Kern. 361-396. New York: Academic Press.

Hopfield, J.J. 1982. Neural networks and physical systems with emergent collective computational abilities. Proc. Natl. Acad. Sci. USA 79 : 2554-2558.

Hopfield, J.J. 1983. Unlearning has a stabilising effect on collective memories. Nature 304 : 158.

Hopfield, J.J., and D.W. Tank. 1985. Neural computation of decisions in optimisation problems. Biolog. Cybern. 52 : 1-25.

Israel, D.A., W.H. Barry, D.J. Edell, and R.G. Mark. 1984. An array of microelectrodes to stimulate and record from cardiac cells in culture. Amer. J. Physiol 247 : H669-H674.

Jobbling, D.T., J.G. Smith, and H.V. Wheal. 1981. Active microelectrode array to record from the mammalian central nervous system in vitro. Med. Biol. Engin. 19 : 533-560.

Keeton, W.T. 1980. Biological Science. 97-98. W.W. Norton & Co.

Kell, D.B. 1987. The principles and potential of electrical admittance spectroscopy: an introduction. In Biosensors: Fundamentals and applications. Edited by A. F. P. Turner, T. Karube and G. Wilson. Oxford: Oxford University Press.

King, C.A., J.E.M. Heaysman, and T.M. Preston. 1979. Experimental evidence for the role of long range forces in fibroblast-substrate interaction. Exp. Cell. Res. 119 : 406-410.

Kleinfeld, D., K.H. Kahler, and P.E. Hockberger. 1988. Controlled outgrowth of dissociated neurons on patterned substrates. J. Neurosci. 8 (11) : 4098-4120.

Kleinfeld, D., G.F. Raccuia, and H.J. Chiel. 1988. Circuits with bistable outputs. Soc. Neur. abstr. 14 : 841.

Levi-Montal Chini, R., and K.R. Seshan. 1982. Long term cultures of embryonic and mature insect nervous and neuroendocrine systems. In Tissue culture of the nervous system. Edited by G. Sato. 95-123. New York: Plenum.

Lucas, J.H., L.E. Czisny, and G.W. Gross. 1986. Adhesion of cultured mammalian CNS neurons to flame-modified hydrophobic surfaces. Vitro Cell. & Dev. Biol. 27 : 37-43.

Manning, G.W., and S.P. Akuja. 1969. Electrical activity of the heart. Illinois: C.C. Thomas.

Maroudas, N.G. 1973. Chemical and mechanical requirements for fibroblast adhesion. Nature 244 : 353-355.

Martin, G.R., and H. Rubin. 1974. Exp. Cell Res. 85 : 319.

McNeal, D.R. 1976. Analysis of a model for excitation of mylinated nerve. IEEE Trans. Biomed. 23 (4) : 329-337.

McNeil, V.M., L.D. Clark, and D.J. Edell. 1987. Optimisation of the noise performance of active neural transducers. Japan:

McRoberts, J.A., M. Taub, and M.H. Saier. 1981. The Madden Darby Canine Kidney (MDCK) cell line. In Functionally Differentiated Cell Lines. Edited by G. Sato. 117-140. New York: Alan R. Liss.

Middleton, C.A. 1982. Cell contacts and the locomotion of epithelial cells. In Cell Behaviour. Edited by R. Bellairs, A. Curtis and G. Dunn. Cambridge: Cambridge University Press.

Miller, C., and C.S. Henriquez. 1988. Three dimensional finite element solution for biopotentials: erythrocyte in an applied field. IEEE Trans. Biomed. 9 : 712-718.

Miller, F.R., and R. Dacheux. 1976. Dendritic and somatic spikes in mudpuppy amacrine cells: identification and TTX sensitivity. Brain Res. 104 : 157-162.

Miller, J.P., W. Rall, and J. Rinzel. 1985. Synaptic amplification by active membrane in dendritic spines. Brain Res. 325 (1-2) : 325-350.

Mimura, Y. 1986. The mechanism of overhang formation in diazide/novalak photoresist film by chlorobenzene soak process. J. Vac. Sci. Technol. B 4 (15-21)

Nelson, P.G., E.A. Neale, and R.L. Macdonald. 1981. Electrophysiological and structural studies of neurons in dissociated cell cultures of the central nervous system. In Excitable cells in tissue culture. Edited by P. G. Nelson and M. Lieberman. 39-74. New York: Plenum.

Nerbonne, J.M., and A.M. Gurney. 1989. Development of excitable membrane properties in mammalian sympathetic neurons. J. Neurosci. 9 (9) : 3272-3286.

Oliver, A.P., R.J. Wyatt, D.L. Peterson, and M.C. Peckerar. 1986. Fabricated array microelectronics in a system for study of cultured nerve cells. Airlie House, Virginia, USA:

Paddock, S.W. 1989. Tandem scanning reflected-light microscopy of cell-substratum adhesions and stress fibres in Swiss 3T3 cells. J. Cell Sci. 93 : 143-146.

Panofsky, W.K.H., and M. Phillips. 1962. Classical electricity and magnetism. New York: Addison-Wesley.

Parsons, T.D., D. Kleinfeld, F. Raccuia-Behling, and B.M. Salzberg. 1989. Optical recording of the electrical activity of synaptically interacting aplysia neurons in culture using potentiometric probes. Biophys. J. 56 : 213-221.

Pickard, R.S. 1979. A review of printed circuit microelectrodes. J. Neurosci. M. 1 : 301-318.

Pine, J. 1980. Recording action potentials from cultured neurons with extracellular microcircuit electrodes. J. Neurosci. M. 5 : 13-22.

Plonsey, R. 1969. Bioelectric phenomena. 203-209. New York: McGraw-Hill.

Pooler, J.P., and G.S. Oxford. 1973. Photoalteration of lobster giant axons in calcium-free and calcium-rich media. J. Membr. Biol. 12 : 339.

Purves, D., and J.W. Lichtman. 1985. Principles of neural development. 205-227. New York: Sinauer.

Rall, W. 1962. Electrophysiology of a dendritic neuron model. Biophys. J. 2 : 145-167.

Rattay, F. 1988. Modelling the excitation of fibres under surface electrodes. IEEE Trans. Biomed. 35 (3) : 199-202.

Rauvala, H., R. Pihlaskari, J. Laitinen, and J. Merenmies. 1989. Extracellular adhesive molecules in neurite growth. Bioscience Reports 9 (1) : 1-12.

Rayport, S.G., and S. Schacher. 1986. Synaptic plasticity in vitro: cell culture of identified aplysia neurons mediating short-term habituation and sensitization. J. Neurosci. 6 (3) : 759-763.

Reddy, J.N. 1984. An introduction to the finite element method. New York: McGraw-Hill.

Regehr, W.G. 1988. Neuron-microdevice connections. Ph.D, California Institute of Technology. USA.

Regehr, W.G., J. Pine, and D.B. Rutledge. 1988. A long term in vitro silicon-based microelectrode-neuron connection. IEEE Trans. Biomed. 35 (12) : 1023-1031.

Reinberg, A.R. 1979. Plasma deposition of inorganic thin films. Ann. Rev. Mater. Sci. 9 : 341-372.

Robinson, D.A. 1968. The electrical properties of metal microelectrodes. Proc. IEEE 56 : 1065-1071.

Rubenstein, J.T., F.A. Spelman, M. Soma, and M.F. Suesserman. 1987. Current density profiles of surface mounted and recessed electrodes for neural prostheses. IEEE Trans. Biomed. 34 (11) : 864-875.

Schmid, R.D. 1988. International workshop at the gesellschaft für biotechnologische forschung (gbf), Brunswick, FRG, 23-26 June, 1987. Biosensors 3 (4) : 239-249.

Shaw, G.L., E. Harth, and A.B. Scheibel. 1982. Cooperativity in brain function: assemblies of approximately 30 neurons. Exp. Neurology 77 : 324-358.

Singer, I.I., D.M. Kazazis, and S. Scott. 1989. Scanning electron microscopy of focal contacts on the substratum attachment surface of fibroblasts adherent to fibronectin. J. Cell Sci. 93 : 147-154.

Smith, G.D. 1978. Numerical solution of partial differential equations. 2nd ed. Oxford: Clarendon.

Standen, N.B., P.T.A. Gray, and M.J. Whitaker. 1987. Microelectrode techniques: The plymouth workshop handbook. Cambridge: The company of biologists.

Stepnoski, R.A., A. Laporte, S. Raccuia-Behling, G.E. Blonder, R.F. Slusher, and D. Kleinfeld. 1991. Non-invasive detection of transmembrane potential in cultured neurons via light scattering. in press

Strasa, F.L. 1985. Applied finite element analysis for engineers. CBS College Publishing.

Stremler, F.G. 1982a. Introduction to Communication Systems. 136-141. Reading Ma.: Addison Wesley.

Stremler, F.G. 1982b. Introduction to Communication Systems. 178-180. Reading Ma.: Addison Wesley.

Sugano, T. 1985. Applications of plasma processes to VLSI technology. New York: John Wiley & Sons Inc.

Syed, N.I., A.G.M. Bulloch, and K. Lukowiak. 1990. In vitro reconstruction of the respiratory central pattern generator of the mollusk lymnaea. Science 250 : 282-285.

Tank, D.W., C.S. Cohan, and S.B. Kater. 1986. Cell body capping of array electrodes improves measurements of extracellular voltages in micro-cultures of invertebrate neurons. Airlie House, Arlinton, Virginia, USA:

Tank, D.W., and J.J. Hopfield. 1987. Collective computation in neuronlike circuits. Sci. Am. 257 (6) : 104-114.

Tank, D.W., and D. Kleinfeld. 1986. The relation between electrode placement and the amplitude of the extracellularily recorded action potentials. Biophysical J. 49 : 233a.

Taub, M., and M.H. Saier. 1979. An established but differentiated kidney epithelial cell line (MDCK). Meth. Enzymol. 58 : 552.

Thomas, C.A., Jr. 1972. A miniature microelectrode array to monitor the bioelectric activity of cultured cells. Exp. Cell Res. 74 : 61-66.

Turner, A.F.P., T. Karube, and G. Wilson. 1987. Biosensors: Fundamentals and applications. Oxford: Oxford University Press.

Veltink, P.H., J.A. Van Alste, and B.K. Boom. 1988. Simulation of intrafascicular and extraneural nerve stimulation. IEEE Trans. Biomed. 35 (1) : 69-75.

Verscheuren, H. 1985. Interference reflection microscopy in cell biology: methodology and applications. J. Cell. Sci. 75 : 279-301.

Weiss, L. 1961. The measurement of cell adhesion. Exp. Cell Res. Suppl. 8 : 141-153.

Widrow, B., and M.A. Lehr. 1990. 30 years of adaptive neural networks: perceptron, madeline, and back propogation. In Procedings of the IEEE. 1415-1442.

Wilson, R.J.A., J.A.T. Dow, and S.E. Blackshaw. 1991. Topographical discontinuities modify the outgrowth of leech retzius neurons grown in culture. Proc. Physiological Soc.:

Wilson, R.J.T. 1990. Dept of Cell Biology, University of Glasgow.

Wong, G.R., E.C. Martel, and S.B. Kater. 1983. Conditioning factor(s) produced by several moluscan species promote neutite outgrowth in cell culture. J. Exp. Biol. 105 : 389-393.

Zambuto, M. 1989. Semiconductor Devices. 112-172. New York: McGraw Hill.

Zucker, R.S. 1989. Short-term synaptic plasticity. Ann. Rev. Neurosci. 12 : 13-31.